

STATUS OF THESIS

Title of thesis

STUDIES ON THE NONLINEAR INTERACTIONS
ASSOCIATED WITH MOORED SEMI SUBMERSIBLE
OFFSHORE PLATFORMS

I YASSIR MOHAMMEDNOUR ELFADUL ABBAS

hereby allow my thesis to be placed at the Information Resource Center (IRC) of Universiti Teknologi PETRONAS (UTP) with the following conditions:

1. The thesis becomes the property of UTP
2. The IRC of UTP may make copies of the thesis for academic purposes only
3. This thesis is classified as

Confidential

Non-confidential

If the thesis is confidential, please state the reason:

The contents of the thesis will remain confidential for _____ years.

Remarks on disclosure:

Endorsed by

Signature of Author

Signature of Supervisor

Permanent address:
Civil Dept., College of Eng.,
Sudan University of Science and Technology,
P.O. Box: 407-Khartoum, Sudan.

Prof. Dr. Kurian V. John

Date: _____

Date: _____

UNIVERSITI TEKNOLOGI PETRONAS
STUDIES ON THE NONLINEAR INTERACTIONS ASSOCIATED WITH
MOORED SEMI SUBMERSIBLE OFFSHORE PLATFORMS

By

YASSIR MOHAMMEDNOUR ELFADUL ABBAS

The undersigned certify that they have read, and recommend to the Postgraduate Studies Programme for acceptance this thesis for the fulfillment of the requirements for the degree stated.

Signature: _____

Main Supervisor: Prof. Dr. Kurian V. John

Signature: _____

Co-Supervisor: Assoc. Prof. Dr. Indra Sati Hamonangan Harahap

Signature: _____

Head of Department: Assoc. Prof. Ir. Dr. Mohd Shahir Liew

Date: _____

STUDIES ON THE NONLINEAR INTERACTIONS ASSOCIATED WITH
MOORED SEMI SUBMERSIBLE OFFSHORE PLATFORMS

By

YASSIR MOHAMMEDNOUR ELFADUL ABBAS

A Thesis

Submitted to the Postgraduate Studies Programme

as a Requirement for the Degree of

DOCTOR OF PHILOSOPHY

CIVIL ENGINEERING DEPARTMENT

UNIVERSITI TEKNOLOGI PETRONAS

BANDAR SERI ISKANDAR,

PERAK

MAY 2011

DECLARATION OF THESIS

Title of thesis

STUDIES ON THE NONLINEAR INTERACTIONS
ASSOCIATED WITH MOORED SEMISUBMERSIBLE
OFFSHORE PLATFORMS

I YASSIR MOHAMMEDNOUR ELFADUL ABBAS

hereby declare that the thesis is based on my original work except for quotations and citations which have been duly acknowledged. I also declare that it has not been previously or concurrently submitted for any other degree at UTP or other institutions.

Witnessed by

Signature of Author

Signature of Supervisor

Permanent address:
Civil Dept., College of Eng.,
Sudan University of Science and Technology,
P.O. Box: 407-Khartoum, Sudan.

Prof. Dr. Kurian V. John

Date: _____

Date: _____

ABSTRACT

The design of moored semi submersible systems constitutes a challenging engineering problem in which, the platform offset, stability, payload and system-optimized cost requirements are to be met simultaneously. This problem is complicated by the incomplete understanding of the nonlinearities associated with the multiple interactions such as wave to wave, wave to platform, platform to mooring, fluid to mooring and mooring to seabed. In this study, an attempt has been made to probe into these nonlinearities through numerical, experimental, and parametric studies.

In the numerical study, moored semi submersibles were analyzed in the time domain. The dynamic equilibrium conditions were satisfied through a set of coupled nonlinear differential equations for the six DOF motions. For representing the platform to mooring nonlinear interactions, the 6x6 mooring stiffness matrix was derived based on the mooring stiffness and on the fairlead coordinates relative to the structure CG. For the evaluation of the slow frequency horizontal motions of the platform, the second order wave forces resulting from the second order temporal acceleration and the structural first order motions were formulated. For the assessment of the fluid to mooring and mooring to seabed nonlinear interactions, a deterministic approach for the dynamic analysis of a multi-component mooring line was formulated. The floater motion responses were considered as the mooring line upper boundary conditions. Lumped parameter approach was adopted for the mooring line modeling. Mooring to seabed nonlinear interactions were modeled assuming that the mooring line rested on an elastic dissipative foundation. A numerical dynamic analysis method in the time domain was developed and results for various mooring lines partially lying on different soils were validated by conducting a comparative study against published results. The contribution of the soil characteristics of the seabed to the dynamic behavior of mooring line was investigated for different types of soil.

Two phases of experimental studies were conducted to provide benchmark data for validating the numerical methods. In the first phase, the seakeeping performance of a semi submersible with eight circular columns was studied. The model was built to scale of 1:100 using Froud's law of similitude. The tests were conducted for head, beam and quartering seas. In the second phase, a semi submersible with six circular columns was modeled using the same scale as for the first semi submersible. Linear mass-spring system was arranged to facilitate measurements of the horizontal drift forces. The system natural periods, still water damping, nonlinear viscous damping, drag coefficient and inertia coefficient information were evaluated from the free decay tests. Seakeeping tests were conducted for head and beam model orientations. The measured drift forces were compared to available formulae in the literature to assess the available semi-empirical methods for evaluation these forces. In both experimental phases, twin-hulled conventional semi submersibles were considered. By comparing the results of the numerical and experimental models, the validity of the numerical method was established.

Based on the validated numerical algorithm, a number of parametric studies were conducted for investigating the contributions of various design parameters on the dynamics of moored semi submersibles. The effects of pretension, mooring line configuration, clump weight, cable unit weight, elongation, breaking strength and pretension angle on the behavior of multi-component mooring line, were investigated by using an implicit iterative solution of the catenary equations. On the other hand, using linearized frequency domain analysis, the contributions of platform payload, platform dimensions, number of columns, number of mooring lines, the wave environment mathematical model, the wave characteristics and the operating (intact or damage) conditions to the responses of moored semi submersibles were investigated.

The experimental and published results verified the efficiency of the developed numerical model for prediction of the wave frequency and low frequency motions and mooring dynamic tension responses of the semi submersible. Moreover, experimental results indicated that in addition to the modeling of the mooring system stiffness, typical or hybrid modeling of the mooring system and attachments are necessary for the critical assessment of the mooring system damaged conditions.

ABSTRAK

Dalam merekabentuk sistem bertambatan separuh tenggelam, beberapa cabaran dalam konteks kejuruteraan seperti keseimbangan dan kestabilan pelantar, muatan, dan kos yang optimum harus dipenuhi dalam satu masa. Kekangan ini akan menjadi semakin mencabar sekiranya tidak memahami ciri-ciri ketidaklelurusan dalam pelbagai interaksi termasuk interaksi antara ombak-ombak, ombak-pelantar, pelantar-penambat, bendalir-penambat, dan akhir sekali interaksi antara penambat-dasar laut. Dalam kajian ini, satu usaha telah dilakukan untuk menyiasat ciri-ciri ketidaklelurusan melalui kajian berangka, eksperimen dan juga kajian berparameter.

Dalam kajian berangka, bertambatan separuh tenggelam telah dianalisis dengan menggunakan kaedah domain masa. Keadaan keseimbangan dinamik telah dipenuhi melalui siri persamaan untuk pembezaan tak lurus yang digabungkan untuk enam gerakan darjah kebebasan. Bagi mewakili interaksi tak lurus antara pelantar-penambat, matriks 6×6 kekakuan tambatan telah dihasilkan berdasarkan kekakuan penambat dan koordinat pengawal tali yang diukur secara relatif pada pusat graviti bagi struktur tersebut. Untuk penilaian pergerakan secara melintang pada frekuensi rendah bagi sesebuah pelantar, siri daya gelombang darjah kedua yang dihasilkan daripada pecutan sementara darjah kedua dan pergerakan struktur darjah pertama telah dirumuskan. Untuk penilaian interaksi antara bendalir-penambat dan penambat-dasar laut, satu pendekatan yang merupakan sebagai penentu untuk analisis dinamik bagi tali tambatan pelbagai komponen telah dirumuskan. Tindak balas pergerakan apungan telah dianggap sebagai keadaan batasan atas untuk tali tambatan. Kaedah Parameter Tergumpal telah digunakan sebagai pemodelan tali tambatan. Interaksi tak lurus antara penambat-dasar laut telah dimodelkan dengan menganggap tali tambatan diletakkan pada landasan disipatif elastik. Satu kaedah analisis berangka dinamik secara domain masa telah dihasilkan dan hasil kajian terhadap tali tambatan yang dipasang pada jenis tanah yang berbeza telah disahkan dengan melakukan satu kajian perbandingan terhadap hasil kajian yang telah

diterbitkan. Sumbangan ciri-ciri tanah dasar laut terhadap tindakan dinamik bagi tali tambatan telah dikaji untuk beberapa jenis tanah.

Dua fasa eksperimen telah dilakukan bagi mendapatkan data untuk digunakan sebagai pengesahan kaedah berangka. Bagi fasa pertama, kajian tentang prestasi struktur terhadap keadaan sekeliling bagi separuh tenggelam yang dilengkapi dengan lapan tiang bulat telah dilakukan. Model tersebut telah dibina dengan skala 1:100 dengan menggunakan perumpamaan Hukum Froud. Kajian tersebut telah dijalankan terhadap hulu, alur-alur, dan juga laut-laut penyukuan. Bagi fasa kedua, sebuah model semi-submersible yang dilengkapi dengan enam tiang bulat telah dihasilkan dengan menggunakan skala yang sama seperti model yang pertama. Sistem lurus jisim-spring telah disusun bagi memudahkan aktiviti mengukur kekuatan layangan secara melintang. Ujian susut bebas telah digunakan untuk mengkaji maklumat tentang tempoh masa semulajadi bagi sesebuah sistem, peredaman air yang statik, peredaman kelikatan tidak linear, faktor seretan, dan faktor inersia. Ujian Ketahanan Laut telah dilakukan ke atas orientasi model untuk hulu dan alur laut. Daya-daya hanyut yang telah diukur akan dibandingkan dengan formula sedia ada untuk menggunakan kaedah separuh empirik sedia ada bagi menilai daya-daya ini. Bagi kedua-dua fasa eksperimen, separuh tenggelam konvensional yang dilengkapi dengan dwi-badan kapal telah diambil kira. Dengan membandingkan hasil kajian antara model berangka dan model eksperimen, keberkesanan kaedah berangka telah dapat dibuktikan.

Berdasarkan algoritma berangka yang telah disahkan, beberapa kajian berparameter telah dilakukan untuk mengkaji penyumbangan beberapa parameter terhadap ciri-ciri dinamik bagi bertambatan separuh tenggelam. Kesan - kesan pra-tegangan, susunan tali tambatan, berat pasak, unit berat kabel, pemanjangan, kekuatan pemutusan, dan sudut pra-tegangan terhadap sifat tali tambatan pelbagai komponen, telah dikaji dengan menggunakan penyelesaian iteratif implisit dari persamaan katenari. Selain daripada itu, sumbangan muatan pelantar, dimensi pelantar, bilangan tiang, bilangan tali tambatan, model matematik bagi model sekeliling, ciri-ciri gelombang dan keadaan (keutuhan dan kerosakan) operasi terhadap tindak balas bertambatan separuh tenggelam telah dikaji dengan menggunakan analisa domain frekuensi lurus.

Hasil kajian melalui eksperimen dan hasil kajian yang telah diterbitkan mengesahkan bahawa model berangka yang telah dibangunkan adalah efisien untuk meramal frekuensi ombak dan frekuensi rendah pergerakan dan tindakbalas tegangan dinamik penambat bagi separuh tenggelam. Lebih-lebih lagi, hasil kajian melalui eksperimen menunjukkan perlunya model kekukuhan sistem penambat, model khas atau hibrid bagi sistem penambat dan pemasangan adalah perlu untuk penilaian yang kritikal bagi kerosakan sistem penambatan.

In compliance with the terms of the Copyright Act 1987 and the IP Policy of the university, the copyright of this thesis has been reassigned by the author to the legal entity of the university,

Institute of Technology PETRONAS Sdn Bhd.

Due acknowledgement shall always be made of the use of any material contained in, or derived from, this thesis.

© YASSIR MOHAMMEDNOUR ELFADUL ABBAS, 2011
Institute of Technology PETRONAS Sdn Bhd
All rights reserved.

ACKNOWLEDGEMENTS

Thanks and Praises to Allah before and after, under Whose provision and blessing this work was carried out. I would like to express my sincere thanks to my study advisor Prof. Kurian V. John for his guidance, inspiration and encouragement throughout the study. Special thanks extend to Dr. Indra Sati Hamonangan Harahap, my co-advisor, for giving valuable suggestions.

The assistance of the Universiti Teknologi PETRONAS staff, particularly the Civil Engineering staff and the offshore laboratory technicians, is gratefully acknowledged. The financial support for this study was provided by the PETRONAS Carigali Sdn Bhd and the Institute of Technology PETRONAS Sdn Bhd. Furthermore, I am grateful for the grant given by the Sudan University for Science and Technology. Through all the trials and challenges, I have faced over this study; I would thank everyone who contributed keeping me patient to overcome these tackles specially my UTP supportive colleagues.

DEDICATION

To my father and mother

To my wife and daughter

To my brothers and sisters

To my family members

To my friends

TABLE OF CONTENTS

Abstract	v
Abstrak	vii
Acknowledgements	xi
Dedication	xii
Table of Contents	xiii
List of figures	xvii
List of tables	xxi
List of Abbreviations	xxii
Nomenclature	xxiii
CHAPTER 1 INTRODUCTION	1
1.1 Chapter overview	1
1.2 Development of offshore platforms	1
1.3 Floating platform systems	5
1.3.1 Semi submersible platforms	7
1.3.2 Station-keeping systems	8
1.4 Problem statement	9
1.5 Objectives of the study	11
1.6 Scope of the study	11
1.7 Overview of the thesis	12
1.8 Chapter Summary	13
CHAPTER 2 LITERATURE REVIEW	15
2.1 Chapter overview	15
2.2 Reported studies	15
2.2.1 Wave frequency responses	16
2.2.2 Low frequency responses	18
2.2.3 Responses to extreme environmental conditions	21
2.2.4 Addition of heave plates	25
2.2.5 Innovation semi submersibles	27
2.2.6 Station-keeping systems	31
2.2.6.1 Mooring to seabed interactions	39
2.3 Critical literature review	41
2.3.1 Wave frequency responses	41
2.3.2 Low frequency response	41
2.3.3 Responses to extreme environmental conditions	43
2.3.4 Addition of heave plates	43

2.3.5 Innovation semi submersibles	44
2.3.6 Station-keeping systems	44
2.3.6.1 Mooring to seabed interactions	47
2.4 Chapter Summary	48
CHAPTER 3 WAVE TO WAVE AND WAVE TO PLATFORM INTERACTIONS	51
3.1 Chapter overview	51
3.2 Hydrostatic analysis of floating structures	51
3.3 Hydrodynamic theory	52
3.3.1 Nonlinear boundary value problem	53
3.3.2 The conventional solution for the NBVP	56
3.3.2.1 Linear Airy wave theory	57
3.3.3 Mathematical spectrum models	58
3.3.3.1 Pierson-Moskowiz spectrum	59
3.3.3.2 The JONSWAP spectrum model	59
3.4 Wave force on semi submersibles	60
3.4.1 The force (Morison) equation	60
3.4.2 First order wave frequency forces	61
3.4.3 Second order low frequency forces	63
3.4.3.1 Integration of the force equation	64
3.5 Chapter summary	67
CHAPTER 4 ANALYSIS OF MOORING LINES	69
4.1 Chapter overview	69
4.2 Quasi-static analysis	69
4.2.1 Catenary equations	70
4.2.2 Multi-component mooring lines analysis	72
4.2.2.1 Initial configuration	73
4.2.2.2 Nonlinear force-excursion relationship for negative horizontal excursions	75
4.3 Hydrodynamic analysis	77
4.3.1 Problem definition	77
4.3.2 Algorithm	78
4.3.3 Mooring to seabed interactions	82
4.3.4 Solution procedure	83
4.3.5 Upper-end boundary condition	90
4.3.6 Programming aspects	90
4.4 Chapter summary	92
CHAPTER 5 DYNAMIC ANALYSIS OF PLATFORM	95
5.1 Chapter overview	95
5.2 Frequency domain analysis	95
5.2.1 Equation of motion	96
5.2.2 Force LTFs	97
5.2.3 Hydrodynamic force coefficients	99

5.2.4 Programming aspects.....	101
5.3 Time domain analysis	102
5.3.1 Co-ordinate systems	103
5.3.2 First order analysis	103
5.3.2.1 Structure physical mass matrix	105
5.3.2.2 Added mass matrix.....	105
5.3.2.3 Hydrostatic stiffness matrix.....	107
5.3.2.4 Mooring system stiffness matrix	108
5.3.3 Low frequency second order analysis	109
5.3.4 Ramp function.....	110
5.3.5 Programming aspects.....	111
5.4 Chapter summary	114
CHAPTER 6 EXPERIMENTAL TESTS	115
6.1 Chapter overview	115
6.2 Test facility and instrumentations.....	115
6.3 Choice of the scale and physical modelling law.....	120
6.4 The semi submersible-A tests.....	123
6.4.1 General.....	123
6.4.2 Model description.....	123
6.4.3 Mooring system.....	125
6.4.4 Seakeeping tests	127
6.5 The semi submersible-B tests	130
6.5.1 General.....	130
6.5.2 Model description.....	131
6.5.3 Laboratory tests.....	133
6.5.3.1 Model hydrostatic data tests	133
6.5.3.2 Static offset test.....	134
6.5.3.3 Free vibration tests	134
6.5.3.4 Seakeeping tests.....	136
6.6 Chapter summary	141
CHAPTER 7 RESULTS AND DISCUSSION	143
7.1 Chapter overview	143
7.2 Parametric study on deepwater mooring lines (Numerical results).....	143
7.2.1 Pretension effect.....	144
7.2.2 Mooring line configuration effect	145
7.2.3 Clump weight effect	146
7.2.4 Cable unit weight effect.....	147
7.2.5 Elongation (Cable axial stiffness) effect	148
7.2.6 Pretension angle effect.....	149
7.3 Dynamic analysis of mooring lines (numerical and validation results).....	150
7.4 Wave frequency responses (numerical vs. experimental results).....	161
7.4.1 Low frequency responses (experimental vs. numerical)	168
7.4.1.1 Static-offset test (experimental results).....	168
7.4.1.2 The free-decay test (numerical vs. experimental results)	169
7.4.1.3 Seakeeping tests (numerical vs. experimental results)	170
7.4.2 Mooring damage conditions (experimental results).....	178

7.5 Case studies (Numerical results).....	181
7.6 Chapter summary.....	208
CHAPTER 8 CONCLUSION.....	209
8.1 Conclusions.....	209
8.1.1 Wave frequency motion analysis.....	210
8.1.2 Second order motion analysis model.....	211
8.1.3 Consequences following mooring line damage.....	211
8.1.4 The hydrodynamic mooring analysis and the seabed-line interactions	211
8.1.5 Investigations on the moored semi submersible design parameter	212
8.2 Future studies	213
REFERENCES.....	214
APPENDIX A EVALUATION OF FIRST ORDER WAVE FORCES.....	226
APPENDIX B BEYROT METHOD FOR MOORING LINES QUASI-STATIC ANALYSIS.....	237
PUBLICATIONS LIST.....	243

LIST OF FIGURES

Fig 1.1: Progression of fixed platforms in the GOM - depths in meters	3
Fig 1.2: Ultra-deepwater (> 1524m) wells drilled in the GOM	3
Fig 1.3: Troll A gas platform, world's tallest concrete structure	5
Fig 1.4: Deepwater systems	6
Fig 1.5: Typical semi submersible offshore platform.....	8
Fig 3.1: Structure Keel, CG, CB and MC definition	52
Fig 3.2: Schematic diagram for a progressive wave train.....	57
Fig 3.3: PM vs. JONSWAP wave spectrum.....	60
Fig 3.4: Velocity of an element along the i^{th} column arising from rotational motions	62
Fig 3.5: The numbering system for the semi submersible	63
Fig 4.1: Freely hanging cable segment in static equilibrium	70
Fig 4.2: Multi-component mooring line.....	72
Fig 4.3: Flow chart for the evaluation of a multi-component mooring line initial configuration	74
Fig 4.4: Flow chart for the evaluation of the nonlinear force-excursion relationship for a multi-component mooring line.....	76
Fig 4.5: Multi-component mooring line Lumped mass model.....	78
Fig 4.6: Flow chart for a multi-component mooring line hydrodynamic analysis.....	92
Fig 5.1: Fitted vs. measured results for drag coefficient (smooth cylinder in waves)	100
Fig 5.2: Fitted vs.measured results for inertia coefficient (smooth cylinder in waves)	101
Fig 5.3: Flow chart for the frequency domain analysis	102
Fig 5.4: Platform's motion and mooring model definitions.....	103
Fig 5.5: Flow chart for the linear dynamic analysis	112
Fig 5.6: Flow chart for the nonlinear dynamic analysis.....	113
Fig 5.7: Solution convergence curve related to Fig. 5.6	114
Fig 6.1: UTP wave basin.....	117
Fig 6.2: UTP basin wave maker system.....	118
Fig 6.3: Plan of the semi submersible-A model	124
Fig 6.4: Section 1 of the semi submersible-A model.....	125
Fig 6.5: The semi submersible-A model prior tests.....	125
Fig 6.6: Single mooring line configuration (Semi submersible-A)	126
Fig 6.7: Mooring system setup plan (Semi submersible-A)	127
Fig 6.8: Seakeeping test setup for head seas (Semi submersible-A)	128
Fig 6.9: Seakeeping test setup for beam seas (Semi submersible-A).....	128
Fig 6.10: Seakeeping test setup for quartering seas (Semi submersible-A).....	129
Fig 6.11: Plan of the semi submersible-B model	132
Fig 6.12: Section 1 of the semi submersible-B model.....	132
Fig 6.13: The semi submersible-B model during tests	132
Fig 6.14: Restraining system (semi submersible-B).....	134
Fig 6.15: Plan of the seakeeping tests setup (semi submersible-B).....	138
Fig 6.16: Section 1 of the seakeeping tests setup (semi submersible-B).....	138
Fig 7.1: Effect of the initial pretension on the mooring tension.....	145

Fig 7.2: Effect of the mooring configuration on the fairlead vertical tension	146
Fig 7.3: Effect of the clump weight on the fairlead vertical tension.....	147
Fig 7.4: Effect of the cable unit weight on the fairlead vertical tension	148
Fig 7.5: Effect of the elongation on the fairlead horizontal tension.....	149
Fig 7.6: Effect of pretension angle on the mooring line stiffness	150
Fig 7.7: Seabed Soils Vertical reaction per line embedment.....	151
Fig 7.8: Mooring No 1 initial configuration	152
Fig 7.9: Mooring No 2 initial configuration	152
Fig 7.10: Mooring No 3 initial configuration	152
Fig 7.11: Frequency response of mooring line No.1 upper end dynamic tension	154
Fig 7.12: Frequency response of mooring line No.2 upper end dynamic tension	154
Fig 7.13: Mooring line No.2 upper end horizontal dynamic tension time history....	155
Fig 7.14: Mooring line No.2 upper end vertical dynamic tension time history.....	156
Fig 7.15: Mooring line No.1 dynamic configuration	156
Fig 7.16: Mooring line No.2 dynamic configuration	157
Fig 7.17: Mooring line No.3 dynamic configuration	157
Fig 7.18: A MCML with distributed clump weight	158
Fig 7.19: Soil contribution to the horizontal dynamic restoring forces (Mooring No. 4)	159
Fig 7.20: Soil contribution to the vertical dynamic restoring forces (Mooring No. 4)	159
Fig 7.21: Soil damping contribution to the horizontal dynamic tension	160
Fig 7.22: Soil damping contribution to the vertical dynamic tension	161
Fig 7.23: Surge response to regular sea wave ($H = 6$ m, $\omega = 0.314$ rad/s).....	162
Fig 7.24: Heave response for regular sea wave ($H = 6$ m, $\omega = 0.314$ rad/s)	162
Fig 7.25: Pitch response to regular sea wave ($H = 6$ m, $\omega = 0.314$ rad/s).....	163
Fig 7.26: Surge RAO to head seas	164
Fig 7.27: Heave RAO to head seas	164
Fig 7.28: Pitch RAO to head seas	165
Fig 7.29: Surge RAO to quartering seas.....	165
Fig 7.30: Heave RAO to quartering seas.....	166
Fig 7.31: Pitch RAO to quartering seas.....	166
Fig 7.32: Sway RAO to beam seas.....	167
Fig 7.33: Heave RAO to beam seas	167
Fig 7.34: Roll RAO to beam seas.....	168
Fig 7.35: Static offset test results with linear and nonlinear data fitting.....	169
Fig 7.36: Simulation of surge free-decay test	170
Fig 7.37: Simulation of sway free-decay test.....	170
Fig 7.38: Drift force comparisons-head seas	171
Fig 7.39: Drift force comparisons-beam seas	172
Fig 7.40: Drift coefficient comparisons-head seas.....	173
Fig 7.41: Drift coefficient comparisons-beam seas.....	173
Fig 7.42: Surge response PSD to HRW1.....	174
Fig 7.43: Surge response PSD to HRW2.....	174
Fig 7.44: Surge response PSD spectrum to HRW3.....	175
Fig 7.45: Sway response PSD to BRW1	175
Fig 7.46: Sway response PSD to BRW2	176
Fig 7.47: Sway response PSD to BRW3	176
Fig 7.48: Comparisons of surge RA to HBC 1~8	177

Fig 7.49: Comparisons of sway RA to BBC 1~8	177
Fig 7.50: Effect of M_1 failure to MRW1 on platform the surge response	178
Fig 7.51: Effect of M_2 failure to MRW2 on platform the surge response	179
Fig 7.52: LC1 reading for M1 failure to MRW1	180
Fig 7.53: LC2 reading for M1 failure to MRW1	180
Fig 7.54: LC1 reading for M2 failure to MRW2	181
Fig 7.55: LC2 reading for M2 failure to MRW2	181
Fig 7.56: Plan of the dimensions related to Table 7.8	182
Fig 7.57: Section 1 of the dimensions related to Table 7.8	182
Fig 7.58: Force-excursion relationship for single line (All cases except a_1)	184
Fig 7.59: Force-excursion relationship for single line (Case a_1)	185
Fig 7.60: Nonlinear mathematical model representing force-excursion relationship for single line (All cases except a_1)	185
Fig 7.61: Nonlinear mathematical model representing force-excursion relationship for single line (Case a_1)	186
Fig 7.62: Force-excursion relationship for single line (Comparisons)	186
Fig 7.63: Mooring system configuration (All cases except a_4 and a_6)	187
Fig 7.64: Mooring system configuration (Case a_4)	187
Fig 7.65: Mooring system configuration post-damage (Case a_6)	188
Fig 7.66: Mooring system restoring force-excursion relation (X-axis)	188
Fig 7.67: Nonlinear X-axis spring mathematical model (case a_1)	189
Fig 7.68: Nonlinear X-axis spring mathematical model (case a_4)	189
Fig 7.69: Nonlinear X-axis spring mathematical model (case a_6)	190
Fig 7.70: Nonlinear X-axis spring mathematical model (All except a_1 , a_4 and a_6) ...	190
Fig 7.71: Mooring system restoring force-excursion relation (Y-axis)	191
Fig 7.72: Nonlinear Y-axis spring mathematical model (case a_1)	191
Fig 7.73: Nonlinear Y-axis spring mathematical model (case a_4)	192
Fig 7.74: Nonlinear Y-axis spring mathematical model (case a_6)	192
Fig 7.75: Nonlinear Y-axis spring mathematical model (All except a_1 , a_4 and a_6) ...	193
Fig 7.76: Nonlinear mathematical model representing force-negative excursion relationship for single line (All cases except a_1)	193
Fig 7.77: Nonlinear mathematical model representing force-positive excursion relationship for single line (All cases except a_1)	194
Fig 7.78: Nonlinear mathematical model representing force-negative excursion relationship for single line (Case a_1)	194
Fig 7.79: Nonlinear mathematical model representing force-positive excursion relationship for single line (Case a_1)	195
Fig 7.80: Surge response time trace to head bi-chromatic wave given in Table 7.9.	196
Fig 7.81: mooring tension response time traces to head bi-chromatic wave given in Table 7.9	196
Fig 7.82: Comparison for motion amplitudes between case a_0 and b	197
Fig 7.83: Comparison for M#1 tension amplitudes between case a_0 and b	197
Fig 7.84: Comparison for motion amplitudes between case a_0 and b	198
Fig 7.85: Comparison for M#1 tension amplitudes between case a_0 and b	198
Fig 7.86: Comparison for motion amplitudes between case a_0 and d	199
Fig 7.87: Comparison for M#1 tension amplitudes between case a_0 and d	199
Fig 7.88: Comparison for motion amplitudes between case a_0 and e	200
Fig 7.89: Comparison for M#1 tension amplitudes between case a_0 and e	200
Fig 7.90: Comparison for motion amplitudes between case a_0 and f	201

Fig 7.91: Comparison for M#1 tension amplitudes between case a_0 and f	201
Fig 7.92: Comparison for motion amplitudes between case a_0 and g	202
Fig 7.93: Comparison for M#1 tension amplitudes between case a_0 and g.....	202
Fig 7.94: Comparison for motion amplitudes between case a_0 and h	203
Fig 7.95: Comparison for M#1 tension amplitudes between case a_0 and h.....	203
Fig 7.96: Comparison between case a_0 , i_1 and i_2 for surge amplitudes	204
Fig 7.97: Comparison between case a_0 , i_1 and i_2 for sway amplitudes.....	204
Fig 7.98: Comparison between a_0 , a_1 and a_2 cases for surge amplitudes	205
Fig 7.99: Comparison between a_0 , a_1 and a_2 cases for sway amplitudes	205
Fig 7.100: Comparison between a_0 , a_3 and a_4 cases for surge amplitudes.....	206
Fig 7.101: Comparison between a_0 , a_3 and a_4 cases for sway amplitudes	206
Fig 7.102: Comparison between a_0 , a_5 and a_6 cases for surge amplitudes.....	207
Fig 7.103: Comparison between a_0 , a_5 and a_6 cases for sway amplitudes.....	207

LIST OF TABLES

Table 1.1: Floating systems as of 2002.....	7
Table 2.1: Typical natural periods of semi submersibles.....	42
Table 3.1: Second order wave force components.....	64
Table 6.1: Specification of the wave maker system	116
Table 6.2: Model to prototype multipliers	122
Table 6.3: The semi submersible-A data (Scale 1:100).....	124
Table 6.4: Multi-component mooring line properties.....	126
Table 6.5: The semi submersible-B data (full scale)	131
Table 6.6: Regular waves for head seas (semi submersible-B).....	139
Table 6.7: Regular waves for beam seas (semi submersible-B).....	140
Table 6.8: Bi-chromatic waves for head and beam seas (semi submersible-B).....	140
Table 6.9: Random waves for head seas (semi submersible-B).....	141
Table 6.10: Random waves for beam seas (semi submersible-B).....	141
Table 6.11: Regular waves for line failure study (semi submersible-B)	141
Table 6.12: Random waves for line failure study (semi submersible-B)	141
Table 7.1: Basic data for a multi-component mooring line analysis.	144
Table 7.2: Sea bed soils data	150
Table 7.3: General data used to analyze Mooring lines No. 1-3	152
Table 7.4: Particulars of chain used in Mooring No. 1, 2 & 3	152
Table 7.5: Mooring line tensions.....	153
Table 7.6: Mooring No 4 Initial configuration data	158
Table 7.7: Single-compnet mooring data	182
Table 7.8: Case studies general data.....	183
Table 7.9: Bi-chromatic wave data for case a ₀	195

LIST OF ABBREVIATIONS

CB	Center of buoyancy
CG	Center of gravity
DOF	Degree of freedom
EOM	Equation of motion
FE	Finite element
GOM	Gulf of Mexico
LMM	Lumped mass method
LHS	Left hand side
LTF	Linear transfer function
MC	Metacenter
MODU	Mobile offshore drilling unit
MWL	Mean water level
RAO	Response amplitude operator
RHS	Right hand side

NOMENCLATURE

<i>Symbol</i>	<i>Definition</i>
A_{r_x}, A_{r_z}	Projected area of the concentrated attachments in x and z directions respectively
A_x, A_z	Upper end motion amplitudes in x and z directions respectively
$B^{(0)}, B^{(1)}, B^{(2)}$	Still water (linear) damping, wave (linear) damping and viscous (nonlinear) damping respectively
$C_A(\omega)$	Frequency dependant added mass coefficient ($= C_M(\omega) - 1$)
C_{A_x}, C_{A_z}	Added mass coefficients of the concentrated attachments in x and z directions respectively
C_A, C_d, C_m	Added mass, drag force and inertia force coefficients respectively
C_{D_n}, C_{D_t}	Added mass coefficients of the mooring line in normal and tangential local directions respectively
C_{D_x}, C_{D_z}	Fluid drag coefficients of the concentrated attachments in x and z directions respectively
$C_M(\omega)$	Frequency dependant inertia force coefficient
$D, D_{j-1/2}$	Diameter of cylinder, cable element $j - 1/2$
E, A	Cable tangent modulus of elasticity and cross-sectional area respectively
$\tilde{E}_j, \tilde{F}_j, \tilde{G}_j$	Coefficient functions for the tension correction equations
$F_{A_x j}, F_{A_z j}$	The added mass force raised on node j in x and z directions respectively
F_{n_j}, F_{t_j}	Fluid drag force of the mooring line in normal and tangential local directions respectively lumped on node j
$F_{P_x hull 1,2}$	The resultant force applied on hull faces (face 1, 2, 3 & 4, see Fig 3.5) due to undisturbed wave dynamic pressure
$F_{P_y hull 1,2}$	The total sway (y-component) force of inertia and drag on the hulls
$F_{z hull 1,2}$	The total heave (z-component) force of inertia and drag on the hulls
F_{x_j}, F_{z_j}	Total external force applied on node j in x and z directions respectively
$F_{x_t}, F_{y_t}, F_{z_t}$	The total horizontal surge (x-axis) force, total sway (y-axis) force and the total vertical heave (z-axis) force respectively
GM_r, GM_p	Metacentric height for roll and pitch
H, L_w, T_w	Height, length and period of the incident wave respectively
H_s	Significant wave height
I	The first suspended node of the mooring line
I_A	Water plane area moment of inertia
$L_{j-1/2}$	Unreformed length of element $j - 1/2$

L_{ch_0}, L_{ch}	The original and instantaneous chord length of a mooring line
L, L_u	The stressed and the unstressed (original) cable length respectively
L_p	Length of the lower hull
$M_{A_j}, M_{A_n_j}$	The equivalent added mass of $j-1/2$ and $j+1/2$ mooring elements in normal and tangential local directions respectively, lumped on node j
$M_{Ax_{att_j}}, M_{Az_{att_j}}$	Added mass of the concentrated attachments at node j in x and z directions respectively
M_{I_i}, M_{D_i}	The moments of the horizontal inertia and drag forces on the column i about an axis perpendicular to the wave direction
M_{att_j}	Submerged mass of the concentrated attachments at node j
$M_{xhull_{1,2}}$	The moments of the horizontal inertia and drag forces on the hulls about x-axis
$M_{xvhull_{1,2}}$	The moments of the vertical inertia and drag forces on the hulls about x-axis
M_{y_p}	The moments of the dynamic pressure on the hull faces about y- axis
$M_{x_t}, M_{y_t}, M_{z_t}$	The total roll moments (about x-axis), the total pitch moments (about y-axis), the total yaw moments (about z-axis) respectively
$\bar{M}_{x_j}, \bar{M}_{z_j}$	Virtual mass for node j (include the lumped submerged mass and submerged/ added mass of the concentrated attachments) in x and z directions respectively
$M_{zhull_{1,2}}$	The moments of the horizontal inertia and drag forces on the hulls about z-axis
M_j	The equivalent submerged mass of $j-1/2$ and $j+1/2$ mooring elements lumped on node j
N_q, N_c, N_γ	Bearing capacity coefficients of the soil underlying the mooring line
$P_{n_{1j-1/2}}, P_{t_{1j-1/2}}$	Fluid drag force per unit length on element $j-1/2$ near end, in normal and tangential local directions respectively
$P_{n_{2j-1/2}}, P_{t_{2j-1/2}}$	Fluid drag force per unit length on element $j-1/2$ far end, in normal and tangential local directions respectively
T, T_o	The initial and the increased average line tension respectively
$T_{j-1/2}$	Axial dynamic tension on element $j-1/2$
T_n	Natural period of oscillation
\bar{T}_N	Non-dimensional dynamic tension at the upper end of mooring line
V_{att_j}	Volume of the concentrated attachments at node j
W_{att_j}	Submerged weight of the concentrated attachments at

	node j
W_j	Equivalent submerged weight of $j-1/2$ and $j+1/2$ mooring elements lumped on node j
X_A, Y_A, Z_A	Coordinates of mooring anchor relative to the global system
X_f, Y_f, Z_f	Coordinates of the instantaneous mooring fairlead relative to the global system
$X_{f_o}, Y_{f_o}, Z_{f_o}$	Coordinates of the original mooring fairlead relative to the global system
X_g, Y_g, Z_g	Coordinates of the structure CG relative to global system
X_j, Z_j	Co-ordinates of node j in x and z directions respectively
$Y_{c_{ih}}$	The moment lever arm of column i , for moments about z -axis (see Fig 3.5 for $i=7$).
a, f, k	The amplitude, cyclic frequency and number ($= 2\pi/L$) of the incident wave respectively
c_j	Current velocity at node j
c	Cohesion of the soil underlying the mooring line
d	Upper end height above sea level at the mooring initial configuration
d_w	Water depth
$f_{n_{1j-1/2}}, f_{t_{1j-1/2}}$	Fluid drag force on element $j-1/2$ near end, in normal and tangential local directions respectively
f_{x_j}, f_{z_j}	Fluid drag force lumped on node j in x and z directions respectively
$f_{x_{att_j}}, f_{z_{att_j}}$	Fluid drag force on attachment at node j in x and z directions respectively
$f_{z_{soil}}$	Soil reactive force at node j in z direction
$\bar{f}_{x_j}, \bar{f}_{z_j}$	Virtual external force node j (include the fluid drag force of line/attachment, weight of line attachment and soil reactive force) in x and z directions respectively
g	Gravitational acceleration
h	Draft
k	System spring constant
k_{soil}	Stiffness of the soil underlying the mooring line
m	Structure physical mass
$m_{j-1/2}$	Submerged mass per unit length of element $j-1/2$
n	The platform surface direction normal vector, which is pointing outward.
q, q_u	Soil overburden pressure at the mooring line level of embedment and the ultimate bearing capacity at of the soil underlying the mooring line respectively

$r_{n1\ j-1/2}, r_{t1\ j-1/2}$	Relative velocity on element $j-1/2$ near end, in normal and tangential local directions respectively
$r_{n1\ j-1/2}, r_{t1\ j-1/2}$	Relative velocity on element $j-1/2$ far end, in normal and tangential local directions respectively
r_{x_j}, r_{z_j}	Relative velocity at node j in x and z directions respectively
r_x, r_y, r_z	Radius of gyration for roll, pitch and yaw motions respectively
t	Time
u, v, w	Three components of a fluid particle velocity in a rectangular Cartesian (x, y, z) fixed on the MWL.
\dot{u}, \dot{v}	The fluid particle acceleration in x, y directions respectively.
w_o, w_t	Submerged unit weight of un-stretched and stretched cable respectively
x, y, z	Cartesian co-ordinate system used for the definition of the wave kinematics
x_j, z_j	Displacement of node j in x and z directions respectively
\dot{x}_j, \dot{z}_j	Velocity of node j in x and z directions respectively
\ddot{x}_j, \ddot{z}_j	Acceleration of node j in x and z directions respectively
$\ddot{x}_g, \dot{x}_g, x_g$	Acceleration, velocity and displacement of the structure CG respectively in the direction of the wave propagation
<i>Greeks</i>	
Δ	The displaced volume by the structure
ρ	Fluid mass density
$\eta(x, y, t)$ or η	The free surface position relative to z -axis.
ω	Circular frequency of the incident wave
$\ddot{\alpha}_g, \dot{\alpha}_g, \alpha_g$	Angular acceleration, velocity and displacement of the structure CG respectively
θ	Constant of the Wilson- θ time integration scheme
θ_t, θ_b	Line resultant tension angle with x -axis at top and bottom end respectively
$\theta_{j-1/2}$	Orientation angle of element $j-1/2$ (Angle of element $j-1/2$ with the positive x -axis measured counterclockwise)
$\bar{\theta}_j$	Average angle of node j (Angle of the tangent at node j with the positive x -axis measured counterclockwise)
$\sigma_{1_j}, \sigma_{2_j}, \sigma_{3_j}$	Functions used for defining the governing EOM of a multi-component mooring line
$\alpha_j, \beta_j, \gamma_j, \kappa_j, \mu_j, \psi_j$	Functions used to define governing EOM solution
$\delta T_{j-1/2}^{n+\theta\Delta t}$	Correction of the tension at element $j-1/2$
$\varepsilon_{j-1/2}^{n+\theta\Delta t}$	Element $j-1/2$ error function

ε	Coefficient of the upper end motion ramp function.
ϕ_w	The model orientation angle or the angle of the incident wave
φ_x, φ_z	Phase angle for the upper end motion in x and z directions respectively
ω_o	Peak circular frequency
ω_f	Frequency of the upper end motion respectively
$\bar{\omega}_f$	The non-dimensional frequency of the upper end motion
$\omega_{j-1/2}$	Submerged weight per unit length of element $j - 1/2$
ε_{soil}	Damping ratio of the soil underlying the mooring line
γ, ϕ	Mass density and internal friction angle of the soil underlying the mooring line respectively
Δt	Time step
ω_n	Frequency of oscillation corresponding to the natural frequency of the system
β	Phase (lagging) angle
ζ	Total damping to critical damping ratio
ξ	A non-dimensional perturbation parameter ($2a/L_w$)
Φ	The velocity potential function
$\Phi^{(n)}$	the n^{th} order solution for Φ
$\sum_{i=3}^{10}$	The summation over the corner columns (3 to 6) and the middle columns (7 to 10) as shown in Fig 3.5

Chapter 1

INTRODUCTION

1.1 Chapter overview

In view to the high demand for oil and gas, the industry has increased its activity into deep and ultradeep offshore fields. The offshore oil and gas industry was born near the coast of Louisiana off GOM in about 5m water depth in 1947. By 1974, the offshore production had increased to 14% of the global production, and in 2010 the global production had increased to 33% of the global production. At this development rate, it is anticipated that the major contribution will come from the offshore oil and gas industry soon. In this chapter, the historical development of offshore platforms is presented, with a special focus on floating platforms. The importance of semi submersible platforms and its station-keeping systems are discussed. Furthermore, the problem of this study is stated, followed by the study objectives and scope. Finally, a general overview of this thesis content is presented.

1.2 Development of offshore platforms

An offshore structure can be defined as a structure which has no fixed access to dry land and may be required to stay in a tolerable position in all weather conditions. Offshore structures may be fixed to the seabed or may be floating. Floating structures may be moored to the seabed, dynamically positioned by thrusters or may be allowed to drift freely. While the majority of the offshore structures support the exploration and production of oil and gas, other major structures, e.g. for harnessing the power from the sea, offshore bases, offshore airports are also coming into existence.

The offshore exploration of oil and gas dates back to the nineteenth century. The first offshore oil wells were drilled from extended piers into the waters of Pacific Ocean, at Summerland's, California in the 1890 (and offshore Baku, Azerbaijan in the Caspian Sea). However, the birth of the offshore industry is commonly considered to have taken place in 1947 when Kerr-McGee completed the first successful offshore well in the GOM in 4.6 m of water off Louisiana. The drilling derrick and draw works were supported on 11.6 m x 21.6 m wooden decked platform built on 61 cm pilings driven to a depth of 31.7 m. Since the installation of this first platform in the GOM over 60 years ago, the offshore industry has developed many innovative structures, both fixed and floating, placed in progressively deeper waters and in more challenging and hostile environments. By 1975, the water depth encountered by offshore structures had extended to 144 m. Within the next three years the water depth dramatically leapt twofold with the installation of COGNAC platform that was made up of three separate structures, one set on top of another at 312 m. COGNAC held the world record for water depth for a fixed structure from 1978 until 1991. Five fixed structures were built in water depths greater than 328 m in the 1990s. The deepest of these is the Shell Bullwinkle platform in 412 m installed in 1991. The progression of fixed structures into deeper waters up to 1988 is shown in Fig 1.1. Since 1947, more than 10,000 offshore platforms of various types and sizes have been constructed and installed worldwide. As of 1995, 30% of the world's production of crude came from offshore. Recently, new discoveries have been made in increasingly deeper waters. In 2003, 3% of the world's oil and gas supply came from deepwater (> 305m) offshore production. This is projected to grow to 10% in the next ten years. The bulk of the new oil will come from deep and ultra deepwater production from three offshore areas, known as the "Golden Triangle": the GOM, West Africa and Brazil. Fig 1.2 illustrates the recent growth in ultra-deepwater drilling in the GOM. Drilling activity is indicative of future production [1].

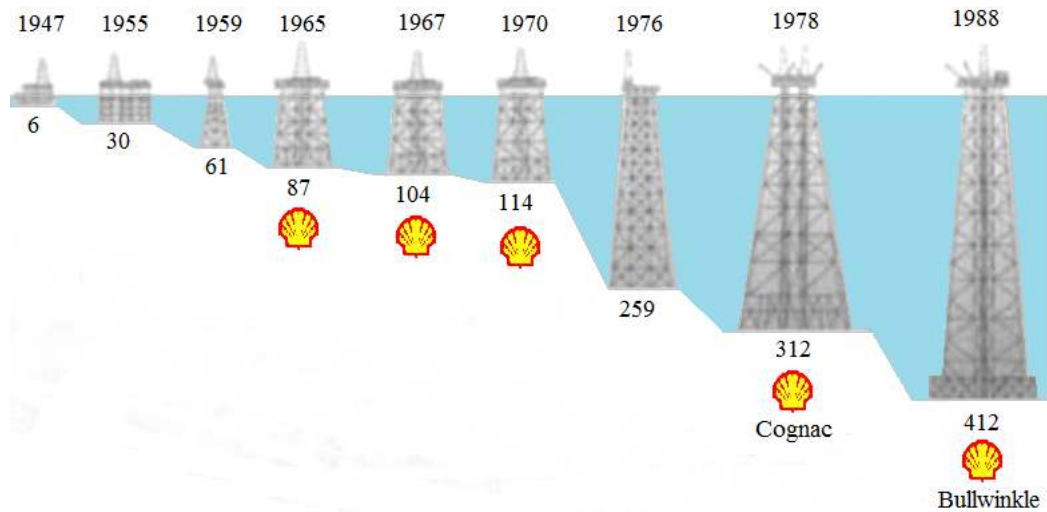


Fig 1.1: Progression of fixed platforms in the GOM - depths in meters
(Source: Handbook of offshore Eng., Chakrabarti, 2005)

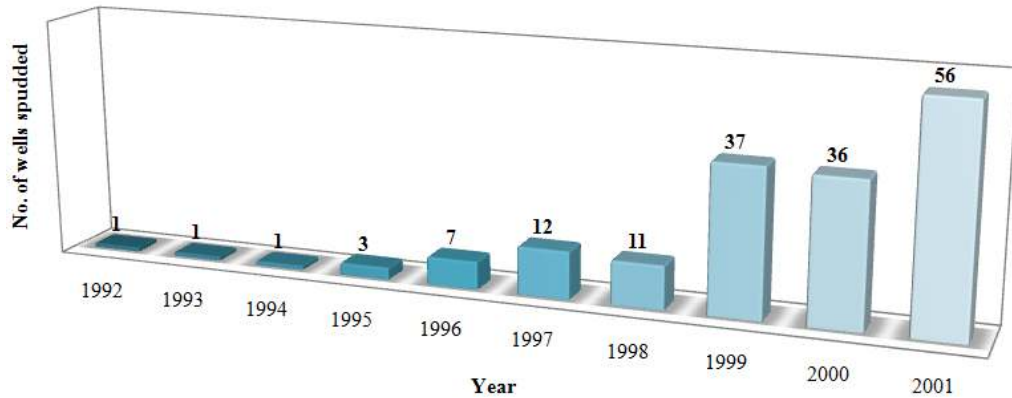


Fig 1.2: Ultra-deepwater (> 1524m) wells drilled in the GOM
(Source: Handbook of offshore Eng., Chakrabarti, 2005)

Fixed structures became increasingly expensive and difficult to install with increased water depths. An innovative and cheaper alternative to the fixed structure, namely, the Lena guyed tower was introduced in 1983. The platform was built in such a way that the upper truss structure could deflect with the wave and wind forces. Piles extending above the sea floor could bend, and horizontal mooring lines attached midway up to the platform could resist the largest hurricane loads. The Lena platform was installed in 305 m of water. Two more “compliant” towers were installed in the GOM in 1998: Amerada Hess Baldpate in 502 m and ChevronTexaco Petronius in 535 m. Petronius is the world’s tallest free standing structure.

Although nearly all of these platforms were of steel construction, around two dozen large concrete structures were installed in the very hostile waters of the North

Sea in the 1980 and early 1990 and several others offshore Brazil, Canada and the Philippines. Among these, the Troll A gas platform is the tallest concrete structure in existence as shown in Fig 1.3. It was installed offshore of Norway in 1996. Its total height is 369 m and it contains 245,000 m³ of concrete (equivalent to 215,000 home foundations). Gravity structures differ from other fixed structures in that they are held in place strictly by the weight contained in their base structures. The Troll platform, as shown in Fig 1.3 for example, penetrates 36 m into the seabed under its own weight.

Bottom-founded structures, with the notable exception of the Gravity Base Structures (GBS e.g. Condeeps), are typically constructed from welded steel tubular members. These members act as a truss supporting the weight of the processing equipment, and the environmental forces from waves, wind and current. Bottom-founded structures are called “fixed” when their lowest natural frequency of flexural motion is above the highest frequency of significant wave excitation. They behave as a rigid platform and are designed to resist the full dynamic forces of the environment. “Compliant” bottom-founded structures are usually designed so that their lowest natural frequency is below the energy in the waves. Waves, wind and current cause these structures to deflect, but the magnitude of the dynamic loads is greatly reduced. This allows economical bottom-founded structures to be designed for water depths, which would not be practical for fixed structures [1].

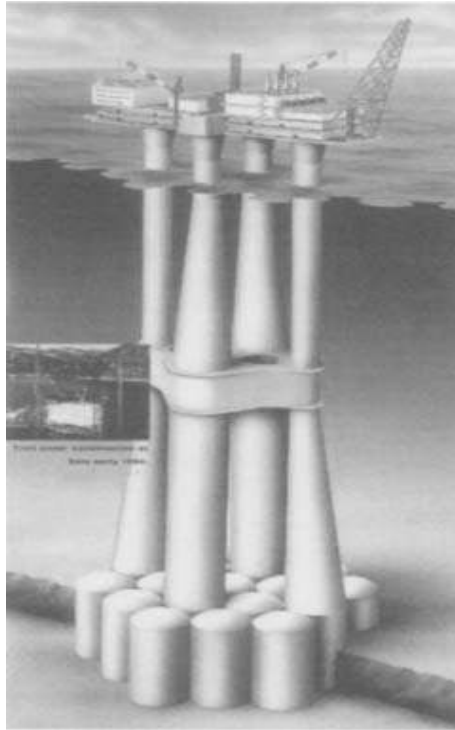


Fig 1.3: Troll A gas platform, world's tallest concrete structure
(Source: *Handbook of offshore Eng.*, Chakrabarti, 2005)

Another type of bottom-supported structure namely compliant tower behaves like a fixed structure in a mild environment. Such a structure is designed with the ability to behave both as a fixed and as a compliant structure. Compliancy is achieved using options such as taut wires connected to heavy chains on seabed or disconnectable pile connections. Thus, when the applied lateral wind, wave and current forces exceed the design limit, chains are lifted off the seabed or the pile connections are released, to turn the fixed structure into a rotationally compliant structure (i.e. from zero degrees of freedom to two degrees of freedom about the seabed).

1.3 Floating platform systems

The first floating production system, a converted semi submersible, was installed on the Argyle field by Hamilton in the UK North Sea in 1975. The first ship-shaped floating production and storage system was installed in 1977 by Shell International for the Castellon field, offshore Spain. There were 40 semi submersible floating production systems (FPSs) and 91 ship-shaped floating production and storage systems (FPSOs) in operation or under construction for deepwaters as of 2002. The

types of production concepts available for deepwater production are illustrated in Fig 1.4.

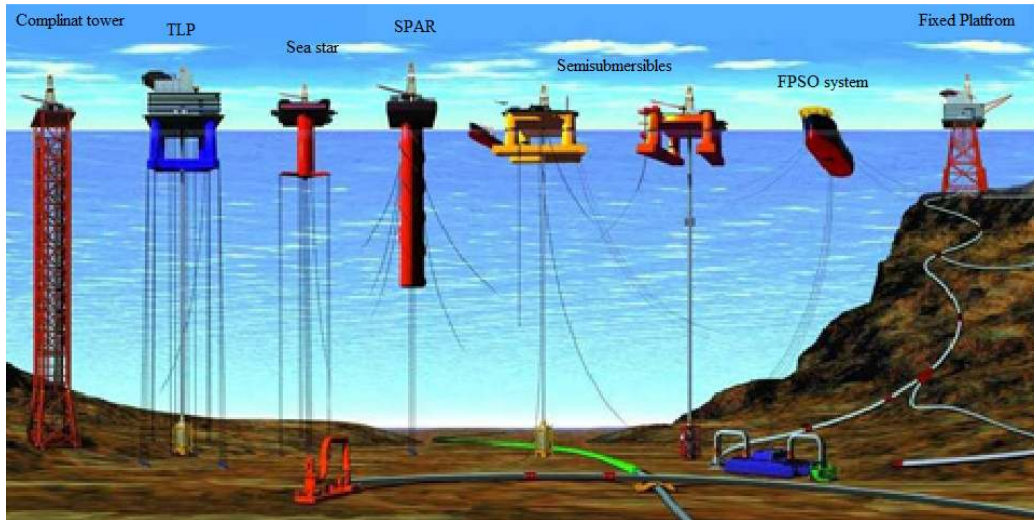


Fig 1.4: Deepwater systems

(Source: GOM national oceanic and atmospheric association, 2010)

Floating platforms generally have too much motion during extreme storms. A group of engineers in California invented a floating system in the early 1970s, which could be tethered to the sea floor, effectively making it a tethered compliant platform. This gave rise to what is called the Tension Leg Platform (TLP). The first commercial application of this technology, and the first dry tree completion from a floating platform, was the Conoco Hutton TLP installed in the UK sector of the North Sea in 1984. Dry trees are possible on a TLP because the platform is heave-restrained by vertical tendons, or tethers. This restraint limits the relative motion between the risers and the hull, which allows flow lines to remain connected in extreme weather conditions. The deep draft Spar platform is not heave-restrained, but its motions are sufficiently benign that risers can be supported by independent buoyancy cans, which are guided in the center well of the spar.

Floating structures have various degrees of compliancy. Neutrally buoyant structures, such as semi submersibles, spars and drill ships are dynamically unrestrained and are allowed to have six degrees of freedom (heave, surge, sway, pitch, roll and yaw). Positively buoyant structures, such as the Tension Leg Platforms (TLPs) and Tethered Buoyant Towers (TBTs) or Buoyant Leg Structures (BLS) are tethered to the seabed and are heave-restrained. All these of structures are structurally

rigid and compliancy is achieved using the mooring system. The sizing of floating structures is dominated by considerations of buoyancy and stability. Topside weight for these structures is more critical than it is for a bottom-founded structure. Semi submersibles and ship-shaped hulls rely on water plane area for stability. The centre of gravity is typically above the centre of buoyancy. The Spar platform is designed so that its centre of gravity is lower than its centre of buoyancy, making it intrinsically stable. Positively buoyant structures depend on a combination of water plane area and tether stiffness to achieve stability [1]. Floating platforms may be classified by their use as mobile drilling-type or production type. The number of units in these categories installed worldwide is shown in Table 1.1.

Table 1.1: Floating systems as of 2002
(Source: Handbook of offshore Eng., Chakrabarti, 2005)

Drilling			
Mobile Offshore Drilling Units (MODUs)		Semi submersibles	112
		Ship-shaped platforms	25
		Barges	12
Production			
Neutrally Buoyant	Floating Production Storage and Offloading Systems (FPSO)	Ship-shaped platforms	85
	Floating Storage and Offloading (FSO)	Barges	67
	Floating Production Systems (FPS)	Semi submersibles	41
		Spars	13
		Wellhead control buoys	2
Positively Buoyant	Conventional TLPs		19
	Mini-TLPS (TLPs and TLWPs)		7
Total			383

1.3.1 Semi submersible platforms

As indicated in Table 1.1, about 40% of the floating structures available worldwide up to 2003 are semi submersibles serving primarily as drilling and production systems. Semi submersibles are multi-legged floating structures with large deck. These legs are interconnected at the bottom with horizontal buoyant members called pontoons or underwater hulls. Some of the earlier semi submersibles resemble the ship form with twin pontoons having a bow and a stern. This configuration was considered desirable for relocating the unit from drilling one well to another either under its own power or

being towed by tugs. Early semi submersibles also included significant diagonal cross bracing to resist the prying and racking loads induced by waves [2]. Fig 1.5 shows typical conventional semi submersible.

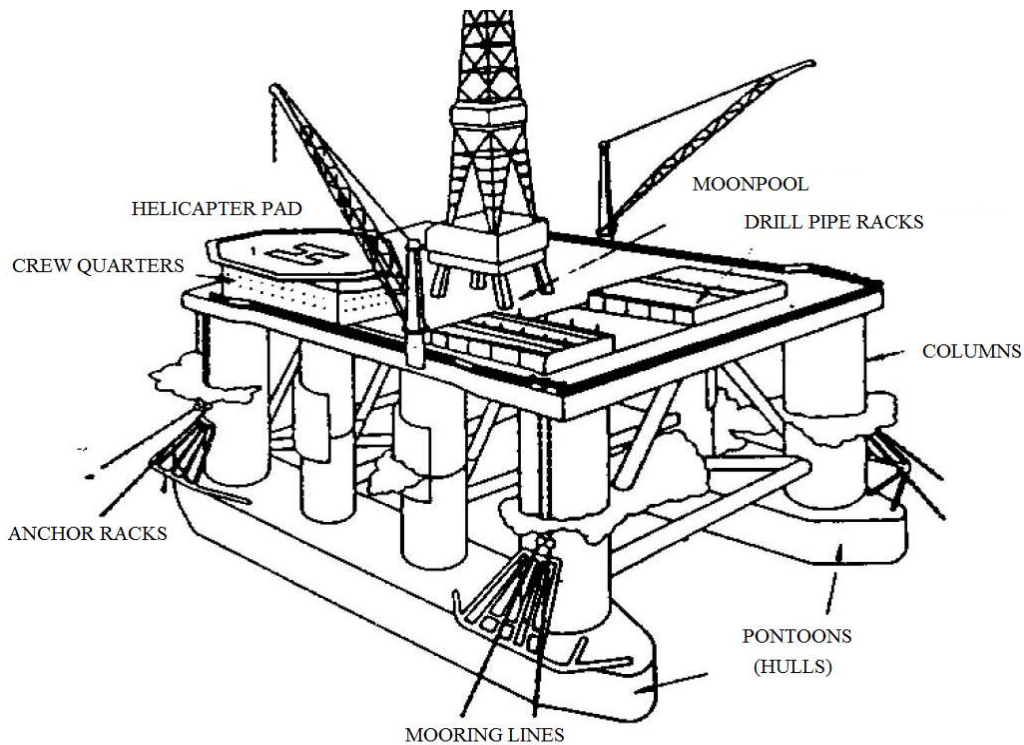


Fig 1.5: Typical semi submersible offshore platform
 (Source: Indomigas Oil and Gas-Indonesia, 2009)

1.3.2 Station-keeping systems

The station-keeping system for ships and other floating platforms can be achieved by spread mooring, single point mooring, turret mooring or dynamic positioning system. The spread mooring consists of multiple legs connected to the platform by fairleads and to seabed by the anchors. They are normally arranged in symmetrical pattern, attached to the bow and stern (in case of FPSOs). The single point mooring system consists of a circular floating buoy anchored to the seabed by means of four, six or eight chain legs draped radially in a catenary curve, the bottom ends of the chains fixed to the seabed by either conventional anchor legs or piles. Turret mooring system is an equipment designed and built to moor the structure in its location of operation. This system allows to weathervane so as to keep its bow head to the prevailing wind and current. On the other hand, the dynamic positioning system

consists of a position reference system, usually acoustic, coupled with computer-controlled thrusters around the platform to compensate current, wave and wind forces in a dynamic controlled mode to keep the platform on predetermined location and heading at sea. The dynamic positioning can be used as the sole source of station keeping or for assisting catenary mooring. Although dynamic positioning system offers greater mobility, conventional mooring has the advantage of being able to retain station-keeping ability in extreme weather conditions and requires substantially less capital and running cost. Therefore, conventional mooring continues to be adopted as an effective station-keeping means for the majority of floating structures and provides a more reliable deepwater mooring solution.

Mooring lines for deepwater operations may be made up of chain, wire rope, synthetic rope, or a combination of them. There are many possible combinations of line types, size, location and size of the clump weight or buoys that can be used to achieve the given mooring performance requirements. Chain and wire are the most popular mooring line materials currently in use. Of the two, the chain is more popular with about 85% of all semi submersibles using it for station keeping due to its durability and contribution to the anchor holding capacity. The wire is much lighter and provides a greater restoring force than chain and requires lower pretension. This becomes increasingly important as the water depth increases. The wire rope needs careful maintenance due to long term abrasion where it is in contact with the seabed [3].

1.4 Problem statement

The design of moored semi submersible systems constitutes a challenging engineering problem, in which the platform offset, stability, payload and system optimized cost requirements are to be met simultaneously. This problem is complicated by the incomplete understanding of the nonlinearities associated with the multiple interactions such as wave to wave, wave to platform, platform to mooring, fluid to mooring and mooring to seabed. Moreover, the design certifying authorities like the American Petroleum Institute (API) [4] have increased these challenges by limiting the floater stability, offset and the intact mooring tension responses in case of

disconnection of single or two mooring lines in operating or survival conditions. This process usually starts with definition of the system and the environment. Subsequently, the mean offset is evaluated from the total steady forces. The latter include the steady environmental (wind, current, nonlinear wave drift) forces and the steady thrust reactive forces in case of using thrust assisted mooring system (TAMS). An optimization process then evaluates the mooring stiffness, line pretension condition and the steady offset.

The evaluation of the oscillatory (time-dependent) forces and the associated system responses (platform motions and line tensions) is the most important and difficult process in the above mentioned problem. These include forces and responses of the first order (wave frequency), second order (low frequency) incident wave forces and second order (low frequency) forces reacted from thrusters (if TAMS were used). The next step in the problem solution is the assessment of the mooring system for intact and damage conditions. The assessment of the intact condition may be done through the application of frequency domain analysis, while the assessment of the damage conditions should be done in time domain due to the highly nonlinear line seabed interactions. An integrated nonlinear dynamic analysis of the coupled platform-mooring system is required for the final design.

Since the middle of the last century, the number of authors who have been working on research areas including analysis and design of conventional moored semi submersibles, improvements on the conventional semi submersible motion characteristics, innovation of semi submersible (up to 6th generation semi submersibles) and analysis and design of mooring systems. It has been proven that the peak moored semi submersible system responses result from the second order wave forces since the eigen-frequencies of these systems lie outside the wave frequencies. The problem of deterministic nonlinear hydrodynamic analysis of conventional catenary moored conventional semi submersibles has not been attempted yet. Thus, the primary objective of this study is to get a clear idea about the nonlinearities associated with the interaction of the floating system, its boundaries and its attachments (namely the environment, mooring lines and the seabed).

1.5 Objectives of the study

As mentioned previously, the main objective of this study is to provide an efficient nonlinear hydrodynamic analysis approach for moored semi submersibles. The general objectives of this study are listed below:

1. To develop a complete and deterministic numerical model for the evaluation of the platform motions of moored semi submersibles in the time domain and in the frequency domain. Furthermore, the contribution of the mooring system to the dynamics of semi submersibles for the wave frequency forces is to be investigated.
2. To develop a computationally effective numerical model for the evaluation of peak horizontal responses of moored semi submersibles based on the second order wave exciting forces and to assess the available semi-empirical procedure for the evaluation of the steady wave drift forces by comparisons with experimental results.
3. To produce well documented test results functioning as benchmark data for numerical models' validation and to prove the validity of the numerical models for the prediction of the first order (wave frequency) and the second order (low frequency) drift forces based on first order diffraction theory.
4. To investigate the consequences following the damage of single mooring line on the behaviour of moored semi submersibles.
5. To develop a complete programmable quasi-static analysis of multi-component fully suspended or partially grounded mooring lines for catenary mooring lines. Furthermore, to develop and validate a numerical model for the nonlinear hydrodynamic analysis of mooring systems in the time domain with emphasis on the mooring to seabed interactions.
6. To investigate the contributions of the various design parameters on responses of moored semi submersibles.

1.6 Scope of the study

The scope of the research is follows:

1. The environment was limited to uni-directional long crested waves.

2. Only stationary semi submersibles were considered.
3. The contributions of risers were not considered in the numerical or experimental modelling.
4. Station keeping systems were limited to catenary mooring systems without thrusters.
5. For the model tests, a nonlinear mass-spring system was adopted for the validation of the first order numerical model. For the validation of the second order numerical model and the investigation of the line failure consequences, a linear mass-spring system was adopted for the model tests.

1.7 Overview of the thesis

Chapter 1 is an introductory chapter. Chapter 2 presents a general summary of the literature pertaining to the subject of this thesis. The reported researches are classified in six categories and a general description of each category is given including historical perspective. From the reported literature, a critical discussion is presented focusing on the research objectives.

Chapter 3 is concerned with fluid-fluid and fluid-structure interactions, including hydrostatic and hydro-dynamic interactions. Furthermore, this chapter presents the methodology for evaluating wave hydrodynamic forces up to second order on semi submersibles.

Chapter 4 deals with the mooring systems. A methodology for analyzing fully suspended or partially grounded single or multi-component mooring lines in a quasi-static manner is given. A deterministic lumped mass approach for the nonlinear analysis of mooring lines taking the fluid to mooring interactions in consideration is presented with a special focus on the nonlinearities associated with mooring to seabed interactions.

Chapter 5 presents the methodology for the hydrodynamic analysis of floating rigid platform in the frequency domain and the time domain. In the frequency domain, the hydrodynamic force LTFs are derived from first principles for the evaluation of the 3 DOF motion in the horizontal plane. The latter are used for the evaluation of

one component of the second order forces for the 3DOF platform motions for the low frequency second order drift forces in the time domain. Furthermore, a methodology for the evaluation of 6 DOF platform motion responses and mooring forces in the time domain with development of the mooring-floater interactions are presented. It should be noted that in this chapter programming flow charts are given for the analysis in the frequency domain and the time domain.

Chapter 6 presents the methodology for the physical modeling of structure and environments. Model specification and construction, test setup and facilities are described for two different semi submersible models. The laboratory tests are described with special focus on station keeping tests.

Chapter 7 presents the results of the numerical models. The analysis of catenary moored semi submersibles and the associated experimental measurements are compared for different semi submersible configuration results. All results are accompanied by descriptive and critical discussions.

Chapter 8 concludes this study by giving a general overview to the problem discussed throughout the thesis. The conclusions addressing each objective are mentioned. Finally, recommendations for further improvements and research are proposed.

1.8 Chapter Summary

Introduction of this study was presented. The historical developments of offshore platforms in general and floating platforms in particular were presented. Semi submersible platforms and station-keeping systems were described. Furthermore, the problem of this study was stated followed by the study objectives and scope. At the end of this chapter, a general overview of the thesis contents was presented.

Chapter 2

LITERATURE REVIEW

2.1 Chapter overview

In this chapter, the research studies on the dynamic analysis of moored semi submersibles reported in the literature over the last forty years are discussed. These studies are categorized into six general research directions. The development and the critical review on each of the category is presented.

2.2 Reported studies

In this literature survey, the reported researches are grouped into six categories based on the research direction. It should be noted that a considerable research work has been reported on very large floating (VLF) semi submersibles. For example, the FE hydrodynamic analysis of pontoon semi submersible and hybrid type VLF and its experimental validation were presented by [5]. Also, the wind lift force on VLF semi submersibles was studied by [6]. However, this research category is not included in this literature survey since the uses of these structures are not feasible for oil and gas industry. Also, very few studies have been reported studying the effect of fully coupled platform-mooring-riser global motion analysis as investigated by [7]. In this paper, the dynamic effects of mooring lines and risers on platforms motions were investigated by comparing the conventional quasi-static and the fully coupled global motion analysis for deepwater semi submersible in 1700m water depth.

2.2.1 Wave frequency responses

In this category, various types of hydrodynamic analysis of conventional semi submersibles subjected to wave frequency forces are discussed. The earliest study was conducted by Hooft. Wave frequency forces and motion responses of floating semi submersible were evaluated assuming that the submerged part of the platform could be sub-divided into typical slender elements. This, however, was valid only when the dimensions of the elemental part were smaller than one fifth of the wave length. The results obtained by this method were validated by comparing with model test results, and it was found that the numerical results differed within 5% from the experimental results [8].

Hooft hypotheses were followed by a number of researchers for the prediction of the floating platform motion and mooring tension responses like [9]-[12]. An intensive comparison study on the methods for calculating the semi submersible wave motions was conducted by [9]. The calculation results on the validity of 34 programs were examined by conducting comparisons with experimental results. These programs were classified into five groups based on the theoretical background of each program. Programs in the first class made use of the 3D potential theory with or without viscous damping correction. In the second class, Hooft method with Morison formula was adopted. In programs of the third class, use of the Hooft method with 2D potential theory was adopted. In the fourth and fifth classes, the programs adopted a mixture of the first and the third classes and the second and the third classes respectively. The results indicated that most of the programs provide virtually the same results for surge and sway, and these results were in a good agreement with the experimental results. For other motions, it was found that there was no good agreement between programs and it was concluded that by using appropriate force coefficients, the simple Morison method was able to obtain accurate results as good as those using the 3D potential theory.

Two computational methods were developed to predict the motion and forces on semi submersibles by [10]. The first method was based on 2D potential theory and another one was based on 3D potential theory. Validation studies between the developed methods and experimental results were conducted. These studies showed

that the computational methods could be applied to provide motion and mooring load data both in the frequency and the time domain in which the performance of the semi submersible may be well predicted in the early design stage.

A parametric study on the free vibration of semi submersibles was conducted by [11]. The effect of the variation of the length, draft and hull spacing on the natural frequencies and mode shapes was investigated. The analyzed semi submersible was modeled as a space frame having a total of 12 DOFs, with three translational and three rotational DOFs at each node. For a partially submerged member, a node was placed at the water level. The element stiffness matrix of the space frame was formed by the standard displacement method, the mass was lumped to obtain the mass matrix and the total load on the deck was found from the buoyancy calculations. The eigen values were evaluated by simultaneous iteration method. It was found that the variation was less sensitive to lower modes of vibration and more pronounced for higher modes.

The motions of a moored semi submersible in regular waves were studied both numerically and experimentally by [12]. Numerically, the semi submersible was modeled as an externally constrained floating platform, as composed of several rigidly connected parts. The idealized equations of motion of each part were obtained in a common reference system fixed on the platform. A consistent formulation of the wave-induced internal forces between two parts as well as the external constraining forces was evaluated. Experimentally, model tests were carried out using a 1:36 scale model of the semi submersible Glomar Arctic. Good agreement was achieved between the numerical results of platform motions and internal forces and those from model tests. Numerical results obtained with and without mooring lines indicated that the mooring effect on the platform motions and internal forces were insignificant in the wave frequency range.

The motions of a semi submersible drilling platform were experimentally evaluated in order to predict their effects on the comfort and activities of the crew by [13]. The motions of the platform in the three rotational and three translational axes were evaluated from translational accelerations measured near three corners of the main deck. Results indicated that the horizontal motions at the drill floor exceeded

the average threshold of perception defined in international standard ISO-6897 by more than a factor of two. It was concluded that the current models were inadequate for evaluating the motions of ships and floating platforms with respect to their effects on the performance of manual tasks and research was required to establish improved criteria for assessing the severity of such motions.

2.2.2 Low frequency responses

The earliest study in this category was [14]. It was showed that for a 2D case of an infinitely long cylinder floating in regular waves with its axis perpendicular to wave direction, only part of the incident wave will be reflected while the rest will be transmitted underneath the cylinder. Using this assumption, the wave drifting (reflection) force was evaluated. Also, it was shown that the drifting force for regular waves is proportional to the square of the wave height. Based on assumptions made in [14], [15] presented different formulations for the wave drift force using the first order diffraction theory. Results from these formulations were found to agree with each other and with experimental data in most cases. Later, based on [14] assumptions and tests on a rectangular barge, [16] presented a numerical method for the evaluation of the slow varying drifting force in the time domain of regular wave groups and irregular wave trains.

Based on the same assumptions made by [14]-[15], [17] developed a numerical method to evaluate the drifting force spectral density of the irregular waves from the spectral density of the drifting force coefficient in regular waves. The influence of the low frequency wave drifting force on the motions of moored platforms and the loads in the mooring system, was demonstrated from results of model tests in irregular waves.

Significant contributions on the low frequency second order wave drifting force based on 3D potential theory of moored semi submersible were demonstrated by [18]. This theory yielded four second order components. These components were due to 1) the relative wave elevation, 2) the velocity squared terms, 3) first order motion and 4) products of angular motion and acceleration. Also, a method for the evaluation of the time independent quadratic transfer functions was given. A numerical method was

developed based on a direct integration 3D potential theory with five contributions for second order wave component, identified by [19]. Further improvements on the 3D potential theory by considering the viscous contributions were made by [20].

The analysis of the second order oscillations was carried out in the frequency domain by [21]. The slow drift oscillations of a moored large volume structure were studied in a wave flume. The recordings of irregular wave input and the resulting mooring forces were analyzed by the spectral technique suggested. The experimental results were compared to [20] theory results. The results were found to be very sensitive to the drift force coefficient. Therefore, it was recommended to determine these coefficients very carefully through the experimental tests.

In the same direction, an approximate method to compute the drift forces on semi submersible platforms were presented by [22]. The interactions between the columns were treated in a simplified approach following [8] method. Including the effects of phase shifts in the waves, the drift forces computed by this simplified approach were compared with the drift forces obtained by use of a panel method approach. For the two platforms used in the comparison, the agreement of the results by both methods was quite satisfactory. This approximate method was suitable for estimating the drift forces on floating platform platforms with vertical cylinders at early design stage.

Moreover, the low frequency damping of a moored semi submersible drilling platform was studied by [23]. Numerical extinction tests in still water and regular waves were used. Mean wave forces were calculated at zero forward speed. The influence of drag forces was represented by the modified Morison equation. The platform as used by [9] for the comparative mooring study was analyzed in irregular beam waves. The computed time series of sway response as well as the corresponding response spectrum compared fairly with model test measurements, demonstrating that this procedure to determine low-frequency damping could be used effectively in the early design stage.

The effect of the forward speed of a ship on the hydro-dynamic drift forces was studied by [24]. The governing equations of the problem, including forward speed were solved in time domain enabling simulation of non-harmonic waves. Based on the perturbation technique, formulae for the drift forces and moments were derived. It

was assumed that the stationary waves generated by the platform do not influence the drift forces substantially. The formulated governing equations were solved using the boundary-element method with a new algorithm combining the integral equations with the boundary conditions. It was shown that this algorithm is stable for all relevant speeds and grid sizes. The results of the developed algorithm were compared with results based on frequency domain approaches found in the literature, and good convergence was achieved. It was concluded that the maximum value of the horizontal drift force increased considerably with the forward speed.

The nonlinear force and response of floating platforms was studied in the frequency domain and the time domain by [25]. Particular emphasis was given to the influence of the nonlinear drag force in predicting mean and low frequency viscous drift forces. The linear 3D potential theory in the time domain was adopted. The results of this model were compared with those obtained by using Morison equation model and the agreement was found to be good, establishing the validity of the numerical model. It was concluded that the frequency domain method can be used for the initial design stage, while the time domain method was recommended for the final design stage.

A new hybrid wave model (HWM) for the prediction of the wave kinematics of the unidirectional irregular wave train was introduced by [26]. The numerical model was extensively examined using various wave spectra and was found to be convergent and accurate. The application of the hybrid wave model were demonstrated by comparison with two sets of laboratory measurements and with the linear random wave theory and its stretching and extrapolation modification by [27]. It was concluded that the hybrid wave model is more accurate and reliable than the linear random wave theory especially near steep wave crest.

An efficient method was developed to predict the slow motion responses of slender compliant offshore structures in the unidirectional irregular waves and currents by [28]. The environmental loads were evaluated using the modified version of Morison equation based on the slender platform approximation. The HWM was used to predict the wave kinematics accurately up to the second order of the wave steepness. The second-order forces due to convective acceleration, free-surface

fluctuation, time-varying structural displacement and axial divergence were also included. The results of the numerical method achieved good agreement with experimental results for spar and floating jacket platforms. It was noted that the predicted slow drift motions using Wheeler stretching and linear exploration wave kinematics models, did not agree well with the physical measurements.

Different analytical and numerical methods to evaluate the dynamic response of Spar platforms due to unidirectional and multidirectional waves, current and wind were presented by [29]. Focus on the second order difference frequency forces and structural responses was done. Some numerical predictions in the time domain using Morison equation and the second order diffraction theory were compared to the measured laboratory and field data. The statistical nature of the response was also studied. Good agreement between results was achieved for the numerical results using the HWM.

Recently, the low frequency responses of semi submersible and other floating platforms were studied by [30]. The problem was formulated using dynamic frequency domain models for low frequency viscous excitation and damping of floating structures subjected to current and irregular waves. The basis of the models was the drag term in the Morison equation. The loads were quantified in terms of power spectrum density functions using Pinkser approach. It was found that the platform motion frequency domain spectrum agreed with the spectrum from a time domain calculation.

2.2.3 Responses to extreme environmental conditions

In this category, the semi submersible dynamics under survival conditions are considered. An experimental work aimed to determine the motion response characteristics and operating limits of semi submersibles in abnormal heel and trim angles was studied by [31]. A model in 1:100 scale of a moored semi submersible with four columns and twin pontoons was investigated. For head, beam and quartering wave directions, tests were undertaken at five angles of trim and heel, namely: even keel, two wards (windward damage) and two away (leeward damage) from the waves in 7 m regular seas with periods of 7 s to 25 s. In all cases, 6DOF

motion responses were obtained. The RAO curves for small angles of trim and heel showed a little change from an even keel. However, at large angles, substantial increases in roll and particularly pitch motion occurred over a band of wave periods 9 s to 13 s. Over this band, all motions contained not only the wave frequency but also a significant sub-harmonic component at half the wave frequency. Under these conditions, leeward damage consistently produced the largest motion. The most extreme motion measured resulted in a pitch RAO of 19.8 degrees for a wave of 6.9 m height and wave of 12 s period in quartering seas.

Furthermore, the partial damage to one column of a twin hulled semi submersible was simulated experimentally by [32]. Four damage conditions representing partial damage to one column were simulated. Test results showed that the natural frequencies of the platform in damage conditions are higher than either those of pitch and roll in similar conditions. These natural frequencies in pitch and roll begin to approach that of the damaged column or the sea state. The value of the natural frequency itself increased much more slowly with increase in damage condition. It was inferred that the nonlinear wave pressure term played only a minor role in the asymmetry of motions of the platform but the mooring characteristics have a significant influence in the platform motions.

Moreover, nonlinear coupled numerical simulations to predict the dynamic response of semi submersibles in extreme environments were formulated by [33]. The effects of thrusters and mooring line damping were carried out to find the total extreme motions and mooring forces. In formulating the motion equations of the coupled system, nonlinear stiffness characteristics of the catenary mooring lines were taken into account. The nonlinear, coupled motion equations were solved simultaneously in the time domain using Adam's numerical integration technique. Surge, sway, heave and yaw DOFs were considered in the analysis. It was concluded that mooring lines could reduce the slowly varying surge response by about 40% in moderate weather conditions when thrusters are not in use. However, in extreme weather conditions, slowly varying surge response reduction was about 7%, and it was enough to prevent a failure. In addition, the biggest contribution to the total surge extreme comes from the mean surge value in extreme weather conditions while

the mean and slowly varying mooring forces contribute significantly to the total surge. The first order mooring forces were negligible.

Also in this research category, the consequences of specific extreme sea conditions on the seakeeping behavior of a semi submersible were investigated by [34]. The numerical time domain investigation using a panel method and the potential theory was compared to frequency domain results. The characteristics of the embedded rogue were varied to analyze the dynamic response of the semi submersible in extreme wave sequences. For validation of the numerical models, the selected sea condition was generated in a physical wave tank and the sea keeping behavior of the semi submersible was evaluated to model scale. Numerical results and the measurements at the model scale agreed well in the frequency domain and the time domain.

On a semi submersible of type GVA 4000, the dynamic responses to reported rogue wave were investigated in the time domain and validated throughout in comparison with frequency domain and commercial software (WAMIT) results by [35]. The numerical time domain investigation using panel method and potential theory was compared to frequency domain results. For time domain analysis the commercial code (TiMIT) was used to provide the motions and forces on the wetted platform of the semi submersible in rogue waves as time series. Corresponding response amplitude operators were also calculated with WAMIT. The satisfactory agreement of TiMIT and WAMIT results proved the capability of numerical codes based on potential theory. The resulting response spectra were then transformed into the time domain using Fourier's transformation. The seakeeping performance of the semi submersible was tested in a physical wave tank while the selected sea conditions were modeled at model scale. It was found that the maximum response was directly related to the freak wave height.

More development on the full 3D simulation of the impact of a rogue wave on semi submersibles using the smoother particle hydrodynamics for TLP and spread taut spread mooring system was undertaken by [36]. This simulation was conducted using the Smoother Particle Hydrodynamics (SPH) technique. Two different mooring configurations were considered: Tension Leg Platform (TLP) and Taut Spread

Mooring (TSM) system. It was found that for a wave normal to the platform side, the heave and surge responses of the platform, significantly differed for the two mooring systems. The TLP system underwent large surge but comparatively smaller heave motions than TSM system. The degree of pitch was very similar. The total tension in the cables was approximately four times higher in the TSM system and exceeded the strength of the cables used in the simulation. It was concluded that for a rogue wave impact, the TLP configuration is more desirable and SPH seems to be an attractive alternative to standard methods for simulating coupled interactions of highly nonlinear breaking waves and structural motions.

Recently, an intensive research studying the consequences of hurricanes Katrina and Rita in the GOM on the offshore oil and gas industry was conducted following those events. The damage caused by these hurricanes was statistically investigated by [37]. It was reported that Hurricanes Katrina and Rita, which entered GOM on 26 August 2005 and 26 of September 2005 respectively, caused the largest number of destroyed and damaged platforms and pipelines, besides the highest number of MODUs set drift in the history of GOM operations. In total, hurricanes Katrina and Rita destroyed 113 platforms and five drilling rigs and severely damaged 19 others. Furthermore, 19 out of 28 MODUs lost their moorings and became drifted far. Most of these platforms were older, small producers in relatively shallow waters. The analysis indicated that the prevalent cause for damage to the integrity of platform structures was the loading caused by the wave inundation of the deck.

Also, numerical predictions for the MODUs horizontal motions under these hurricanes were developed by [38]. This study employed a simplified equation describing only the horizontal motions (surge, sway and yaw) on a MODU under the impact of steady wind, current and wave forces. The simplified hydrodynamic model neglected the first and second order oscillatory wave forces, unsteady wind forces, wave drift damping and the effects of the platform oscillation on the steady wind and current forces. For validation, the predicted drifting trajectories of two MODUs were compared with the corresponding measurements recorded by the global positioning system (GPS). Comparisons showed that the simplified hydrodynamic model was capable of predicting the drift in MODU.

2.2.4 Addition of heave plates

In this category, a number of authors contributed towards the improvement of the motion characteristics of conventional semi submersibles by adding heave plates. The first attempt of this type was made by [39]. Experimental and theoretical work aimed to enhance the wave induced motion characteristics for semi submersible platforms by incorporating a pneumatic compliancy, was achieved using open bottom tanks mounted on the platform. This was achieved with open bottom tanks mounted on the platform. As a result, the heave, roll and pitch motions were substantially reduced. Regular and irregular wave tests were performed on a scale model enabling the motion reduction capabilities of such a system to be evaluated. Test data was compared with a multi-degree of freedom dynamic response calculation in the frequency domain, in which, Morison equation was used for calculating wave-induced forces on the semi submersible. The proposed system seemed to be effective in mitigation of the semi submersible vertical motions.

In addition, a new deep draft semi submersible named DPS 2001 with a retractable heave plate was developed by [40]. The system combined the advantages of a semi submersible with the operation motion advantages of a truss spar type floater. The truss/heave plate was in a retracted configuration during fabrication and towing, which allowed the deck to be installed and commissioned inshore. The feasibility of DPS 2002 was demonstrated by carrying out a preliminary design. Total steel weight for the hull system was comparable to platforms with comparable motions. Global responses were estimated and were found to be superior to typical semi submersibles. Because of the heave plate, DPS 2002 motions were significantly less than that of conventional semi submersibles and ship-type hulls.

Likewise, the addition of heave plate to an existing deep draft semi submersible with external extendable columns supporting the heave plate to achieve desirable motions was proposed by [41]. It was found that the heave motion characteristics for this system were similar to those of spar platforms. The riser technology presently used on spars with keel joints and stress joints was applied to a dry tree semi-design assuming the motions were similar by mean of replacing the soft tank in spar with heave plate for the semi submersible. The heave plate connectors were designed

considering not only the hydrodynamic loadings but also horizontal tension and stroke riser loads at the keel as well, which would give enormous moments at the keel and stress joints. The results showed that the proposed modification is suitable for a dry tree solution.

Moreover, parametric investigations adopting the hydrodynamic analysis of a conceptual dry tree semi submersible with heave plates for drilling and production platforms were studied by [42]. In this study, calculations showed that increasing the diameter of pontoon relative to the diameter of the column reduced the vertical forces, assuming a predetermined heave plate area and draft. Also, the hull form of the dry tree semi submersible can be optimized to control the cancellation period, magnitude of the heave RAO below the cancellation period and the heave natural period. The relative areas of the column and pontoon were varied to demonstrate the global effects of the hydrodynamic forces acting on these structural components while the area of heave plate was kept constant.

Furthermore, a design optimization study by proposing heave plates to the base of each column to enhance the stability of semi submersible platforms was done by [43]. The design was refined by multiple try and error iterations aimed at enhancing the hydrodynamic performance of the platform while minimizing its cost. It was found that for efficient optimization of platforms, a method of handling complex nonlinear multiple variables is necessary. The genetic optimization method was selected to estimate the dimensions of an offshore structure subjected to physical requirements including structural weight, horizontal motion, vertical motion and rotation in operating and extreme sea-states, the air gap, mooring size, etc. For this purpose, a simplified hydrodynamic model was developed to capture the parametric sensitivity of the platform responses to primary design parameter. Preliminary results, with static constraints, showed a linear relation between payload and the platform displacement.

In the same research area, extensive numerical and experimental motion analysis and comprehensive model testing were carried out to investigate the global performance of a conventional semi submersible configured with heave plate by [44]. The design case was a GOM deepwater environment, similar to that for a Spar located

in 1680 m of water, with eight top tensioned risers (TTR) supported on top of the semi submersible hull with tensioners, a spread mooring and a 10,000 T operating payload. Extensive numerical and experimental motion analysis and comprehensive model testing were carried out to validate the in-place behavior of such a solution. The analytical and model test results demonstrated that the excitation of a semi submersible hull by wind, wave and current can be adequately mitigated by the proper placement and sizing of a heave plate system. The analysis and testing indicated that achieving suitable motions in a cost effective manner, require incorporating fabrication and installation issues into the heave plate system. The in-place behavior of this solution was validated, proving that the concept provides a viable cost effective dry tree floating solution for deep developments.

Recently, two semi submersible designs proposing heave plates for the new GOM met-ocean criteria post Katrina hurricane, with a common topside and riser payload were developed by [45]. The comparison was based on hull dimensions, including heave plate and structural support construction. Performance focused on riser response, especially stroke and tension. In both cases, the design met the criterion of keeping the riser stroke under 10 m. However, damaged conditions, such as broken mooring and a flooded hull compartment, need to be further investigated. The analysis demonstrated the flexibility in relative sizes of the hull and heave plate to provide an optimum design for a particular riser count and layout. It was concluded that both versions of the dry semi submersible can be designed to support TTRs with stroke ranges of less than 10 m. Heave motion was sensitive to the relative sizes of pontoon width and height, heave plate draft and hull draft. For both designs, heave motion was less sensitive to the column draft change than to the heave plate draft.

2.2.5 Innovation semi submersibles

The semi submersible development is reaching sixth generation now. This was achieved through the contribution of a considerable number of researchers. The studies regarding the developments in this area are grouped in this fifth category. An early improvement in deck payload and motion response to waves obtained by separating the buoyancy and hydrostatic stability contributing members of the

structure was described by [46]. In this study, the buoyancy was supplied by bottle legs directly below the platform deck and the hydrostatic stability was maintained by articulated stabilizers from submerged out-riggers on the outer perimeter of the platform keel. The stabilizers had small excess buoyancy and behaved as inverted pendulums. These innovations made the platforms to be designed with a deck payload in a range of 10,000 T to 12,000 T. It was concluded that the large distance of the stabilizer water plane areas from the platform centerline led to large hydrostatic stability. This gave the platforms in deeper draft lower wave induced motions. Moreover, separation of buoyancy, stability and deck support functions within the structure allowed more effective optimization for each of them.

Likewise, the design of column stabilized semi submersible with a jacking mechanism, which enabled the platform to change its draft from 50 m to 10 m was introduced by [47]. The platform was targeted for the development of marginal deepwater fields. The platform absorbed the advantages from both purpose-built deep draft platforms and conventional shallower draft semi submersibles. It has combined excellent motion response characteristics with the ability for conventional dry dock inspection, maintenance, re-fitting and re-use. The motion and stability characteristics of the proposed system were studied in the frequency domain. Results proved that the proposed platform was extremely versatile, when compared to conventional semi submersible, and have a much better motion response.

Moreover, a dry tree semi submersible (DTS) platform with buoyancy-tensioned tie-back risers attached to the risers below the upper wave and current zone with the highest hydrodynamic loading, was presented by [48]. The main advantages, comparisons with alternative techniques and the DTS platform motions were studied. The DTS was a conventional semi submersible unit with buoyancy tensioned tieback risers. The tieback riser buoyancy cans were attached to the risers below the upper wave and current zone with the highest hydrodynamic loading. An open tubular truss tower with spacer grids at regular intervals was fixed to the platform at deck and pontoon levels, taking up horizontal riser forces and maintaining distance between the risers down to the level of the lowest buoyancy can. This riser guide was kept in an elevated position flush with the platform bottom during transport and tow. It was concluded that the DTS concept avoided the disadvantages of dry tree concept with

riser tensioners, which rapidly lost payload capacity in deepwater because of the increasing weight of the riser system. When compared to spar, the DTS had a substantially better steel weight to payload ratios.

Another innovation, the production drilling (DP) semi submersible representing the next generation for ultra deepwater activities was developed by [49]. A system engineering approach that included total field development, from the reservoir to pipeline was used to identify high impact technologies. The net effect was a significant reduction in topside drilling and process operating payloads and hull size relative to a conventional PD semi submersible with the same capabilities. A case study for 3,000 m GOM field development revealed that a 20% capex reduction was achieved along with a three month schedule compression to first oil. All technologies used were in commercial application, with industry-wide acceptance. It was concluded that the next generation PD semi submersible would both enable and provide a step change in the economics of producing hydrocarbon reservoir in ultra deepwater basins around the world.

As a new offshore concept, a truss pontoon semi submersible (TPS) was introduced by [50]. In this system, a truss spar was used to create the added mass by the heave plates. The effect of the heave plates on the vertical motion of the floating structure was demonstrated. A TPS was analyzed utilizing the linear diffraction theory as well as the linear part of the Morison equation. The effect of both regular and random waves was studied. The results from the Morison equation of the surge and heave exciting forces and pitch exciting moment were compared with the linear diffraction theory results. The analytical heave and pitch and pitch motion results were also compared with the model test results. The close agreement of the analysis results with the experimental results suggested that the simplified Morison equation could be used for the TPS analysis without sacrificing the quality of the results. However, good engineering judgment was required for estimating the values of the hydrodynamic coefficients as well as the amount of damping introduced in the structure. It was also found that the heave plates introduce large added mass and considerable damping in the system motion in the vertical direction such that the resonance becomes less of a problem. This suggested that the TPS concept might have merits as a heave-controlled floating production in the deepwater development.

A case study for the validation of the procedure, that compares full depth model test results of a semi submersible in water depth 1,250 m (model scale 1:100) against the extrapolated full depth results obtained from a truncated system of 500 m was conducted by [51]. The sway, roll and heave responses and line tension were compared. The results showed that the hybrid verification procedure was able to predict the change in the system response going to the full depth due to increased line dynamics. It was concluded that the hybrid verification process relies heavily on the tuned model of the platform being meaningful at both depths.

On the construction techniques, wave exciting tests of a semi submersible floating structure model with a proposed mechanical connector of 1:100 scale and the numerical analysis using the hydro-elastic response analysis program VODAC were carried out by [52]. Mechanical connectors were used instead of welding to connect two units. It was confirmed that the existence of the new type of the mechanical connectors did not degrade the response characteristics of the semi submersible floating structure.

The vortex induced motion (VIM) of a deep draft semi submersible with four square columns was numerically formulated, experimentally measured in model tests and observed in a prototype configuration by [53]. A formulation was developed to predict the distribution of VIM amplitudes, which can be used to estimate VIM induced fatigue damage. Froude scaling was used to model the hull and displacement in 1:50 scale. The effects of waves and external damping on VIM were investigated. Results showed that a relatively small sea state does not influence the VIM response. The additional damping, up to 10 % of equivalent linear damping, did not increase the VIM response amplitudes. This led to a recommendation that for performing VIM test, the damping is an important consideration.

Recently, A new concept of LNG FPSO based on a deep draft, small water plane, low center of gravity and large radius of gyration semi submersible hull was introduced by [54]. These characteristics made the platform respond with low motions. Global performance and sloshing analysis for the LNG FPSO hull and the conventional FPSO hull were performed to compare their operating performance for West Africa and the Northwest Australia environments. Results showed the new hull

form has appreciable advantages over the conventional ship type LNG FPSO. The lower motion response of the new LNG BOX makes it possible to use efficient LNG liquefaction processes well proven in onshore application, steel catenary risers, spread mooring line and membrane type LNG cargo containment system. These features made offshore floating LNG liquefaction more economical and an attractive solution to the mid and large size stranded LNG gas fields.

2.2.6 Station-keeping systems

This category discusses the studies related to investigations on the station keeping systems. A quasi-static analysis technique for the 3D marine cable structures based on the FE formulation was presented by [55]-[56]. Hydrodynamic as well as the gravity forces were treated as distributed forces on the cable elements, while part of the inertia forces were lumped at the nodes of the model. This separation of the forces into distributed and concentrated forces, allowed the use of long cable elements. From the given forces and the given position of the ends of the cable, the algorithm determined the complete geometry of the cable, its end forces and its tangent stiffness matrix. The equilibrium configuration of the assembly was approached by successive iterations, which decrease the imbalance of the forces that exists at the previous iteration. Special procedure for the rapid convergence of the solution was presented.

An iterative numerical scheme based on the catenary equations for the quasi-static analysis of multi-component mooring lines for horizontal positive excursions was presented by [57]. The material and geometry nonlinearities were taken into consideration with no hydrodynamic effects taken into account. Further development of this method namely the quasi-static analysis of multi-component mooring lines for vertical excursions, was made by [58].

The magnitude of the mooring loads with slowly varying drift forces, was examined by [59]. The analysis was performed using the time domain simulation in conjunction with model tests. An engineering assessment of the quasi-static approach was made, which proposed the use of combined quasi-static and time domain analysis in the design of semi submersible mooring systems. It was concluded that the quasi-

static approach at best is only an approximate approach with deviation for both model test and time domain results by as much as $\pm 40\%$. Hence, it was recommended that all mooring system designs should be confirmed by time domain simulations and model tests.

In the same direction of Raman, an overview of the analysis methods and design procedures used for catenary mooring systems was conducted by Patel and Brown [60]. Particular emphasis on the application of these mooring systems to floating production platforms was taken into consideration. Modern trends of in automated analysis procedure for mooring systems designs were described. Also, an overview of the new design features and operating techniques that are increasingly being utilized were presented. For the quasi-static analysis, use of the [55]-[56] method was adopted.

The earliest study on the dynamic analysis of mooring lines was conducted by [61]. Starting with Walton and Polachech approach, theoretical and experimental results on the dynamic tensions and motions of the multi-component mooring lines were presented by [62]. Special attention was given to the dynamic behavior of mooring lines under the excitation caused by the motion of floating platforms using the LMM. The material nonlinearity of the mooring line was incorporated in the numerical model. Time histories of the dynamic tensions predicted by the numerical method were compared with experimental measurements and excellent agreement was achieved. Also, lifting and grounding approach for the simulation of the seabed line interaction was formulated. This approach was based on forcing the first suspended node to ground smoothly for preventing the unrealistic impact. For this purpose, special mass modifiers for the first two suspended nodes were introduced. Based on Nakajima assumptions, a computer algorithm using LMM was established by [63]. Results of this algorithm were compared with harmonic oscillation test tests for different lines and water depths at different model scales. The formulated algorithm was proven to be an effective tool to quantify the dynamic behavior of multi-component mooring configurations. It was concluded that the dynamic tensions in mooring systems may affect the low frequency motions of the moored structure.

The influence of using different time integration schemes to solve the dynamic equations of motion applicable to a mooring line was studied by [64]. The four time integration schemes investigated were the central difference (CD), Houbolt, Wilson- θ and Newmark- β schemes. An assessment of the stability, accuracy and the influence of the time step size for each scheme were presented. It was concluded that for the evaluation of long-term dynamic tension of a mooring line, the CD scheme might be ruled out since it was limited smaller time step than required for other schemes. On the remaining schemes, Wilson- θ presented the smoothest solution with minimum time step.

Using Nakajima model, formulation of a mooring line dynamic model through the use of the LMM was presented by [65]. A model to account for both friction and suction effects as well as lifting and grounding of nodes was discussed in some detail. Results were presented, which illustrated the seabed interference effects upon the total dynamic solution. It was concluded that the seabed friction and suction effects are negligible for deepwater mooring systems. Also, the control of the nodal lifting and grounding by the adopted method was difficult.

Also based on Nakajima model, a dynamic analysis scheme for the prediction of the dynamic behavior of tether cable and attached remote operated vehicle (ROV) system was developed by [66]. The scheme was valid for the analysis of single, nonlinear 3D and static/dynamic model of a submersible cable and attached system. The LMM with Houbolt integration algorithm and Newmark- β were basically employed. Several wave tank experiments were performed and the results were compared with numerical ones. The developed scheme proved to be effective and reliable for the dynamic analysis of the cable-ROV system.

The dynamics of mooring lines for deepwater applications with submerged buoys attached to them were studied both experimentally and numerically by [67]. The theoretical background was outlined and the experimental setup as well as the data acquisition system were detailed. The obtained experimental results were compared with numerical predictions using both time and frequency domain computer codes. Also, the beneficial effects of buoys in reducing the mooring line dynamic tension

were investigated. This was conditioned by the proper selection of the size, number and location of the buoys.

The earliest study using the FE method for the analysis of mooring lines was conducted by [68]. A numerical approach for evaluating the static and dynamic response of general 3D cable structures totally immersed in a moving fluid was presented. The FE method was used to model the nonlinearities associated with the geometry, hydrodynamics and material. Results obtained using incremental/iterative solution techniques were discussed. Also, a FE model for the dynamic analysis of cable suspended in water was presented by [69]. Global existence and uniqueness of the solution of the truncated system was shown for a slightly simplified equation describing the motion of the cable having negligible added mass and supported by fixed end-points. Based on this, along with published results on local existence and uniqueness of solutions for symmetrizable hyperbolic systems, global results for the initial value problem were conjugated. Furthermore, a numerical model for the assessment of the dynamic behavior of mooring lines taking into account the hydrodynamic forces exerted by the surrounded fluid based on FE formulations was presented by [70]. In order to stress the importance of the dynamic analysis, comparisons of the method results with those of the quasi-static approach were presented. It was concluded that the quasi-static methods are not sufficient to describe the characteristics of the restoring forces especially for deepwater platforms.

The dynamic positioning control, which was designed using a linear mathematical model obtained from nonlinear motion equations of the platform for a semi submersible, was studied by [71]. In such a control, motions caused by linear wave exciting forces add to the drift of the platform. It was not possible for the thrusters to resist this wave frequency motion because the linear exciting force is very strong. A controller was designed using a linear mathematical model obtained from nonlinear motion equations of the platform for the purpose of maintaining a given position without responding to linear exciting force in the wave frequency range. Model tests were carried out and it was found that the designed controller performed well. Model experiments were conducted in oblique incident waves and some successful results were achieved.

The analysis using quasi-static, dynamic and matching methods for the platform and mooring line-buoy systems of deepwater mooring system for a semi-submerged drilling platform was studied by [72]. The motion equations for the floating structures were solved by the Green's function method with numerical panel approach and the mooring line-buoy kinetics and kinematics problems were formulated as a combined nonlinear initial-value and two-point boundary-value problem. In this study, it was reported that the quasi-static method with matching approach for platform and mooring line-buoy system could be applied to determine the parameter of motions for moored floating structure, especially including number, size and position for buoy. Also, this method can be used to determine the parameter of motions for moored floating structure.

The slow motions in the horizontal plane of a mooring systems under time independent external excitation was analyzed using nonlinear 3D, large deformation FE model by [73]. Three qualitatively mooring line models were developed and used to cover a wide range of applications, ranging from an extensible taut nonlinear string to an inextensible heavy cable. A nonlinear, three dimensional, large deformation nonlinear elastic strain FE model was used for all intermediate cases. Numerical solution of the latter problem was achieved through a global Newton's iteration. It was concluded that the mooring systems might oscillate autonomous external excitation or experience complicated and operationally hazardous long-term response.

The slow and intermediate frequency motion of the nonlinear dynamics of spread mooring systems (SMS) using a 3D nonlinear large deformation FE model was studied by [74]. The mathematical model consists of the slow-motion maneuvering equations in the horizontal plane including quasi-steady hydrodynamic forces up to the third order, memory effect, nonlinear forces from mooring lines, riser dynamics and environmental loads due to current, wind and wave-drift. A three dimensional nonlinear large deformation FE model was used to calculate quasi-static riser dynamics in the analysis of mooring dynamics. It was shown that the large amplitude slow motion of SMS was due to resonance of the mooring system natural frequency. The slow-varying drift represents only one of the mechanisms that can instigate such motions. Mean drift forces could also cause large amplitude oscillations. Further,

slowly varying drift forces might reduce dramatically and even eliminate such motions.

Also, a parametric study considering the effects of cable diameter, shape of the cable, current profile and time on the excursion and vertical position of the buoy using the nonlinear dynamic FE analysis of single point mooring systems using incremental time integration Wilson- θ method was investigated by [75]. Case studies were carried out for taut and slack mooring systems using multiple numbers of buoys. It was found that the shape of the cable governs its drag coefficient and the variation in the excursion of the buoy and configuration of the cable could be modified by manipulating buoy force and by providing streamlined sheaths having reduced drag coefficients. Also, it was observed that addition of subsurface buoys reduces the tension in the cable.

A 6DOF FE code was developed for the nonlinear static and dynamic analysis of mooring lines and marine risers by [76]. The geometric and the environmental load nonlinearities were considered. The Newton iteration method was selected to solve the mooring line nonlinear algebraic governing differential equations while for dynamic problems, the first order differential equations were solved by the first order Adams-Moulton method. The reliability and accuracy of the program were demonstrated by comparing numerical solutions with the analytical solutions, experimental data and numerical results by other programs.

The stiffness coefficients of the mooring lines in 6DOF of a floating structure were derived based on the differential changes of mooring lines' tensions caused by static motions of the floating platform by [77]. The performance of a moored floating breakwater was theoretically investigated under the action of normal regular waves. Special attention was given to the effect of different configuration of the mooring lines. A three dimensional model of the mooring lines for the static and the dynamic analysis was used. It was concluded that the modification of the initial configuration of the mooring line affected the stiffness and drag damping of the mooring line and the transition from slack to the taut mooring line led to increase of the stiffness of the mooring line, especially on the vertical plane.

Furthermore, an adaptive dynamic relaxation technique using Newmark's direct integration algorithm for static analysis of catenary mooring lines was proposed by [78]. The added artificial damping was controlled adaptively in the relaxation process to accelerate convergence. For stability and acceleration of convergence, detailed control procedures for the time step, load increment and other parameter were presented. Application of the proposed numerical scheme to the static analysis of a number of catenary mooring lines with different nonlinear boundary conditions was made. Results from a comparative study indicated that this method is numerically more robust.

Also, a linearized frequency domain dynamic analysis of mooring lines was studied to evaluate the large motion of slender structures by [79]. The viscous drag damping was linearized by evaluating linearized equivalent damping coefficient through iteration. The linearized frequency domain results were compared with results from nonlinear simulations for a towing cable, a mooring line and a lazy-wave riser. It was found that the frequency domain simulations gave basically similar results to those of time domain with higher cable tensions for mooring lines partly lying on the seabed since the implemented frequency domain method did not take into account the effect of cable seabed interaction.

In addition, the catenary equations were solved by transformation to a single polynomial equation of eight degrees by Laguerre's iteration for a three component mooring made up of two lines connected at a point buoy or sinker by [80]. An estimation scheme for a static catenary equation was used instead of discretisation scheme. The problem was transformed to a single polynomial equation of eight degrees and solved by Laguerre's iteration. The elongation of the lines was shown to be equivalent to small uncertainties in the weight per unit length. The techniques described provide alternative, more robust convergence and where there was no buoy or sinker, the solution was in closed form.

Similar to [76] work, an efficient 2D FE model for the numerical analysis of mooring cables and seabed interaction were built by [81]. Geometric shape and dynamics of mooring lines were evaluated in the time domain. A hybrid beam element was employed to simulate the mooring cable while the seabed was simulated

by application of different soil constitutive models. Tensions and offsets of the mooring cables at the fairlead point were compared accounting for friction effect between cables and seabed. It was concluded that the frictional contact between seabed and mooring cables must be considered in deepwater mooring design and elastic and elastic-plastic soil model of the seabed resulted in the same stress value. Hence, the elastic foundation method was adequate for solving this kind of problems.

Also, the stiffness coefficients were evaluated using a 2D FE model with eight noded isoparametric element of the slack mooring lines derived from basic catenary equations of the cable by [82]. The hydrodynamic coefficients and wave exciting forces were evaluated using a 2D FE technique with eight noded isoperimetric element. The theoretical model was supported by an experimental model conducted in a wave flume. The motion responses and mooring forces were measured for three different mooring configurations. The comparisons between the theoretical and experimental measurements showed good agreement except at the roll resonance frequency. In this study, it was concluded that the mooring line forces were significantly affected by the mooring line configuration and mooring forces at lower excitation frequencies.

Recent development on the dynamic analysis of mooring lines, that allow for large mooring elongation was introduced as an extended scheme by [83]. The predicted tensions and the trajectory of the mooring lines based on the extended numerical scheme were found in satisfactory agreement with those of laboratory measurements. The prediction based on numerical schemes for mooring lines assume that the mooring lines were inextensible or undergo small elongation match poorly. It was concluded that since mooring lines with inserted springs are often used in the model tests of a moored deepwater floating offshore structure, the extended numerical scheme was useful in designing a mooring line model for the wave basin tests and in examining the corresponding measured responses of the floating structure model and tensions in its mooring line system.

2.2.6.1 Mooring to seabed interactions

Several attempts have been made to investigate the effects of this nonlinear interaction to the dynamic response on the mooring system. The effect of soil on mooring system dynamics through development of two FE numerical models was conducted by [84]. In addition, centrifuge tests were conducted in order to verify and calibrate the numerical tools. The first FE method implicitly modeled the embedded portion of the mooring line by lumping their effects at one generalized element at the seafloor surface. The other method explicitly modeled the local soil resistance along the embedded line. The basic components in both models included a nonlinear spring and two dashpots. Experimental tests indicated significant energy absorption behavior of the embedded mooring line. It was concluded that the mooring line forces considering the line-soil interactions might become much lower if this interaction is not considered.

The effect of current and seabed friction on mooring line tension and energy dissipation were studied in both the time domain and the frequency domain by [85]. In the time domain, the nonlinear hydrodynamic drag force and soil stiffness and friction were taken in consideration. In the frequency domain, the drag force was linearized by statistical linearization method and the mooring to seabed interaction was modeled by the stochastic linearization technique with constant Coulomb frictional force. The comparison between the time domain and the frequency domain results were found to be good and promising. It was concluded that the seabed friction increased the energy dissipation.

The dynamics of catenary moorings in the region surrounding the touchdown point were studied using experiments and numerical simulations by [86]. Special emphasis was kept on mooring line tension shocks when the touchdown point speed exceeds the transverse wave speed. The analytical derivation of the shock criterion was reviewed and verified using experimental results. Simulations of the touchdown model were modeled using the elastic foundation approach and they were found to be accurate for cases with or without shocks.

A new method for modeling the interaction between the mooring line and seabed without considering the frictional and impact effects in the frequency domain were

introduced by [87]. The section of the cable interacting with the seabed was truncated and replaced with system of nonlinear springs with stiffness values linearized from static catenary equations. These springs simulate the behavior of the truncated cable and the time varying boundary condition at the touchdown. The cable-spring was analyzed in the frequency domain with a centered finite difference scheme. The proposed method was shown to increase the accuracy of the mooring line frequency domain analysis.

A numerical method to model the interactions of low tensions cables with the seabed were presented by [88]. The seabed was modeled as an elastic foundation with linear damping and prescribed topology. The finite difference scheme in the time domain was adopted for the numerical algorithm. The developed numerical algorithm was used to simulate the 2D cable lying, dropping and towing in an uneven seabed. The results were compared to the results found in the literature and with the closed form solution for a perfectly elastic cable and found to have good convergence.

The use of the slip line method or the method of characteristics to solve the classical geotechnical bearing capacity problem of a vertically loaded rigid strip footing rested on cohesive-frictional half space was adopted by [89]. The results confirmed the exact plasticity of the bearing capacity problem. Also, the indentation of the touchdown region of pipelines was studied by [90]. The bottom interactions were modeled by the rigid plastic seabed. Analytic solution of the problem verified the field observation that large indentations can occur, particularly when the line tension is low. In addition, a laboratory testing program was initiated to investigate the potential changes in stiffness for soils in the touchdown point region of a steel catenary riser by [91]. The tests were performed using a T-bar apparatus, which was used to determine the shear strength of clay soils. The normalized stiffness was found to match experimental results, which were obtained with pipe tests for upload-reload cycle of loading and hence confirming the normalized technique.

Recently, 3D experiments investigating that interaction of a model steel catenary riser with the seabed was conducted by [92]. The model riser pipe was 7.65 m long and 110 mm diameter and was loaded by both monotonic and cyclic motions via a computer-controlled actuation system. In these experiments, the pipe was placed on a

bed of sand for benchmarking purposes. Numerical analysis was used to determine the nonlinear distribution of the soil reaction along the length of the embedded line. Result from numerical and experimental models were compared and good agreement was found. In addition, a straightforward procedure for the evaluation of the touchdown point and the distribution of the bearing pressure was given.

2.3 Critical literature review

2.3.1 Wave frequency responses

This category is associated with the analysis and design of conventional moored semi submersibles for the dominant wave frequency excitation. In this research area, most of the studies were following the hypothesis adopted by [8], assuming that the total hydrodynamic effect may be estimated by adding effects on individual elements. Only few studies, such as [93], considered the dynamic interference between the vertical members. However, there is no complete and deterministic approach for six degrees of freedom hydrodynamic coupled analysis. Also, the interactions between the mooring system and the floating platform in 3D analysis have not been reported so far. Although some parametric studies were made, there is no available study on the effects of the semi submersible element dimensions and spacing, the wave characteristics and the operating conditions on the wave frequency motions.

2.3.2 Low frequency response

In this category, the analysis and design of conventional moored semi submersible to drift excitation was attempted. The most intensive work regarding this category was conducted by [18]-[20]. Stationary floating platforms in irregular waves are subjected to large, so called first order wave forces, which are linearly proportional to the wave height and which have the same frequencies as the waves. They are also subjected to small, so-called second order, mean and low frequency wave forces. The frequencies of the second order low frequency components are associated with the frequencies of the wave groups occurring in irregular waves. In case of mooring systems, the second order wave forces are of great importance. When the incident waves include slowly

varying components, the frequency of these components may be close to the natural frequency of the mooring system, thus possibly causing breakage of anchor lines and the mooring system [24].

The components of mean and low frequency second order wave forces can affect different structures in different ways and though of the same origin, they have been called by different names. The horizontal components of the mean and low frequency second order wave forces are also known as wave drift forces because, under the influence of these forces, an unrestrained floating platform undergoes a steady slow drift motion in the general direction of the wave propagation. The vertical components of the second order wave forces are sometimes known as suction forces. These components of the second order forces have been identified as causing the phenomena of the steady tilt of semi submersibles with low initial static stability as indicated by [94]-[96]. Depending upon the frequency of the waves, it has been found that the difference in the suction forces can result in a tilting moment, which can cause the platform to tilt away from the oncoming waves. This effect is of importance in specifying the static stability requirements for semi submersibles.

Semi submersibles are usually designed such that their natural frequencies, in various modes of platform motion, lie outside the frequency range of maximum wave energy. The typical natural periods of semi submersible platforms given by [2] and [25] are presented in Table 2.1. It can be seen from this table that the risk of existence of springing forces is high in the horizontal (surge, sway and yaw) degrees of freedom and should be considered in the design of the mooring system.

Table 2.1: Typical natural periods of semi submersibles

Mode of Motion	Natural Period (s)
Surge, Sway	> 60
Heave	20~25
Pitch, Roll	20~30
Yaw	>100

The second order reactive force component due to the effect of free surface fluctuation (FSF) on the hydrostatic stiffness and added mass was found to produce sum-frequency forces and has no contribution to the difference frequency force [28]. Also, it was shown in [29] that the second order force due to convective acceleration was very close to the negative of that due to FSF. Also, the second order force due to

axial divergence was shown to have the smallest contribution to total second order force [28].

Second order forces and the related phenomenon to regular, group and irregular wave trains were taken into consideration with an emphasis on the low frequency damping. There is no an appropriate methodology and efficient computational technique for the evaluation of the second order forces due to low frequency resulting from wave to wave interactions applicable to semi submersible. Furthermore, semi-empirical methods used for the evaluation of the steady drift forces assuming no dynamic interference have not been justified for floating structures with an array of vertical cylinders like semi submersibles.

2.3.3 Responses to extreme environmental conditions

The research in the third direction was subjected to damage conditions of semi submersibles in rogue waves during hurricanes. Various experimental investigations were carried out by different researchers after the Alexander Kielland and the Ocean Ranger disasters [97]. Moreover, considerable research was made following the damage caused by hurricanes Katrina and Rita in GOM by 2005. Most of the studies were concentrating on the hydrostatic stability and the structure integrity. Number of authors have reported that the improvement of the performance of mooring can contribute effectively towards preventing platform dragging. There has not been any work reported on this improvement. Reviewing current air-gap standards to avoid deck inundation and foundation failures and recent hurricanes need to be included in the met-ocean data to inform re-evaluation of the current design standards. Also, the effects of damaged mooring lines have not been reported in the literature.

2.3.4 Addition of heave plates

The fourth research direction was about the motion characteristics of conventional semi submersibles with heave plates. The foundation for this research category was established by [39]. Research results demonstrated that the excitation of a semi submersible hull by the environment can be adequately mitigated by the proper

placement and sizing of a heave plate system. It was reported that further research was needed to assess the responses (especially stroke and tension responses) of risers attached to deep draft semi submersibles equipped with heave plates.

2.3.5 Innovation semi submersibles

The fifth research area reported in the literature covers the innovation and new generation semi submersibles. This research was initiated by [39]. All innovations aimed to improve the structure hydrostatic and hydrodynamic stability characteristics. This research area is always under great demand, since sustainable development is required by the oil and gas industry.

2.3.6 Station-keeping systems

The final (six) research area is on the station keeping facilities, including mooring systems; thruster assisted mooring systems and dynamic positioning systems for stationary semi submersible. Mooring systems are used intensively for stationing floating production platforms such as semi submersibles. The mooring system is a conventional network of multi-component lines, each of which is either a single cable connecting to a bottom anchor or a multi-component combination of anchor, clump weight, chains and cables. The most common mooring system employed is the catenary system due to its topological simplicity. With increasing water depth, the required weight of the mooring lines increases and multi-component mooring lines with concentrated or distributed clump weights is usually used. The weight of the mooring lines become a limiting factor in the design of the platforms in deepwater.

Dynamic analysis accounted for the time varying effects due to mass, damping, and fluid-line relative acceleration. In this approach, the time varying fairlead motions were calculated from the platform's surge, sway, heave, pitch, roll, and yaw motions. Dynamic models were used to predict the mooring line responses to the fairlead motions, as recognized by the API [4]. Two methods, frequency domain and time domain analyses were used for predicting dynamic mooring loads. In the time domain method, all nonlinear effects including line stretch, line geometry, fluid

loading, and sea bottom effects were modeled. On the other hand, the frequency domain method is always linear and the linear principle of superposition is used. Methods to approximate nonlinear effects in the frequency domain and their limitations should be investigated to ensure acceptable solutions for the intended operation.

Based on the reported literature, the quasi-static analysis of mooring lines utilizing the nonlinear catenary equations is considered as the general accepted method for mooring system design. The assumptions adopted ignoring the fluid to mooring and mooring to seabed nonlinear interactions made this approach to have significant limitations regarding the computation efficiency and accuracy of the results. Traditionally, the inclusion of mooring line effects in the analysis of the motions of moored floating structures was carried out using the quasi-static methods [65]. In this approach, the mooring line was assumed to respond statically to the environmental actions and floating platform motion excitation. This quasi-static behavior of mooring systems was possible because the response of the mooring platform was normally outside the frequency range of the mooring system. However, this kind of analysis ignores the effect of line dynamics, which in some situations may be a significant element in the dynamic analysis of a moored offshore platform [3]. From both theoretical and experimental research, it has been established that the dynamic behavior of a mooring line induced by high frequency oscillations of the upper end contributes significantly to the line tensions and the motions [63].

In the mooring system design, a quasi-static analysis method was often used for evaluating the performance of a mobile mooring system, and the effects of line dynamics were accommodated using a relatively conservative safety factor. With the advent of moorings in very deepwater, a more rigorous dynamic analysis is required for the final design of a permanent mooring system, and the factor of safety is relaxed to remove some uncertainty in line tension prediction. [60] suggested using the method given by [55]-[56]. This method becomes more complicated for analyzing multi-component mooring lines compared to the method introduced by [57]-[58].

For the dynamic analysis of mooring systems, most researchers adopt one of two methods, either lumped mass method (LMM) or finite element method (FEM). The

LMM is the most widely adopted method [64]. The application of LMM to the dynamic mooring problem was first applied by [61]. They provided some details of the formulation and solution techniques neglecting the mooring material elasticity, but information was given about the fluid reactive forces and method validation. The explicit difference scheme was adopted to solve the problem with conditionally stable outputs. Other studies using this method [62]-[63], [65]-[66], [98] gave a summary of the formulation and solution providing case studies and discussions. [62] extended the model of [61]. They included material elasticity and seafloor lifting and grounding model neglecting the grounded part of the mooring line by forcing the first two suspended node masses that touched the seafloor to vanish.

The LMM involved lumping of all effects of mass, external forces and internal reactions at a finite number of points along the line. The behavior of a continuous mooring line was modeled as a set of concentrated masses connected by mass-less springs. By applying the dynamic equilibrium conditions and equation of stress/strain continuity to each mass, a set of discrete equations of motion was derived. In this method, material damping, bending and torsional stiffness were usually neglected [65]-[70]. This approach of modeling the mooring line basically resulted in the partial differential equations (PDEs), which were replaced by a set of ordinary differential equations (ODEs). The latter equations were solved in time domain using an appropriate time integration scheme.

On the other hand, the FEM utilizes interpolation functions to describe the behavior of a given internal variable to an element in terms of the displacements of the nodes in generalized co-ordinate system. The equations of motion for a single element are obtained by applying the interpolation functions to kinematic and constitutive relations and the equations of the dynamic equilibrium. The solution procedure is similar to the LMM. Various models based on the FEM have been presented either using linear or higher shape functions [68]-[70], [75]. The FEM has the advantage that it can be extended to analyze lines having significant bending and torsional stiffness amounts. However, computer codes based on this method have lesser computation efficiency when compared with the LMM algorithms.

Considerable research has been done considering this area, especially for the uncoupled quasi-static analysis of mooring systems [73], [83]. Some authors adopt the frequency domain or time domain analysis. It was found that the frequency domain simulations gave basically similar results to those of time domain with higher cable tensions for mooring lines partly lying on the seabed because the frequency domain method did not take into account the effect of mooring to seabed interaction. On the other hand, some studies on the line to seabed interactions were done with no frictional contact between seabed and mooring cables being considered. Further research is needed to model all nonlinearities associated with mooring lines, including the mooring to seabed interactions.

2.3.6.1 Mooring to seabed interactions

Recently, considerable work has been done to study the static and dynamic analysis of mooring lines. Preliminary analysis results conducted by the US Navy indicated that the resulting mooring line forces using some form of soil-structure interaction were less than those evaluated assuming fixed end conditions [84]. Meanwhile, intensive work was done on seabed-risers-pipelines' interactions. [90] extended the analysis of the pipe-laying on a rigid-plastic seabed, and confirmed the field observation that large indentations occurred, particularly when the tension was low. A laboratory testing program was initiated by [91] to investigate potential changes in stiffness for soils in the TDP region of a steel catenary riser. [92] introduced a form for the nonlinear soil reaction for SCR pipe lying on a bed of sand numerically and experimentally based on an exact soil bearing capacity following [89] calculations. [92]'s soil interaction model represented a benchmark work for future studies on seabed-line interactions.

Seabed interaction belongs to one of two scenarios: the frictional effects between the seabed and the mooring line and the lifting and grounding (LG) interactions and applied in [62],[65]. The first scenario is a physical effect usually considered in case of relatively long grounded lines (e.g. pipelines). Very little literature deals directly with seabed friction on mooring lines such as given by [85]. The second scenario is a

modeling problem which plays an important role in the mooring line dynamic response system [86].

Three basic approaches were used to model this bottom interaction in numerical simulations. The first approach was to cut the mooring off at the TDP and attach an equivalent linear spring and/or dashpot, which was used in frequency domain models [87] and in some time domain models as given by [99]. This approach was valid for small dynamic motions about the static TDP. The second approach was the lift-off and grounding approach introduced by [62] and modified by [65]. In this method, the grounded part of the mooring line was neglected and the masses of the nodes approaching the seabed were reduced in order to avoid unrealistic impact. Mass modifiers based on parabolic mass distribution of the line were applied as multipliers of the lumped masses to the suspended first two nodes. These mass modifiers allowed the node grounding smoothly, reducing the nodal mass to zero at the seabed. This approach simulated a rigid bottom with no impact allowed to occur (especially for nodes attached with clump weight) and a smooth rolling and unrolling of the cable. The third approach was to model the seabed as an elastic foundation. This was used in [63], [68], [86], [88] and by [100]. Although this model has been associated difficulties in determining appropriate stiffness and damping values for a given liquefied soil, it was the most convenient model for the mooring to seabed interaction problem.

2.4 Chapter Summary

The research studies handling the dynamic analysis of moored semi submersibles reported in the literature over the few decades were surveyed and categorized into six general motivations, the development and the critical review of each category was presented. The summary of critical literature review is given bellow:

1. Lot of research has been conducted for the analysis of conventional moored semi submersibles to first order excitation. Very few studies have taken the proximity of vertical cylinders in consideration. A deterministic approach for six degrees of freedom hydrodynamic coupled analysis taking floating platform–mooring system interactions in 3D analysis is needed. Also, a

parametric study for the station-keeping characteristics for different semi submersible configuration is needed.

2. Lot of work regarding steady and low frequency second order hydrodynamic forces and responses of conventional semi submersible have been made. Still, there is a gap for finding computationally efficient methodology for the assessment of these components.
3. Numerous studies have been reported for the analysis of mooring line, most of them considering the quasi-static responses of mooring lines. Yet, an efficient methodology is needed for the evaluation of nonlinear force-excursion relationship for single lines fully suspended or partially lying on the seabed and for multi-component mooring. Also, a complete modelling of the nonlinearities associated with catenary shaped mooring lines in time domain is not available.

Chapter 3

WAVE TO WAVE AND WAVE TO PLATFORM INTERACTIONS

3.1 Chapter overview

In this chapter, the method of investigation the wave to wave and wave to platform interactions are presented. The hydrostatic stability conditions and the methods for evaluating the platform hydrostatic characteristics are described. Also, the nonlinear hydrodynamic boundary value problem formulated from the wave to wave and wave to platform interactions is formulated. The conventional nonlinear solution of the problem and the simplified solution are presented together with the methodology for simulation of the random sea energy. Also, the methodology for the evaluation of the hydrodynamic wave forces on semi submersibles is also presented.

3.2 Hydrostatic analysis of floating structures

The hydrostatic stability of compliant floating offshore structures plays an important role in their design and operating effectiveness. In case of conventional rigid floating structures, like semi submersibles, the hydrostatic stability is the limited criterion for the deck payload capacity. Therefore, it is important to consider the hydrostatic stability of a compliant structure very carefully for its impact on its payload performance and on its dynamic response in waves [2]. The key analytic areas for hydrostatic analysis include the platform mass distribution, CG to keel point distance (KG), CB to keel point distance (KB), radius of gyration for roll, pitch and yaw motions (r_x, r_y, r_z) and MC heights for roll and pitch (GM_x, GM_y). The definition of keel, CG, CB and MC height of the structure are presented in Fig 3.1.

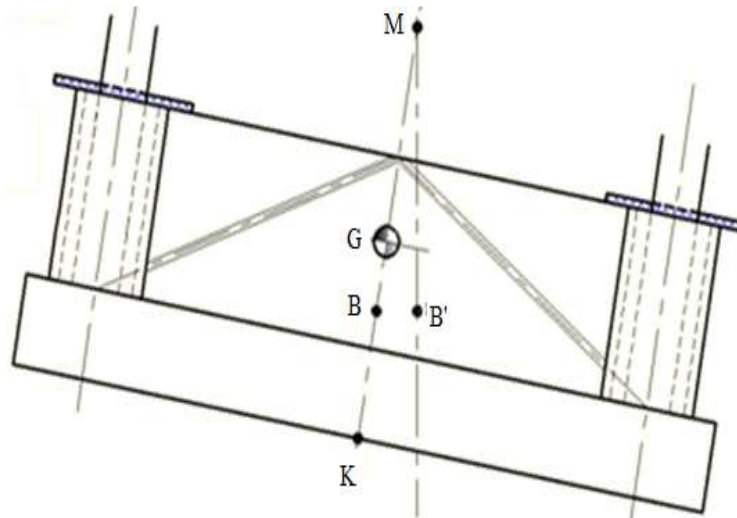


Fig 3.1: Structure Keel, CG, CB and MC definition

For a floating system to be positively stable, the GM should be positive. The MC can be likened to the centre of oscillation of a suspended pendulum. Therefore, GM becomes the length of the string, and for the pendulum to swing in a stable oscillation and return to its original position, the centre must be above the pendulum. For a submerged object to be stable, the CG must be below the CB. However, since the point of action of buoyancy is fixed along the line of gravity and does not change, the metacenter is B itself. The criterion $GM > 0$ thus still holds well. In this study for the evaluation of these quantities, the total mass of structure was distributed by the mass weight ratios for the elements of the structure. The distance KG was located by the averaging the relative distance of the member CG weighted by their masses. In a similar manner, the CB was located for the displaced water. The MC height (as defined in Fig 3.1 is given by Eq 3.1.

$$GM = KB + BM - KG \quad (3.1)$$

where

$$BM = \frac{I_A}{\Delta}$$

3.3 Hydrodynamic theory

Theoretical simulation of water waves and sea motion in general involves rigorous mathematical analysis. The basic hydrodynamic equations that govern the wave

kinematics are the equation of continuity (Laplace's equation) and the equation of the conservation of the momentum (Bernoulli's equation). The form and solution of these equations vary depending on the intended application of the wave kinematics. However, in general, all solutions assume incompressible, inviscid and irrotational fluid particles. The simplest solution of the hydrodynamic equations involves further assumption, that the waves are of small amplitude compared to the water depth and the wave length. This solution was introduced by Airy (1845) and became known as the linear Airy wave theory.

Higher order wave theories are not based on the assumption of small amplitude to solve the hydrodynamic equations. Instead, they include terms higher than first order in the solution. Stoke (1847) developed equations for waves of finite amplitude by accounting for terms up to fifth order. The successively higher order theories give wave surface profiles that are steeper and flatter in the trough than those given by the linear wave theory. Dean (1965) developed the stream function wave theory which is numerical solution to the hydrodynamic equations and has demonstrated good agreement with experimental wave channel test results for a wide range of H/T^2 ranges [101]. Many other analytical and numerical wave theories have been developed and are available in the literature.

Most of the recent water wave theories are based on environmental parameter of water depth, wave height and wave depth. Generally, these theories have been developed by solving a boundary value problem (BVP) through simplifying the problem utilizing certain assumptions. The general solution of the BVP is not possible due to the nonlinearities associated with the governing equation and the boundary conditions. The perturbation parameter is the general approximation technique used for deepwater wave problem as presented in following sections.

3.3.1 Nonlinear boundary value problem (NBVP)

For the formulation of the water waves nonlinear boundary value problem, it was assumed that the fluid is ideal (inviscid and incompressible), the flow is irrotational and continuous and the atmospheric pressure outside the fluid is constant. Moreover,

the floor of the ocean is flat, impermeable, intermediate with respect to long waves and deep to short waves. Furthermore, the wave amplitude is small compared to the wave length and water depth. The continuity of the flow implies mass conservation of the fluid. This condition is mathematically represented by the continuity equation in-terms of the fluid velocity (V) as expressed in Eq 3.2.

$$\nabla V = 0 \quad (3.2)$$

where

$$\nabla = \frac{\partial}{\partial x} \vec{i} + \frac{\partial}{\partial y} \vec{j} + \frac{\partial}{\partial z} \vec{k} \quad (3.3)$$

The ir-rotational fluid flow implies that the existence of fluid velocity potential Φ [102], from which the three components of the fluid particle velocity are evaluated as given by Eq 3.3.

$$\vec{u} = \frac{\partial \Phi}{\partial x}, \quad \vec{v} = \frac{\partial \Phi}{\partial y}, \quad \vec{w} = \frac{\partial \Phi}{\partial z}$$

Substituting Eq 3.3 in Eq 3.2, the governing (Laplace's) equation for the NBVP is obtained as given by Eq 3.4.

$$\frac{\partial^2 \Phi}{\partial x^2} + \frac{\partial^2 \Phi}{\partial y^2} + \frac{\partial^2 \Phi}{\partial z^2} = 0 \quad (3.4)$$

The general form of the NBVP governing equation is expressed in Eq 3.5.

$$\nabla^2 (\Phi^{(1)} + \Phi^{(2)} + \dots) = 0 \quad (3.5)$$

The solutions of Eq 3.3~3.4 provide the wave kinematics. The Bernoulli's equation was used to define the wave kinetics as given by Eq 3.6.

$$\rho \frac{\partial \Phi}{\partial t} + p + \rho g z + \frac{\rho}{2} \left(\frac{\partial^2 \Phi}{\partial x^2} + \frac{\partial^2 \Phi}{\partial y^2} + \frac{\partial^2 \Phi}{\partial z^2} \right) = f(t) \quad (3.6)$$

where p is the hydrodynamic pressure and $f(t)$ is an arbitrary function (time dependant). Since the fluid is bounded by the ocean bottom, the free surface and the floating platform, the governing differential equation must satisfy the conditions at theses boundaries. Using the assumption that the floor of the ocean is flat, the boundary condition at the ocean bottom states that the fluid vertical velocity component is zero at the bottom, as expressed in Eq 3.7.

$$\frac{\partial \Phi}{\partial z} = 0, \text{ at } z = -d \quad (3.7)$$

At the point of intersection of the platform and the fluid, the velocity of water particles must be the same as the velocity of the platform V_n as expressed in Eq 3.8.

$$\frac{\partial \Phi}{\partial n} = V_n, \text{ on the surface of the platform} \quad (3.8)$$

The free surface is governed by two boundary conditions, kinematic and dynamic [103]. The first boundary condition states that a fluid particle lying on the free surface at one instant of time will continue to remain on the free surface. Mathematically, this condition is expressed in Eq 3.9.

$$\frac{\partial \Phi}{\partial z} = \frac{\partial \eta}{\partial t} + u \frac{\partial \eta}{\partial x} + v \frac{\partial \eta}{\partial z}, \text{ at } z = \eta \quad (3.9)$$

Assuming constant pressure on the free surface, the dynamic free surface condition is derived from the Bernoulli's equation (Eq 3.6) as given by Eq 3.10.

$$\rho \frac{\partial \Phi}{\partial t} + \rho g \eta + \frac{\rho}{2} \left(\frac{\partial^2 \Phi}{\partial x^2} + \frac{\partial^2 \Phi}{\partial y^2} + \frac{\partial^2 \Phi}{\partial z^2} \right) = f(t) \quad (3.10)$$

The exact solutions for the potential function in the Laplace's governing equation with the present state of knowledge is not possible due to the nonlinear free surface boundary conditions (the product of velocity with the free surface slope in the kinematic conditions and the velocity square terms in the in the dynamic condition). In addition, the free surface where the conditions are applied is time dependant and its location is unknown. In this study, the most popular approach to solve the problem is adopted, which called the perturbation method. Based on the assumption of small wave amplitude, this method can be used to obtain an approximate solution, which partially satisfies the free surface boundary conditions. In this method, the solution for the potential function and the wave elevation are assumed to take the form of a power series [104] as given by Eq 3.11~3.12.

$$\Phi = \sum_{n=1}^{\infty} \xi^n \Phi^{(n)} \quad (3.11)$$

$$\eta = \sum_{n=1}^{\infty} \xi^n \eta^{(n)} \quad (3.12)$$

On the solution of the BVP, firstly substituting Eq 3.11~3.12 into the governing equation (Eq 3.5) and the boundary conditions in the absence of the platform (Eq 3.7, 3.9~3.10). Secondly, the free surface boundary conditions (Eq 3.9~3.10) are expanded into truncated Taylor series at the desired solution order and about the still water level ($z = 0$). Finally, the governing equation and boundary conditions can be grouped and solved at each order of wave steepness starting with the first order equations.

3.3.2 The conventional solution for the NBVP

The potential elevation for the interaction of irregular incident waves with frequencies ω_1 and ω_2 ($\omega_1 < \omega_2$) having amplitudes of a_1 and a_2 , were derived up to the second order by [105] using a conventional perturbation approach. This derivation has been used by many researchers, for example [26]-[29]. The first and the second order incident wave potentials are given by Eq 3.13~3.14 respectively.

$$\phi^{(1)} = \sum_{j=1}^N \frac{a_j g}{\omega_j} \frac{\cosh k_j(z+d_w)}{\cosh k_j d_w} \sin \theta_j \quad (3.13)$$

$$\begin{aligned} \phi^{(2)} &= \sum_{j=1}^N \frac{3}{8} a_j^2 \omega_j \frac{\cosh 2k_j(z+d_w)}{\sinh^4 k_j d_w} \sin 2\theta_j + \sum_{i=1}^N \sum_{j=1}^N A_{-} \frac{\cosh k_{-}(z+d_w)}{\cosh k_{-} d_w} \sin \theta_{-} \\ &+ \sum_{i=1}^N \sum_{j=1}^N A_{+} \frac{\cosh k_{+}(z+d_w)}{\cosh k_{+} d_w} \sin \theta_{+} \end{aligned} \quad (3.14)$$

where

$$A_{\mp} = \pm \frac{a_i a_j \omega_j (\alpha_i \alpha_j \mp 1)}{2} \left[\frac{2\lambda(1 \mp \lambda)(\alpha_i \alpha_j \pm 1) \mp \lambda^3 (\alpha_j^2 - 1) + \alpha_i^2 - 1}{(\alpha_j - \alpha_i \lambda)^2 - (1 - \lambda)^2} \right]$$

$$k_{\mp} = k_j \mp k_i, \lambda = \frac{\omega_i}{\omega_j}, \theta_{\mp} = \theta_j \mp \theta_i, \theta_j = k_j x - \omega_j t + \beta_j, \alpha_j = \coth k_j d$$

k_j is the number of the wave component j and d_w is the water depth. It is worth mentioning here that only the second term of Eq 3.14 is relevant to second order slow frequency forces since this study aimed to evaluate the forces which may cause the dynamic amplification.

3.3.2.1 Linear Airy wave theory

A linearized solution of the previously mentioned BVP has been introduced by Airy (1845) and became known as the linear (Airy) wave theory (LWT). The LWT was found to give wave forces close to those obtained using higher order wave theories, provided a proper method of calculating wave forces is used with suitable choice of the hydrodynamic force coefficients [29], [106]. In addition, the LWT was shown to provide good solution in deepwater (when $d_w/L_w > 0.5$). The linear wave theory was used since it is simple and reliable over a large segment of whole wave regime and sufficient to obtain the kinematics of waves to be used in the analysis of semi submersible platforms in deepwater for the range of water depths, wave periods and wave heights used for the first order analysis. A schematic diagram of an elementary, sinusoidal progressive wave is presented in Fig 3.2.

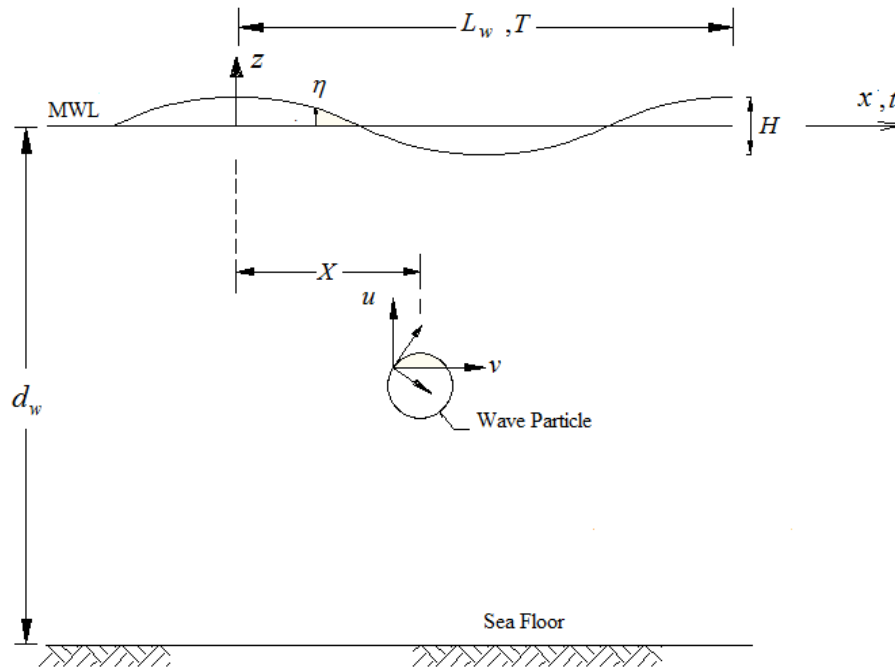


Fig 3.2: Schematic diagram for a progressive wave train

For the LWT, only the first order terms in the governing equations and the boundary conditions of the BVP are retained (Eq 3.5~3.10). The solution (Eq 3.13) is obtained by assuming that the velocity potential and wave elevation have the form represented by the first terms of Eq 3.13~3.12. The velocity of the fluid particle was evaluated by plugging Eq 3.13 in Eq 3.14 and the fluid acceleration was evaluated as the first derivative of the velocity with respect of time. Thus by the LWT, the wave

kinematics at depth z below the MWL are given by Eq 3.15~3.20. It should be noted that in LWT, the wave length is related to the water depth by the linear dispersion (Eq 3.13) relationship. This was evaluated by plugging the first order velocity potential (Eq 3.13) in the combined free surface boundary condition, evaluated by eliminating $\eta^{(1)}$ from the free surface boundary conditions (Eq 3.9~3.10). Applying first order velocity (Eq 3.13) potential to the dynamic boundary condition (Eq 3.12), the wave profile was obtained (Eq 3.20). It should be noted that the formulae for the wave kinematics, dispersion relationship and the wave profile (Eq 3.15~3.20) are for random wave with N regular components. The same formulae were used for regular waves with only one component (without summation and random phase).

$$u = \sum_{j=1}^N \frac{a_j g}{\omega_j} \frac{\cosh k_j(z + d_w)}{\sinh k_j d_w} \cos \theta_j \quad (3.15)$$

$$v = \sum_{j=1}^N \frac{a_j g}{\omega_j} \frac{\sinh k_j(z + d_w)}{\sinh k_j d_w} \sin \theta_j \quad (3.16)$$

$$\dot{u} = \sum_{j=1}^N \frac{a_j g}{\omega_j} \frac{\cosh k_j(z + d_w)}{\sinh k_j d_w} \sin \theta_j \quad (3.17)$$

$$\dot{v} = - \sum_{j=1}^N \frac{a_j g}{\omega_j} \frac{\sinh k_j(z + d_w)}{\sinh k_j d_w} \cos \theta_j \quad (3.18)$$

$$\omega^2 = gk \tanh k d_w \quad (3.19)$$

$$\eta = \sum_{j=1}^N a_j \cos \theta_j \quad (3.20)$$

Generally, in the design of offshore structures, an important step is to select the most appropriate mathematical wave spectrum representing the wave energy of the site where the structure is proposed.

3.3.3 Mathematical spectrum models

The mathematical spectrum models are generally based on one or more parameter (e.g. significant wave height, wave period, shape factor, etc.). The most common single parameter spectrum is the Pierson-Moskowitz (PM) model based on the significant wave height or wind speed. There are several two parameter spectra available, some of these, which are commonly used, are Bretschneider, Scott, the International Ship Structures Congress (ISSC) and the International Towing Tank

Conference (ITTC). A Joint North Sea wave Project (JONSWAP) spectrum is a five-parameter spectrum, but usually three of the parameter are held constant. A more complex spectral model has been presented by Ochi and Hubble, which is six-parameter spectrum. It describes two peaks in the energy spectrum (e.g. in a wind generated sea mixed with swell) [103]. In this study, PM and JONWAP mathematical spectrums were adopted for the modeling of the random sea energies.

3.3.3.1 Pierson-Moskowiz spectrum

The PM spectrum describes the energy of wind-generated sea-state, which has been used by many of engineers and it was found that it is one of the most representative spectrum for many areas over the world. The PM spectrum model is mathematically presented by Eq 3.21.

$$S(\omega) = \frac{0.0081g^2}{(2\pi)^4} \omega^{-5} \exp\left[-1.25\left(\frac{\omega}{\omega_o}\right)^{-4}\right] \quad (3.21)$$

where

$$\omega_o = \frac{0.161g}{H_s}$$

3.3.3.2 The JONSWAP spectrum model

During a joint North Sea wave project, Hasselman *et al.* [103] developed JONSWAP mathematical spectrum model. The JONSWAP spectrum accounts for the effect of fetch-limited condition and is much sharply peaked than the PM spectrum. The JONSWAP spectrum model is given by Eq 3.22.

$$S(\omega) = \frac{0.0081g^2}{(2\pi)^4} \omega^{-5} \exp\left[-1.25\left(\frac{\omega}{\omega_o}\right)^{-4}\right] \gamma^{\exp\left[-\frac{(\omega-\omega_o)}{(2\tau^2\omega_o^2)}\right]} \quad (3.22)$$

where γ is the Peakedness parameter (taken as 2.0) and τ is the shape parameter (taken as 0.07 for $\omega \leq \omega_o$ or 0.09 for $\omega > \omega_o$). A comparison between the PM and

JONSWAP spectra wave energy distribution for the same wave characteristics (significant height of 3.25 m and peak frequency of 0.654 rad/s) are shown in Fig 3.3. It can be seen from the figure that at the peak frequency the JONSWAP spectrum gives higher power with narrow banded energy distribution. For this reason, JONSWAP spectrum is usually used for simulating the storm environmental conditions, while PM spectrum is used for simulating the operational conditions.

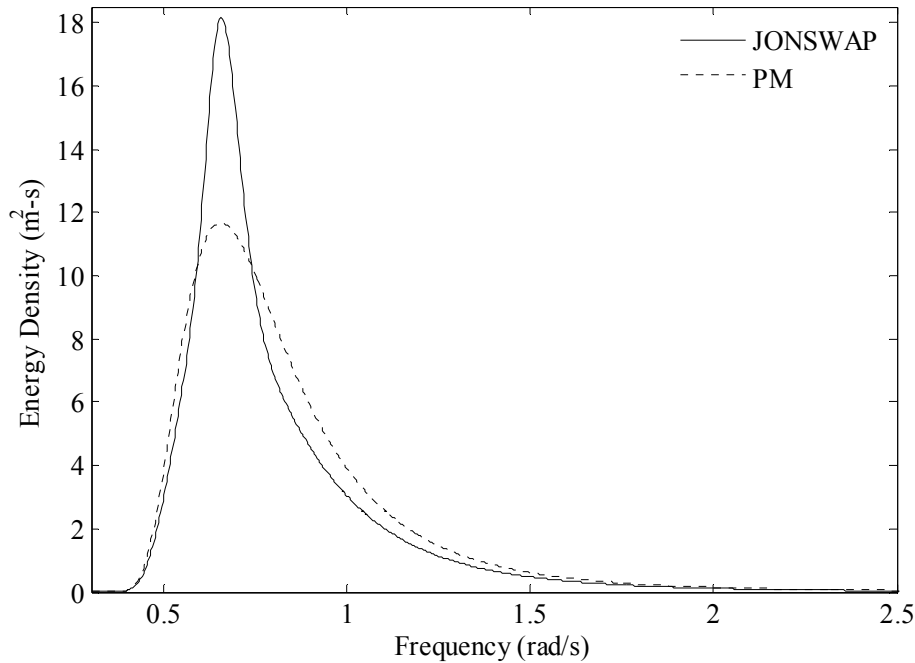


Fig 3.3: PM vs. JONSWAP wave spectrum

3.4 Wave force on semi submersibles

3.4.1 The force (Morison) equation

The original version of force (Morison) equation was proposed by [107] for the evaluation of the excited wave force on vertical pile, which is composed of two inertia and drag components. This equation is considered semi-empirical equation and was proved reliable for evaluating forces on slender rigid cylinders. Later, for compliant structures the original force equation was modified to account for relative velocity and acceleration between the structure and the fluid particles. The drag (F_D) and inertia

(F_I) forces on an element of a unit length of the cylinder are given by Eq 3.23~3.24 respectively. This formula of the force equation was used for evaluation of wave frequency forces.

$$F_D = \rho C_d \frac{D}{2} U_{rel} |U_{rel}| \quad (3.23)$$

$$F_I = \rho \frac{\pi D^2}{4} (C_m \dot{u} - C_A \ddot{x}) \quad (3.24)$$

where U_{rel} is the wave-structure relative velocity. On the other hand, [108] suggested a nonlinear axial divergence term to be added to the modified force equation. In this thesis, this form of force equation is called Rainey modified force (Morison) equation. This form of equation will be discussed when nonlinear wave forces are considered.

3.4.2 First order wave frequency forces

In the following formulation, wave forces and moments were derived based on the modified force (Morison) equation (Eq 3.23~3.24) for the analysis of the 3D first order motion responses for semi submersibles in the time domain. For each structural member, the relative velocity and acceleration were calculated based on the element position and the structure CG angular acceleration as shown in Fig 3.4. The member relative velocity and acceleration were evaluated by Eq 3.25~3.26.

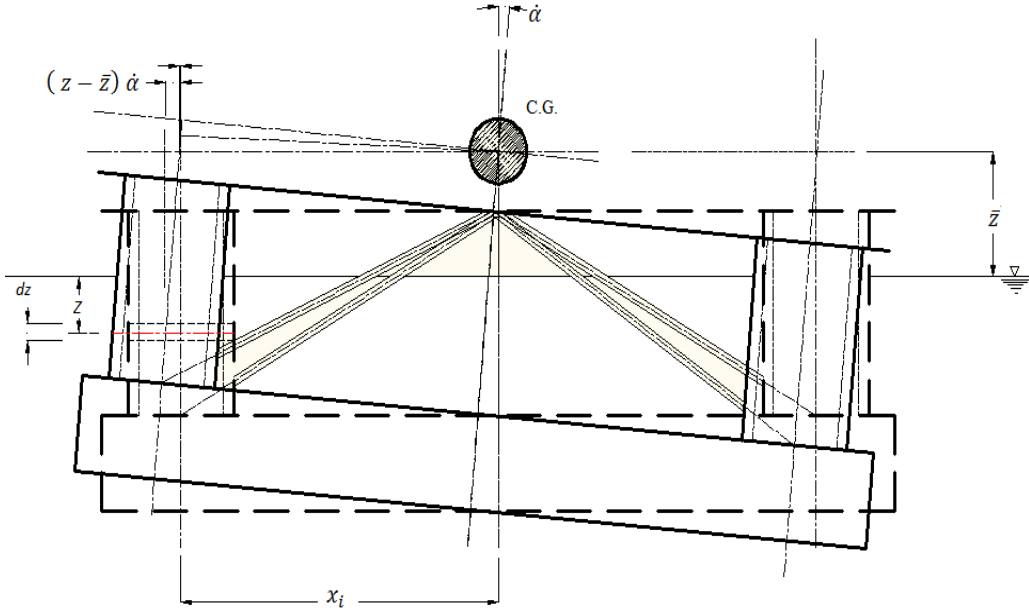


Fig 3.4: Velocity of an element along the i^{th} column arising from rotational motions

$$U_{rel} = u - \left[\dot{x}_g - (z - \bar{z})\dot{\alpha}_g + \frac{1}{2} x_i \dot{\alpha}_g^2 \right] \quad (3.25)$$

$$\ddot{x} = \ddot{x}_g - \left[(z - \bar{z})\ddot{\alpha}_g - \frac{1}{2} x_i \ddot{\alpha}_g^2 \right] \quad (3.26)$$

For the evaluation of the wave force, Eq 3.23~3.24 were numerically integrated along the wetted length of each column and over the whole length of hull to obtain the total instantaneous force on the structure. The moments of these forces about the structure CG were found by multiplying the force equations by appropriate moment arms and then integrated over the whole length of each cylinder to obtain the total moments. The details of the complete evaluation of the wave forces and moments are presented in Appendix A. A summary of the resultant forces and moments are given by Eq 3.27~3.32. The related numbering system of the semi submersible is shown in Fig 3.5.

$$F_{x_t} = \sum_{i=3}^{10} (F_{I_i} + F_{D_i}) \cos \phi_w + F_{p_{x_{hull1,2}}} \quad (3.27)$$

$$F_{y_t} = \sum_{i=3}^{10} (F_{I_i} + F_{D_i}) \sin \phi_w + F_{p_{y_{hull1,2}}} \quad (3.28)$$

$$F_{z_t} = F_{z_{hull1,2}} \quad (3.29)$$

$$M_{x_t} = - \sum_{i=3}^{10} (M_{I_i} + M_{D_i}) \sin \phi_w + M_{x_{hull1,2}} + M_{xv_{hull1,2}} \quad (3.30)$$

$$M_{y_t} = \sum_{i=3}^{10} (M_{I_i} + M_{D_i}) \cos \phi_w + M_{y_p} \quad (3.31)$$

$$M_{z_t} = \sum_{i=3}^{10} (F_{I_i} + F_{D_i}) Y_{c_{ih}} + M_{z_{hull1,2}} \quad (3.32)$$

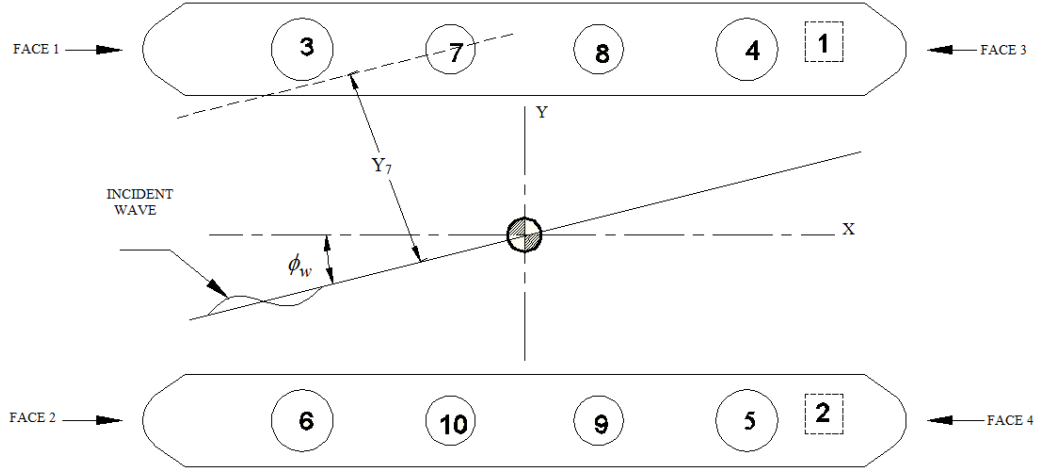


Fig 3.5: The numbering system for the semi submersible.

3.4.3 Second order low frequency forces

In the following formulations, only low frequency second order wave drift were considered since they may cause dynamic amplification in the horizontal plane of a moored as indicated in Table 2.1. These hydrodynamic forces were evaluated using the Rainey modified force equation [95] as given by Eq 3.33 for a unit length of a vertical cylinder. It is worth mentioning that the wave acceleration in Eq 3.33 is due to temporal (change with time) and convective (change with space) accelerations as demonstrated by Eq 3.34. The latter acceleration is nonlinear in nature.

$$F_x = K_I \dot{u} - K_{M_I} \ddot{x}_g + K_D (u - \dot{x}_g) |u - \dot{x}_g| + K_M (u - \dot{x}_g) \frac{\partial \omega}{\partial z} \quad (3.33)$$

$$\dot{u} = \frac{\partial u}{\partial t} + u \frac{\partial u}{\partial x} + w \frac{\partial u}{\partial z} \quad (3.34)$$

where

$$K_I = \rho C_M(\omega) \frac{\pi D^2}{4}, \quad K_{M_I} = \rho C_A(\omega) \frac{\pi D^2}{4}, \quad K_D = \rho C_D(\omega) \frac{D}{2}$$

3.4.3.1 Integration of the force equation

For a vertical cylinder having draft of h , the total wave force acting on it was evaluated by integrating Eq 3.33 over the whole length. Thus, up to second order, the wave force on a cylinder is given by Eq 3.35.

$$\begin{aligned}
 F_x = & \int_{-h}^0 K_I \dot{u}^{(1)} dz - \int_{-h}^0 K_{M_I} \ddot{x}_g^{(1)} dz - \int_0^\eta K_{M_I} \ddot{x}_g^{(1)} dz + \int_0^\eta K_I \dot{u}^{(1)} dz \\
 & + \int_{-h}^0 K_I \frac{\partial u^{(x)(1)}}{\partial t} dz + \int_{-h}^0 K_I \frac{\partial u^{(2)}}{\partial t} dz + \int_{-h}^0 K_I \left(u^{(1)} \frac{\partial u^{(1)}}{\partial x} + w^{(1)} \frac{\partial u^{(1)}}{\partial z} \right) dz \\
 & + \int_{-h}^0 K_D |u - \dot{x}_g|^{(1)} (u - \dot{x}_g)^{(1)} dz + \int_{-h}^0 K_M (u - \dot{x}_g)^{(1)} \frac{\partial w^{(1)}}{\partial z} dz
 \end{aligned} \tag{3.35}$$

Only the first and the second terms of Eq 3.35 give first order force and added mass. This equation suggests seven second order components as given in Table 3.1 ordered respectively from the third term. It was decided to consider only significant second order force component for the sake of simplicity and efficient computational procedure. As mentioned in 2.3.2, the second order reactive force component due to effect of free surface fluctuation (FSF) on the hydrostatic stiffness and added mass was not considered in this formulation because it was found that it is producing sum-frequency forces and had no contribution to the difference frequency force. Also, the second order force due to convective acceleration was very close to the negative of that due to FSF. Thus, these two second order force components cancel each other and were not considered. Furthermore, the second order force due to axial divergence was not considered because it was proven to have the smallest contribution total second order force. In the following formulation, only second order force associated with the horizontal (surge, sway and yaw) motions will be considered.

Table 3.1: Second order wave force components

No	Description
1	second order added mass component
2	second order force component due to FSF
3	second order force component due to structural displacement
4	second order force component due to second order temporal acceleration
5	second order force component due to convective acceleration
6	second order force component due to Morison incident drag force
7	second order force component due axial divergence

The second order force component due to second order temporal acceleration is given by Eq 3.36.

$$F^{(2)1} = \int_{-h}^0 K_I \frac{\partial u^{(2)}}{\partial t} dz = K_I \int_{-h}^0 \frac{\partial^2 \phi_-^{(2)}}{\partial x \partial t} dz \quad (3.36)$$

where

$$\frac{\partial^2 \phi_-^{(2)}}{\partial x \partial t} = \sum_{i=1}^N \sum_{j=i+1}^N \frac{0.25g^2 AH_* k_- \omega_-}{gk_- \tanh k_- d_w - \omega_-^2} \frac{\cosh k_- (z + d_w)}{\cosh k_- d_w} \sin \theta_-$$

$$A = \frac{\omega_-}{\omega_*} k_* (1 + \tanh k_i d_w) + \frac{1}{2} \left(\frac{k_i^2}{\omega_i \cosh^2 k_i d_w} - \frac{k_j^2}{\omega_j \cosh^2 k_j d_w} \right)$$

$$\omega_- = \omega_i - \omega_j > 0, \quad k_- = k_i - k_j, \quad H_* = H_i H_j, \quad \omega_* = \omega_i \omega_j, \quad \theta_- = \theta_i - \theta_j$$

The hydrodynamic forces on a floating structure are calculated at the instantaneous position instead of its original position [109]. The second order force due to first order structural motion is given by Eq 3.37.

$$F^{(2)\delta} = K_I \int_{-h}^0 \frac{\partial u^{(x)(1)}}{\partial t} dz \quad (3.37)$$

where $\partial u^{(x)(1)}/\partial t$ denotes the contribution of the structural displacement to the horizontal acceleration. For irregular wave train containing N regular components, the wave acceleration at the displaced position is given by Eq 3.38.

$$\frac{\partial u^{(x)(1)}}{\partial t} = \sum_{j=1}^N a_j \omega_j \frac{\cosh k_j (z + d)}{\cosh k_j d} \sin [k_i (x_g + X' - Y'\theta) - \omega_j t + \beta_j] \quad (3.38)$$

where X', Y' are the co-ordinates of the element relative to the platform co-ordinate system (defined in Chapter 5) and θ is the yaw motion. Expanding the sine term by Taylor series around the mean position and retaining terms up to second order as given by Eq 3.39.

$$\sin [k_i (x_g^{(1)} + X' - Y'\theta^{(1)}) - \omega_i t + \beta_i] = \sin \Theta_i + k_i (x_g^{(1)} - Y'\theta^{(1)}) \cos \Theta_i \quad (3.39)$$

where

$$\Theta_i = k_i X' - \omega_i t + \beta_i$$

The first term of the RHS of Eq 3.39 corresponds to the first order force evaluated at the mean position, while the second term constitutes the contribution of the structural displacement to the second order wave forces.

Letting

$$x_g^{(1)} = \sum_{j=1}^N \bar{X}_{g_j}^{(1)} \sin \Theta_j \quad (3.40)$$

$$\theta^{(1)} = \sum_{j=1}^N \bar{\theta}_j^{(1)} \sin \Theta_j \quad (3.41)$$

where $\bar{X}_{g_j}^{(1)}$ is the transitional first order motion amplitude in the direction of the wave propagation of the structure CG and $\bar{\theta}_j^{(1)}$ is the yaw first order motion amplitude. Substituting Eq 3.40 and the first part of the second term of the RHS of Eq 3.39 into Eq 3.38. Eq 3.42 is obtained as follows.

$$\frac{\partial u^{(x)(1)}}{\partial t} = \sum_{i=1}^N \left(a_i \omega_i k_i \frac{\cosh k_i (z + d_w)}{\cosh k_i d_w} \cos \Theta_i \right) \sum_{j=1}^N \bar{X}_{g_j}^{(1)} \sin \Theta_j \quad (3.42)$$

Letting

$$C_i = a_i \omega_i k_i \frac{\cosh k_i (z + d_w)}{\cosh k_i d_w}$$

Thus, the nonlinear temporal acceleration due to the structural transitional displacement is given by Eq 3.43.

$$\frac{\partial u^{(x)(1)}}{\partial t} = \sum_{i=1}^N \sum_{j=1}^N C_i \bar{X}_{g_j}^{(1)} \cos \Theta_i \sin \Theta_j \quad (3.43)$$

Taking the low frequency part of the $\cos \Theta_i \sin \Theta_j$ term as given by Eq 3.44.

$$\frac{\partial u^{(x)(1)}}{\partial t} = \sum_{i=1}^N \sum_{j=1}^N C_i \bar{X}_{g_j}^{(1)} \cos \Theta_i \sin \Theta_j \quad (3.44)$$

where

$$\Theta_- = \Theta_i - \Theta_j$$

Substituting Eq 3.44 in Eq 3.37, the second order force due to transitional motion is evaluated in the direction of the wave propagation. Similarly, substituting Eq 3.41

and the second part of the second term of the RHS of Eq 3.39 into Eq 3.42. The nonlinear temporal acceleration due to the structure rotational motion was evaluated as given by Eq 3.45 and the low frequency second order force component due to rotational motion (yaw) motion is given by Eq 3.46.

$$\frac{\partial u^{(\theta)(1)}}{\partial t} = \frac{Y'}{2} \sum_{i=1}^N \sum_{j=i+1}^N \left(C_i \bar{\theta}_j^{(1)} - C_j \bar{\theta}_i^{(1)} \right) \sin \Theta \quad (3.45)$$

$$F^{(2)\theta} = K_I \int_{-h}^0 \frac{\partial u^{(\theta)(1)}}{\partial t} dz \quad (3.46)$$

3.5 Chapter summary

In this chapter, the method for the assessment evaluation of the hydrostatic stability and the related characteristics were described. Mathematical formulation for the nonlinear boundary value problem representing wave to wave and wave to platform interactions were given together with the general and simplified solutions of the problem. The PM and JONSWAP mathematical spectrums, which were used for simulating the random sea environments and a comparison between the two were presented. Finally, the derivations of the hydrodynamic wave forces up to second order on semi submersibles were presented.

Chapter 4

ANALYSIS OF MOORING LINES

4.1 Chapter overview

In this chapter, the basics of the quasi-static analysis procedure are given. Moreover, a programmable mathematical derivation for establishing the nonlinear force-excursion relationship is presented. A deterministic nonlinear hydrodynamic analysis adopting the lumped mass approach in the time domain is given with mathematical model for the upper end boundary condition. Finally, assuming the mooring line lies on an elastic dissipative foundation, a mathematical model for the nonlinear mooring to seabed interactions is developed.

4.2 Quasi-static analysis

In this analysis method, it has been assumed that the behavior of each mooring line may be modeled by nonlinear spring with tension-displacement relationship. This relationship depends upon the line length, weight, elastic properties and the water depth. This assumption is based on the following condition. If the station-keeping response of a moored offshore platform deemed to be outside the exciting frequency range of the mooring system, the mooring line would only respond statically to the in-plane motions of the platform. Therefore, the static catenary equations can be used [3].

4.2.1 Catenary equations

A catenary is the curve formed by suspending a uniform cable of zero bending stiffness between two points. Classical theory for the static catenary shape forms the basis for an upper bound calculation on the restraint stiffness for cable stayed offshore structures. Since the bending stiffness EI is zero, such a cable achieves its stiffness only through a change in shape as the tension force T and T_o as shown in Fig 4.1. Classical theory leads to the equation of the catenary curve and relation among system variables ($L, w_t, T, T_o, \theta_t, \theta_b$).

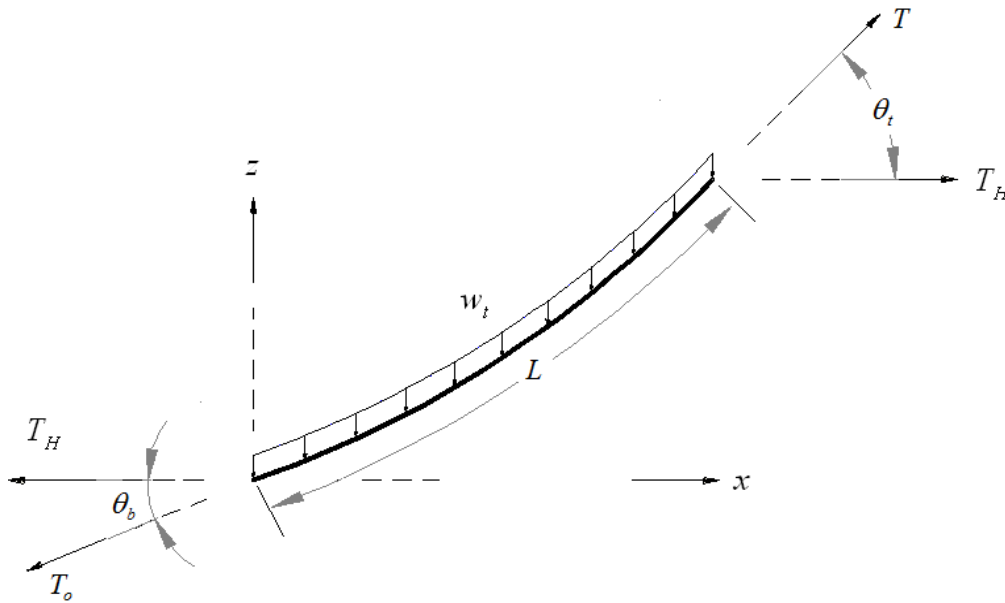


Fig 4.1: Freely hanging cable segment in static equilibrium

The governing differential equation for the catenary segment (Fig 4.1), expressed in terms of (x, z) coordinates is defined in Eq 4.1.

$$\frac{d^2z}{dx^2} = \frac{w_t}{T_H} \left[1 + \left(\frac{dz}{dx} \right)^2 \right]^{\frac{1}{2}} \quad (4.1)$$

Since the cable bending stiffness is neglected, the resultant end tensions T_o and T are tangential to the catenary curve [110]. For static equilibrium, the horizontal component of tension remains unchanged. Vertical equilibrium of this catenary segment (Fig 4.1) is satisfying the condition stated in Eq 4.2, in which L is the length of the segment, given by Eq 4.3.

$$T \sin \theta_t - T_o \sin \theta_b = w_t L \quad (4.2)$$

$$L = \int_x \left[1 + \left(\frac{dz}{dx} \right)^2 \right] \quad (4.3)$$

A closed form solution for the catenary governing equation (Eq 4.1), giving the x, z coordinates of the catenary curve is given by Eq 4.4-4.5.

$$x = C \left(\sinh^{-1} \tan \theta_t - \sinh^{-1} \tan \theta_b \right) \quad (4.4)$$

$$z = C \left(\cosh \sinh^{-1} \tan \theta_t - \cosh \sinh^{-1} \tan \theta_b \right) \quad (4.5)$$

where C is the mooring parameter, given by Eq 4.6.

$$C = \frac{T_H}{w_t} \quad (4.6)$$

As stated in 2.3.6, [60] suggested using the formulations given by [55]-[56]. They developed the catenary equations into a mathematical procedure and computer algorithm to derive the end forces and tension distribution in catenary from the value of its end coordinates, line elasticity and line length. This method is called ‘‘Peyrot’s method’’ in this thesis. For the sake of completeness, the detail of Peyrot’s method is given in Appendix B. In this study, from computational efficiency point of view, the Peyrot’s method was adopted for partially or wholly suspended single component mooring lines. Peyrot method becomes more complicated for analyzing multi-component mooring lines compared to the method introduced by [57]-[58]. The latter method was used in this study for the quasi-static analysis of multi-component mooring lines. They formulated the catenary equations into a mathematical procedure to derive the end forces and geometry of multi-component mooring line taking into account the limitations of the previous methods. The quasi-static analysis for multi-component mooring lines in positive and vertical excursions was given. In this study, a similar procedure was derived for multi-component mooring line analysis for negative excursions.

4.2.2 Multi-component mooring lines analysis

The nonlinear force-excursion relationship for the multi-component mooring line, as shown in Fig 4.2, was evaluated based on the catenary equations (Eq 4.4~4.5) and applying step by step iterative scheme.

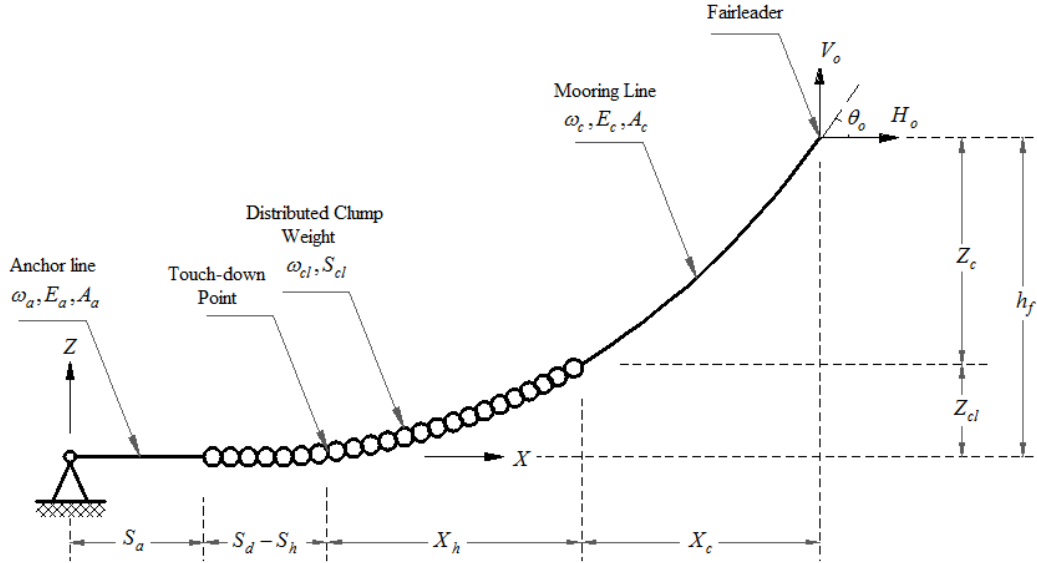


Fig 4.2: Multi-component mooring line.

The following assumptions were made for the purpose of this nonlinear analysis:

1. The sea-floor is flat, rigid and provides friction-less support to the part of the mooring line lying on it.
2. The mooring natural frequency lies outside the dominant exciting frequency. Hence, the mooring line would only respond statically to the in-plane motions of the platform.
3. The distributed clump weight segment is inextensible.
4. The effect of the line dynamics due to wave and current environmental loading is neglected.
5. The anchor point prevents transitional movements of the mooring line at anchor level.
6. Horizontal (positive and negative) and vertical excursions of the mooring line are considered.

The extension of any segment under increased line tension can be approximately evaluated by Eq 4.7. While, the modified unit weight due to stretching is given by Eq 4.8.

$$L = L_u \left[1 + \frac{(T - T_o)}{EA} \right] \quad (4.7)$$

$$w_t = \frac{L}{L_u} w_o \quad (4.8)$$

4.2.2.1 Initial configuration

For the initial configuration evaluation, the flow chart given Fig 4.3 and Eq 4.9 ~ 4.14 were used. It should be noted that e_{\max} was taken as 1%.

$$V_o = H_o \tan \theta_o \quad (4.9)$$

$$V_1 = H_o \tan \theta_1 \quad (4.10)$$

$$L_{34} = \frac{V_o - V_1}{w} \quad (4.11)$$

$$e_i = (z_c + z_{cl}) - h_f \quad (4.12)$$

$$\theta_{1_{i+1}} = \begin{cases} 1.001\theta_{1_i} \rightarrow e_i > 0 \\ 0.999\theta_{1_i} \rightarrow e_i \leq 0 \end{cases} \quad (4.13)$$

$$x_o = x_c + x_h + (L_{23} - S_{23}) + L_{34} \quad (4.14)$$

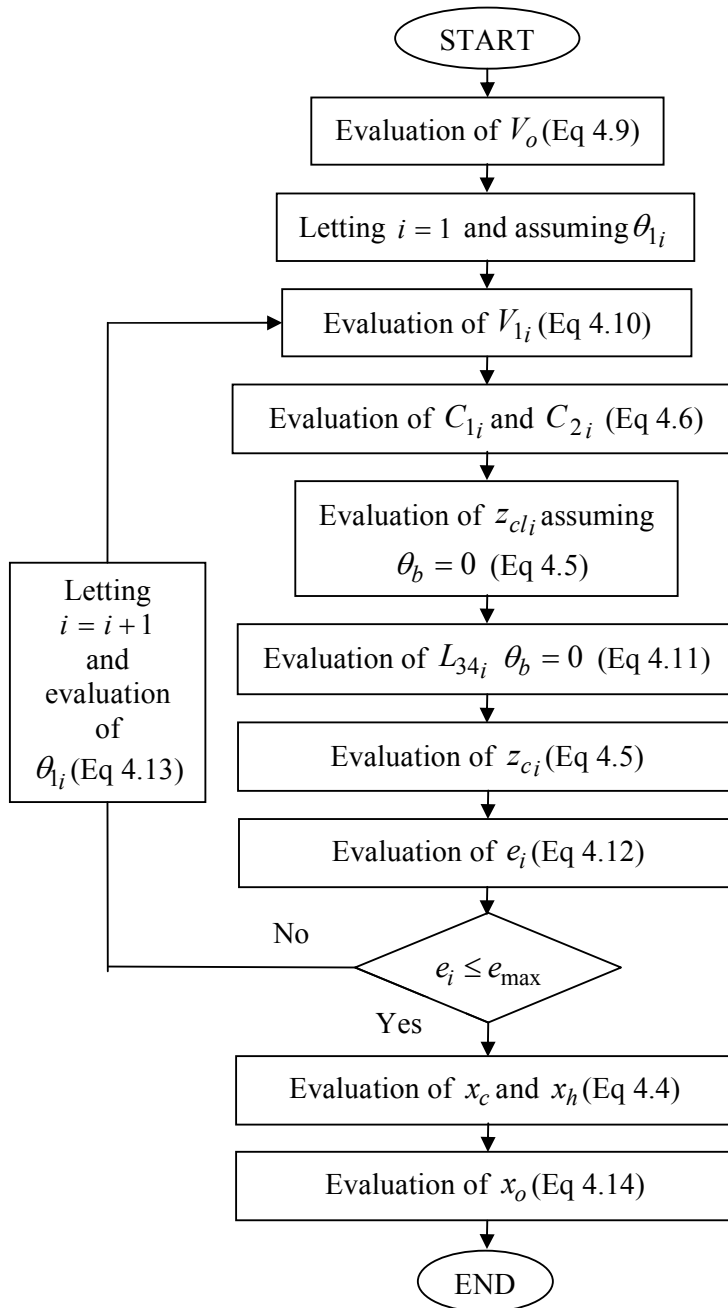


Fig 4.3: Flow chart for the evaluation of a multi-component mooring line initial configuration

4.2.2.2 Nonlinear force-excursion relationship for negative horizontal excursions

Starting with initial configuration, the vertical force V_o was decreased to allow for negative excursions. The corresponding horizontal force was estimated iteratively, ending with new configuration. The procedure was continued until specified value of negative excursion is reached, depending on the ultimate configuration allowed for negative excursions (usually it is the taut mooring configuration for lines with positive excursions). The related flow chart given is Fig 4.4, in which Eq 4.15~4.19 were used. It should be noted that ΔV was taken as 1 kN and $E_{x_{\max}}$ was 50 m.

$$V_{o_{i+1}} = V_{o_i} - \Delta V \quad (4.15)$$

$$V_{1_{i+1}} = V_{o_{i+1}} - \omega L_{34} \geq 0 \quad (4.16)$$

$$H_{o_{i+1}} = H_o - \frac{e_i(H_{o_{i-1}} - H_{o_i})}{e_{i-1} - e_i} \quad (4.17)$$

$$x_f = x_c + x_h + (L_{23} - S_{23}) + L_{34} \quad (4.18)$$

$$E_x = x_f - x_o \quad (4.19)$$

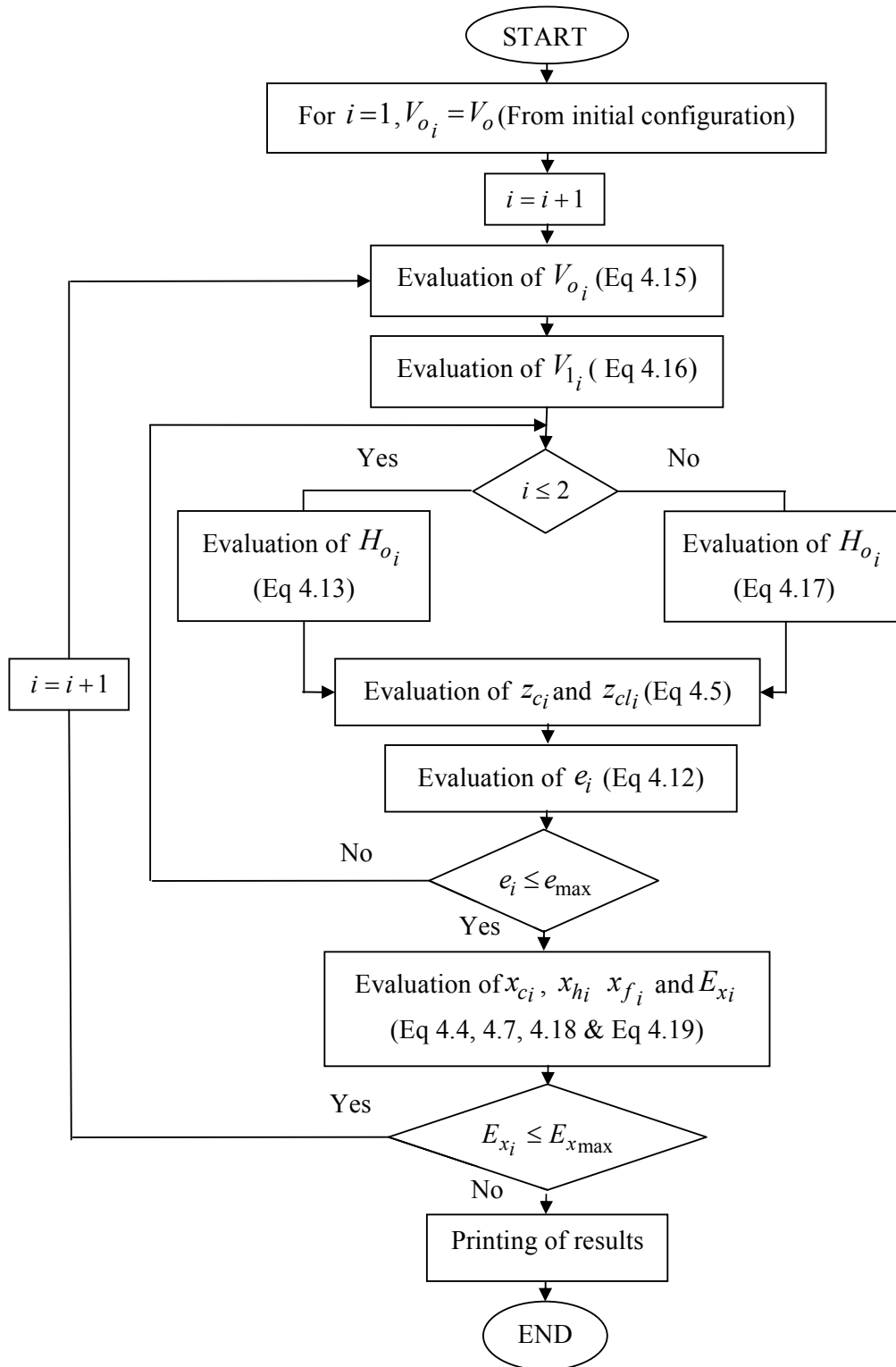


Fig 4.4: Flow chart for the evaluation of the nonlinear force-excursion relationship for a multi-component mooring line (Negative excursions)

4.3 Hydrodynamic analysis

4.3.1 Problem definition

A Multi-Component Mooring Line (MCML) connected to a floating structure subjected to the environment consisting of wind, waves and current was subjected to line-end loads, weight, buoyancy, sea-floor reactive forces, line/attachments inertia and fluid reactive forces. The following assumptions were used in the mathematical problem formulation:

1. The evaluation of the responses of the floating structure and the mooring to the environment excitation could be made separately since motions of the floating structure were not affected significantly by the mooring line tensions.
2. The mooring line remained in the vertical plane through both ends and the anchor boundary condition was not allowed to respond to the applied forces. Hence the motions of the mooring fairlead represented the predefined upper node boundary condition for the analysis of the mooring line.
3. The continuous distribution of mooring line mass was replaced by a discrete distribution of lumped masses at a finite number of points “nodes” where all internal and external forces were considered to act. These nodes were connected by a series of straight mass-less spring segments “elements”.
4. The forces considered were the element tensions (assumed to be constant per element), the global fluid loading, the seabed reactive forces, the inertia forces and effective weights, all lumped carefully at nodes.
5. The mooring line rested on a bed of elastic foundation and the touchdown point (TDP) was a variable during the oscillating excitation.
6. The line was fully flexible in the bending directions, and only the secant stiffness of the line was considered in the analysis.
7. The modified version of Morison equation, which accounted for the relative fluid/line velocities, was sufficient for the evaluation of the hydrodynamic forces. These forces were initially evaluated in the element local coordinates with special attention given for force transfer coefficients. Linear loading variation per element was assumed.

8. The hydrodynamic force transfer coefficients were independent of the wave/ upper end motion excitation frequencies. Hence constant values of the hydrodynamic force transfer coefficients were adopted.

4.3.2 Algorithm

The mathematical model adopted in this study was a modification of the LMM [65]-[63]-[61]-[62] and [98]. The mooring line was represented by a set of masses interconnected by springs as shown in Fig 4.5. In order to derive the governing equations of motion (GEOM) for the j^{th} lumped mass, Newton's law of motion was applied in global system co-ordinates.

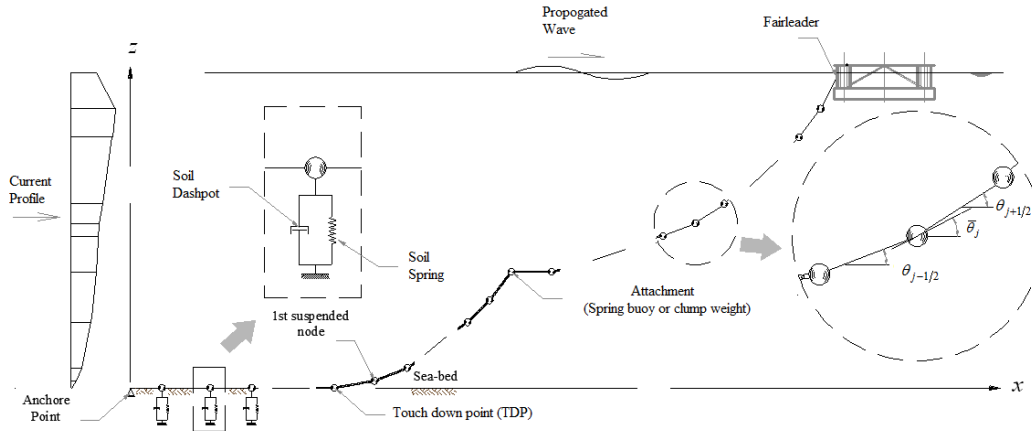


Fig 4.5: Multi-component mooring line Lumped mass model.

The nodal accelerations in the global were resolved to the node local co-ordinate in terms of the node average angle $\bar{\theta}_j$, which was given by Eq 4.20.

$$\bar{\theta}_j = \frac{1}{2}(\theta_{j-1/2} + \theta_{j+1/2}) \quad (4.20)$$

The nodal forces due to added mass in the local co-ordinate were given by Eq 4.21~4.22.

$$F_{A_x j} = \left(M_{A_t j} \cos^2 \bar{\theta}_j + M_{A_n j} \sin^2 \bar{\theta}_j \right) \ddot{x}_j + \left(\left(M_{A_t j} - M_{A_n j} \right) \sin \bar{\theta}_j \cos \bar{\theta}_j \right) \ddot{z}_j \quad (4.21)$$

$$F_{A_z j} = \left(\left(M_{A_t j} - M_{A_n j} \right) \sin \bar{\theta}_j \cos \bar{\theta}_j \right) \ddot{x}_j + \left(M_{A_t j} \sin^2 \bar{\theta}_j + M_{A_n j} \cos^2 \bar{\theta}_j \right) \ddot{z}_j \quad (4.22)$$

Applying equilibrium conditions at node j , the external forces should balance the reactive forces as given by Eq 4.23~4.24. It should be noted here that the hydrodynamic and soil reactive forces were considered as external forces and transferred to the RHS of the equilibrium equation with negative signs. This will be discussed in detail later.

$$\begin{aligned} & \left(\bar{M}_{x_j} + M_{A_t_j} \cos^2 \bar{\theta}_j + M_{A_n_j} \sin^2 \bar{\theta}_j \right) \ddot{x}_j \\ & + \left(\left(M_{A_t_j} - M_{A_n_j} \right) \sin \bar{\theta}_j \cos \bar{\theta}_j \right) \ddot{z}_j = F_{x_j} \end{aligned} \quad (4.23)$$

$$\begin{aligned} & \left(\left(M_{A_t_j} - M_{A_n_j} \right) \sin \bar{\theta}_j \cos \bar{\theta}_j \right) \ddot{x}_j \\ & + \left(\bar{M}_{z_j} + M_{A_t_j} \sin^2 \bar{\theta}_j + M_{A_n_j} \cos^2 \bar{\theta}_j \right) \ddot{z}_j = F_{z_j} \end{aligned} \quad (4.24)$$

Letting:

$$\sigma_{1_j} = \bar{M}_{x_j} + M_{A_t_j} \cos^2 \bar{\theta}_j + M_{A_n_j} \sin^2 \bar{\theta}_j \quad (4.25)$$

$$\sigma_{2_j} = \left(M_{A_t_j} - M_{A_n_j} \right) \sin \bar{\theta}_j \cos \bar{\theta}_j \quad (4.26)$$

$$\sigma_{3_j} = \bar{M}_{z_j} + M_{A_t_j} \sin^2 \bar{\theta}_j + M_{A_n_j} \cos^2 \bar{\theta}_j \quad (4.27)$$

where

$$M_{A_t_j} = \frac{\rho\pi}{8} C_{A_t} \left(D_{j-1/2}^2 L_{j-1/2} + D_{j+1/2}^2 L_{j+1/2} \right) \quad (4.28)$$

$$M_{A_n_j} = \rho \frac{\rho\pi}{8} C_{A_n} \left(D_{j-1/2}^2 L_{j-1/2} + D_{j+1/2}^2 L_{j+1/2} \right) \quad (4.29)$$

$$M_j = \frac{1}{2} \left(m_{j-1/2} L_{j-1/2} + m_{j+1/2} L_{j+1/2} \right) \quad (4.30)$$

$$M_{A_x \text{ att } j} = C_{A_x} \rho V_{\text{att } j} \quad (4.31)$$

$$M_{A_z \text{ att } j} = C_{A_z} \rho V_{\text{att } j} \quad (4.32)$$

The ODEs given in Eq 4.21~4.22 could be written in a simple matrix form as given by Eq 4.33, which represented the GEOM of the studied MCML.

$$\begin{bmatrix} \sigma_{1j} & \sigma_{2j} \\ \sigma_{2j} & \sigma_{3j} \end{bmatrix} \begin{Bmatrix} \ddot{x}_j \\ \ddot{z}_j \end{Bmatrix} = \begin{Bmatrix} F_{xj} \\ F_{zj} \end{Bmatrix} \quad (4.33)$$

The external forces considered were the element tensions above and below the node, the nodal lumped submerged weight, the weight of node attachment (if applicable), the global fluid loading due to drag force on the node adjacent elements and due to drag concentrated on node attachment. By evaluating the external force components along the global co-ordinate reference coordinate system, the LHS of Eq 4.21~4.22 was given by Eq 4.34~4.35.

$$F_{xj} = T_{j+1/2} \cos \theta_{j+1/2} - T_{j-1/2} \cos \theta_{j-1/2} - \bar{f}_{xj} \quad (4.34)$$

$$F_{zj} = T_{j+1/2} \sin \theta_{j+1/2} - T_{j-1/2} \sin \theta_{j-1/2} - \bar{f}_{zj} \quad (4.35)$$

where

$$\bar{f}_{xj} = \left(f_{xj} + f_{xattj} \right) \quad (4.36)$$

$$\bar{f}_{zj} = \left(f_{zj} + f_{zattj} + W_j + W_{attj} + f_{zsoil} \right) \quad (4.37)$$

$$W_j = \frac{1}{2} (w_{j-1/2} L_{j-1/2} + w_{j+1/2} L_{j+1/2}) \quad (4.38)$$

Substituting Eq 4.36~4.38 into Eq 4.33, Eq 4.39 was obtained.

$$\begin{bmatrix} \sigma_{1j} & \sigma_{2j} \\ \sigma_{2j} & \sigma_{3j} \end{bmatrix} \begin{Bmatrix} \ddot{x}_j \\ \ddot{z}_j \end{Bmatrix} = \begin{Bmatrix} T_{j+1/2} \cos \theta_{j+1/2} - T_{j-1/2} \cos \theta_{j-1/2} - \bar{f}_{xj} \\ T_{j+1/2} \sin \theta_{j+1/2} - T_{j-1/2} \sin \theta_{j-1/2} - \bar{f}_{zj} \end{Bmatrix} \quad (4.39)$$

Fluid forces were evaluated through the application of Morison equation to each element as though it was a smooth cylinder. This was initially calculated in a local coordiante system, and then the fluid loading in global coordinate system was evaluated through the application of the standard rotation transformation procedure. In addition to the drag on the line elements, there was also the hydrodynamic drag on any concentrated substance attached to the mooring line such as spring buoy or clump weight. The procedure for evaluation of fluid drag forces was according to the following steps:

1. Evaluation of relative fluid-line nodal velocities in global co-ordinate system as given by Eq 4.40~4.41. The linear Airy wave theory (Eq 3.15~3.16) was

adopted for evaluation of the wave velocities. It should be noted that the wave length was obtained using an iterative technique applying the dispersion relation (Eq 3.19).

$$r_{x_j} = \dot{x}_j - (u_j + c_j) \quad (4.40)$$

$$r_{z_j} = \dot{z}_j - v_j \quad (4.41)$$

2. Transformation of the nodal relative velocities to local axes using the element orientation angle average angles as given by Eq 4.42~4.45.

$$r_{t1_{j-1/2}} = r_{x_{j-1}} \cos\theta_{j-1/2} + r_{z_{j-1}} \sin\theta_{j-1/2} \quad (4.42)$$

$$r_{t2_{j-1/2}} = r_{x_j} \cos\theta_{j-1/2} + r_{z_j} \sin\theta_{j-1/2} \quad (4.43)$$

$$r_{n1_{j-1/2}} = r_{z_{j-1}} \cos\theta_{j-1/2} - r_{x_{j-1}} \sin\theta_{j-1/2} \quad (4.44)$$

$$r_{n2_{j-1/2}} = r_{z_j} \cos\theta_{j-1/2} - r_{x_j} \sin\theta_{j-1/2} \quad (4.45)$$

3. Evaluation of the fluid reactive forces per unit length for line elements in local co-ordinates assuming that nodal orientations were equal to the adjacent element orientations as given by Eq 4.46~4.49.

$$P_{t1_{j-1/2}} = \frac{\rho}{2} C_{Dt} D_{j-1/2} \left| r_{t1_{j-1/2}} \right| r_{t1_{j-1/2}} \quad (4.46)$$

$$P_{t2_{j-1/2}} = \frac{\rho}{2} C_{Dt} D_{j-1/2} \left| r_{t2_{j-1/2}} \right| r_{t2_{j-1/2}} \quad (4.47)$$

$$P_{n1_{j-1/2}} = \frac{\rho}{2} C_{Dn} D_{j-1/2} \left| r_{n1_{j-1/2}} \right| r_{n1_{j-1/2}} \quad (4.48)$$

$$P_{n2_{j-1/2}} = \frac{\rho}{2} C_{Dn} D_{j-1/2} \left| r_{n2_{j-1/2}} \right| r_{n2_{j-1/2}} \quad (4.49)$$

4. Evaluation of member end resultant fluid forces, assuming linear force-length variation through nodes, as given by Eq 4.50~4.57.

$$f_{n1_{j-\frac{1}{2}}} = \frac{L_{j-1/2}}{6} \left(2P_{n1_{j-1/2}} + P_{n2_{j-1/2}} \right) \quad (4.50)$$

$$f_{n2_{j-\frac{1}{2}}} = \frac{L_{j-1/2}}{6} \left(P_{n1_{j-1/2}} + 2P_{n2_{j-1/2}} \right) \quad (4.51)$$

$$f_{n1_{j+\frac{1}{2}}} = \frac{L_{j+1/2}}{6} \left(2P_{n1_{j+1/2}} + P_{n2_{j+1/2}} \right) \quad (4.52)$$

$$f_{n2_{j+\frac{1}{2}}} = \frac{L_{j+1/2}}{6} \left(P_{n1_{j+1/2}} + 2P_{n2_{j+1/2}} \right) \quad (4.53)$$

$$f_{t1_{j-\frac{1}{2}}} = \frac{L_{j-1/2}}{6} \left(2P_{t1_{j-1/2}} + P_{t2_{j-1/2}} \right) \quad (4.54)$$

$$f_{t2_{j-\frac{1}{2}}} = \frac{L_{j-1/2}}{6} \left(P_{t1_{j-1/2}} + 2P_{t2_{j-1/2}} \right) \quad (4.55)$$

$$f_{t1_{j+\frac{1}{2}}} = \frac{L_{j+1/2}}{6} \left(2P_{t1_{j+1/2}} + P_{t2_{j+1/2}} \right) \quad (4.56)$$

$$f_{t2_{j+\frac{1}{2}}} = \frac{L_{j+1/2}}{6} \left(P_{t1_{j+1/2}} + 2P_{t2_{j+1/2}} \right) \quad (4.57)$$

5. Evaluation of resultant nodal forces in local coordinate system as given by Eq 4.58~4.59, then using the standard transformation matrix to evaluate the nodal resultant fluid forces in the global coordinate system, and in case of available nodal attachment, the drag on attachment added to the lumped nodal drag as given by Eq 4.60.

$$F_{n_j} = f_{n2_{j-1/2}} + f_{n1_{j+1/2}} \quad (4.58)$$

$$F_{t_j} = f_{t2_{j-1/2}} + f_{t1_{j+1/2}} \quad (4.59)$$

$$\begin{Bmatrix} f_{x_j} \\ f_{z_j} \end{Bmatrix} = \begin{bmatrix} \cos \bar{\theta}_j & -\sin \bar{\theta}_j \\ \sin \bar{\theta}_j & \cos \bar{\theta}_j \end{bmatrix} \begin{Bmatrix} F_{t_j} \\ F_{n_j} \end{Bmatrix} + \frac{\rho}{2} \begin{Bmatrix} A_{r_x} C_{D_x} |r_{x_j}| r_{x_j} \\ A_{r_z} C_{D_z} |r_{z_j}| r_{z_j} \end{Bmatrix} \quad (4.60)$$

4.3.3 Mooring to seabed interactions

As indicated in 2.3.6.1, both seabed Nakajima and elastic foundation seabed models were considered for the purpose of investigating seabed contributions to the mooring line dynamic analysis in this study. Assuming that the mooring line rested on elastic-dissipative bed of soil, this foundation was replaced by linear spring (having zero stiffness for line invert elevations above the soil surface, allowing the line to lift from

the soil without resistance) with a dashpot as shown in Fig 4.5. Thus, the soil reactive forces were estimated by Eq 4.61 for $z_j < 0$ and by Eq 4.62 for $z_j \geq 0$.

$$f_{z_{soil}} = \frac{k_{soil}}{2} (L_{j-1/2} + L_{j+1/2}) \varepsilon_j + \varepsilon_{soil} \dot{z}_j \sqrt{2k_{soil} \bar{M}_{z_j} (L_{j-1/2} + L_{j+1/2})} \quad (4.61)$$

$$f_{z_{soil}} = 0 \quad (4.62)$$

The stiffness k_{soil} for the line invert elevation below the sea bed was evaluated as secant stiffness to a nominal embedment from the theoretical bearing capacity curve for a strip footing in drained soil with width equal to the contact width of the soil-mooring line [92]. The Terzaghi equation for the soil bearing capacity given in Eq 4.63 was used to evaluate the soil stiffness [89]. The bearing capacity factors N_q , N_c and N_γ are given by Eq 4.64~4.66, where is B the foundation width [111].

$$q_u = cN_c + qN_q + \frac{1}{2} \gamma B N_\gamma \quad (4.63)$$

$$N_q = e^{\pi \tan \phi} \tan^2 \left(\frac{\pi}{4} + \frac{\phi}{4} \right) \quad (4.64)$$

$$N_c = \frac{N_q - 1}{\tan \phi} \quad (4.65)$$

$$N_\gamma = 2(N_q + 1) \tan \phi \quad (4.66)$$

4.3.4 Solution procedure

To facilitate the solution, the governing EOM presented in Eq 4.33 was rearranged into a form of functional dependencies as given by Eq 4.67.

$$\begin{Bmatrix} \ddot{x}_j \\ \ddot{z}_j \end{Bmatrix} = \frac{1}{\lambda_j} \begin{bmatrix} \sigma_{3j} & -\sigma_{2j} \\ -\sigma_{2j} & \sigma_{1j} \end{bmatrix} \begin{Bmatrix} T_{j+1/2} \cos \theta_{j+1/2} - T_{j-1/2} \cos \theta_{j-1/2} - \bar{f}_{x_j} \\ T_{j+1/2} \sin \theta_{j+1/2} - T_{j-1/2} \sin \theta_{j-1/2} - \bar{f}_{z_j} \end{Bmatrix} \frac{\overline{\Delta t}^2}{\Delta t^2} \quad (4.67)$$

where

$$\lambda_j = \sigma_{1j} \sigma_{3j} - \sigma_{2j}^2 \quad (4.68)$$

Rearranging Eq 4.67 in the form given by Eq 4.69~4.72.

$$\begin{aligned} \dot{\ddot{x}}_j = & \frac{\overline{\Delta t}^2}{\lambda_j} \left[\left(T_{j+1/2} \cos \theta_{j+1/2} - T_{j-1/2} \cos \theta_{j-1/2} - \bar{f}_{x_j} \right) \right. \\ & \left. - \sigma_{2_j} \left(T_{j+1/2} \sin \theta_{j+1/2} - T_{j-1/2} \sin \theta_{j-1/2} - \bar{f}_{z_j} \right) \right] / \overline{\Delta t}^2 \end{aligned} \quad (4.69)$$

$$\begin{aligned} \ddot{x}_j = & \frac{\overline{\Delta t}^2}{\lambda_j} \left[\left(\sigma_{3_j} \cos \theta_{j+1/2} - \sigma_{2_j} \sin \theta_{j+1/2} \right) T_{j+1/2} \right. \\ & \left. - \left(\sigma_{3_j} \cos \theta_{j-1/2} - \sigma_{2_j} \sin \theta_{j-1/2} \right) T_{j-1/2} + \left(\sigma_{2_j} \bar{f}_{z_j} - \sigma_{3_j} \bar{f}_{x_j} \right) \right] / \overline{\Delta t}^2 \end{aligned} \quad (4.70)$$

$$\begin{aligned} \ddot{z}_j = & \frac{\overline{\Delta t}^2}{\lambda_j} \left[\sigma_{1_j} \left(T_{j+1/2} \sin \theta_{j+1/2} - T_{j-1/2} \sin \theta_{j-1/2} - \bar{f}_{z_j} \right) \right. \\ & \left. - \sigma_{2_j} \left(T_{j+1/2} \cos \theta_{j+1/2} - T_{j-1/2} \cos \theta_{j-1/2} - \bar{f}_{x_j} \right) \right] / \overline{\Delta t}^2 \end{aligned} \quad (4.71)$$

$$\begin{aligned} \ddot{z}_j = & \frac{\overline{\Delta t}^2}{\lambda_j} \left[\left(\sigma_{1_j} \sin \theta_{j+1/2} - \sigma_{2_j} \cos \theta_{j+1/2} \right) T_{j+1/2} \right. \\ & \left. - \left(\sigma_{1_j} \sin \theta_{j-1/2} - \sigma_{2_j} \cos \theta_{j-1/2} \right) T_{j-1/2} + \left(\sigma_{2_j} \bar{f}_{x_j} - \sigma_{1_j} \bar{f}_{z_j} \right) \right] / \overline{\Delta t}^2 \end{aligned} \quad (4.72)$$

Letting

$$\alpha_j = \frac{\overline{\Delta t}^2}{\lambda_j} \left(\sigma_{3_j} \cos \theta_{j+1/2} - \sigma_{2_j} \sin \theta_{j+1/2} \right) \quad (4.73)$$

$$\beta_j = \frac{\overline{\Delta t}^2}{\lambda_j} \left(\sigma_{3_j} \cos \theta_{j-1/2} - \sigma_{2_j} \sin \theta_{j-1/2} \right) \quad (4.74)$$

$$\gamma_j = \frac{\overline{\Delta t}^2}{\lambda_j} \left(\sigma_{1_j} \sin \theta_{j+1/2} - \sigma_{2_j} \cos \theta_{j+1/2} \right) \quad (4.75)$$

$$\kappa_j = \frac{\overline{\Delta t}^2}{\lambda_j} \left(\sigma_{1_j} \sin \theta_{j-1/2} - \sigma_{2_j} \cos \theta_{j-1/2} \right) \quad (4.76)$$

$$\mu_j = \frac{\overline{\Delta t}^2}{\lambda_j} \left(\sigma_{2_j} \bar{f}_{z_j} - \sigma_{3_j} \bar{f}_{x_j} \right) \quad (4.77)$$

$$\psi_j = \frac{\overline{\Delta t}^2}{\lambda_j} \left(\sigma_{2_j} \bar{f}_{x_j} - \sigma_{1_j} \bar{f}_{z_j} \right) \quad (4.78)$$

The GEOM were solved as given by Eq 4.79~4.80.

$$\ddot{x}_j = (\alpha_j T_{j+1/2} - \beta_j T_{j-1/2} + \mu_j) / \overline{\Delta t}^2 \quad (4.79)$$

$$\ddot{z}_j = (\gamma_j T_{j+1/2} - \kappa_j T_{j-1/2} + \psi_j) / \overline{\Delta t}^2 \quad (4.80)$$

The GEOM time domain solution given by Eq 4.79~4.80 needed an appropriate numerical time integration scheme. Generally, two numerical integration schemes are available for the problem solution, explicit and implicit schemes. The general forms of the explicit/implicit schemes are given by Eq 4.81~4.82 respectively.

$$\ddot{x}_j^{n+1} = f(x_j^{n+1}, x_j^n, x_j^{n-1}, \dots, x_j^1) \quad (4.81)$$

$$\ddot{x}_j^{n+1} = f(x_j^{n+2}, x_j^{n+1}, x_j^n, \dots, x_j^1) \quad (4.82)$$

As mentioned in 2.2.6, the influence of different time integration implicit and explicit schemes used to solve the GEOM applicable to the mooring line was studied systematically in [64]. The time integration schemes investigated were the central difference explicit scheme (CD), and three implicit schemes, namely Houbolt, Wilson- θ and Newmark- β . An assessment of the stability, accuracy and the influence of time step size for each scheme were discussed. This study concluded that the CD scheme might be ruled out because it was limited to smaller time step than required for the implicit schemes. The Newmark- β scheme was not recommended by the authors for the cited problem because it produced an extremely inaccurate and irregular solution in case of lifting cable and sub-sea attachments. Also, it took roughly twice computation time of other implicit schemes considered. Of the two remaining time schemes, it was found that there was little difference in using either scheme but the Houbolt scheme needed a special starting procedure, and thus the authors did not recommend it. Of the three implicit methods, it was proven that Wilson- θ presented the smoothest solution and it was recommended for the general solution of the cable dynamic problem. Depending upon previous recommendations, the Wilson- θ numerical integration scheme was adopted in this study for the solution of the GEOM of the MCMLs. In the Wilson- θ scheme, a linear variation of acceleration was assumed over the time interval. If the time increased from t to $t + \tau$, where $(0 \leq \tau \leq n + \theta \overline{\Delta t}) \theta \geq 1.0$ in this study θ was taken as 1.4. It was assumed that acceleration at time $t + \tau$ was given by Eq 4.83.

$$\ddot{x}_j^{n+\tau} = \ddot{x}_j^n + \frac{\tau}{\theta \overline{\Delta t}} (\ddot{x}_j^{n+\theta \overline{\Delta t}} - \ddot{x}_j^n) \quad (4.83)$$

By integration, the nodal velocities and displacements at time $t + \tau$ were given by Eq 4.84~4.85.

$$\dot{x}_j^{n+\tau} = \dot{x}_j^n + \ddot{x}_j^n \tau + \frac{\tau^2}{2\theta\Delta t} (\ddot{x}_j^{n+\theta\Delta t} - \ddot{x}_j^n) \quad (4.84)$$

$$x_j^{n+\tau} = x_j^n + \dot{x}_j^n \tau + \ddot{x}_j^n \frac{\tau^2}{2} + \frac{\tau^3}{6\theta\Delta t} (\ddot{x}_j^{n+\theta\Delta t} - \ddot{x}_j^n) \quad (4.85)$$

Applying Eq 4.84~4.85 at time $n + \theta\Delta t$, nodal velocities and displacements were obtained as in Eq 4.86~4.89.

$$\dot{x}_j^{n+\theta\Delta t} = \dot{x}_j^n + \frac{\theta\Delta t}{2} (\ddot{x}_j^{n+\theta\Delta t} + \ddot{x}_j^n) \quad (4.86)$$

$$x_j^{n+\theta\Delta t} = x_j^n + \dot{x}_j^n \theta\Delta t + \frac{(\theta\Delta t)^2}{6} (\ddot{x}_j^{n+\theta\Delta t} + \ddot{x}_j^n) \quad (4.87)$$

$$\dot{z}_j^{n+\theta\Delta t} = \dot{z}_j^n + \frac{\theta\Delta t}{2} (\ddot{z}_j^{n+\theta\Delta t} + \ddot{z}_j^n) \quad (4.88)$$

$$z_j^{n+\theta\Delta t} = z_j^n + \dot{z}_j^n \theta\Delta t + \frac{(\theta\Delta t)^2}{6} (\ddot{z}_j^{n+\theta\Delta t} + \ddot{z}_j^n) \quad (4.89)$$

The nonlinearities present in the GEOM solution (Eq 4.33) made the closed form solution not possible. Thus, iterative procedure to achieve results of prescribed accuracy was adopted. The solution procedure could be broken down into the following steps:

1. A state of equilibrium of the line was chosen based on initial upper end restoring forces. This could be the quasi-static condition of the mooring line found from catenary equations or numerical integration methods, and must represent a consistent solution to a void instability of the solution, from which it was possible to extrapolate forward in time.
2. A set of tentative values for the displacements were determined for the next time step by applying Eq 4.82~4.83, 4.90, 4.92 using tentative estimate for the tensions at the next time step. For a first estimate, these were considered to be the tensions at the previous time step.
3. In general, the tentative displacements obtained at time $n + \theta\Delta t$ did not satisfy the condition that element length evaluated from the updated nodal coordinates should be equal to the distance calculated from the material constitutive relation (Hook's law in this case). The latter requirement formed

the constraints equation for the iterative procedure. From this, a set the tension corrections could be derived and applied to the original tension estimates to obtain a second set of better tension estimates. Letting k indicate the tension related iteration index, the new tension estimate was given by Eq 4.90. It should be noted that Eq 4.90 was subjected to the iteration starting condition ${}^1T_{j-1/2}^{n+\theta\Delta t} = T_{j-1/2}^n$ for $k = 0$. The constraint equation or segment error function was formulated as given in Eq 4.91. Expanding the segment error function ${}^{k+1}\mathcal{E}_{j-1/2}^{n+\theta\Delta t}$ as a truncated first order Taylor series about $\left({}^{k+1}T_{j-3/2}^{n+\theta\Delta t}, {}^{k+1}T_{j-1/2}^{n+\theta\Delta t}, {}^{k+1}T_{j+1/2}^{n+\theta\Delta t}\right)$, Eq 4.92 was obtained.

$${}^{k+1}T_{j-1/2}^{n+\theta\Delta t} = {}^{k+1}\tilde{T}_{j-1/2}^{n+\theta\Delta t} + \delta T_{j-1/2}^{n+\theta\Delta t} \quad (4.90)$$

$$\begin{aligned} {}^{k+1}\mathcal{E}_{j-1/2}^{n+\theta\Delta t} &= \left({}^{k+1}X_j^{n+\theta\Delta t} - {}^{k+1}X_{j-1}^{n+\theta\Delta t}\right)^2 + \left({}^{k+1}Z_j^{n+\theta\Delta t} - {}^{k+1}Z_{j-1}^{n+\theta\Delta t}\right)^2 \\ &\quad - \left[L_{j-1/2} \left(1 + \frac{{}^{k+1}T_{j-1/2}^{n+\theta\Delta t}}{(EA)_{j-1/2}} \right) \right]^2 \end{aligned} \quad (4.91)$$

$$\begin{aligned} {}^{k+1}\mathcal{E}_{j-1/2}^{n+\theta\Delta t} &= {}^{k+1}\tilde{\mathcal{E}}_{j-1/2}^{n+\theta\Delta t} + \frac{\delta^{k+1}\mathcal{E}_{j-1/2}^{n+\theta\Delta t}}{\delta^{k+1}T_{j-1/2}^{n+\theta\Delta t}} \delta^{k+1}T_{j-1/2}^{n+\theta\Delta t} + \frac{\delta^{k+1}\mathcal{E}_{j-1/2}^{n+\theta\Delta t}}{\delta^{k+1}T_{j-1/2}^{n+\theta\Delta t}} \delta^{k+1}T_{j-1/2}^{n+\theta\Delta t} \\ &\quad + \frac{\delta^{k+1}\mathcal{E}_{j-1/2}^{n+\theta\Delta t}}{\delta^{k+1}T_{j+1/2}^{n+\theta\Delta t}} \delta^{k+1}T_{j+1/2}^{n+\theta\Delta t} + \dots = 0 \end{aligned} \quad (4.92)$$

Updating nodal coordinates at time $n+\theta\Delta t$ by adding the nodal displacements (Eq 4.90 and Eq 4.92) to the original nodal coordinates, Eq 4.93~4.96 were obtained.

$$\begin{aligned} f_1(T_{j+1/2}, T_{j-1/2}) &= {}^{k+1}X_j^{n+\theta\Delta t} = X_j^n + \dot{x}_j^n \theta \Delta t + \frac{(\theta \Delta t)^2}{3} \ddot{x}_j^n \\ &\quad + \frac{\theta^2}{6} (\alpha_j T_{j+1/2} - \beta_j T_{j-1/2} + \mu_j) \end{aligned} \quad (4.93)$$

$$\begin{aligned} f_2(T_{j-1/2}, T_{j-1/2}) &= {}^{k+1}X_{j-1}^{n+\theta\Delta t} = X_{j-1}^n + \dot{x}_{j-1}^n \theta \Delta t + \frac{(\theta \Delta t)^2}{3} \ddot{x}_{j-1}^n \\ &\quad + \frac{\theta^2}{6} (\alpha_{j-1} T_{j-1/2} - \beta_{j-1} T_{j-1/2} + \mu_{j-1}) \end{aligned} \quad (4.94)$$

$$f_3(T_{j+1/2}, T_{j-1/2}) = {}^{k+1}Z_j^{n+\theta\Delta t} = Z_j^n + \dot{z}_j^n \theta \Delta t + \frac{(\theta \Delta t)^2}{3} \ddot{z}_j^n$$

$$+ \frac{\theta^2}{6} (\gamma_j T_{j+1/2} - \kappa_j T_{j-1/2} + \psi_j) \quad (4.95)$$

$$\begin{aligned} f_4(T_{j-1/2}, T_{j-1/2}) &= {}^{k+1}Z_{j-1}^{n+\theta\bar{\Delta}t} \\ &= Z_{j-1}^n + \dot{z}_{j-1}^n \theta \Delta t + \frac{(\theta \bar{\Delta} t)^2}{3} \ddot{z}_{j-1}^n \\ &+ \frac{\theta^2}{6} (\gamma_{j-1} T_{j-1/2} - \kappa_{j-1} T_{j-1/2} + \psi_{j-1}) \end{aligned} \quad (4.96)$$

4. The partial derivatives were evaluated (Eq 4.97~4.100) and substituted in segment error function (Eq 4.91), by expressing the segment error function in terms of functions $f_1 \sim f_4$ given by Eq 4.97.

$$\begin{aligned} \delta^{k+1} \varepsilon_{j-1/2}^{n+\theta\bar{\Delta}t} &= [f_1(T_{j+1/2}, T_{j-1/2}) - f_2(T_{j-1/2}, T_{j-1/2})]^2 \\ &+ [f_3(T_{j+1/2}, T_{j-1/2}) - f_4(T_{j-1/2}, T_{j-1/2})]^2 \\ &- \left[L_{j-1/2} \left(1 + \frac{{}^{k+1}T_{j-1/2}^{n+\theta\bar{\Delta}t}}{(EA)_{j-1/2}} \right) \right]^2 \end{aligned} \quad (4.97)$$

$$\frac{\delta^{k+1} \varepsilon_{j-1/2}^{n+\theta\bar{\Delta}t}}{\delta^{k+1} T_{j-1/2}^{n+\theta\bar{\Delta}t}} = \frac{\theta^2}{3} \left[\left({}^{k+1}X_j^{n+\theta\bar{\Delta}t} - {}^{k+1}X_{j-1}^{n+\theta\bar{\Delta}t} \right) \beta_{j-1} + \left({}^{k+1}Z_j^{n+\theta\bar{\Delta}t} - {}^{k+1}Z_{j-1}^{n+\theta\bar{\Delta}t} \right) \kappa_{j-1} \right] \quad (4.98)$$

$$\begin{aligned} \frac{\delta^{k+1} \varepsilon_{j-1/2}^{n+\theta\bar{\Delta}t}}{\delta^{k+1} T_{j-1/2}^{n+\theta\bar{\Delta}t}} &= - \left\{ \frac{\theta^2}{3} \left[\left({}^{k+1}X_j^{n+\theta\bar{\Delta}t} - {}^{k+1}X_{j-1}^{n+\theta\bar{\Delta}t} \right) (\beta_j + \alpha_{j-1}) \right. \right. \\ &+ \left. \left({}^{k+1}Z_j^{n+\theta\bar{\Delta}t} - {}^{k+1}Z_{j-1}^{n+\theta\bar{\Delta}t} \right) (\kappa_j + \gamma_{j-1}) \right] \\ &+ \left. \left[\frac{2L_{j-1/2}^2}{(EA)_{j-1/2}} \left(1 + \frac{{}^{k+1}T_{j-1/2}^{n+\theta\bar{\Delta}t}}{(EA)_{j-1/2}} \right) \right] \right\} \end{aligned} \quad (4.99)$$

$$\frac{\delta^{k+1} \varepsilon_{j+\frac{1}{2}}^{n+\theta\bar{\Delta}t}}{\delta^{k+1} T_{j+\frac{1}{2}}^{n+\theta\bar{\Delta}t}} = \frac{\theta^2}{3} \left[\left({}^{k+1}X_j^{n+\theta\bar{\Delta}t} - {}^{k+1}X_{j-1}^{n+\theta\bar{\Delta}t} \right) \alpha_{j-1} + \left({}^{k+1}Z_j^{n+\theta\bar{\Delta}t} - {}^{k+1}Z_{j-1}^{n+\theta\bar{\Delta}t} \right) \gamma_{j-1} \right] \quad (4.100)$$

Letting

$$\tilde{E}_j^{n+\theta\bar{\Delta}t} = \frac{\theta^2}{3} \left[\left({}^{k+1}X_j^{n+\theta\bar{\Delta}t} - {}^{k+1}X_{j-1}^{n+\theta\bar{\Delta}t} \right) \beta_{j-1} + \left({}^{k+1}Z_j^{n+\theta\bar{\Delta}t} - {}^{k+1}Z_{j-1}^{n+\theta\bar{\Delta}t} \right) \kappa_{j-1} \right] \quad (4.101)$$

$$\begin{aligned}
\tilde{F}_j^{n+\theta\bar{\Delta}t} &= \frac{\theta^2}{3} \left[\left({}^{k+1}X_j^{n+\theta\bar{\Delta}t} - {}^{k+1}X_{j-1}^{n+\theta\bar{\Delta}t} \right) (\beta_j + \alpha_{j-1}) \right. \\
&\quad \left. + \left({}^{k+1}Z_j^{n+\theta\bar{\Delta}t} - {}^{k+1}Z_{j-1}^{n+\theta\bar{\Delta}t} \right) (\kappa_j + \gamma_{j-1}) \right] \\
&\quad + \left[\frac{2L_{j-1/2}^2}{(EA)_{j-1/2}} \left(1 + \frac{{}^{k+1}T_{j-1/2}^{n+\theta\bar{\Delta}t}}{(EA)_{j-1/2}} \right) \right]
\end{aligned} \tag{4.102}$$

$$\tilde{G}_j^{n+\theta\bar{\Delta}t} = \frac{\theta^2}{3} \left[\left({}^{k+1}X_j^{n+\theta\bar{\Delta}t} - {}^{k+1}X_{j-1}^{n+\theta\bar{\Delta}t} \right) \alpha_{j-1} + \left({}^{k+1}Z_j^{n+\theta\bar{\Delta}t} - {}^{k+1}Z_{j-1}^{n+\theta\bar{\Delta}t} \right) \gamma_{j-1} \right] \tag{4.103}$$

Eq 4.92 was written in the form of Eq 4.104.

$$\tilde{E}_j^{n+\theta\bar{\Delta}t} \delta T_{j-3/2}^{n+\theta\bar{\Delta}t} - \tilde{F}_j^{n+\theta\bar{\Delta}t} \delta^{k+1} T_{j-1/2}^{n+\theta\bar{\Delta}t} + \tilde{G}_j^{n+\theta\bar{\Delta}t} \delta^{k+1} T_{j+1/2}^{n+\theta\bar{\Delta}t} = -{}^{k+1}\tilde{\varepsilon}_{j-1/2}^{n+\theta\bar{\Delta}t} \tag{4.104}$$

A linear system of simultaneous equations was derived in Eq 4.104 to solve for the tension corrections $\delta^{k+1} T_{j-1/2}^{n+\theta\bar{\Delta}t}$. The solution of Eq 4.104 may be made by Gauss's elimination with backward or forward substitution algorithm but being a tri-diagonal system, it was recommended by [63] to use Thomas algorithm for efficient computations. Substituting the tension corrections in Eq 4.93, better estimates of ${}^{k+1} T_{j-1/2}^{n+\theta\bar{\Delta}t}$ were obtained and used with Eq 4.82~4.83, Eq 4.90, Eq 4.92 to gain an improved estimate of the nodal displacement vectors $x_j^{n+\theta\bar{\Delta}t}$ and $z_j^{n+\theta\bar{\Delta}t}$. These were used to update the nodal co-ordinates and the element error functions. This procedure was continued until the latter functions achieved the desired accuracy. In this study, the accepted error in the element length was ± 1 mm. So far, only the acceleration from the Wilson- θ scheme was used. Implicit in the coefficients of Eq 4.71 were the fluid-drag/soil-impact terms in-terms of the nodal velocities. Thus, the nodal velocities were evaluated one step behind the current solution time step because it was not possible to evaluate the nodal velocities at the same time as trying to evaluate nodal displacements. For this reason the time step was small enough for better estimation of the drag force at the current time step.

4.3.5 Upper-end boundary condition

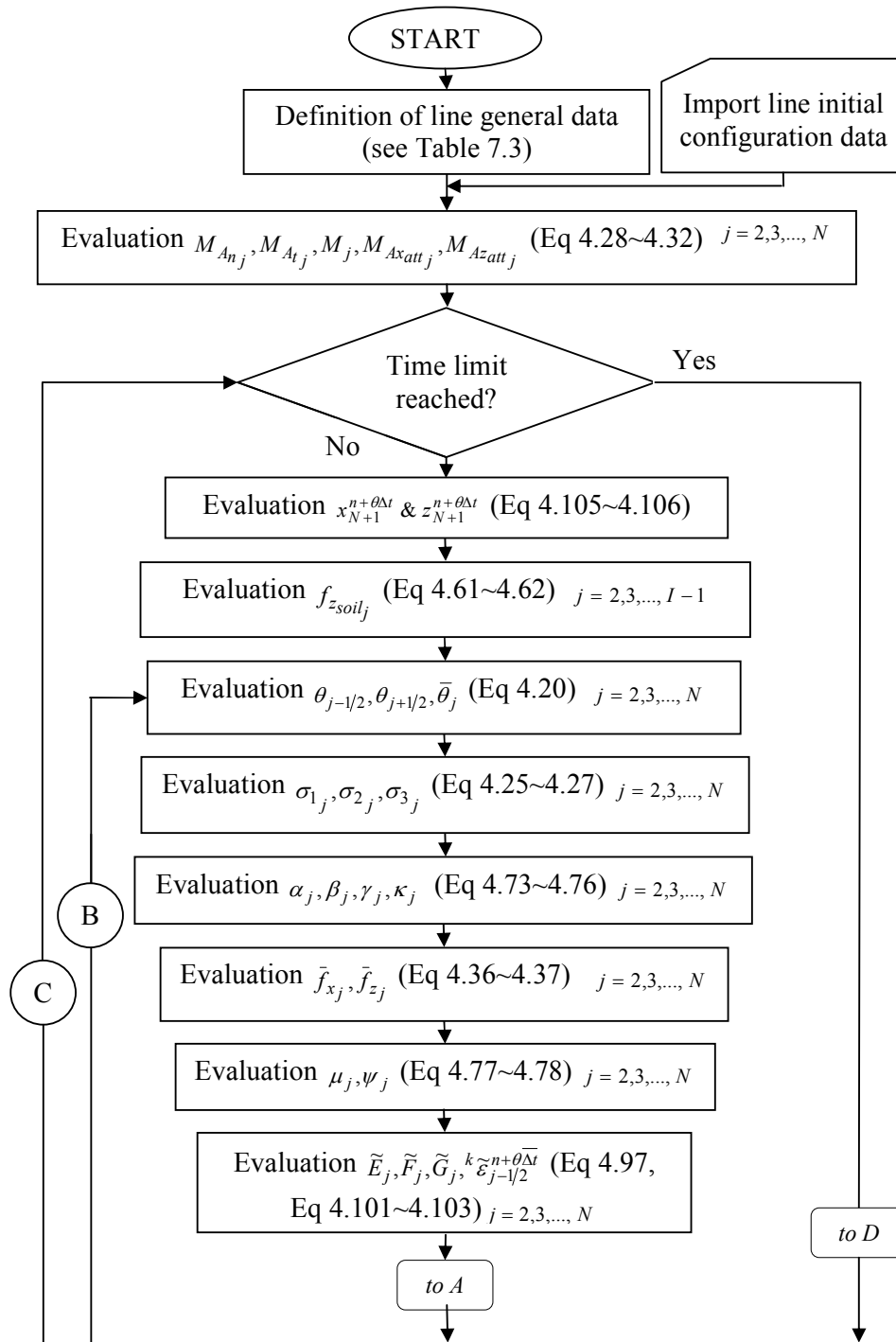
Simulations started by applying a starting function to the UBC. For the mathematical model adopted for the UBC in this study, the formulae for UBC were given by Eq 4.105~4.106.

$$x_{N+1}^{n+\theta\bar{\Delta t}} = \left(1 - e^{-\varepsilon(n+\theta\bar{\Delta t})}\right) A_x \sin\left(w_f(n+\theta\bar{\Delta t}) + \varphi_x\right) \quad (4.105)$$

$$z_{N+1}^{n+\theta\bar{\Delta t}} = \left(1 - e^{-\varepsilon(n+\theta\bar{\Delta t})}\right) A_z \sin\left(w_f(n+\theta\bar{\Delta t}) + \varphi_z\right) \quad (4.106)$$

4.3.6 Programming aspects

Based on the previous mentioned numerical formulation, a computer code was established. The related flow chart is presented in Fig 4.6.



Flow chart for a multi-component mooring line hydrodynamic analysis
(To be continued)

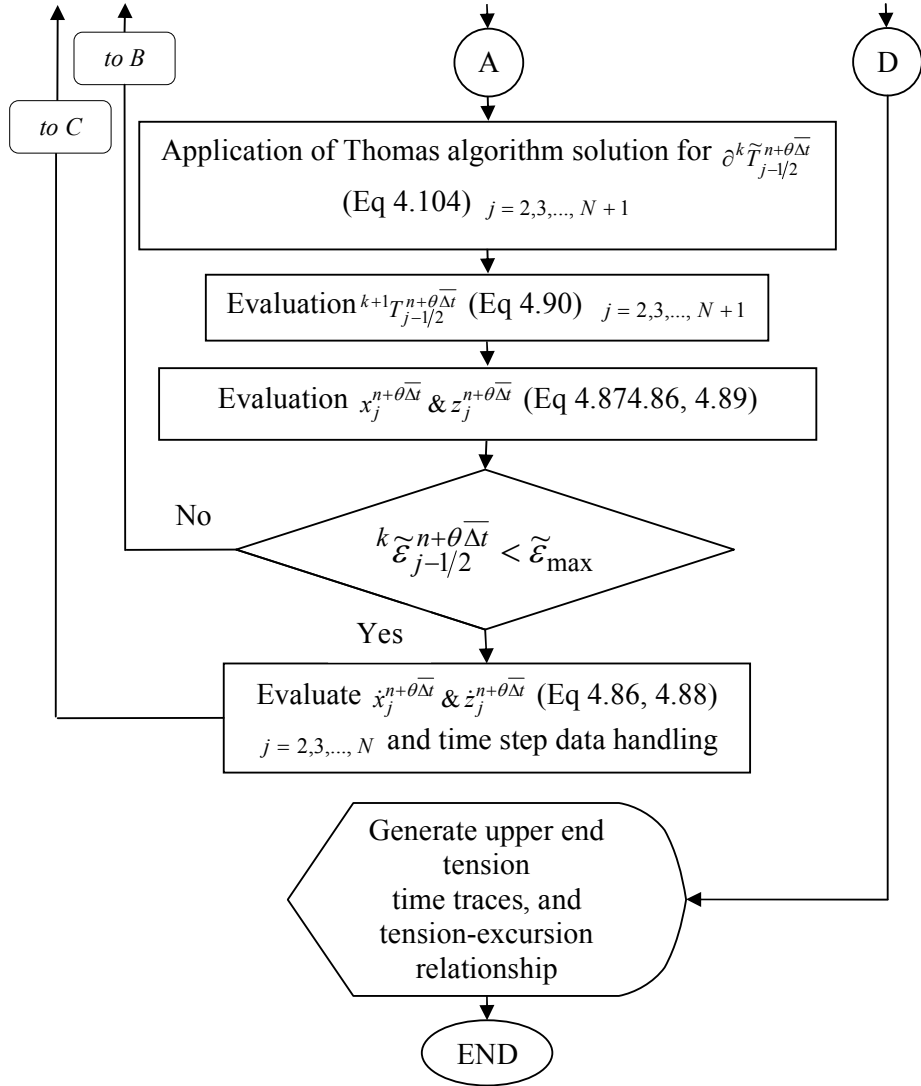


Fig 4.6: Flow chart for a multi-component mooring line hydrodynamic analysis
(Continued)

4.4 Chapter summary

In this chapter, a background about mooring systems and the related structural analysis methods was presented. The basics of the quasi-static analysis procedure were given. Besides, a programmable mathematical derivation for an establishment of the nonlinear force-excursion relationship for negative excursions was presented. An accurate nonlinear hydrodynamic analysis coupled analysis of mooring lines adopting the lumped mass approach in the time domain was given with mathematical

model for the upper end boundary condition. A mathematical model for the nonlinear mooring to seabed interactions was developed.

Chapter 5

DYNAMIC ANALYSIS OF PLATFORM

5.1 Chapter overview

In this chapter, the methodology for the rigid platform dynamic analysis in the frequency domain and the time domain are presented. For the frequency domain analysis, the nonlinear EOM for single DOF is derived and the linearized frequency-dependant solution is presented. Moreover, based on published experimental results and data fitting technique mathematical formulae for the frequency dependant force coefficient are derived. Furthermore, a flow chart showing the iterative linearized analysis of the platform in the frequency domain is presented. For the time domain analysis, the methods for the first order motion analysis and up to second order are given. For first-order 3D motion analysis, the EOM and the related coefficient matrices are presented. A derivation of the mooring system nonlinear stiffness matrix, which represents mooring system-structure interaction, is presented. Finally, the methodology for the 2D nonlinear motion analysis in the time domain is presented with the related programming flow chart.

5.2 Frequency domain analysis

The frequency domain (FD) method is a general approach for evaluating the dynamic responses of the structures. In the FD method, the response amplitude and phase are determined corresponding to each frequency of the wave environment. The RAOs are evaluated from the response and wave spectra. The following procedure for the FD analysis was used for the evaluation of the first order horizontal responses (surge, sway and yaw), which represents one of the inputs to evaluate the low frequency second order forces and the motion responses.

5.2.1 Equation of motion

The EOM was derived based on Newton's second law of motion, the differential EOM of mass spring with dashpot system for surge DOF is given by Eq 5.1.

$$[m + a(\omega)]\ddot{x} + B^{(0)}\dot{x} + B^{(2)}|\dot{x}|\dot{x} + kx = F^{(1)} + F^{(2)} \quad (5.1)$$

where $a(\omega)$ is the frequency dependant added mass and $F^{(1)}, F^{(2)}$ are the linear and nonlinear steady wave force respectively. The nonlinear damping term in Eq 5.1 was linearized by the truncated first term of the Taylor's expansion as given by Eq 5.2.

$$|\dot{x}|\dot{x} = \frac{8}{3\pi} \omega X \quad (5.2)$$

Letting

$$M = m + a(\omega) \quad (5.3)$$

$$B = B^{(0)} + \frac{8B^{(2)}}{3\pi} \omega X \quad (5.4)$$

$$F = F^{(1)} + F^{(2)} \quad (5.5)$$

where M is the total mass of the platform in water Substituting Eq 5.3~5.5 in Eq 5.1, the conventional form of the EOM was used as given by Eq 5.6.

$$M\ddot{x} + B\dot{x} + kx = F \quad (5.6)$$

In this FD analysis, the virtual mass of the system M evaluated in the direction of the wave propagation is given by Eq 5.7.

$$M = m + (h-b) \sum_{k=1}^{Noc} K_{MI_k} + \frac{K_{MIP}}{6} \quad (5.7)$$

where

$$K_{MI_k} = \rho \frac{\pi D_k^2}{4} C_{A_k}(\omega)$$

$$K_{MIP} = \rho \frac{\pi D_p^2}{4} C_{A_p}(\omega)$$

The still water damping $B^{(0)}$ was taken as linear combination of system stiffness and virtual mass as given by Eq 5.8.

$$B^{(0)} = 2\zeta\sqrt{kM} \quad (5.8)$$

The general solution of the EOM (Eq 5.6) constitutes free and forced oscillation, assuming the steady state solution is given by the harmonic function Eq 5.9.

$$x = X \sin(\omega t - \beta) \quad (5.9)$$

Substituting Eq 5.9 in the EOM (Eq 5.6) and elimination of time, the amplitude of the motion X and the associated phase angle β are given by Eq 5.10~5.11.

$$X = \frac{F}{\sqrt{(k - \omega^2 M)^2 + (B\omega)^2}} \quad (5.10)$$

$$\beta = \tan^{-1}\left(\frac{B\omega}{k - \omega^2 M}\right) \quad (5.11)$$

These equations are written in terms of the system natural frequency and damping ratio as given in Eq 5.12~5.13.

$$X = \frac{F/k}{\sqrt{[1 - (\omega/\omega_n)^2]^2 + [2\zeta \omega/\omega_n]^2}} \quad (5.12)$$

$$\beta = \tan^{-1}\left[\frac{2\zeta \omega/\omega_n}{1 - (\omega/\omega_n)^2}\right] \quad (5.13)$$

where

$$\omega_n = \sqrt{\frac{k}{M}}, \quad \zeta = \frac{B}{2\sqrt{kM}}$$

5.2.2 Force LTFs

Since semi submersible platforms are inertia-dominated structures, the contribution of the drag force is small and it was not being considered in the FD analysis. First, the hydrodynamic force (frequency-dependant) on the columns was evaluated in the direction of the wave propagation by Eq 5.14.

$$\begin{aligned} F_c(\omega) &= \sum_{k=1}^{Noc} K_{I_k} \int_{-h+b}^0 a\omega^2 \frac{\cosh k_f(d+z)}{\sinh k_f d} \sin(k_f X_k'' - \beta) dz \\ &= \sum_{k=1}^{Noc} K_{I_k} \frac{a\omega^2}{k_f} \left[1 - \frac{\sinh k_f(d-h+b)}{\sinh k_f d}\right] \sin(k_f X_k'' - \beta) \end{aligned} \quad (5.14)$$

By summing the multiplication of the force arises in each column by associate lever arm, the yaw moment was evaluated as given by Eq 5.15.

$$M_c(\omega) = \sum_{k=1}^{Noc} Y_k'' K_{I_k} \frac{a\omega^2}{k_f} \left[1 - \frac{\sinh k_f(d-h+b)}{\sinh k_f d} \right] \sin(k_f X_k'' - \beta) \quad (5.15)$$

where X_k'', Y_k'' are the member coordinates relative to the wave axes (will be defined in later). The wave force on pontoons is effectively in the sway direction, and is given by Eq 5.16.

$$F_p(\omega) = \sum_{k=1}^{Nop} K_{I_{p_k}} a\omega^2 \frac{\cosh k_f(d-h+0.5b)}{\sinh k_f d} s \int_{-L_p/2}^{L_p/2} \sin[k_f c X_{p_k} + k_f s Y_{p_k} - \beta] dX_{p_k} \quad (5.16)$$

Eq 5.16 is analytically evaluated by Eq 5.17.

$$F_p(\omega) = - \sum_{k=1}^{Nop} K_{I_{p_k}} \frac{a\omega^2 \cosh k_f(d-h+0.5b)}{k_f c \sinh k_f d} s \left[\cos(k_f c X_{p_k} + k_f s Y_{p_k} - \beta) \right]_{-L_p/2}^{L_p/2} \quad (5.17)$$

The yaw moment on the pontoons is given by Eq 5.18.

$$F_p(\omega) = \sum_{k=1}^{Nop} K_{I_{p_k}} a\omega^2 \frac{\cosh k_f(d-h+0.5b)}{\sinh k_f d} s \int_{-L_p/2}^{L_p/2} X_{p_k} \sin[k_f c X_{p_k} + k_f s Y_{p_k} - \beta] dX_{p_k} \quad (5.18)$$

The integration in Eq 5.18 is evaluated by parts, as given by Eq 5.19.

$$I = - \frac{X_{p_k}}{k_f c} \cos(k_f c X_{p_k} + k_f s Y_{p_k} - \beta) + \frac{1}{(k_f c)^2} \sin(k_f c X_{p_k} + k_f s Y_{p_k} - \beta) \quad (5.19)$$

where

$$I = \int_{-L_p/2}^{L_p/2} X_{p_k} \sin[k_f c X_{p_k} + k_f s Y_{p_k} - \beta] dX_{p_k}$$

By summing forces for columns and pontoons in each direction, the horizontal force and moments LTFs are written as given by Eq 5.20~5.22.

$$LTF_{surge} = cg \tanh k_f d \left[1 - \frac{\sinh k_f(d-h+b)}{\sinh k_f d} \right] \sum_{k=1}^{Noc} K_{I_k} \quad (5.20)$$

$$\begin{aligned}
LTF_{sway} &= sg \tanh k_f d \left[1 - \frac{\sinh k_f (d - h + b)}{\sinh k_f d} \right] \sum_{k=1}^{Noc} K_{I_k} \\
&+ g \tan \phi \tanh k_f d \frac{\cosh k_f (d - h + 0.5b)}{\sinh k_f d} \sum_{k=1}^{Nop} K_{I_{p_k}} \quad (5.21)
\end{aligned}$$

$$\begin{aligned}
LTF_{yaw} &= g \tanh k_f d \left[1 - \frac{\sinh k_f (d - h + b)}{\sinh k_f d} \right] \sum_{k=1}^{Noc} |Y_k''| K_{I_k} \\
&+ g \tan \phi \tanh k_f d \frac{\cosh k_f (d - h + 0.5b)}{\sinh k_f d} \sum_{k=1}^{Nop} K_{I_{p_k}} \left| -L_{p_k} + \frac{1}{k_f c} \right| \quad (5.22)
\end{aligned}$$

It should be noted that when $\phi = \pi/2$ the term $\tan \phi$ was replaced by unit in Eq 5.21~5.22.

5.2.3 Hydrodynamic force coefficients

Frequency dependant force coefficients were used for application of the force (Morison) equation based on numerous data given by [103], which were evaluated by data fitting technique. The fitted curves for C_D corresponds to Keulegan Carpenter number KC values are given Eq 5.23.

$$\left. \begin{aligned}
C_D &= 0.227 & KC &= 0 \\
C_D &= -0.0113KC^2 + 0.2785KC & 0 &< KC \leq 15 \\
C_D &= -0.009KC + 1.77 & 15 &< KC \leq 30 \\
C_D &= -0.0726KC + 3.7455 & 30 &< KC \leq 35 \\
C_D &= -0.0238KC^2 + 1.8789KC - 35.55 & 35 &< KC \leq 45 \\
C_D &= 0.0915KC - 3.2958 & 45 &< KC \leq 50.5 \\
C_D &= -0.0175KC + 2.2018 & 50.5 &< KC \leq 75 \\
C_D &= 0.0266KC^2 - 4.029KC + 153.65 & 50.5 &< KC \leq 80
\end{aligned} \right\} (5.23)$$

Also, the fitted curves for C_M corresponds to Keulegan Carpenter number KC values are given Eq 5.24.

$$\begin{array}{l}
 C_M = 2.45652 \\
 C_M = -0.0727KC + 2.4447 \\
 C_M = 0.0029KC^2 - 0.1289KC + 2.7133 \\
 C_M = 0.0013KC^2 - 0.0485KC + 1.7384 \\
 C_M = -0.0248KC + 2.1801 \\
 C_M = -0.008KC^2 + 0.6877KC - 13.251 \\
 C_M = 0.0004KC^2 - 0.0429KC + 2.3322 \\
 C_M = 0.0254KC - 0.3442
 \end{array}
 \left. \begin{array}{l}
 KC = 0 \\
 0 < KC \leq 10 \\
 10 < KC \leq 20 \\
 20 < KC \leq 30 \\
 30 < KC \leq 37 \\
 37 < KC \leq 50 \\
 50 < KC \leq 65 \\
 65 < KC \leq 71
 \end{array} \right\} (5.24)$$

Comparisons between fitted curves (Eq 5.23~5.24) and the test data are shown in for C_M and C_D respectively.

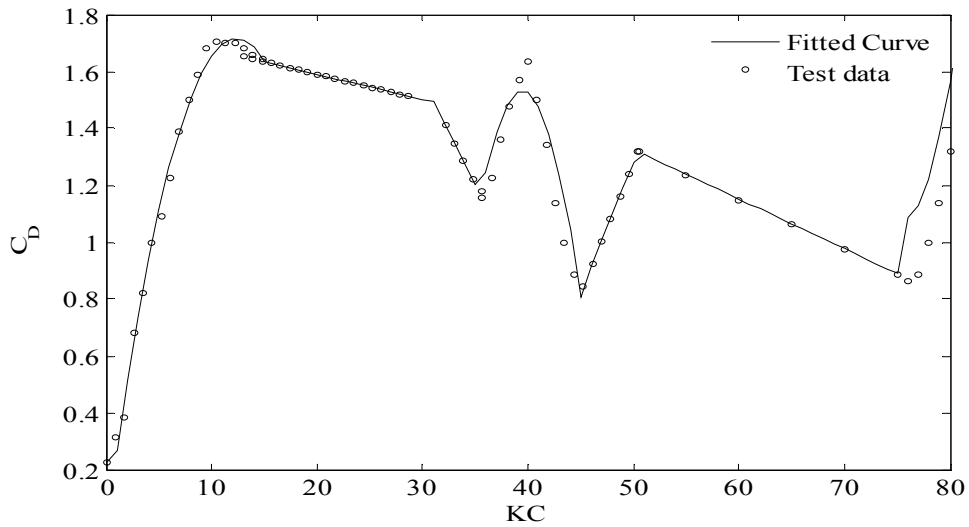


Fig 5.1: Fitted vs. measured results for drag coefficient (smooth cylinder in waves)
 (Source of test data: *Hydrodynamics of offshore structures, Chakrabarti, 1987*)

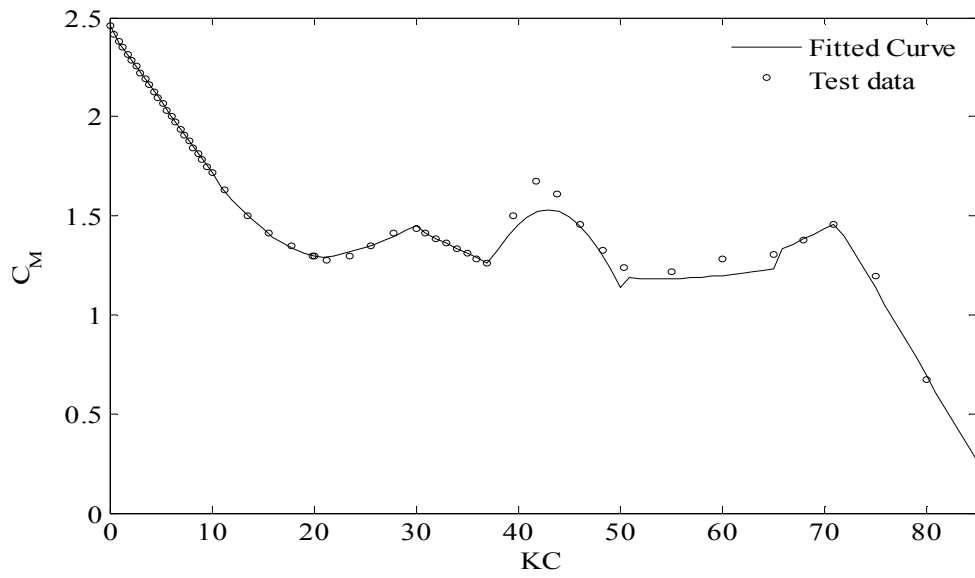


Fig 5.2: Fitted vs.measured results for inertia coefficient (smooth cylinder in waves)
 (Source of test data: *Hydrodynamics of offshore structures*, Chakrabarti, 1987)

5.2.4 Programming aspects

The same procedure was used for the system's horizontal first order responses and the related program flow chart is shown in Fig 5.3.

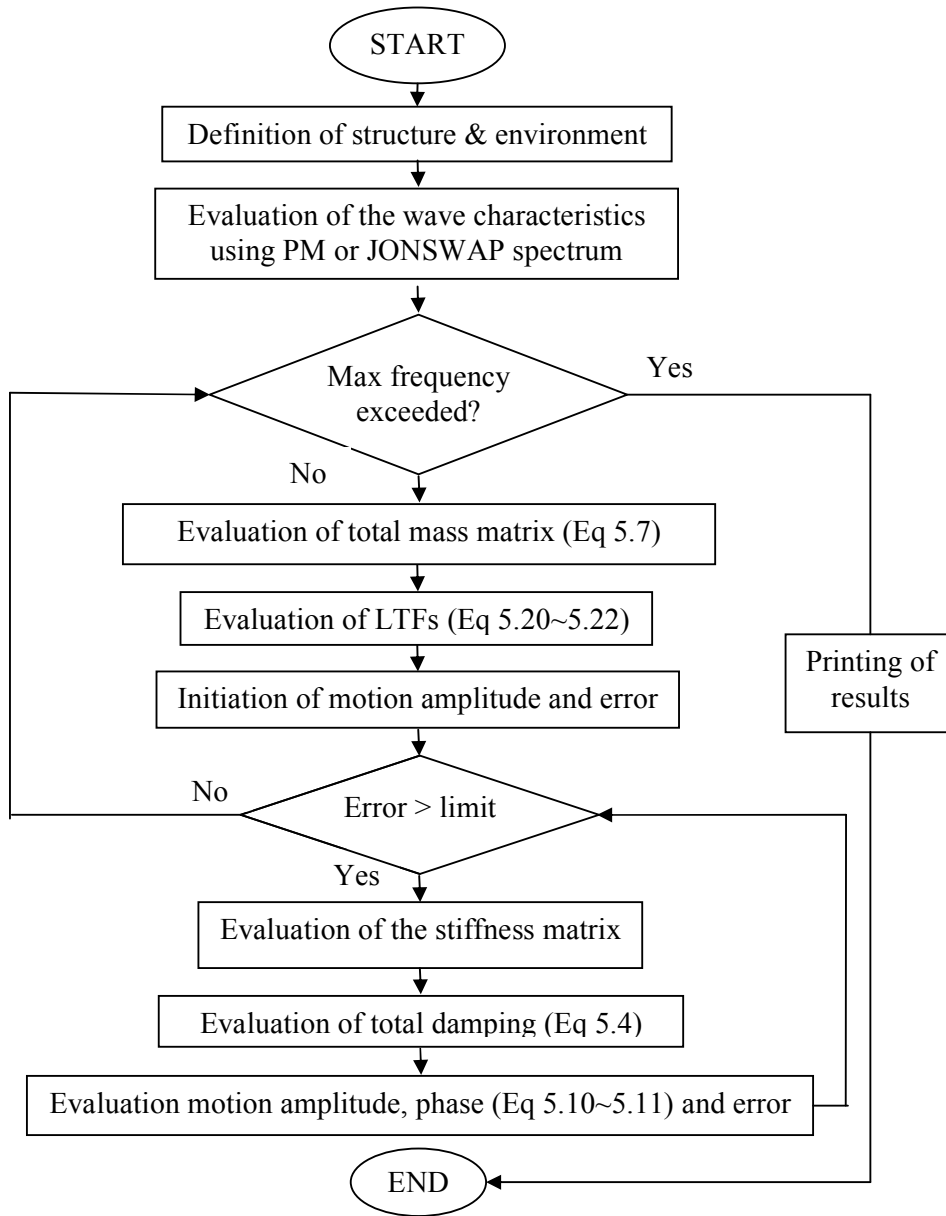


Fig 5.3: Flow chart for the frequency domain analysis

5.3 Time domain analysis

In the time domain analysis, all nonlinearities associated with the EOM for the system were incorporated including nonlinear mooring restoring forces and nonlinear hydrodynamic forces.

as the force vector for each structure element. The forces on a platform are the resultant of a number of components including:

1. The excitation forces due to wave, current or hydrostatic pressure.
2. The restoring forces due to mooring lines and
3. Damping from drag on the structure or the mooring lines, radiation, wave drift damping, etc.

Applying the conditions of equilibrium in the horizontal and vertical directions and rotation about CG, the governing EOM for the rigid platform are derived. They are represented in the matrix form terms of stiffness, mass matrices and force vector as expressed in Eq 5.25~5.27.

$$[M]\{\ddot{X}\} + [K]\{X\} = \{F\} \quad (5.25)$$

$$[M] = [M_s] + [M_a] \quad (5.26)$$

$$[K] = [K_s] + [K_m] \quad (5.27)$$

The assumptions used in Eq 5.25 formulation and their solutions are stated below:

1. The semi submersible platform is assumed to be an assembly of cylindrical elements and rectangular pontoons which have small ratios of cross-sectional dimensions compared to the incident wave lengths. Therefore, the force (Morison) equation formulation is enough to estimate wave incident forces efficiently.
2. The motion amplitudes of the wave are assumed to be small when compared to the effective water depth. Therefore, linear Airy theorem for wave potential flow is satisfactory.
3. Wave forces on individual members are computed as though other members were not present, or in other words hydrodynamic interference between members is ignored.
4. The small contribution of potential damping term due to wave radiation and diffraction effects is neglected in the analysis for platforms with very slender members.

The s and the coefficient matrices appearing in Eq 5.25 were evaluated prior to applying the numerical scheme to evaluate the platform responses to excitation forces.

5.3.2.1 Structure physical mass matrix

Since the reference axes chosen are the principal axes, the physical mass matrix M , is presented in Eq 5.28.

$$[M] = \begin{bmatrix} m & 0 & 0 & 0 & 0 & 0 \\ 0 & m & 0 & 0 & 0 & 0 \\ 0 & 0 & m & 0 & 0 & 0 \\ 0 & 0 & 0 & mr_{rol}^2 & 0 & 0 \\ 0 & 0 & 0 & 0 & mr_{pit}^2 & 0 \\ 0 & 0 & 0 & 0 & 0 & mr_{yaw}^2 \end{bmatrix} \quad (5.28)$$

5.3.2.2 Added mass matrix

Added mass for columns were evaluated by summation of the added mass matrix for each single column. For each column, the added mass is based on the instantaneous wetted length and each column was divided into N number of elements using as given in Appendix A. Numerical integration was used to evaluate the added mass matrix in each column, the following steps shows the columns added mass matrix evaluation procedure:

For element k , z -coordinate measured from MWL is given by Eq 5.29 (Fig A.3).

$$z_k = -(h - b - z_g) + \left(k - \frac{1}{2}\right) dz \quad (5.29)$$

For columns, the coupled added mass matrix was evaluated as given by Eq 5.30.

$$[m_{ac}] = \begin{bmatrix} m_{11,c} & 0 & 0 & 0 & 0 & 0 \\ 0 & m_{22,c} & 0 & 0 & 0 & 0 \\ 0 & 0 & m_{33,c} & 0 & 0 & 0 \\ 0 & m_{42,c} & 0 & 0 & 0 & 0 \\ m_{51,c} & 0 & 0 & 0 & 0 & 0 \\ m_{61,c} & m_{62,c} & 0 & 0 & 0 & 0 \end{bmatrix} \quad (5.30)$$

where

$$m_{11,c} = \sum_{i=3}^{10} \sum_{j=1}^N \rho C_{Ac} \cos \phi \frac{\pi D_i^2}{4} dz$$

$$m_{22,c} = \sum_{i=3}^{10} \sum_{j=1}^N \rho C_{Ac} \sin \phi \frac{\pi D_i^2}{4} dz$$

$$\begin{aligned}
m_{33,c} &= \sum_{i=3}^{10} \rho C_{Ac} \frac{\pi D_i^3}{12} \\
m_{42,c} &= \sum_{i=3}^{10} \sum_{j=1}^N \rho C_{Ac} \cos \phi \frac{\pi D_i^2}{4} (Z_{e_k} - s) dz \\
m_{51,c} &= \sum_{i=3}^{10} \sum_{j=1}^N \rho C_{Ac} \sin \phi \frac{\pi D_i^2}{4} (Z_{e_k} - s) dz \\
m_{61,c} &= \sum_{i=3}^{10} \sum_{j=1}^N \rho C_{Ac} \frac{\pi D_i^2}{4} \cos \phi \tilde{Y}_{c_i} dz \\
m_{62,c} &= \sum_{i=3}^{10} \sum_{j=1}^N -\rho C_{Ac} \frac{\pi D_i^2}{4} \sin \phi \tilde{X}_{c_i} dz \\
\tilde{X}_{c_i} &= -X_{c_i} \cos \phi + Y_{c_i} \sin \phi \\
\tilde{Y}_{c_i} &= X_{c_i} \sin \phi + Y_{c_i} \cos \phi
\end{aligned}$$

A simplified form of the added matrix for hulls was adopted, for a non-elongated platform that has different added mass forces for acceleration components parallel to the three reference axes directions [2]. The first three diagonal terms of the added mass are given by Eq 5.31~5.33.

$$m_{11,h} = \rho C_{m_1} V \quad (5.31)$$

$$m_{22,h} = \rho C_{m_2} V \quad (5.32)$$

$$m_{33,h} = \rho C_{m_3} V \quad (5.33)$$

For a spherical platform of radius a , however, the platform volume and the added mass coefficients are given by Eq 5.34~5.35.

$$V = \frac{4}{3} \pi a^3 \quad (5.34)$$

$$C_{m_1} = C_{m_2} = C_{m_3} = \frac{1}{2} \quad (5.35)$$

The remaining terms of the added mass matrix are obtained by calculating the acceleration reaction forces due to unit linear acceleration along the reference axes, for a platform with center of volume (x_1, y_1, z_1) , these yields the remaining terms, given by Eq 5.36~5.49.

$$m_{12,h} = m_{13,h} = m_{23,h} = 0 \quad (5.36)$$

$$m_{14,h} = m_{25,h} = m_{36,h} = 0 \quad (5.37)$$

$$m_{15,h} = m_{11,h} z_1 \quad (5.38)$$

$$m_{16,h} = -m_{11,h}y_1 \quad (5.39)$$

$$m_{26,h} = -m_{22,h}z_1 \quad (5.40)$$

$$m_{26,h} = m_{22,h}x_1 \quad (5.41)$$

$$m_{34,h} = m_{33,h}y_1 \quad (5.42)$$

$$m_{35,h} = -m_{33,h}x_1 \quad (5.43)$$

$$m_{44,h} = m_{22,h}z_1^2 + m_{33,h}y_1^2 \quad (5.44)$$

$$m_{55,h} = m_{33,h}x_1^2 + m_{11,h}z_1^2 \quad (5.45)$$

$$m_{66,h} = m_{11,h}y_1^2 + m_{22,h}x_1^2 \quad (5.46)$$

$$m_{45,h} = -m_{33,h}x_1y_1 \quad (5.47)$$

$$m_{46,h} = -m_{22,h}x_1z_1 \quad (5.48)$$

$$m_{56,h} = -m_{11,h}x_1y_1 \quad (5.49)$$

A special case of the above derivation is used to obtain the hydrodynamic added mass matrix for the rectangular cross-section hulls. The instantaneous centers of the hulls volume are given Eq 5.50~5.52.

$$x_{1,hull1,2} = \begin{cases} X_g - b_{st} \sin\phi \\ X_g + b_{st} \sin\phi \end{cases} \quad (5.50)$$

$$y_{1,hull1,2} = \begin{cases} Y_g - b_{st} \cos\phi \\ Y_g + b_{st} \cos\phi \end{cases} \quad (5.51)$$

$$z_{1,hull1,2} = \begin{cases} Z_g - (h-b/2) \\ Z_g + (h-b/2) \end{cases} \quad (5.52)$$

5.3.2.3 Hydrostatic stiffness matrix

Contributions to the hydrostatic stiffness matrix, K_h , arise in the heave, roll and pitch DOFs due to buoyancy forces in the water plane cutting members of the hull [2] as given by Eq 5.53.

$$[K_h] = \begin{bmatrix} 0 & 0 & 0 & 0 & 0 & 0 \\ 0 & 0 & 0 & 0 & 0 & 0 \\ 0 & 0 & k_{33} & 0 & 0 & 0 \\ 0 & 0 & k_{43} & k_{44} & 0 & 0 \\ 0 & 0 & k_{53} & k_{54} & k_{55} & 0 \\ 0 & 0 & 0 & 0 & 0 & 0 \end{bmatrix} \quad (5.53)$$

where

$$\begin{aligned}
k_{33} &= \rho g \sum A_{wn} \\
k_{43} &= \rho g \sum y_w A_{wn} \\
k_{53} &= -\rho g \sum x_w A_{wn} \\
k_{54} &= \rho g \sum x_w y_w A_{wn} \\
k_{44} &= \rho g \Delta G M_p \\
k_{55} &= \rho g \Delta G M_r
\end{aligned}$$

5.3.2.4 Mooring system stiffness matrix

For the derivation of the mooring stiffness, K_m , a right handed coordinate system was used as defined in Fig 5.4 for x, y plane. The restoring forces due to spring mooring lines on the platform were derived assuming that the mooring system behavior is perfect elastic and may be replaced with linear springs in x, y and z directions. Therefore, the mooring restoring forces of the mooring system were evaluated by Eq 5.54. It is worth mentioning that, in the derivation of this equation, only terms up to the second order were retained.

$$\begin{Bmatrix} F_{mx} \\ F_{my} \\ F_{mz} \\ M_{mx} \\ M_{my} \\ M_{mz} \end{Bmatrix} = \begin{bmatrix} k_x & 0 & 0 & 0 & -k_x Z_f & k_x Y_f \\ 0 & k_y & 0 & -k_y Z_f & 0 & -k_x X_f \\ 0 & 0 & k_z & 0 & 0 & 0 \\ 0 & -k_y Z_f & 0 & k_y Z_f^2 & 0 & 0 \\ -k_x Z_f & 0 & 0 & 0 & k_x Z_f^2 & 0 \\ k_x Y_f & -k_x X_f & 0 & 0 & 0 & (k_x Y_f^2 + k_y X_f^2) \end{bmatrix} \begin{Bmatrix} X_g \\ Y_g \\ Z_g \\ \theta_x \\ \theta_y \\ \theta_z \end{Bmatrix} \quad (5.54)$$

Thus, the mooring contribution to the system dynamics was represented by the symmetrical stiffness matrix given in Eq 5.55.

$$[K_m] = \begin{bmatrix} k_x & 0 & 0 & 0 & -k_x Z'_f & k_x Y'_f \\ 0 & k_y & 0 & -k_y Z'_f & 0 & -k_x X'_f \\ 0 & 0 & k_z & 0 & 0 & 0 \\ 0 & -k_y Z'_f & 0 & k_y Z'^2_f & 0 & 0 \\ -k_x Z'_f & 0 & 0 & 0 & k_x Z'^2_f & 0 \\ k_x Y'_f & -k_x X'_f & 0 & 0 & 0 & (k_x Y'^2_f + k_y X'^2_f) \end{bmatrix} \quad (5.55)$$

In Eq 5.55, the mooring line spring constants (k_x, k_y, k_z) were obtained from force-excursion nonlinear mooring system analysis (as presented in Chapter 4), as the first derivative of the restoring force corresponds to the desired excursion. It should be noted that for the evaluation of the horizontal spring constants (k_x, k_y), two nonlinear mathematical models were used, based on the line original and instantaneous cord lengths. These mathematical models were estimated by data fitting technique for the nonlinear force-excursion relation. The line original and instantaneous cord lengths are given by Eq 5.56~5.57.

$$L_{cho} = \left[(X_{fo} - X_A)^2 + (Y_{fo} - Y_A)^2 + (Z_{fo} - Z_A)^2 \right]^{1/2} \quad (5.56)$$

$$L_{ch} = \left[(X_f - X_A)^2 + (Y_f - Y_A)^2 + (Z_f - Z_A)^2 \right]^{1/2} \quad (5.57)$$

5.3.3 Low frequency second order analysis

For low frequency motion analysis, the same procedure as presented for first order motion analysis was used but structure DOF were limited to surge, sway and yaw. In addition, the total force was evaluated up to second order using the methodology presented in Chapter 3. For this analysis purpose, large displacement nonlinear solution of the EOM in the time domain applying the dynamic equilibrium through using Newmark- β approach was adopted.

The EOM was solved by an iterative unconditional stable Newmark- β with constant average acceleration with factor $\beta = 1/4$ [112]. The factor γ was taken as $1/2$, assuming no artificial damping. The EOM was written in a form of an effective static equilibrium equation in terms of the new time step force \hat{F}_{i+1} and stiffness \hat{K} and was solved for the time updated displacements X_{i+1} as given by Eq 5.58.

$$\hat{F}_{i+1} = \hat{K}X_{i+1} \quad (5.58)$$

where the effective force vector and stiffness were matrix calculated from Eq 5.59~5.60 respectively.

$$\hat{F}_{i+1} = F_{i+1} + M(a_0 X_i + a_2 \dot{X}_i + a_3 \ddot{X}_i) + B(a_1 X_i + a_4 \dot{X}_i + a_5 \ddot{X}_i) \quad (5.59)$$

$$\hat{K} = K + a_o M + a_1 B \quad (5.60)$$

The time updated (at step $i+1$) acceleration and velocity were calculated from Eq 5.61~5.62.

$$\ddot{x}_{i+1} = a_o(x_{i+1} - x_i) - a_2 \dot{x}_i - a_3 \ddot{x}_i \quad (5.61)$$

$$\dot{x}_{i+1} = \dot{x}_i + a_6 \dot{x}_i + a_7 \ddot{x}_{i+1} \quad (5.62)$$

The related integration constants ($a_o \sim a_7$) are given in Eq5.63 ~5.70.

$$a_o = \frac{1}{\beta \Delta t^2} \quad (5.63)$$

$$a_1 = \frac{\gamma}{\beta \Delta t} \quad (5.64)$$

$$a_2 = \frac{1}{\beta \Delta t} \quad (5.65)$$

$$a_3 = \frac{1}{2\beta} - 1 \quad (5.66)$$

$$a_4 = \frac{\gamma}{\beta} - 1 \quad (5.67)$$

$$a_5 = \left(\frac{\gamma}{2\beta} - 1 \right) \overline{\Delta t} \quad (5.68)$$

$$a_6 = (1 - \gamma) \overline{\Delta t} \quad (5.69)$$

$$a_7 = \gamma \overline{\Delta t} \quad (5.70)$$

5.3.4 Ramp function

To ensure a continuous and gradual transition of wave loads from an initial zero to a fully developed stage at time T_f , ramp function f_{ramp} was used before applying Newmark- β technique for EOM solution in time domain. The wave loads were multiplied by a factor, f_{ramp} , which increases from zero to one as given by Eq 5.71.

$$f_{ramp} = \frac{1}{2} \left[1 - \cos \left(\frac{\pi t}{T_f} \right) \right] \quad (5.71)$$

5.3.5 Programming aspects

For the wave frequency motion analysis, the programming flow chart shown in Fig 5.5 was used, in which smaller time step (typically 0.2 s) were used since the dynamic equilibrium conditions was based on the previous time step. Also, the flow chart shown in Fig 5.6 was used for the nonlinear iterative dynamic analysis of the moored in the time domain. The dynamic equilibrium condition was applied each time step through iteration in the updated wave forces F_i with maximum allowable error of $\varepsilon_{\max} = 0.01\%F_i$. This value of permissible was taken to speed up the convergence with and acceptable accuracy. Usually this procedure converges in 3~5 iterations steps as shown in Fig. 5.7. Thus, to avoid loop iteration without convergence, the iteration counter was limited to fifteen ($j_{\max} = 15$).

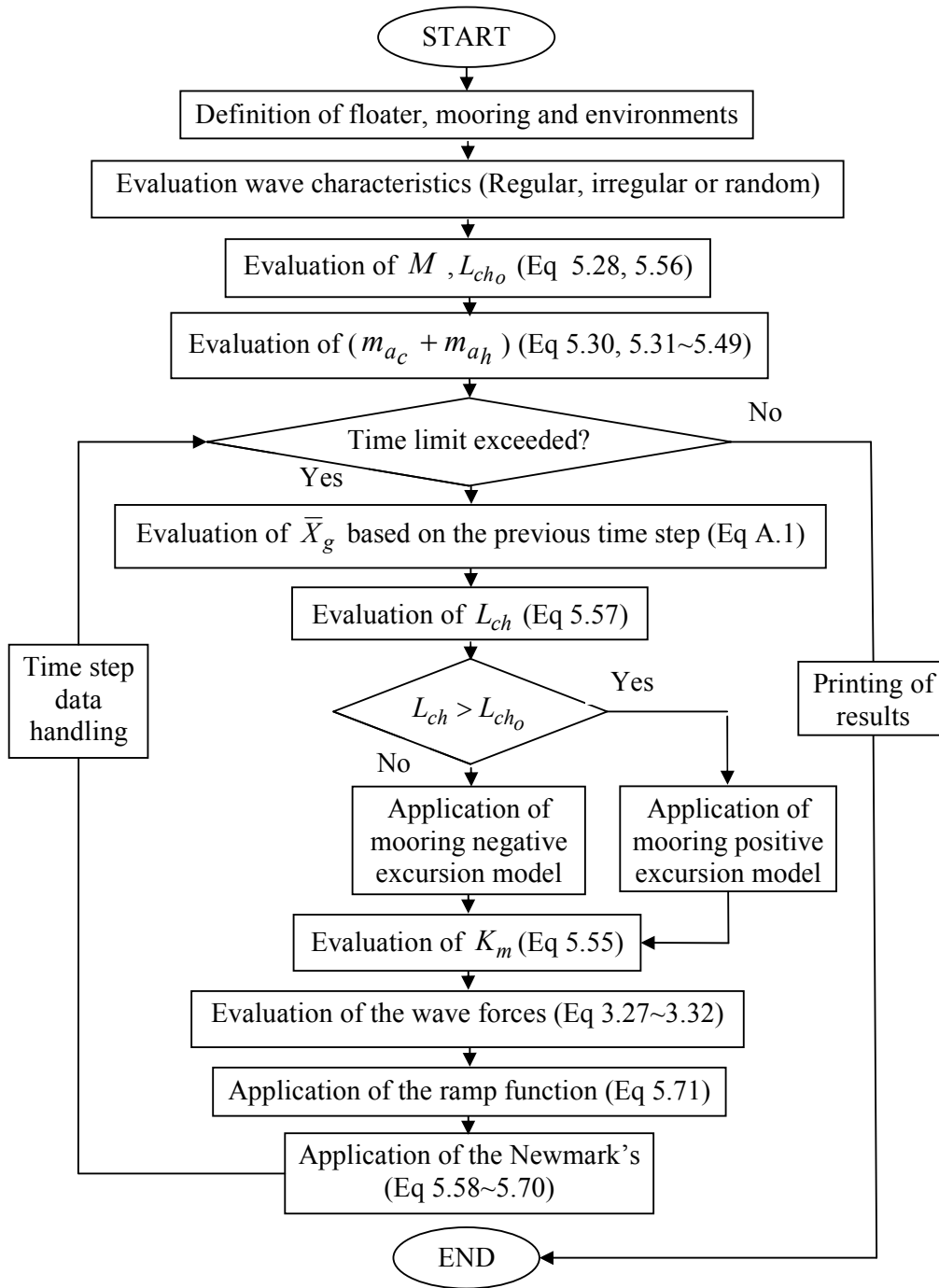


Fig 5.5: Flow chart for the linear dynamic analysis

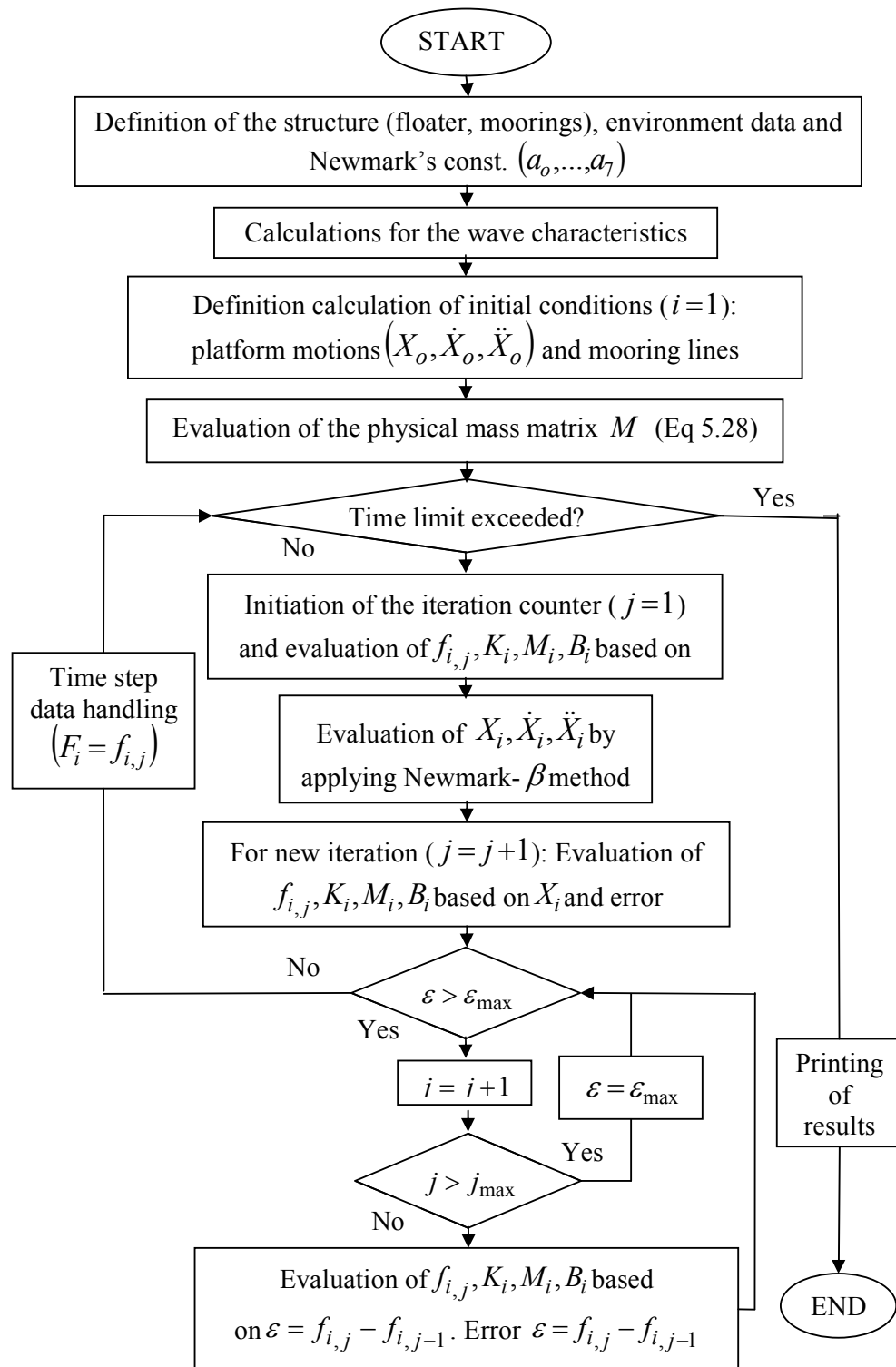


Fig 5.6: Flow chart for the nonlinear dynamic analysis

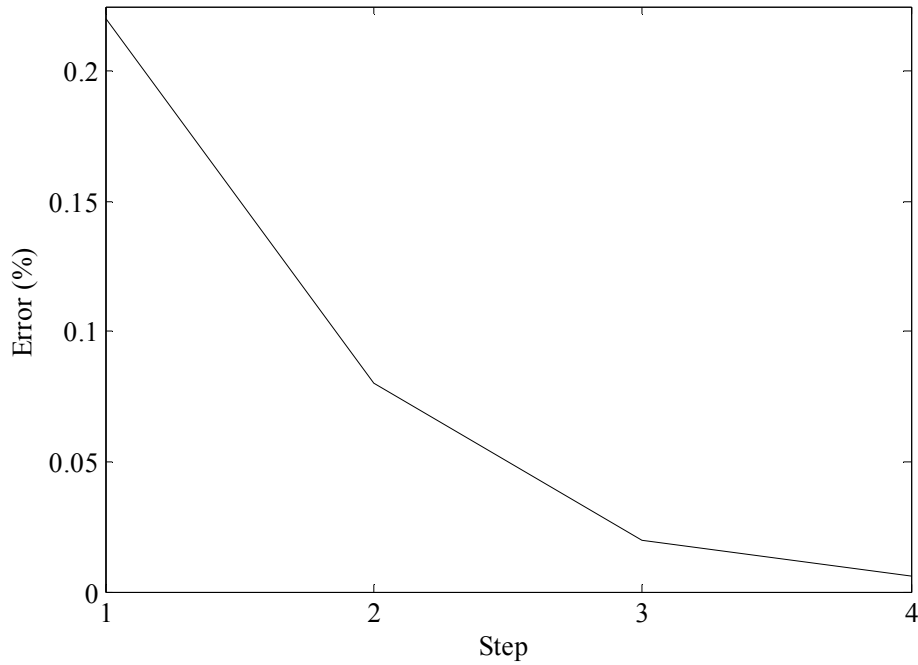


Fig 5.7: Solution convergence curve related to Fig. 5.6

5.4 Chapter summary

In this chapter, the two different methods for the floating platform dynamic analysis were presented. The first method was in the frequency domain, in which, the linearized frequency-dependant solution of the EOM was presented with the related programming flow chart. Mathematical formulae for the frequency dependant force coefficient were presented. The second method was in the time domain, in which, the procedure for the first-order 3D motion analysis was given. The EOM and the related coefficient matrices were presented. The derived mathematical representation of the nonlinear mooring system-structure interactions was given. Finally, a programmable procedure the horizontal nonlinear motion analysis in the time domain was presented.

Chapter 6

EXPERIMENTAL TESTS

6.1 Chapter overview

As indicated previously, the numerical models were developed for linear and nonlinear response analysis for moored semi submersibles. Therefore, it was decided to conduct the experimental studies in two phases. The first experiment phase was aimed to provide data for validating the first order numerical model. The second phase was associated with the second order nonlinear numerical model. In this chapter, the laboratory tests are described. Modeling of the structure, mooring systems and environment are described. Moreover, the instrumentations and data acquisition systems for the tests are described.

6.2 Test facility and instrumentations

All moored sea keeping tests were performed in the Universiti Teknologi PETRONAS (UTP) wave tank. This tank, measures approximately 22 m long, 10 m wide and 1.5 m deep as shown in Fig 6.1. The wave maker system in this tank comprises of wave-maker, remote control unit, signal generation computer and dynamic wave absorption beach. The wave-maker comprises a number of modules, each having eight individual paddles, which can move independently to one another. These paddles move backward and forward horizontally to generate waves in the basin. The wave-maker can generate the following types of sea-states:

1. Irregular 2D/3D short/long crested waves in a direction normal to the wave-maker by using filtered white noise method (FWNM).
2. Irregular 2D/3D short/long crested waves at normal/ oblique angle by using the summation of sine wave method (SSWM).

3. Bi-directional regular/ irregular 2D long crested wave by using SSWM.
4. Sea state that have been created off-line and stored in a file as paddle position.
5. Regular waves at normal/oblique angles.

The Bi-directional or bi-modal waves can be produced through dividing the wave-maker into sections and each section can produce different sea-states and directions. The sea state setup in the same way as wave generated by SSWM. The specifications of the wave maker system are given in Table 6.1.

Table 6.1: Specification of the wave maker system

Description		Value
Paddle	Width (m)	0.62
	Height (m)	1.30
	Stroke (m)	± 0.54
	Velocity (m/s)	0.87
	Force (kN)	1.50
Sea-state available		JONSWAP
		PM
		Derbyshire coastal
		Derbyshire ocean
		ISSC ¹
		ITTC ²
		BTTP
		Neumann
		Bretschneider
		Top hat
Sea-state defined by		Wind speed
		Fetch
		Frequency
		Wave height
		Spectral Density
Wave generation method		FWNM
		SSWM
		Bi-directional
		User defined
Module	No.	2.00
	Width (m)	4.98
Maximum water depth (m)		1.00

¹ International Ship Structure Congress

² International Towing Tank Congress

The wave maker is capable of generating up to 0.3 m and period as short as 0.5 s (model scale). Major random sea spectra, such as JONSWAP, ISSC, PM, Bretschneider, and Ochi-Hubble, can be simulated. Also, custom spectra can be added to the software and calibrated. The progressive mesh beach systems minimize interference from reflected waves during tests. UTP basin also includes a current making system capable of providing a current speed of 0.2 m/s at a water depth of 1m. (the speed varies with water depth). Fig 6.1 shows UTP basin plan and east-west section and Fig 6.2 shows UTP basin wave maker system.

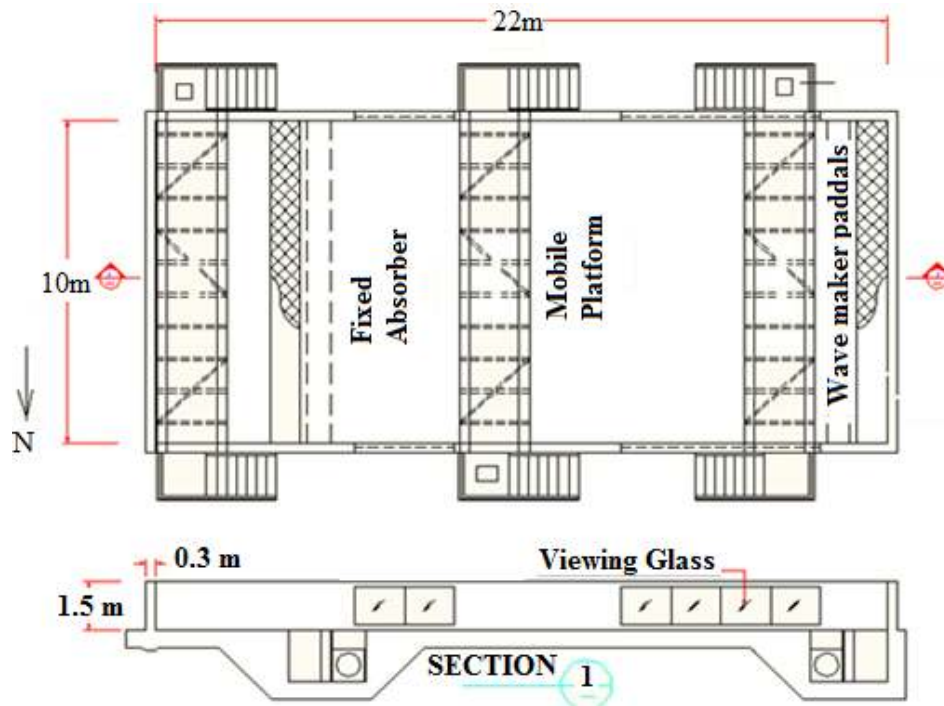


Fig 6.1: UTP wave basin



Fig 6.2: UTP basin wave maker system
(Source: *UTP basin user manual, HR Wallingford, 2008*)

The UTP basin beach consists of foamed filled plates fixed to a rigid framework. The beach efficiency has been verified by absorption coefficient was evaluating the absorption coefficient test, it is found that the absorber coefficient decreased slightly with bigger waves, dropping from 98.1% to 97.4 % as wave height increase from 0.05 m to 0.30 m [113]. The following instrumentation were used during tests: 1) single axis Rieker's inclinometer mainly for inclination tests, 2) six-camera optical tracking (OptiTrack) system to measure 6 DOF motions, 3) resistive HR's wave probes to measure the wave heights, 4) TML's load cells to measure the mooring system loads, 5) TML's accelerometers to measure model acceleration at required locations. The accelerometers and the load cells were connected to TML's smart dynamic strain recorder (data logger) attached to Windows-based data acquisition and analysis program that is suitable for up to 64 analogue input channels. The remaining sensors were attached directly to the data acquisition system. This system consists of three modules: 1) calibration and scaling of inputs, 2) data acquisition and 3) data analysis.

The Rieker's single axis inclination sensor is a complete angle monitoring and early warning system. It was designed to allow for tilt angle measurement in the range $\pm 70^\circ$ and formatted to provide one reading per line. The sensor was supplied with digital LCD display, which can be configured to display degrees, percent grade, or inch per foot rise with either 0.1° or 0.01° resolution. The LCD display model also

provides a relative zero and minimum/maximum angle function. The relative zero allows to temporarily zeroing the digital readout to obtain relative slope changes. The minimum/maximum angle function provides the smallest and largest angle the device has sensed since the last reset. The sensor is powered by an 8-30 VDC non-regulated power supply (default power), with optional 9V battery, 110VAC or 240VAC wall adapters, or cigarette lighter adaptor.

The use of optical tracking (OptiTrack) system is a robust, real-time data, 3D system, in which markers can be attached to multiple objects in known patterns (rigid bodies) within specified volume, allowing them to be tracked in full 6DOF (position and orientation). The tracking tools provide built-in multi-camera calibration and 3D point tracking which automatically hands off between cameras for maximum coverage. The system is equipped with built-in support standard VRPN, which make integrating the real time tracking data with applications a snap. The system comprises of the following components: 1 x calibration square, 1 x hardware key, 2 x rigid body base, 2 x hub, 1 x sync cable (5 m), 1 x calibration wand, reflective markers (LEDs), 1 x tracking tools software, 2 x USB 2.0 active extension cable (15 m). The system is equipped with six cameras, each with a resolution of 640x480 pixels. This system of cameras can track up to 24 LEDs in a maximum working space range of 11m³.

The HR's wave probe compromise of two parallel stainless steel rods with a plastic head and foot. The head is fixed to calibration stem and a mounting block is supplied that allows the calibration stem to be fixed to any vertical surface. The wave probe is equipped with tripod for the use in the wave basin. The probe length is 900 mm and diameter of 6.0 mm. The wave probe is equipped with a simple monitor for measuring rapidly changing water levels. In addition, the TML's load cells used were tension/compression submersible low capacity (250N) cylindrical-shaped (80 mm diameter and 42 mm height) and light weight (0.45 kg) instruments. It can be used for high precision measurement because the internal structure uses both ends fixation beam for the strain sensing element. This sensor having rated output of 3000×10^{-6} strain and can be used in temperature range of $-20^{\circ}\text{C} \sim +70^{\circ}\text{C}$. These sensors are equipped with 60 m length and 6 mm diameter 4-core shielded chloroprene cable.

The used TML's accelerometer is a single axis acceleration transducer. It is compact (16 mmx16 mmx28 mm) and light weight (18g) and has a waterproof structure, which makes it suitable for use wave tank applications in temperature range of $-10^{\circ}\text{C}\sim+50^{\circ}\text{C}$ and water pressure up to 500 kPa. This transducer could measure body acceleration in the range of $\pm 10 \text{ m/s}^2$ with rated output of 1000×10^{-6} strain and frequency response of 50Hz. This transducer is attached to 80 m 4-core shielded vinyl cable, having a diameter of 3.2 mm.

The TML's smart dynamic strain recorder is a compact flash recording type 4-channel dynamic strain recorder and measures strain, DC voltage and thermocouples. At the same time of measurement, measured data are automatically stored on a compact flash card up to 2GB. This data logger measured 15.7 cm x 8.4 cm x 4.2 cm and weighed 0.5 kg. The 4-channel unit can be connected in parallel up to 8 units (total 32 channels). It was configured with built-in un-interrupted power supply (UPS) to function when power supply is suddenly interrupted; the power switch is designed to turn off after recording the measured data on the CF card. The highest sampling speed is 5 μs with one channel and the measured data are recorded on a specified CF memory card at the same speed. For simultaneous data acquisition, its sampling rate is 50 kHz for 4 channels. It should be noted that this data logger is capable for measuring a large strain up to $\pm 80000\times 10^{-6}$ strain.

6.3 Choice of the scale and physical modelling law

The choice of scale of a model test often is limited by experimental facilities available. Optimum scale is determined by comparing the economics of the scale model with that of the experiments. Indeed, too small scale may result in scale effects and errors and too large is often very expensive and may introduce problems for physically handling the model. The primary purpose of this wave tank study is to obtain reliable results by minimizing scale effects and measurements error. Large scale is recommended to minimize the problem of scale effect when Reynolds effect (such as presence of drag force) is important. The common ranges of scale for studies such as breakwater stability are 1:150 to 1:20 in 2D (towing) tanks, and 1:150 to 1:80

in three dimensional wave tanks. The desired range of the scale for offshore structures in two dimensional wave tanks is 1:100 to 1:10.

Modeling laws relate the behavior of the prototype to that of a scaled model in a prescribed manner [97]. There are two generally accepted methods by which scaling laws relating two physical systems are developed. The first one is based on the inspectional analysis of the mathematical description of the physical system under investigation. The dynamics of physical system are described by a system of differential equations. These equations are written in non-dimensional terms. Since the simulated physical system duplicates the full-scale system, these non-dimensional quantities in the differential equations must be equal for both. Thus, the equality of the corresponding non-dimensional parameters governs the scaling laws. This method assures similarity between the two systems but is dependent upon knowing explicitly the governing equations for both the prototype and model. The second method is based on well-known Buckingham Pi theorem. In this approach, the important variables influencing the dynamics of the system are identified first. Then, their physical dimensions are noted. Based on Buckingham Pi theorem, an independent and convenient set of non-dimensional parameters is constructed from these variables. The equality of the pi terms for the model and prototype systems yields the similitude requirements or scaling laws to be satisfied. The model and prototype structural systems are similar if the corresponding pi terms are equal [114].

In case of water flow with a free surface, the gravitational effects predominate. The effect of other factors, such as viscosity, surface tension, roughness ...etc is generally small and can be neglected. In this case, Froude's model law is most applicable. The Froude number, F_r , for the model and the prototype in waves is expressed by Eq 6.1, where the subscripts p, m stand for prototype and model respectively. Assuming geometric similarity $D_p = \lambda D_m$, where λ is the scale factor for the model and D stands for any characteristic dimension of the object. Thus, the prototype velocity is given by $u_p = \sqrt{\lambda} u_m$. In this study, a general assumption was made that the model follows the Froude's law of similitude, the common variables are listed in Table 6.2.

$$F_r = \frac{u_p^2}{gD_p} = \frac{u_m^2}{gD_m} \quad (6.1)$$

Table 6.2: Model to prototype multipliers
(Source: *Offshore structures modeling, Chakrabarti, 1994*)

Variable	Unit	Scale factor
<i>Geometry</i>		
Length	L	λ
Area	L ²	λ^2
Volume	L ³	λ^3
Angle	None	1
Radius of gyration	L	λ
Area moment of inertia	L ⁴	λ^4
Mass moment of inertia	ML ²	λ^5
CG	L	λ
<i>Kinematics and dynamics</i>		
Time	T	$\lambda^{1/2}$
Acceleration	LT ⁻²	1
Velocity	LT ⁻¹	$\lambda^{1/2}$
Displacement	L	λ
Angular acceleration	T ⁻²	λ^{-1}
Angular velocity	T ⁻¹	$\lambda^{1/2}$
Angular displacement	None	1
Spring constant (Linear)	MT ⁻²	λ^2
Damping coefficient	None	1
Damping factor	MT ⁻¹	$\lambda^{5/2}$
Natural period	T	$\lambda^{1/2}$
Displacement	L	λ
<i>Wave mechanics</i>		
Wave height	L	λ
Wave period	T	$\lambda^{1/2}$
Wave length	L	λ
Celerity	LT ⁻¹	$\lambda^{1/2}$
Particle velocity	LT ⁻¹	$\lambda^{1/2}$
Particle acceleration	LT ⁻²	1
Water depth	L	λ
Wave pressure	ML ⁻¹ T ⁻²	λ

6.4 The semi submersible-A tests

6.4.1 General

Following a few catastrophic accidents involving mobile offshore drilling platforms, various studies were carried out to investigate the adequacy of stability criteria applied to offshore mobile platforms which was derived on an empirical basis considering service experience accumulated for ships over many years [97]. In the design of the offshore structures, it is desirable to assess the effects of the environmental forces such as wind, wave and current forces on the platform prior to its construction. Seakeeping performance is of significant importance in platform design due to the stationary nature drilling and production platforms. Knowledge of the anticipated wave forces is critical to the design of the mooring lines. For the purpose of the seakeeping design, its response assessment to environmental forces is usually evaluated using either physical experiments or computational simulations. Traditionally, the evaluation of a prototype platform's seakeeping performance was accomplished by physical experiments using scaled models in a towing or wave tank. This approach, however, requires a detailed model to be built including the complete hull geometry and the mass properties of the model. This process is very costly as model construction often costs large amount of money to fabricate and outfit. In addition, the model basin charges constitute another large amount of money per day. In this experimental study, the primary objective is to provide benchmark data for verification of the first order numerical analysis results. In this experiment phase, the seakeeping performance of the model under study was assessed. This was conducted during the period of 07/09/2009 to 06/12/2009.

6.4.2 Model description

A twin hulled semi submersible physical model was made of acrylic plastic sheets to the scale of 1:100 according to the dimensions shown in Fig 6.3~Fig 6.4. The members were cut using laser techniques and connected by melting and cooling using chloroform chemical compound. The model consisted of two rectangular pontoons

each with four circular columns. The reason for choosing this particular geometry for the semi submersible model was because it had a similar configuration to the Ocean Ranger that had sunk to the bottom of the ocean with the loss of all 84 of its crew [115]. The model was painted in high visibility yellow color for video capturing purposes and draft marks with measurements scale were added to the model corner columns for accuracy and visual purposes. Special ballast containers were placed in the model corner columns to ballast the model to the desired draft. The weights inside these ballast containers could be placed vertically so as to adjust the centre of gravity of the model for the desired MC height. Fig 6.5 shows the semi submersible model prior tests. The principal data for the prototype and the model are given in Table 6.3.

Table 6.3: The semi submersible-A data (Scale 1:100)

Variable		Prototype	Model	
			Scaled	Actual
No of bracing members		16	16	16
Bracing diameter (m)		1	0.01	0.011
Water depth (m)		110	1.1	1.1
Draught (m)		16	0.16	0.16
MC height (m)	Roll	2.88	0.0288	0.028
	Pitch	2.36	0.0236	0.024
Radii of gyration (m)	Roll	34.3	0.343	0.34
	Pitch	35.3	0.353	0.35
	Yaw	40.6	0.406	0.410

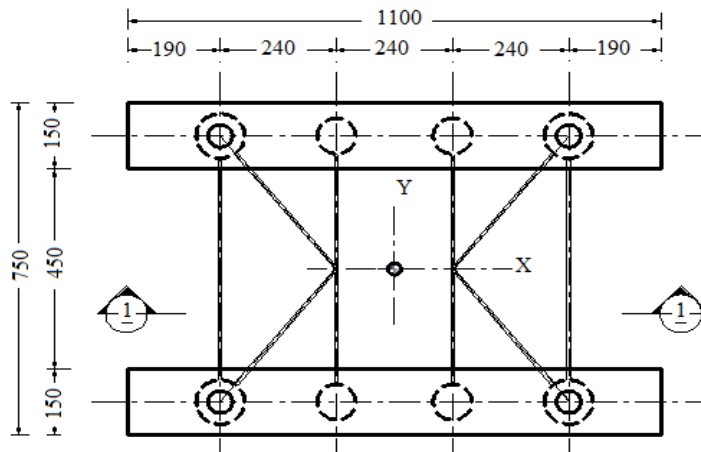


Fig 6.3: Plan of the semi submersible-A model
(All dimensions are in mm)

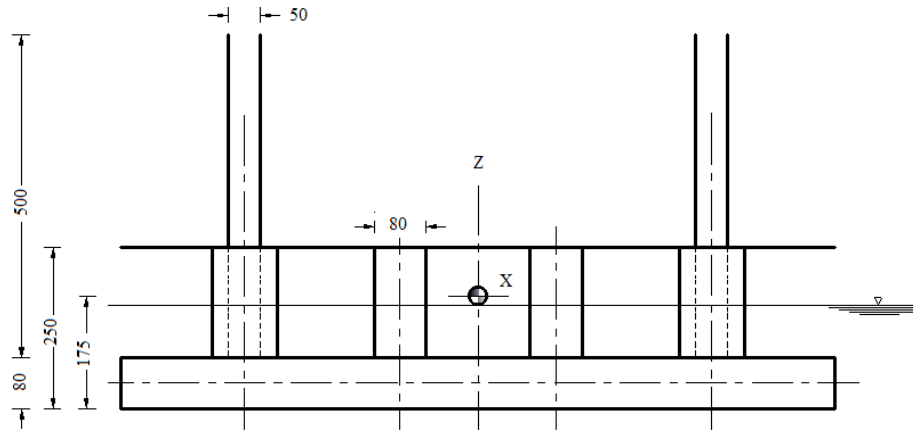


Fig 6.4: Section 1 of the semi submersible-A model
(All dimensions are in mm)



Fig 6.5: The semi submersible-A model prior tests

6.4.3 Mooring system

Modeling of moored platforms involves modeling both the floating structure and the mooring system [3]. Several types of mooring are used for floating structures, the most common being mooring chains, wires and hawsers. In this study, a multi component mooring system was utilized for stationing the model. It consisted of aluminum alloy wire and distributed clump weight made of steel chain as shown in Fig 6.6. The physical characteristics of a single mooring line are given Table 6.4. Four typical mooring lines were connected to the model at fairlead points according to the drawing shown in Fig 6.7. It is worth mentioning that the pretension on the

mooring lines was maintained by attaching small buoys near the mooring fairlead, these buoys having been designed perfectly to provide the desired net buoyancy. Elasticity modulus and breaking strength of the wired part of a mooring line were determined by testing a specified length of the mooring line in the universal testing machine to measure its elongation at various loadings.

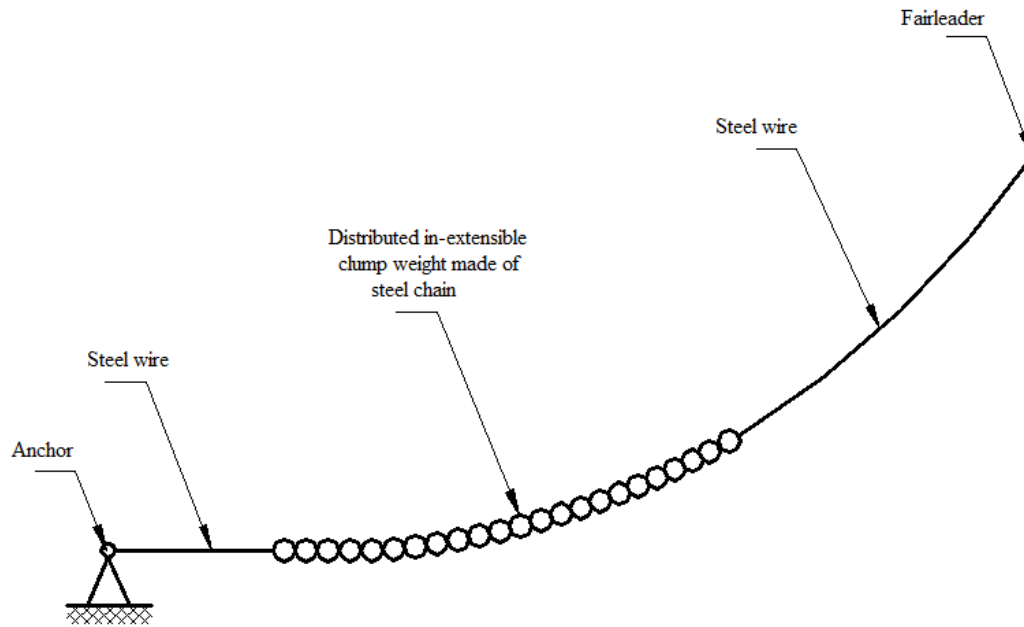


Fig 6.6: Single mooring line configuration (Semi submersible-A)

Table 6.4: Multi-component mooring line properties

Description	Prototype	Model	
		Scaled	Actual
Horizontal pretension component (kg)	70000	70E-3	70E-3
Angle of inclination at fairlead point	30	30	30
Effective diameter of the mooring/anchor	150	1.50	1.55
Effective area of the clump weight (mm ²)	1057	10.57	10.50
Submerged unit weight of	20000	0.020	0.021
Submerged unit weight of clump	83000	0.083	0.083
Mooring line length (m)	120	1.2	1.2
Anchor line length (m)	50	0.5	0.5
Clump weight length (m)	100	1.0	1.0
Height of fairlead point (m)	110	1.1	1.1
Elasticity modulus of mooring/anchor	105	1.045	1.045
Mooring breaking strength (MPa)	360E+3	3.6E+	3.594E
Anchor average holding capacity (kg)	7250E+0	7.25	7.26

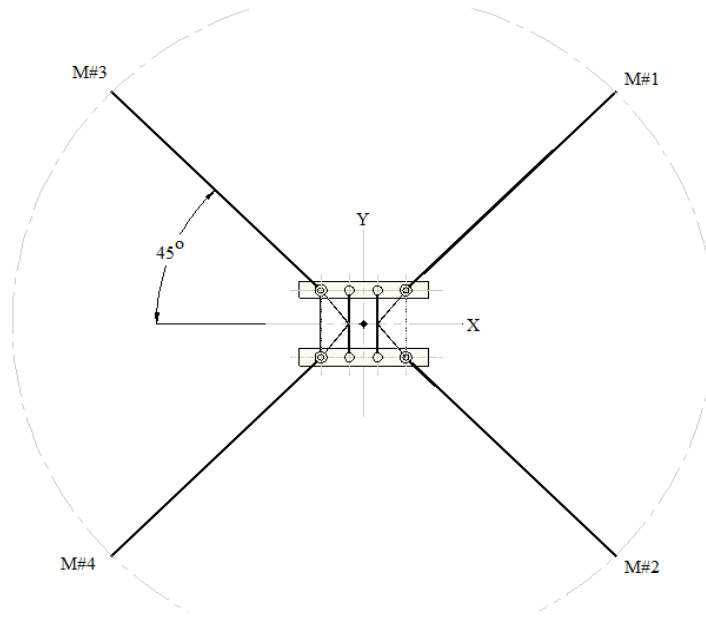


Fig 6.7: Mooring system setup plan (semi submersible-A)

6.4.4 Seakeeping tests

The seakeeping test setup was organized so that the amplitudes of the regular wave trains for all platform motions could be measured visually. Two wave probes, one velocity meter and one video camera were located according to the drawing shown in Fig 6.8~Fig 6.10 to record the wave profile, water particle velocity and the model motion time histories for head, beam and quartering seas respectively. The tests in regular waves were carried out in order to obtain RAOs of the semi submersible physical model. The high quality video camera was used to record the surge, heave and pitch responses of the model for sea, quartering and beam waves. The data were measured in time series for the wave tests and filtered.

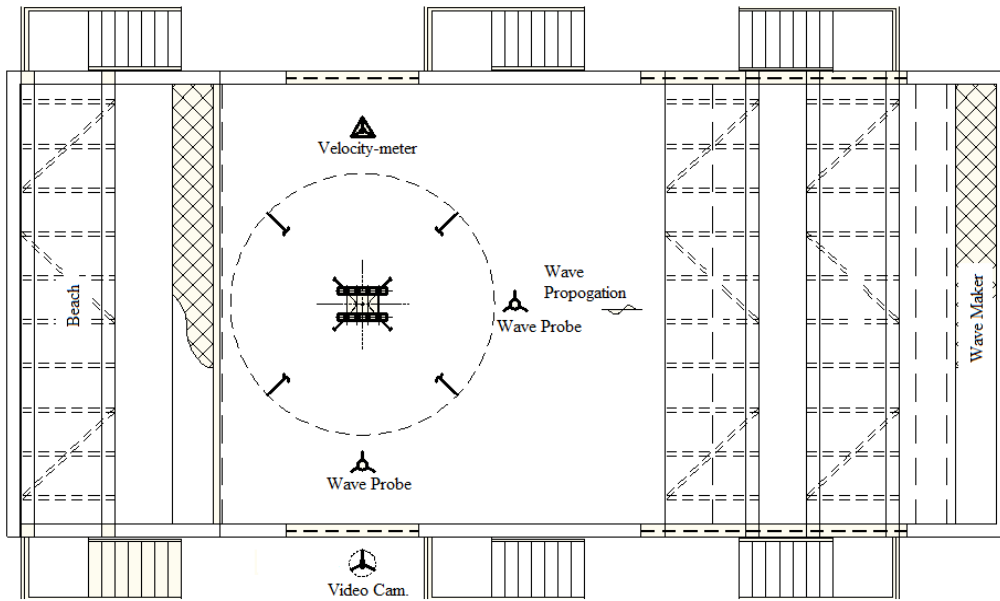


Fig 6.8: Seakeeping test setup for head seas (semi submersible-A)

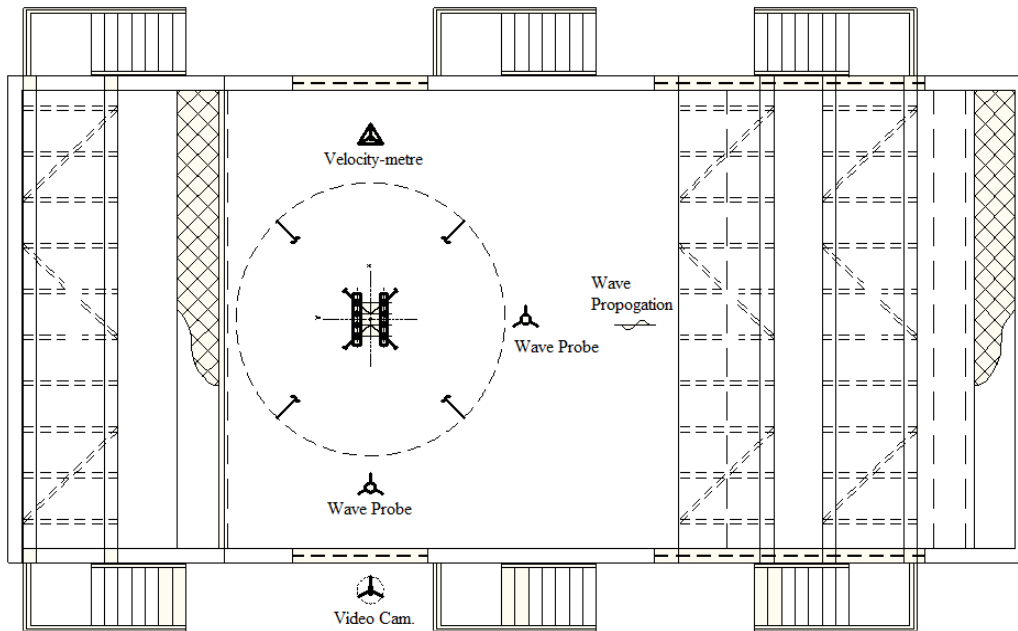


Fig 6.9: Seakeeping test setup for beam seas (semi submersible-A)

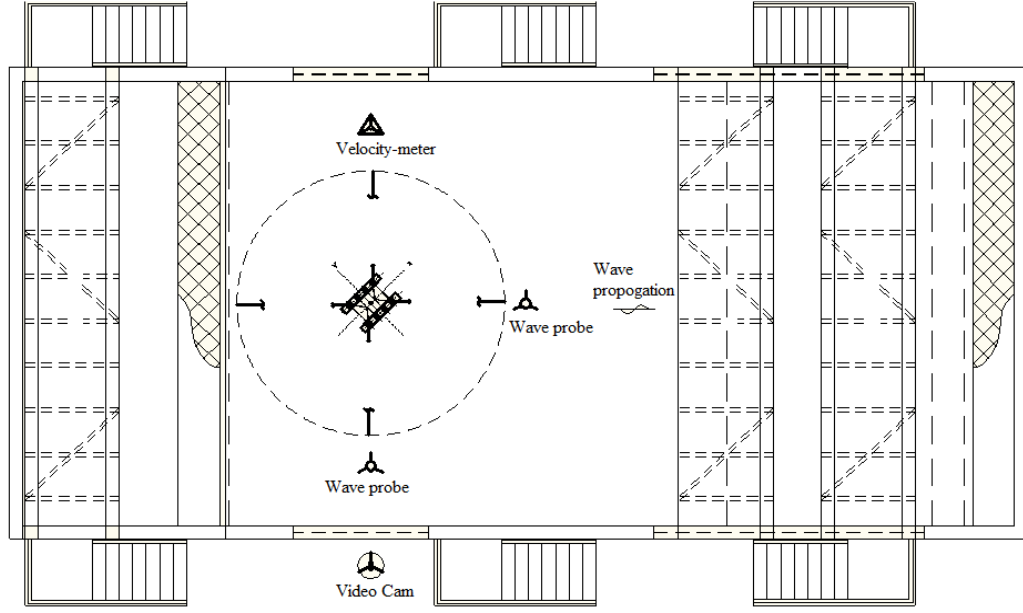


Fig 6.10: Seakeeping test setup for quartering seas (semi submersible-A)

For irregular wave, a PM (Pierson Markowitz) spectrum of 100 mm (model scale) significant wave height was used for the simulation of the sea state energy throughout the test for various semi submersible physical model orientations. For post processing, the data a numerical code was developed using the FFT technique to transfer the physical model irregular response time series to response energy spectra.

The transformation from the time domain to the frequency domain was evaluated by FFT Technique. The energy spectrum was assumed to behave as continuous function of frequency from frequency resolution to the Nyquist frequency. The frequency resolution, Δf , was evaluated by Eq 6.3 and the Nyquist frequency, f_N , was evaluated by Eq 6.4 in terms of the time step, $\overline{\Delta t}$. The total data length, T_s , was divided into eight segments, each segment has an equal number of data points, N , the time step was evaluated by Eq 6.5. For efficient computations N was taken as power of two (128, 256 ...etc). The result of FFT was squared to convert to energy unit [103]. For the response time series, $R(t)$ was transformed to energy spectrum using FFT as shown in Eq 6.2.

$$S(f) = \frac{2\pi}{T_s} \left[\sum_n^N R(n\overline{\Delta t}) e^{2\pi i f (n\overline{\Delta t})} \overline{\Delta t} \right]^2 \quad (6.2)$$

$$\Delta f = \frac{1}{N\Delta t} \quad (6.3)$$

$$f_N = \frac{1}{2\Delta t} \quad (6.4)$$

$$\overline{\Delta t} = \frac{T_s}{8N} \quad (6.5)$$

6.5 The semi submersible-B tests

6.5.1 General

Seakeeping characteristics of a floating structure is in motion under its own power or moored to either sea floor or to another structure by some mechanical means determine its ability to survive the environment. The motion and component loads of the floating system are generally computed analytically and verified with model tests [114]. For designing floating offshore structures, the motions of the structure should be known in addition to the wave forces acting on it, which was routinely obtained through model testing. As mentioned in 2.3.2, for a given platform and position in the horizontal plane, the motions depend on the mooring system and the external forces acting on the platform. Forces caused by a stationary irregular sea are of irregular nature and may be split into two parts: first order oscillatory forces with wave frequency and second order, slowly varying forces with frequencies much lower than the wave frequencies [17]. The motion of a floating structure takes place within two different time scales, the first time scale corresponding to the period of the waves, while the second one having periods much longer than the periods associated with the water waves. The oscillations of the latter time scales have been called the "slow drift oscillations". Even though the origin of these oscillations is a second order effect, it has turned out that these oscillations are responsible for the major part of the loads on a mooring system [21]. In this experiment phase, the model under study was calibrated, followed by the results of the seakeeping tests, which were conducted during the period of 1/11/2010 to 31/12/2010.

6.5.2 Model description

The subject of this investigation was a twin-hulled semi submersible with six circular columns and a displacement of 40,000 T in fresh water. It was decided to construct the model of scale 1:100 from steel plates according to the dimensions given in Fig 6.11~Fig 6.12. The constructed model undergoing tests is shown in Fig 6.13. Table 6.5 shows the summary of the calculated and measured general structural data of the semi submersible (full scale). The twin-hulled semi submersible model was tested for two model orientations (head and beam seas) in the wave tank of the UTP. The model motion and the restraining lines tension responses were measured by optical tracking system and load cells respectively. Data post processing program was prepared to evaluate the response spectra to random waves using the Fast Fourier Technique (FFT). About 80 runs were carried out including model CG evaluation, inclination, free-decay, static offset and seakeeping tests.

Table 6.5: The semi submersible-B data (full scale)

Description		Value	
		Calculated	Measured
Length of the lower hull (m)		100	100
Draft (m)		27	27
Center of gravity (m)	X_g	At mid-ship	At mid-ship
	Y_g	At mid-ship	At mid-ship
	Z_g	19.313 above base line	19.133above base line
Metacentric height (m)	GM_r	5.104	5.091
	GM_p	1.498	1.477
Displacement in fresh water (T)		39,400	39,320
Radius of gyration (m)	r_x	20.981	21.222
	r_y	27.450	27.359
	r_z	24.285	-
Natural periods (s)	$T_{n_{surge}}$	105.5	105.1
	$T_{n_{sway}}$	127.6	127.2
Water depth (m)		110	110

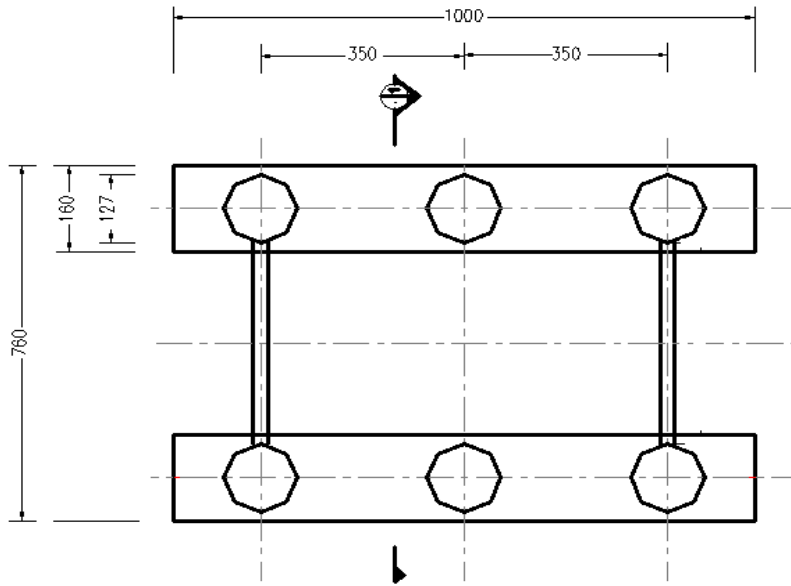


Fig 6.11: Plan of the semi submersible-B model
(All dimensions are in mm)

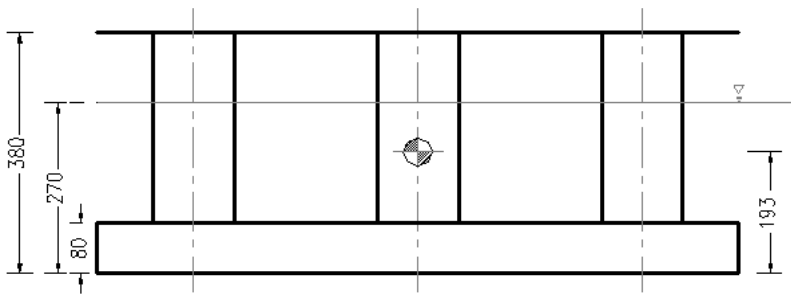


Fig 6.12: Section 1 of the semi submersible-B model
(All dimensions are in mm)

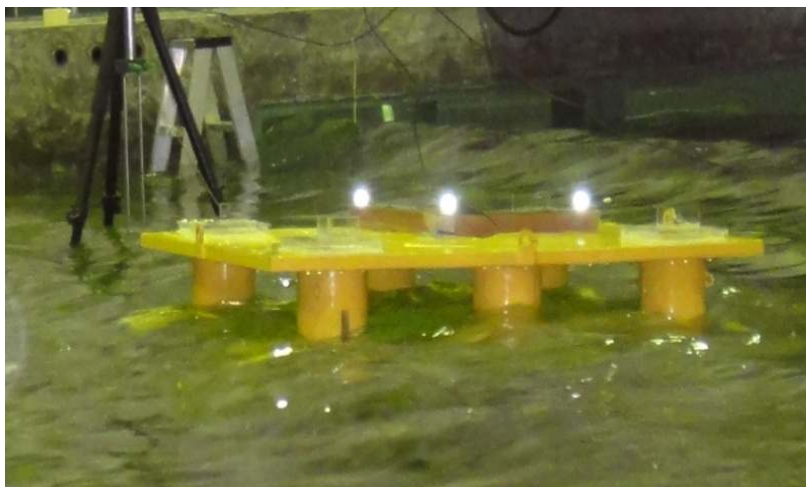


Fig 6.13: The semi submersible-B model during tests

6.5.3 Laboratory tests

6.5.3.1 Model hydrostatic data tests

The basic structural hydrostatic data for model under study was measured in the laboratory and compared to values calculated using the methods mentioned previously for hydrostatic analysis (see Table 6.5). The model center of gravity CG, mass moments of inertia, and MC heights were measured. For x and y axis estimation of the CG position, the model was balanced on a round rod along a particular axis for the determination of the center of gravity along that direction axis. The model was placed transverse on its sides on the rod and moved until the two sides tend to balance and a small displacement on either direction of the rod provided a bias in that direction. Thus, the distance from the edge of the model to the center of the rod gave the location of the CG.

In the z axis, the calibration test was performed by hanging the model from a universal joint such that it was free to swing in the roll and pitch directions. Then, lifting the bow of the model by known load and simultaneously recording the angle of inclination by using an inclinometer, the CG was calculated from the Eq 6.6. It should be noted that five inclination angles were applied to the model and average CG was considered.

$$H_{CG} = \frac{Fd_1}{W \sin \theta} \quad (6.6)$$

where H_{CG} is the distance from the CG to the universal rotational point, F is the lifting force, d_1 is the horizontal moment arm from lifting point to rotational point, W is the model weight and θ is the model's angle of inclination. For the evaluation of radii of gyration, the test setup was the same as for CG test. The model was given a rotational displacement and then allowed to swing freely about the universal joint. By means of six-camera optical tracking system, the natural period of displacement time history was determined. The mass moment of inertia I_g was calculated using Eq 6.7.

$$I_g = \left(\frac{T_N}{2\pi}\right)^2 WH_{CG} - \left(\frac{W}{g}\right)H_{CG} \quad (6.7)$$

where T_N is the period of oscillation. A wet inclination test was performed to measure the MC height GM of the platform in roll and pitch directions. Initially, the model was free floated and known weights were placed on the center of the bow deck support and the trim angle of the model was recorded by using the single axis inclinometer. The GM value was evaluated using Eq 6.8. Five trim angles were applied in each direction and the average GM value was adopted, where F_a is the added weight.

$$GM = \frac{F_a d_1}{W \sin \theta} \quad (6.8)$$

6.5.3.2 Static offset test

Static test was carried out to determine the mooring system stiffness. The model was restrained by four lines ($M_1 \sim M_4$). Two load cells (LC_1 and LC_2) were attached in up and down stream as shown in Fig 6.14. Cables were used as mooring lines and the forces were measured horizontally. Nine set of measurements were taken for every 4m (full-scale) system increment. Forces were applied at the counterweight point by pulling the string and the load cells readings were recorded.

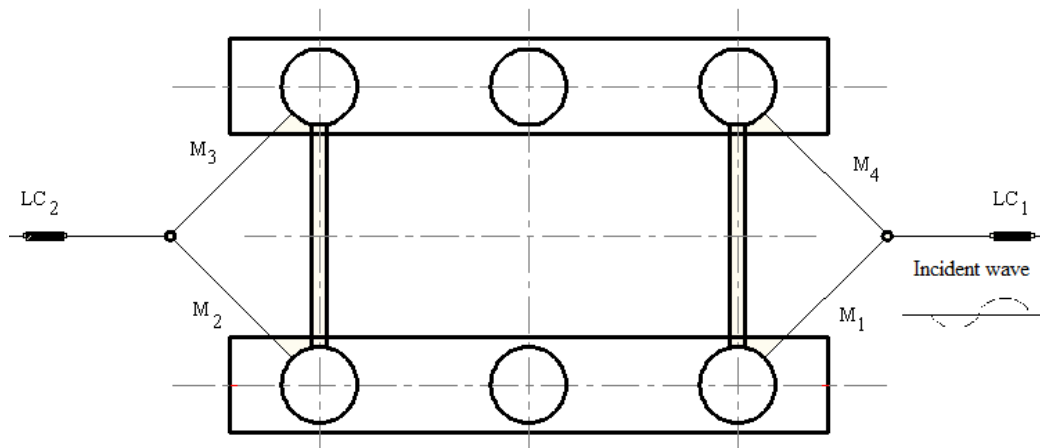


Fig 6.14: Restraining system (semi submersible-B)

6.5.3.3 Free vibration tests

Extensive model test programs and computations among the mean and slowly varying drift forces on slender elements have been carried out by [20]. The findings of this

study confirmed that considerable viscous effects can be present in the low frequency wave forces and the major part of this effect to drift forces is confined to the splash zone. Since tests are treated as mass-spring system, valuable information is obtained from the free vibration of the system regarding the system natural period and damping.

The magnitude of the damping determines the extent of the motions and corresponding mooring loads near the system natural period. When nonlinear damping is present, the EOM for the damped-free oscillation in surge is given in Eq 6.9, which is equivalent to Eq 5.1:

$$M\ddot{x} + C\dot{x} + b_2|\dot{x}|\dot{x} + kx = 0 \quad (6.9)$$

where C is the linear damping coefficient and b_2 is the nonlinear damping coefficient. Eq 6.9 is nonlinear and the close form solution is difficult to obtain. Thus, the following simplification was made by linearizing the nonlinear damping term as given by Eq 6.10.

$$|\dot{x}|\dot{x} = \frac{8}{3\pi} \omega_n x_k \dot{x} \quad (6.10)$$

where x_k is the amplitude of the k^{th} oscillation cycle Substituting Eq 6.10 in Eq 6.9 yields Eq 6.11.

$$M\ddot{x} + \left(C + \frac{8b_2}{3\pi} \omega_n x_k \right) \dot{x} + kx = 0 \quad (6.11)$$

Letting

$$C' = C + \frac{8b_2}{3\pi} \omega_n x_k \quad (6.12)$$

The damping factor (including the linearized term) is given by Eq 6.13.

$$\zeta' = \frac{C'}{2M\omega_n} \quad (6.13)$$

The damping coefficient is related to the logarithmic decrement of three consecutive values by Eq 6.14.

$$\ln \frac{x_{k-1}}{x_{k+1}} = 2\pi\zeta' \quad (6.14)$$

Substituting Eq 6.12~6.13 in Eq 6.14 yields Eq 6.15.

$$\ln \frac{x_{k-1}}{x_{k+1}} = \frac{T_n}{2} \left(\frac{C}{M} + \frac{16b_2}{3MT_n} x_k \right) \quad (6.15)$$

The damping coefficient is given by Eq 6.16.

$$\zeta = \frac{1}{2\pi} \ln \frac{x_{k-1}}{x_{k+1}} - \frac{4b_2}{3\pi M} x_k \quad (6.16)$$

Assuming the nonlinear damping coefficient is approximated by the Morison drag term as given by Eq 6.17.

$$b_2 = \frac{\rho}{2} C_D A \quad (6.17)$$

where A is the projected area of the platform in the direction of the flow. Plugging Eq 6.17 into Eq 6.16 gives Eq 6.18, which represents a straight line by fitting technique for the oscillation peaks, the values of the C_D and ζ were evaluated.

$$\frac{1}{2\pi} \ln \frac{x_{k-1}}{x_{k+1}} = \zeta + \frac{2}{3\pi} \left(\frac{\rho C_D A}{M} \right) x_k \quad (6.18)$$

The inertia coefficient was estimated from the measured natural period using Eq 6.19.

$$C_M = \frac{kT_n^2}{4\pi^2 m} \quad (6.19)$$

6.5.3.4 Seakeeping tests

For evaluating the seakeeping characteristics of the model, it was tested for regular (monochromatic) waves, regular wave groups (bi-chromatic), and random waves. Two typical springs were attached with steel wires on fore and aft side of the model, the springs being chosen to be linear in the range of the anticipated loads. The general objectives of these tests were to evaluate the steady drift forces, platform motion and mooring tension responses to regular waves. The platform and restraining system responses were measured also for bi-chromatic and random seas. All random time traces were transformed to the frequency domain using Fast Fourier Technique (FFT). Two model orientations were configured to simulate head and beam seas.

The hydrodynamic forces on an object floating in regular waves may be resolved into an oscillatory part and a constant part, of which the latter is known as steady drifting force [16], which is responsible for the offset of the structure. Although [116] experimental results showed that the relation between drift force and wave height does not follow the theoretically assumed proportionality with the square of the wave amplitude, the general accepted assumption is that the horizontal second order wave forces, known as wave drifting forces are proportional to the square of the wave amplitude [17]. In this study, this general assumption was used. Therefore, the non-dimensional steady drift force coefficient R_d is defined by Eq 6.20.

$$R_d = \left(\frac{2F_d}{\rho g a^2 B} \right)^{1/2} \quad (6.20)$$

where F_d is the steady drift force and B is the characteristic length of the structure facing the incident wave. By measuring the average mooring force, the height and frequency of the incident wave, the steady drift (reflection) coefficient was evaluated using Eq 6.20. It should be noted that the first few minutes of the run were neglected to avoid the transient low frequency response. The effect of the wave amplitude on the reflection coefficient was studied by taking two wave amplitudes for the same wave frequency. The test duration for each run was one hour (full scale). Tests for regular waves were carried out for the range of the dominant wave frequencies. The measured total restraining was corrected using Eq 6.21 assuming that the difference between the actual wave force and the measured restraining force resulted in horizontal motion accelerations.

$$\bar{F}_d = F_m + m\ddot{x} \quad (6.21)$$

where \bar{F}_d is the actual(corrected) wave drift force, F_m is the measured wave drift force, m is the virtual mass (assumed constant) of the platform and \ddot{x} is the measured acceleration of the structure. The calculated wave drift forces (Eq 6.21) were compared with formulae introduced by [117], which was evaluated by fitting the data for single vertical floating cylinder. Assuming that the steady drift force originates at the splash zone, these formulae were used for the evaluation of the total drift force on semi submersible by summing up the drift of single columns and neglecting the effect of the underwater hulls and the hydrodynamic interference.

Measurements of the mean horizontal wave drift forces on the model in regular waves were carried out using soft spring restraining system, which consisted of horizontal wires with soft linear springs connected to load cells mounted on the model. The test setup is shown in Fig 6.15~Fig 6.16. The test setup was arranged to measure the mean and low frequency slowly varying horizontal wave drift forces by suppressing the model from drifting while leaving the model to respond freely to the first order wave frequency forces. This was made possible by the soft spring wire restraining system attached to the model. It should be noted that the restraining system was pretensioned through pulley system and clamped in a way to ensure that no slacking of the wire occurred during the tests.

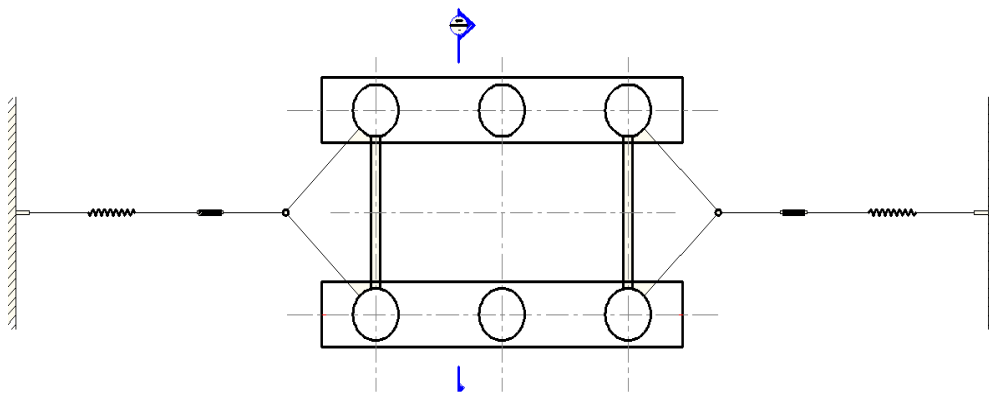


Fig 6.15: Plan of the seakeeping tests setup (semi submersible-B)

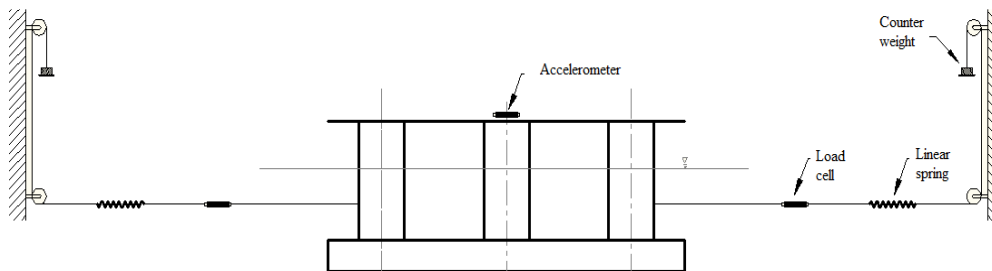


Fig 6.16: Section 1 of the seakeeping tests setup (semi submersible-B)

For measurement of the generated wave profiles, two wave probes were placed. One was in front of the model and the second one in the same line of the model. These remained in place during seakeeping tests. The acquired data includes the model 6DOF motions, mooring loads and the environmental variables (wave height, period ...etc.). The semi submersible-B was tested with two orientations (head ad beam) in variety of wave environments, including ten different regular waves (each with two wave amplitudes), eight different combinations of bi-chromatic waves (based on the natural frequency of the system) and different random sea states. Table

6.6~Table 6.7 summarizes the target and measured regular (mono-chromatic) sinusoidal waves for head and beam seas respectively, which were used for the seakeeping experiments.

Table 6.6: Regular waves for head seas (semi submersible-B)

Test Derive	Wave height (m)		Wave period (s)	
	Target	Measured	Target	Measured
HRG 1.1	0.88	0.80	6	6.11
HRG 1.2	1.80	1.69		
HRG 2.1	1.28	1.36	7	6.93
HRG 2.2	2.60	2.28		
HRG 3.1	1.74	1.43	8	8.08
HRG 3.2	3.50	3.28		
HRG 4.1	2.24	2.05	9	8.89
HRG 4.2	4.50	3.85		
HRG 5.1	2.76	2.68	10	9.91
HRG 5.2	5.50	5.37		
HRG 6.1	3.88	3.43	12	12.08
HRG 6.2	7.80	7.22		
HRG 7.1	5.68	4.76	14	13.87
HRG 7.2	11.40	10.67		
HRG 8.1	3.88	4.21	16	16.12
HRG 8.2	7.80	7.41		
HRG 9.1	2.56	2.49	18	19.13
HRG 9.2	5.10	4.96		
HRG 10.1	0.88	0.54	21	20.88
HRG 10.2	1.80	0.95		

Table 6.7: Regular waves for beam seas (semi submersible-B)

Test Derive	Wave height (m)		Wave period (s)	
	Target	Measured	Target	Measured
BRG 1.1	0.88	0.89	6	5.98
BRG 1.2	1.80	1.59		
BRG 2.1	1.28	1.25	7	6.94
BRG 2.2	2.60	2.30		
BRG 3.1	1.74	1.70	8	7.97
BRG 3.2	3.50	3.21		
BRG 4.1	2.24	2.59	9	9.08
BRG 4.2	4.50	4.72		
BRG 5.1	2.76	2.94	10	10.13
BRG 5.2	5.50	5.87		
BRG 6.1	3.88	3.43	12	11.89
BRG 6.2	7.80	7.30		
BRG 7.1	5.68	5.20	14	14.06
BRG 7.2	11.40	11.00		
BRG 8.1	3.88	4.87	16	16.11
BRG 8.2	7.80	8.44		
BRG 9.1	2.56	2.52	18	17.91
BRG 9.2	5.10	4.93		
BRG 10.1	0.88	0.77	21	21.02
BRG 10.2	1.80	1.03		

Eight bi-chromatic waves were selected in a way that the difference frequency of the wave components approaches the considered natural frequency of the system. The input data for bi-chromatic wave generation for head and beam seas are given in Table 6.8.

Table 6.8: Bi-chromatic waves for head and beam seas (semi submersible-B)

Head seas			Beam seas		
Test Derive	Height (m)	Frequency (rad/s)	Test Derive	Height (m)	Frequency (rad/s)
HBC1	2/2	0.628/0.658	BBC1	2/2	0.628/0.638
HBC2	2/2	0.628/0.668	BBC2	2/2	0.628/0.648
HBC3	2/2	0.628/0.678	BBC3	2/2	0.628/0.658
HBC4	2/2	0.628/0.688	BBC4	2/2	0.628/0.668
HBC5	2/2	0.628/0.698	BBC5	2/2	0.628/0.678
HBC6	2/2	0.628/0.708	BBC6	2/2	0.628/0.688
HBC7	2/2	0.628/0.718	BBC7	2/2	0.628/0.698
HBC8	2/2	0.628/0.728	BBC8	2/2	0.628/0.708

Storm spectra were generated with JONSWAP spectral. During setup phase for the random wave tests, the data collection commenced 20 minutes (full scale) after running wave to allow for the wave to become fully developed at the model location.

In Table 6.9~Table 6.10, the target and measured random wave characteristics for head and beam seas are given respectively.

Table 6.9: Random waves for head seas (semi submersible-B)

Test Derive	Significant height (m)		Peak period (s)	
	Target	Measured	Target	Measured
HRW1	3.25	3.22	9.60	9.49
HRW2	8.50	8.44	11.80	11.40
HRW3	13.0	12.88	14.00	13.93

Table 6.10: Random waves for beam seas (semi submersible-B)

Test Derive	Significant height (m)		Peak period (s)	
	Target	Measured	Target	Measured
BRW1	3.25	3.20	9.60	9.63
BRW2	8.50	8.52	11.80	11.86
BRW3	13.0	13.03	14.00	14.07

In order to investigate the effects of single line of the restraining system failure on the motion and the intact lines response, four seakeeping tests were conducted in head regular and random seas. Each case was made by manually releasing M_1 or M_2 (Fig 6.14) during tests. Table 6.11~Table 6.12 give the target and measured wave characteristics for regular and random seas respectively. In each table, the targeted seas were almost the same but the associated numbers of the derive signal were changed to indicate the line number which was released during the test.

Table 6.11: Regular waves for line failure study (semi submersible-B)

Drive signal	Wave height (m)		Wave period (s)	
	Target	Measured	Target	Measured
MRG1	12	12.22	14	13.89
MRG2	12	12.33	14	14.11

Table 6.12: Random waves for line failure study (semi submersible-B)

Drive signal	Significant height (m)		Peak period (s)	
	Target	Measured	Target	Measured
MRW1	8.50	8.42	11.80	11.67
MRW2	8.50	8.53	11.80	11.71

6.6 Chapter summary

In this chapter, the physical modeling of two semi submersibles was described. Moreover, the structural data and the related restraining system were given. For the semi submersible-A, modeling of the environment the seakeeping test methodology

was presented. For the second semi submersible, the test procedures for the model calibration, the free decaying, the static offset and the seakeeping tests were described.

Chapter 7

RESULTS AND DISCUSSION

7.1 Chapter overview

In this chapter, results of the numerical and experimental models are presented. The method developed for analyzing multi-component mooring lines is adopted for studying the effects of pretension, mooring line configuration, clump weight, cable unit weight, elongation, breaking strength and pretension angle on the nonlinear force-excursion relationship. Also, for multi-component mooring lines, results and discussion for the hydrodynamic analysis are presented. Furthermore, the effects of seabed soil characteristics on mooring dynamics are investigated. The developed methods for the platforms linear and nonlinear analysis in the frequency domain and the time domain are validated by comparisons with experimental results. The former analysis method was used for investigating the effects of the design parameter for different semi submersible configurations on the platform motion and mooring tension responses. Also, experimental results regarding semi submersible mooring damaged conditions are presented and discussed.

7.2 Parametric study on deepwater mooring lines (Numerical results)

The procedure explained in 4.2.2 for analyzing multi-component mooring lines was used to construct the nonlinear force-excursion relationship for a single multi-component mooring line with distributed clump weight for horizontal (positive and negative) and vertical excursions. Table 7.1 shows the basic data used for the purpose of this study. In this study, the fairlead tension and stiffness characteristics of a multi-component catenary mooring line were studied with various parameter for horizontal (positive and negative) and vertical excursions. The effects of pretension, mooring

line configuration, clump weight, cable unit weight, elongation, breaking strength and pretension angle were investigated on the behavior of multi-component mooring line. The mooring line stiffness was evaluated as the first derivative of the tension with respect to the mooring excursion.

Table 7.1: Basic data for a multi-component mooring line analysis.

Parameter	Value
Initial horizontal force (kN)	1000
Angle of inclination at fairlead point (deg)	30
Effective area of the mooring/anchor line (m ²)	0.0032
Effective area of the clump weight (m ²)	0.8782
Submerged unit weight of mooring-anchor lines (kN/m)	0.2932
Submerged unit weight of clump weight (kN/m).	25
Anchor line length (m)	260
Clump weight length (m)	40
Water depth (m)	192
Height of fairlead point above sea-floor (m)	186
Elasticity modulus of mooring/anchor lines (m)	210E+6

7.2.1 Pretension effect

Fig 7.1 shows the pretension effect on the mooring line fairlead tension for 1000 kN, 1400 kN and 1800 kN pretension for horizontal positive excursions. It can be seen that the multi-component mooring line fairlead horizontal tension component was proportional to the pretension for horizontal excursions, while the same was true for vertical fairlead tension component for vertical excursions until the whole clump weight was lifted off the sea floor. There was little effect of pretension on the vertical fairlead tension component for vertical excursions when the whole clump weight was lifted off the sea floor.

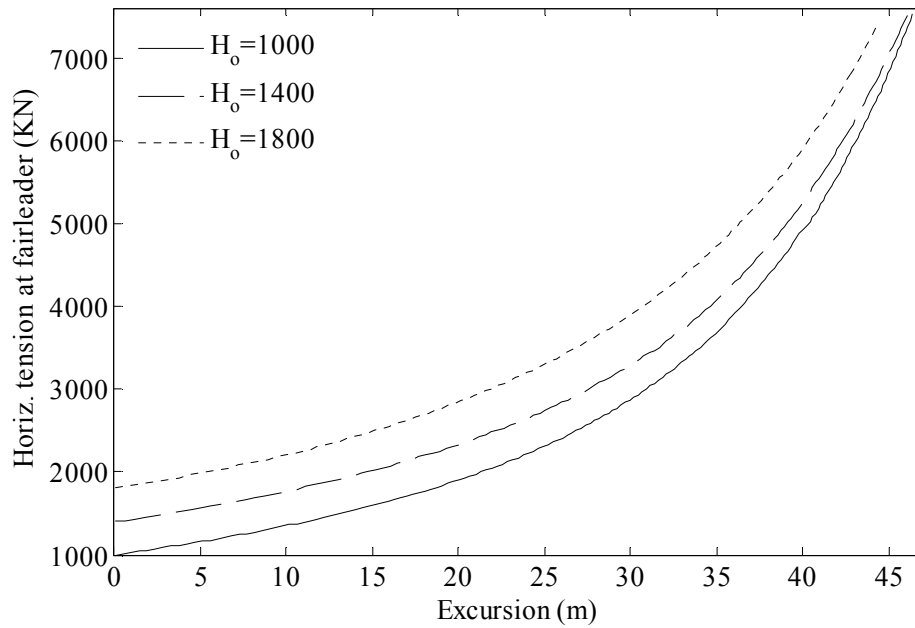


Fig 7.1: Effect of the initial pretension on the mooring tension

7.2.2 Mooring line configuration effect

The effect of mooring length/depth ratio on the vertical excursion was investigated for the ratios 2.67, 3.16 and 3.75. Fig 7.2 shows the L/d ratio effect. It was found that for this level of mooring pretensions, the mooring line fairlead tension and stiffness was independent of the mooring line length since the tension-stiffness curves were identical.

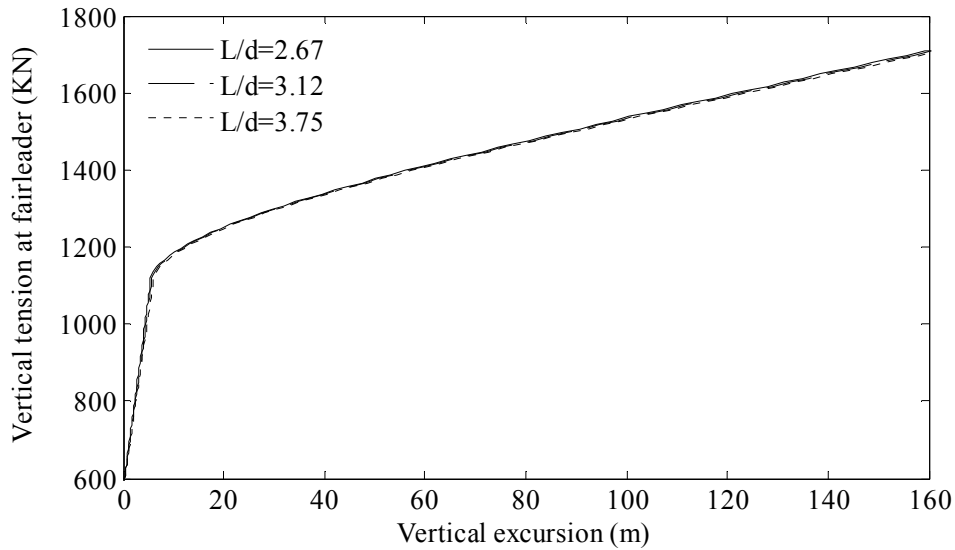


Fig 7.2: Effect of the mooring configuration on the fairlead vertical tension

7.2.3 Clump weight effect

The effect of the clump weight was studied for 1000 kN, 1500 kN and 2000 kN total clump weight for positive horizontal and vertical excursions. Fig 7.3 shows the effect of the distrusted clump for vertical weight excursions. It was noted that the horizontal fairlead tension component was independent of clump weight while the vertical fairlead tension component for vertical excursions was proportional to the clump weight beyond lifting off the whole clump weight. Also, it can be seen from this Figure that the force-excursions relationship was linear for low range of excursions (<10 m) and before lifting off the clump weight.

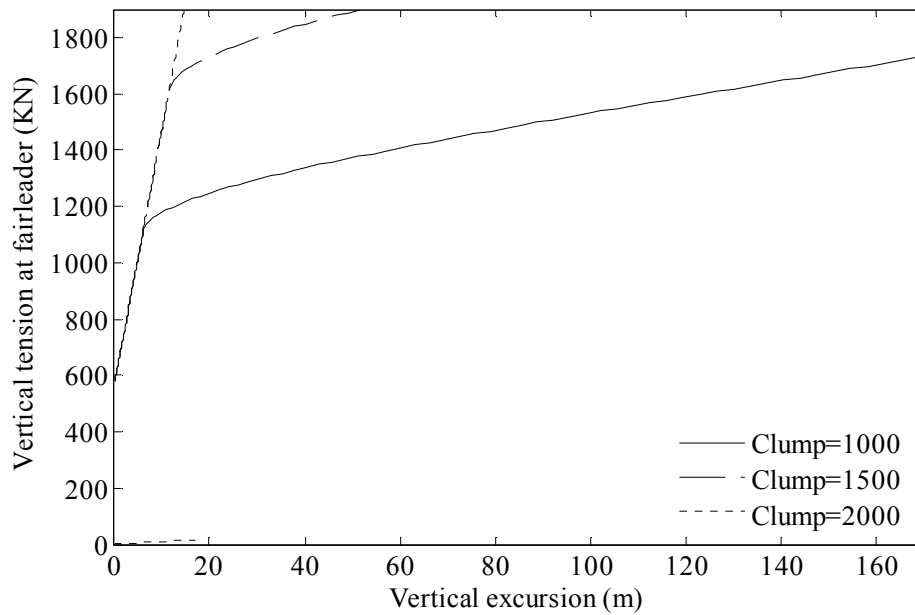


Fig 7.3: Effect of the clump weight on the fairlead vertical tension

7.2.4 Cable unit weight effect

Fig 7.4 shows the nonlinear force-excursion relationship for vertical excursions. The cable unit weight effect was investigated using 0.293 kN/m, 0.493 kN/m and 0.693 kN/m for vertical excursions. It was found that the cable restoring force was proportional to the unit weight of the cable for horizontal positive excursions. This was true for vertical excursions after lifting up the whole clump weight, but the relation was inversely proportional before lifting the clump weight.

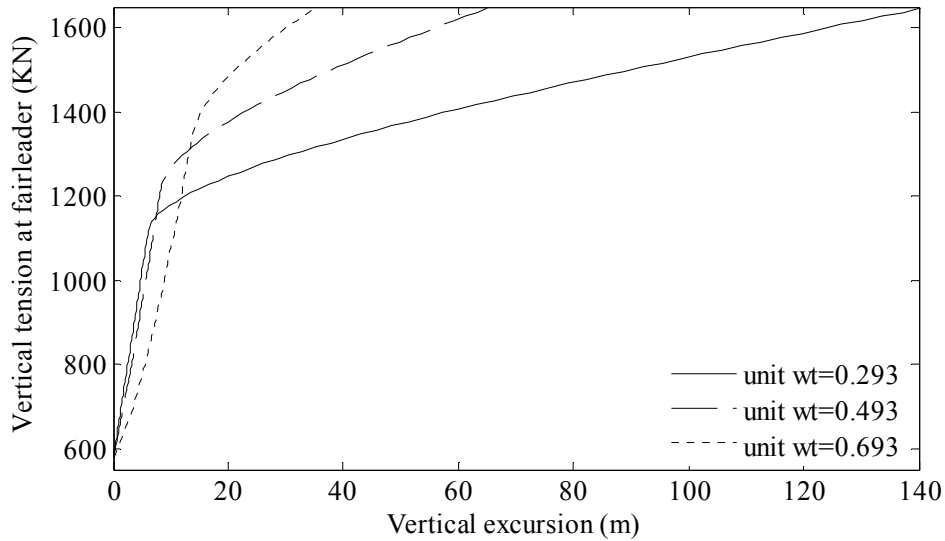


Fig 7.4: Effect of the cable unit weight on the fairlead vertical tension

7.2.5 Elongation (Cable axial stiffness) effect

Fig 7.5 shows the elongation effect for the cable. The elongation effect was studied using $0.672E+6$ kN, and $67.2E+6$ kN axial stiffness for positive excursions. It was noted that for the small tension range of horizontal tension component ($H_o < 2000$ kN), there was little effect of elongation, while in the large range of horizontal tension component ($H_o < 4000$ kN), the effect increased exponentially as shown in the same Figure. For vertical tension component, the effect of the cable axial stiffness was very little, especially beyond lifting off the whole clump weight.

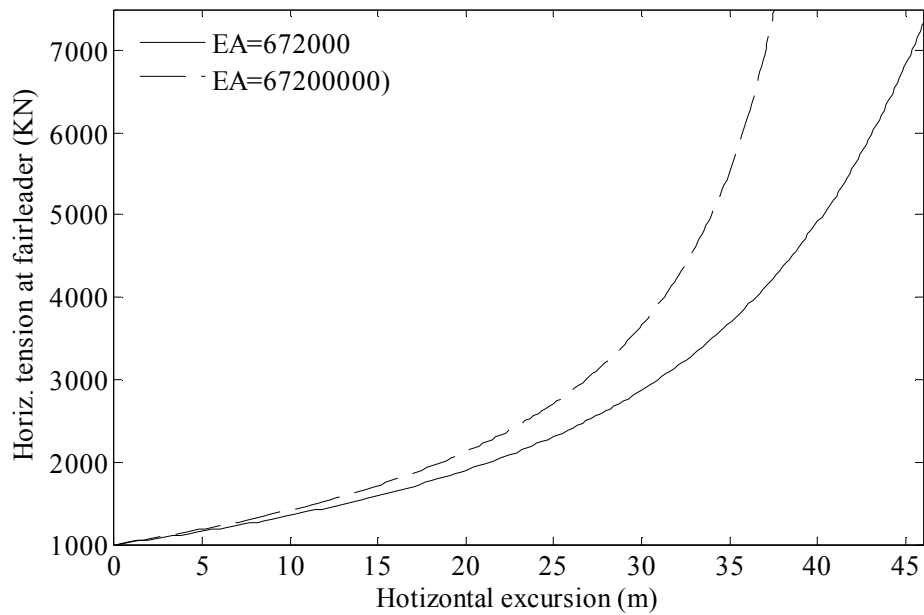


Fig 7.5: Effect of the elongation on the fairlead horizontal tension

7.2.6 Pretension angle effect

The effect of pretension angle was studied using 20°, 30° and 45° angles for positive horizontal and vertical excursions. Fig 7.6 shows the effect of pretension angle for 20°, 30° and 60° for negative horizontal excursions. It was noted that the mooring line horizontal restoring force was inversely proportional to the pretension angle for positive horizontal excursions. Although the mooring horizontal stiffness was proportional to the pretension angle, there was very little effect of pretension angle for negative excursions. For vertical restoring force, the pretension angle was proportional to the vertical restoring force before lifting off the whole clump weight and inversely proportional after lifting off the whole clump weight.

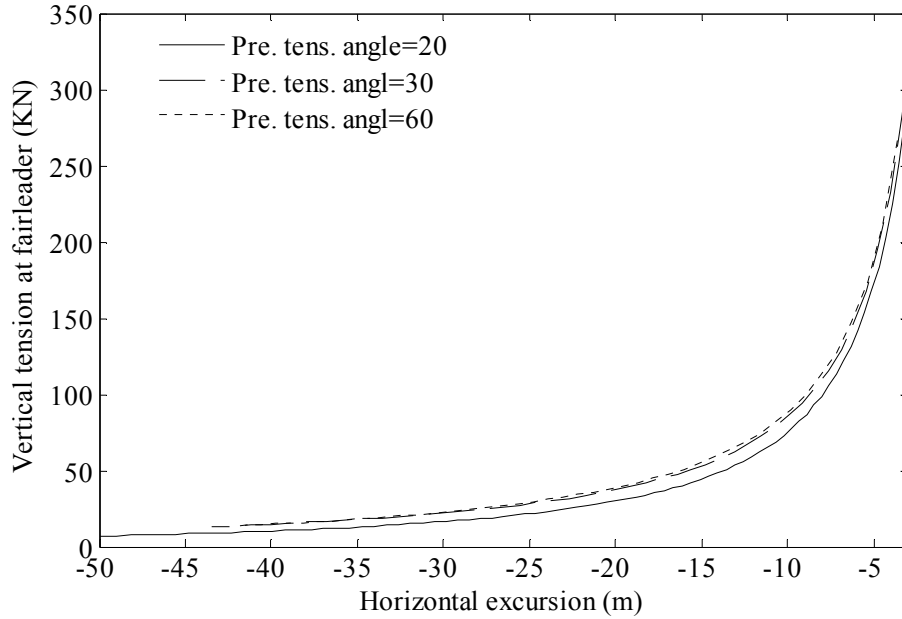


Fig 7.6: Effect of pretension angle on the mooring line stiffness

7.3 Dynamic analysis of mooring lines (numerical and validation results)

The calculated soil spring stiffness and the assumed soil damping ratios (three values) are presented in Table 7.2. The calculated seabed soils vertical reaction per line embedment is presented in Fig 7.7.

Table 7.2: Sea bed soils data

Designation	Type	ϕ (°)	γ (kN/m ³)	c (kPa)	k_{soil} (Pa)	ε_{soil} (%)
Soil A ³ -1	Sand	35	18	0	4500	0, 3, 5
Soil A-2	Silty sand	30	19	0	2600	0, 3, 5
Soil B ⁴ -1	Clay	0	20	15	150	0, 3, 5

³ Cohesive-less soil

⁴ Cohesive soil

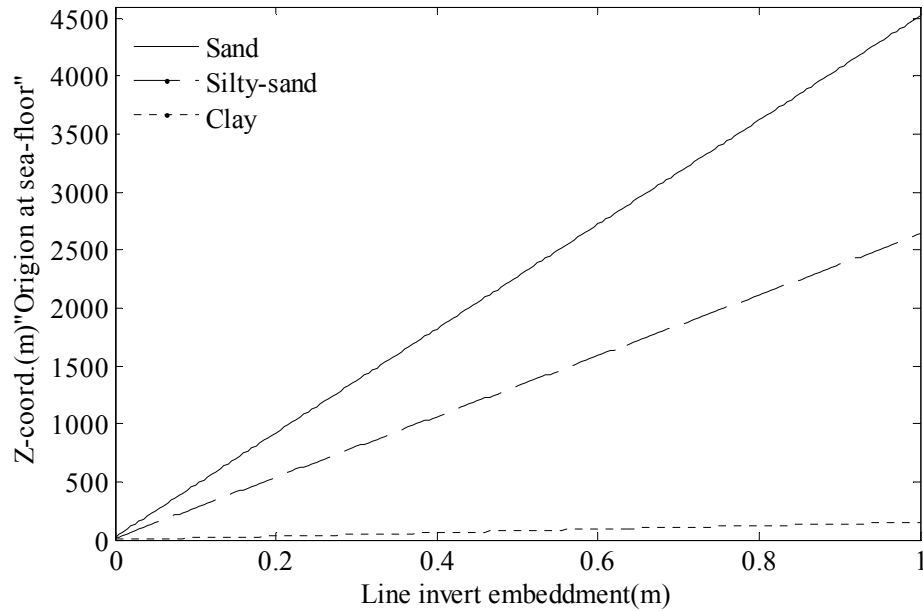


Fig 7.7: Seabed Soils Vertical reaction per line embedment

Based on the mathematical formulation described in Chapter 4, a numerical code named MCMLDYN was developed in the MATLAB 2009a environment, for deepwater MCMLs dynamic analysis. Three case studies were conducted for the validation of the established numerical code. The dynamic behavior of mooring line No. 1, 2 & 3 were assessed numerically using MCMLDYN code and compared to [62] experimental results. The results of mooring line No.1~3 are presented in Fig 7.8~Fig 7.10 respectively, in which, the global co-ordinate system, the node numbers-coordinates, element numbers (inscribed inside circles) and concentrated weights of nodal attachments (spring buoy for mooring line No.2 and clump weight for mooring line No.3) are given. The general data used for the analysis of mooring line No. 1~3 are presented in Table 7.3, while the basic characteristic data for the chain used in Mooring lines No.1~3 are given in Table 7.4 3. The mooring No.1~3 element tensions are given in Table 7.5.

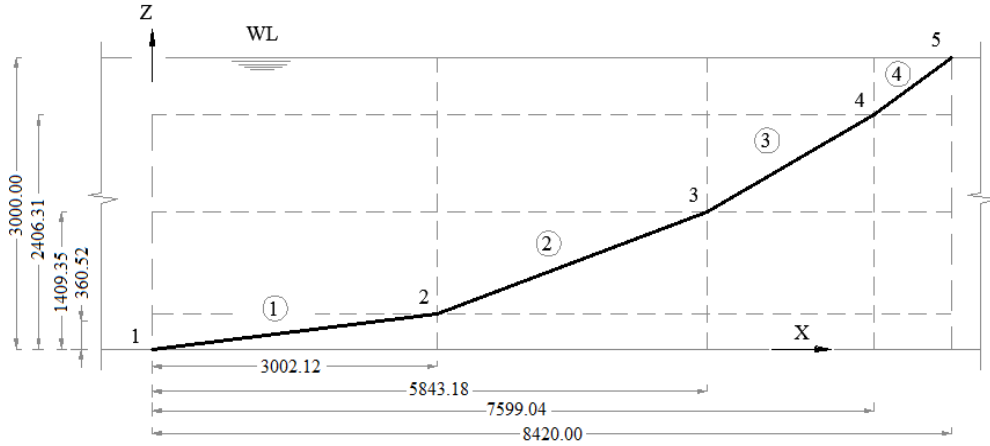


Fig 7.8: Mooring No 1 initial configuration

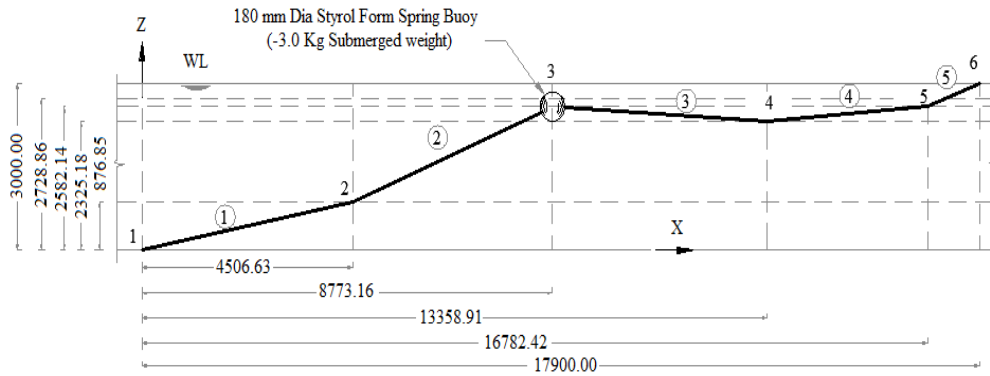


Fig 7.9: Mooring No 2 initial configuration

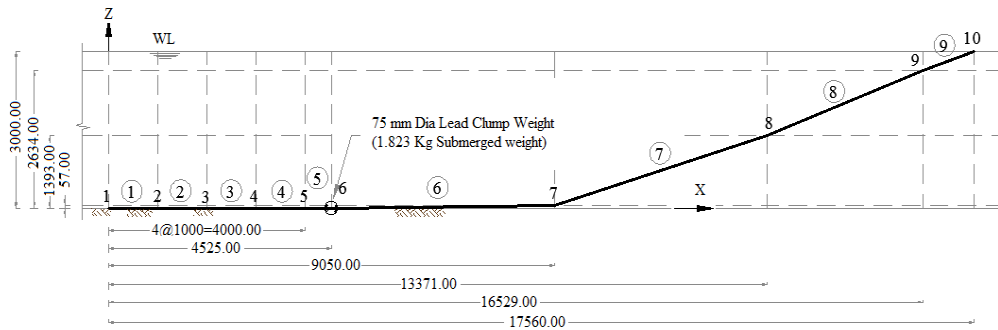


Fig 7.10: Mooring No 3 initial configuration

Table 7.3: General data used to analyze Mooring lines No. 1-3

C_{D_n}	C_{D_t}	C_{A_n}	C_{A_t}	C_{D_x}	C_{D_z}	C_{A_x}	C_{A_z}	Δt (s)	ρ (Kg/m ³)
2.18	0.17	1.98	0.20	1.00	1.00	0.50	0.50	0.02	1025

Table 7.4: Particulars of chain used in Mooring No. 1, 2 & 3

Submerged unit mass (kg/m)	0.194
Diameter (mm)	5.990
Modulus of elasticity (Pa)	0.211

Table 7.5: Mooring line tensions

Mooring No.	Element ID	Tension (kg)
1	1	2.539
	2	2.645
	3	2.871
	4	3.136
2	1	4.596
	2	4.809
	3	4.611
	4	4.583
	5	4.705
3	1-6	9.399
	7	9.745
	8	10.019
	9	10.317

Forced oscillation tests for mooring lines No. 1~3 were conducted [62] in a wave flume containing calm water. The lower ends of the mooring lines were attached rigidly to the bottom of the model basin and the upper ends were attached to a mechanical oscillator, forced to oscillate horizontally with amplitude of 50 mm. The upper end horizontal and vertical tensions were measured by a load cell located at mooring line/mechanical oscillator attachment point, while the tension at the anchored point was measured by a ring gauge.

The non-dimensional tension amplitudes for the horizontal/vertical upper end dynamic tensions for mooring lines No. 1~2 (Eq 7.1) were plotted against the non-dimensional frequency (Eq 7.2) as shown in Fig 7.11~Fig 7.12 respectively. It was noted that for non-dimensional frequency greater than 0.03, the dynamic tension was directly proportional to the upper end motion frequency. At the non-dimensional frequency of 0.12, the dynamic tension increased about three/two times of the initial static tension for mooring lines No. 1~2 respectively. Lower increase of the dynamic tension for mooring line No.2 was due to the existence of spring buoy.

$$\bar{T}_N = \frac{T_N}{2T_{oN}} \quad (7.1)$$

$$\bar{\omega}_f = \omega_f \sqrt{\frac{D_N}{2g}} \quad (7.2)$$

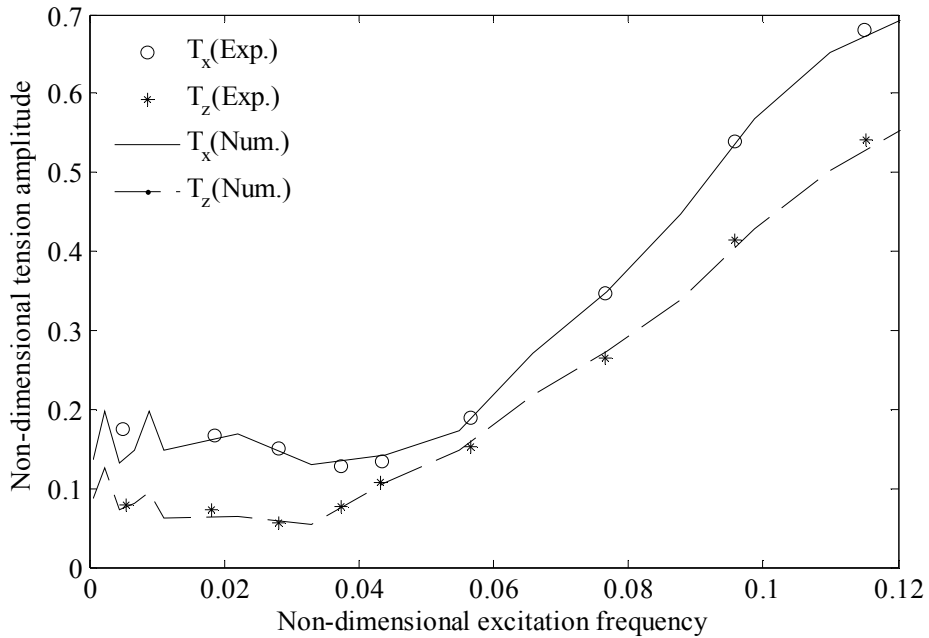


Fig 7.11: Frequency response of mooring line No.1 upper end dynamic tension
 (Source of test data: 14th Offshore Technology Conference; Nakajima, 1982)

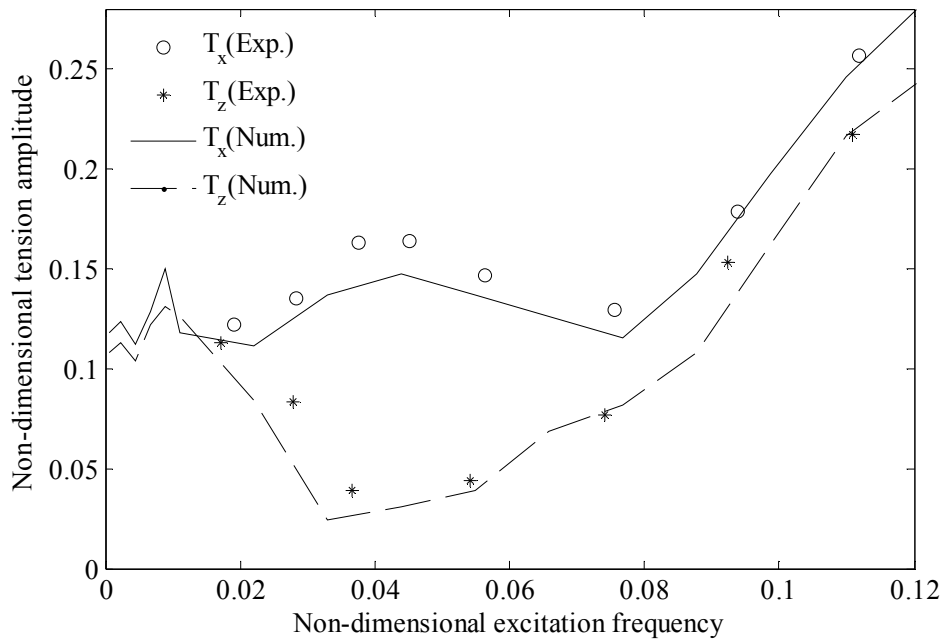


Fig 7.12: Frequency response of mooring line No.2 upper end dynamic tension
 (Source of test data: 14th Offshore Technology Conference; Nakajima, 1982)

Time domain simulations for the upper end dynamic horizontal/vertical tensions were compared to [62] experimental results for upper end sinusoidal motion of 5 rad/s frequency and 50 mm amplitude with no ramp for mooring line No. 3 as shown

in Fig 7.13~Fig 7.14. For the numerical calculations, it was assumed that the grounded part of mooring line No. 3 rested on clay soil (Soil B-1) having 5% damping ratio. It could be seen clearly from Fig 7.11~Fig 7.14 that good agreement was achieved between the dynamic simulations of the mooring lines and Nakajima experimental results. Thus, the adopted numerical model is recommended for the mooring line/seabed interactions assessment with an acceptable degree of confidence.

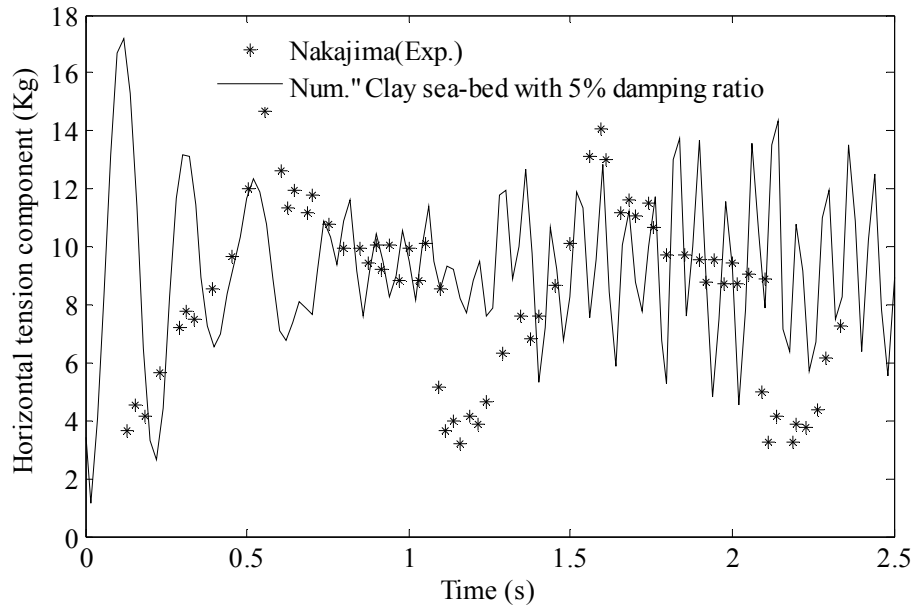


Fig 7.13: Mooring line No.2 upper end horizontal dynamic tension time history
 (Source of test data: 14th Offshore Technology Conference; Nakajima, 1982)

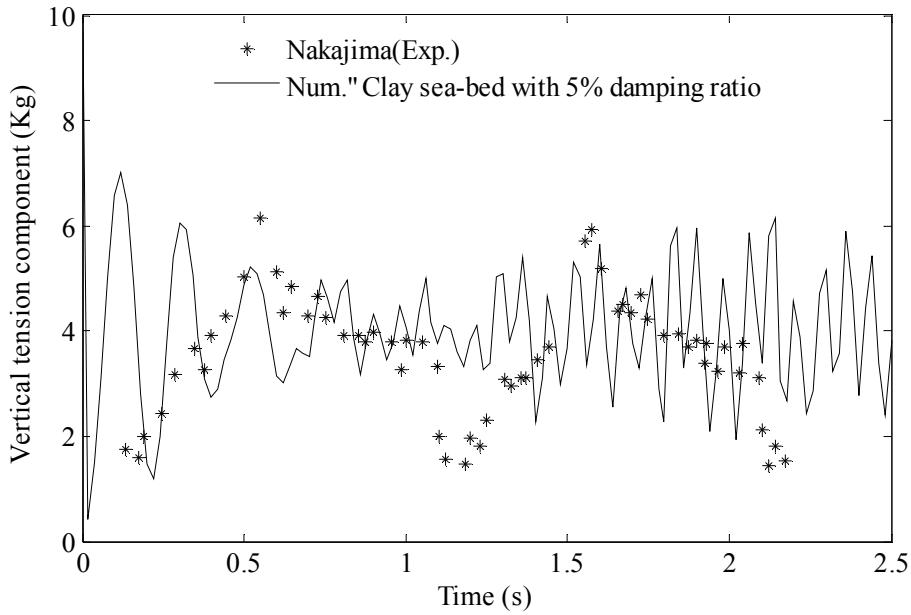


Fig 7.14: Mooring line No.2 upper end vertical dynamic tension time history
 (Source of test data: 14th Offshore Technology Conference; Nakajima, 1982)

Fig 7.15~Fig 7.17 show the mooring line No. 1~3 configuration time history for upper end 50 mm oscillation amplitude at different frequencies in calm water. Mooring line No. 3 was assumed to be resting on clay soil (Soil B-1), having 5% damping ratio.

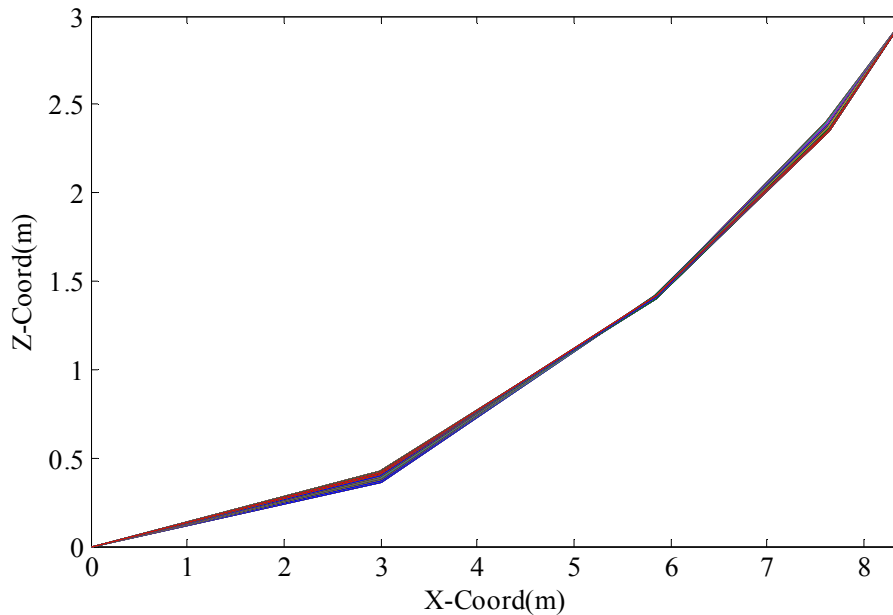


Fig 7.15: Mooring line No.1 dynamic configuration
 ($A_x=50$ mm, $A_z=0$ mm and $w_f=0.503$ rad/sec)

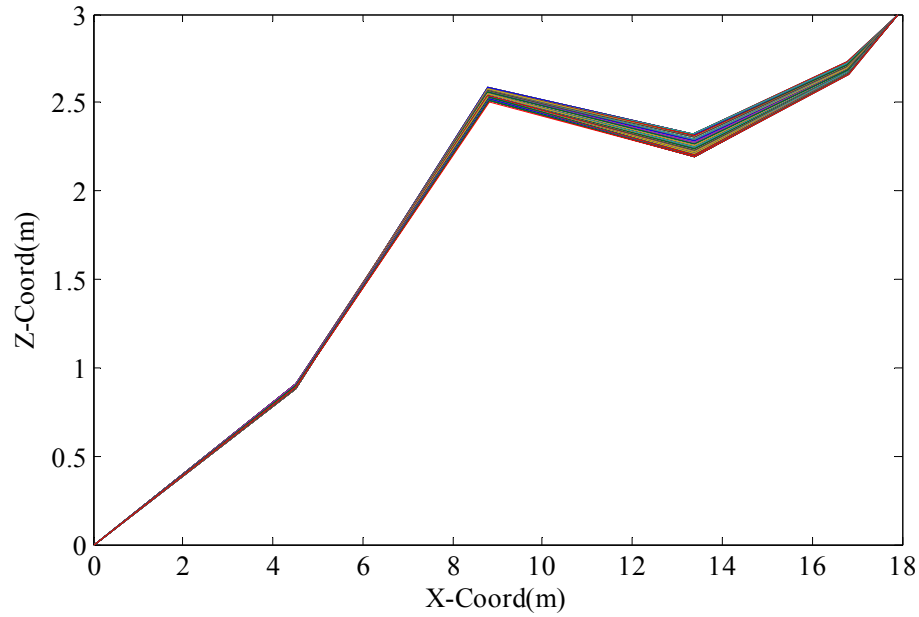


Fig 7.16: Mooring line No.2 dynamic configuration
 ($A_x = 50 \text{ mm}$, $A_z = 0 \text{ mm}$ and $w_f = 1.257 \text{ rad/sec}$)

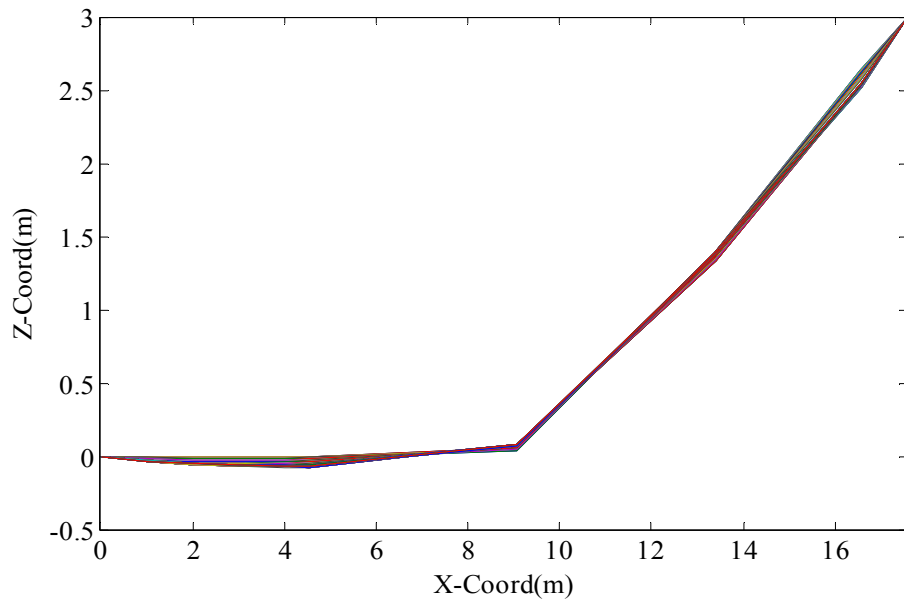


Fig 7.17: Mooring line No.3 dynamic configuration
 ($A_x = 50 \text{ mm}$, $A_z = 0 \text{ mm}$ and $w_f = 2.618 \text{ rad/sec}$)

To study the effect of the seabed on the line dynamics, a MCML as shown in Fig 7.18 was analyzed, assuming it was lying on rigid bed (Nakajima model) and an elastic foundation made of clay, silty sand and sand soils with 5 % damping ratio. The data for the analyzed mooring line is given in Table 7.6.

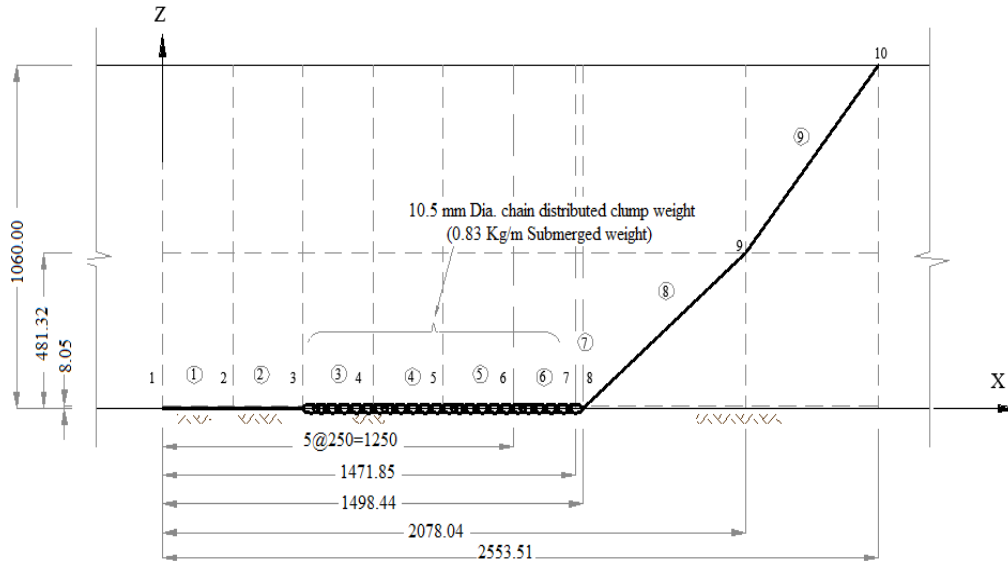


Fig 7.18: A MCML with distributed clump weight

Table 7.6: Mooring No 4 Initial configuration data

Elem. ID	D (mm)	E (GPa)	m (kg/m)	T_o (N)	L (m)
1	1.55	3.600	0.02	0.367763	0.250000
2	1.55	3.600	0.02	0.367763	0.250000
3	10.5	3600	0.83	0.367763	0.250000
4	10.5	3600	0.83	0.367763	0.250000
5	10.5	3600	0.83	0.367763	0.250000
6	10.5	3600	0.83	0.367763	0.221850
7	10.5	3600	0.83	0.385191	0.027778
8	1.55	3.600	0.02	0.476293	0.748279
9	1.55	3.600	0.02	0.580983	0.749116

The horizontal and vertical tension amplitudes of the mooring line were plotted against upper end motion frequencies for a given motion amplitude of 50 mm as shown in Fig 7.19~Fig 7.20. Nakajima model and elastic foundation with a dashpot were used to model the mooring line seabed interactions. The latter model was assumed for three different soils having the same damping ratio of 5 %. Results showed that the elastic foundation model gave lower mooring tensions compared to Nakajima seabed model. It was found that for low frequencies (< 12 rad/s), the second seabed model reduced the mooring tension up to 22 % while for high frequencies (> 12 rad/s) it reduced up to 17 %. Thus, elastic foundation with dashpot seabed model

reduced the mooring tensions especially at low upper end motion excitation frequency.

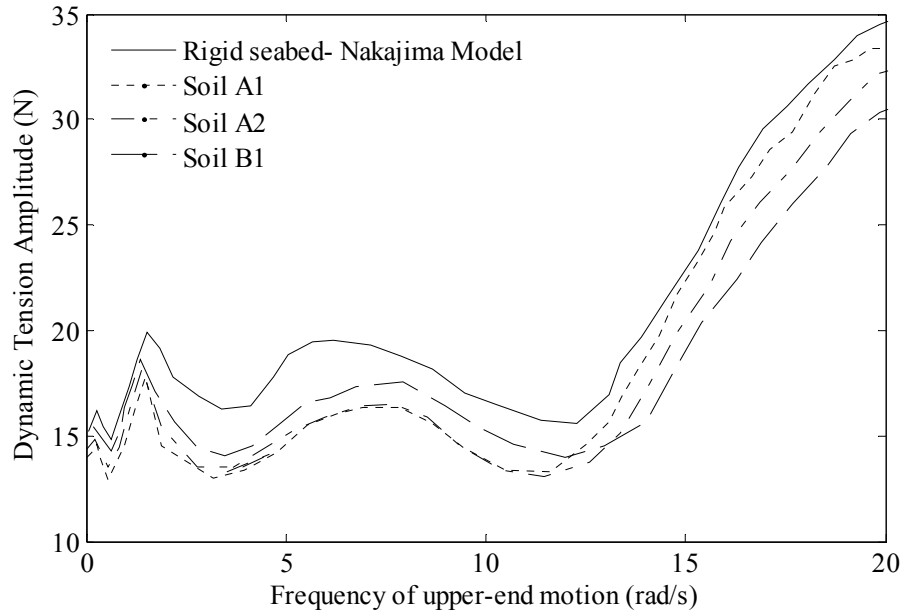


Fig 7.19: Soil contribution to the horizontal dynamic restoring forces (Mooring No. 4)

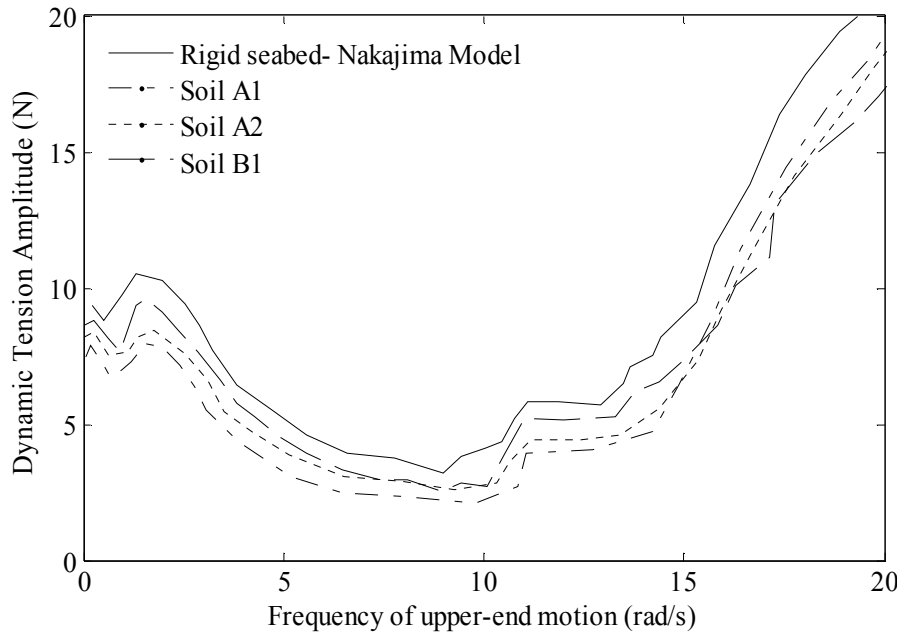


Fig 7.20: Soil contribution to the vertical dynamic restoring forces (Mooring No. 4)

Regarding the soil type, it was noted that for stiff soils, the mooring line tension was low at low frequencies (< 12 rad/s for horizontal tension and < 15 rad/sec for vertical tension), but high at high frequencies. This happened due to the high soil reactions to high frequency line dynamic actions. In other words, stiff soils provided

desired effect to line dynamics (decreased tension) at low frequencies, but it had an adverse effect at high motion frequencies (increased tension).

To investigate the contribution of the soil damping to the mooring line dynamics, the mooring line No. 4 was dynamically analyzed in calm water with upper end motion having different frequencies for a given motion amplitude of 50 mm. It was assumed that the grounded part of the mooring was supported upon clay soil (Soil B-1), which had a damping ratio of 0%, 3% and 5% as shown in Fig 7.21 Fig 7.22. Results indicated that the higher the soil damping, the lower the mooring tensions. Comparing undamped soil to damped soil (5% damping ratio), a maximum of about 3% difference was obtained for horizontal tension at low frequencies (<10 rad/s), while about 4% difference was obtained for horizontal tension at high frequencies (>10 rad/s). On the other hand for the vertical tension, a maximum difference of about 7 % was obtained at low frequencies (< 10 rad/s), and about 9 % at high frequencies (>10 rad/s) when comparing undamped soil to damped soil (5% damping ratio). Thus, the soil damping decreased vertical tensions more than horizontal tensions and decreased tensions at high frequencies more than at low frequencies.

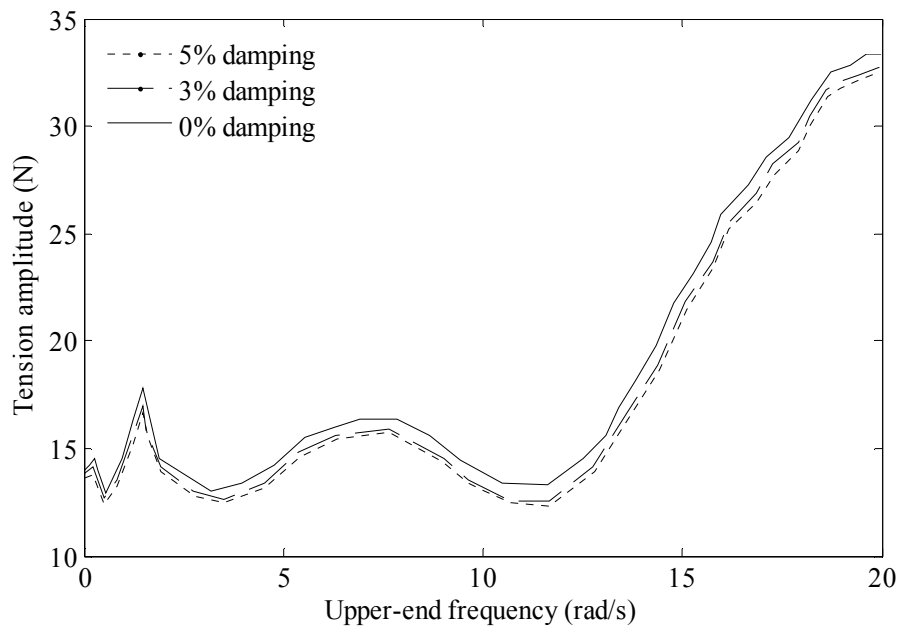


Fig 7.21: Soil damping contribution to the horizontal dynamic tension (Mooring No. 4)

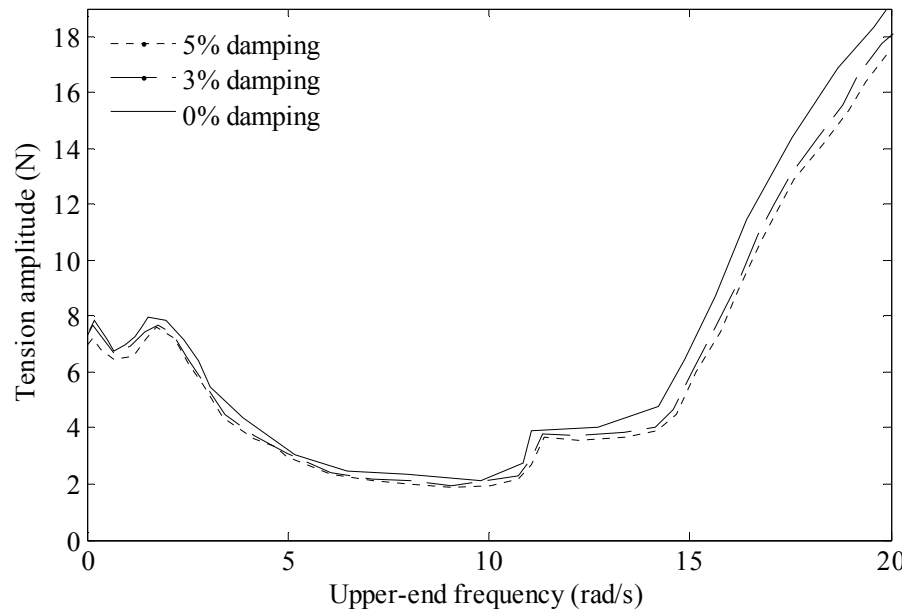


Fig 7.22: Soil damping contribution to the vertical dynamic tension (Mooring No. 4)

7.4 Wave frequency responses (numerical vs. experimental results)

The responses of the semi submersible physical model were determined numerically using the structure dimensions, properties, draft and the generated wave characteristics as inputs and the results were compared with the corresponding experimental data (full scale). The surge, heave and pitch response time histories to a regular wave of 6 m height and 0.314 rad/s frequency propagated at zero heading angle were measured. The numerical results were compared with the corresponding experimental results in Fig 7.23~Fig 7.25. The numerical model fairly well predicted the response amplitudes and periods. The maximum discrepancies were 1.2%, 13.2% and 0.2% below the experimental results for surge, heave and pitch responses respectively. The heave response for low frequency waves differed greater because heave motions were influenced by water depth at low frequency.

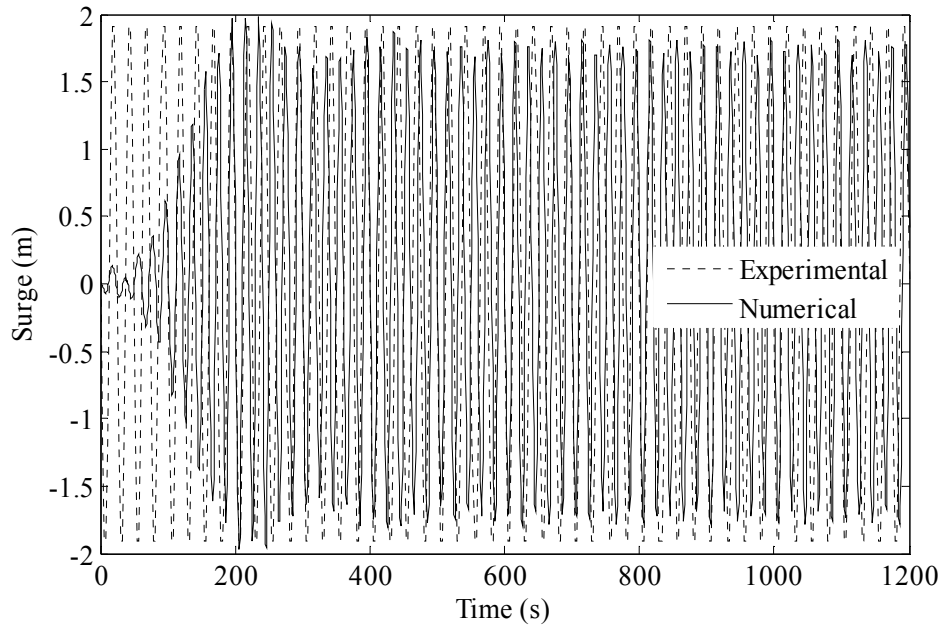


Fig 7.23: Surge response to regular sea wave ($H = 6$ m, $\omega = 0.314$ rad/s)

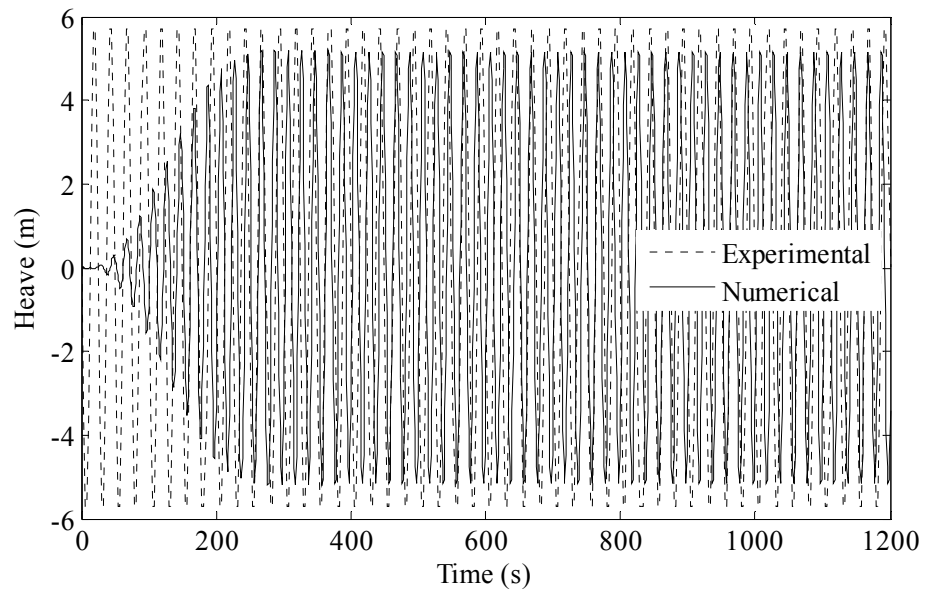


Fig 7.24: Heave response for regular sea wave ($H = 6$ m, $\omega = 0.314$ rad/s)

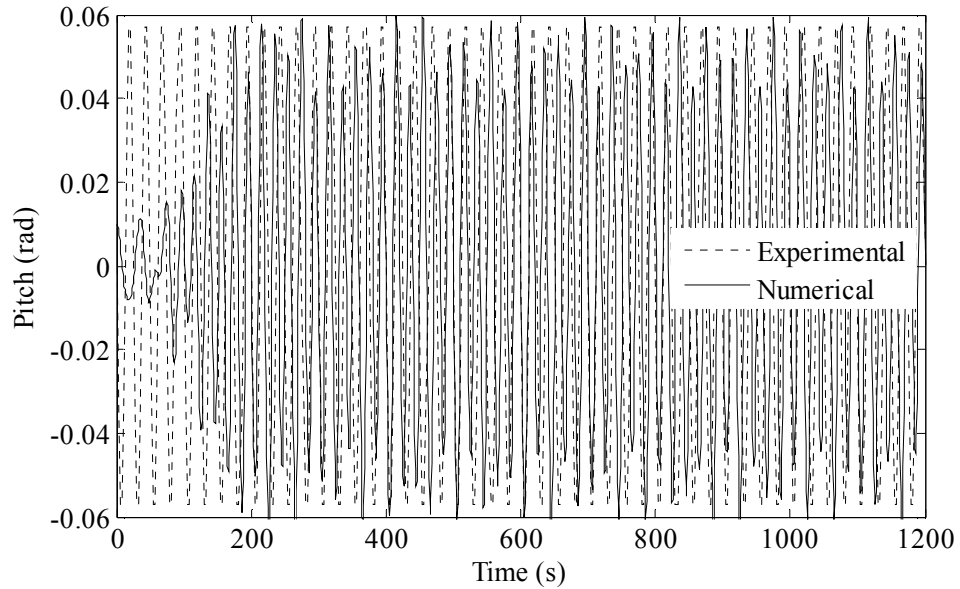


Fig 7.25: Pitch response to regular sea wave ($H = 6$ m, $\omega = 0.314$ rad/s)

The physical model RAOs for surge, heave and pitch of the numerical analysis were compared to the experimental processed results for regular and irregular waves in sea and quartering waves in Fig 7.26~Fig 7.31. The numerical results agreed well with the experimental results. The maximum differences were 20% & 10% for surge 6.7% & 20% for heave and 20% & 12.8% for pitch in sea and quartering waves respectively.

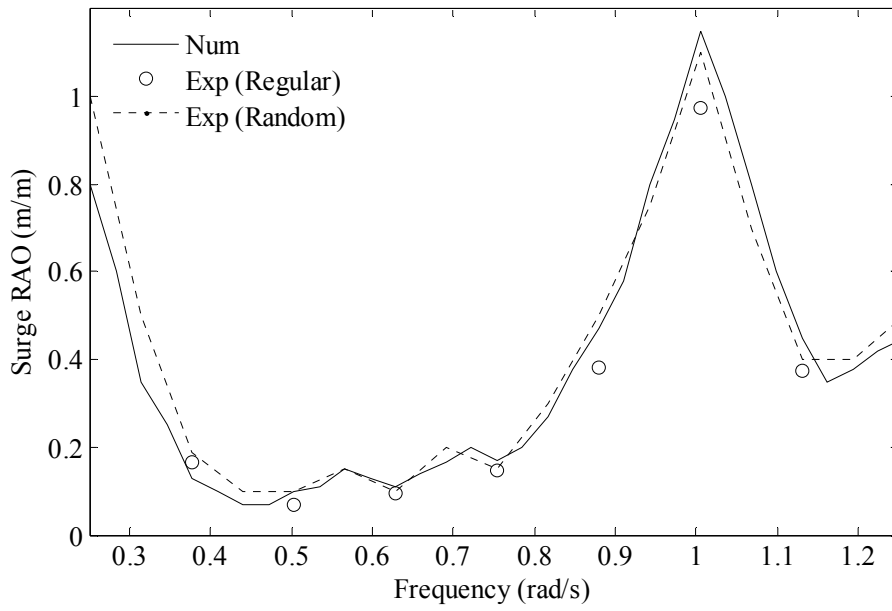


Fig 7.26: Surge RAO to head seas

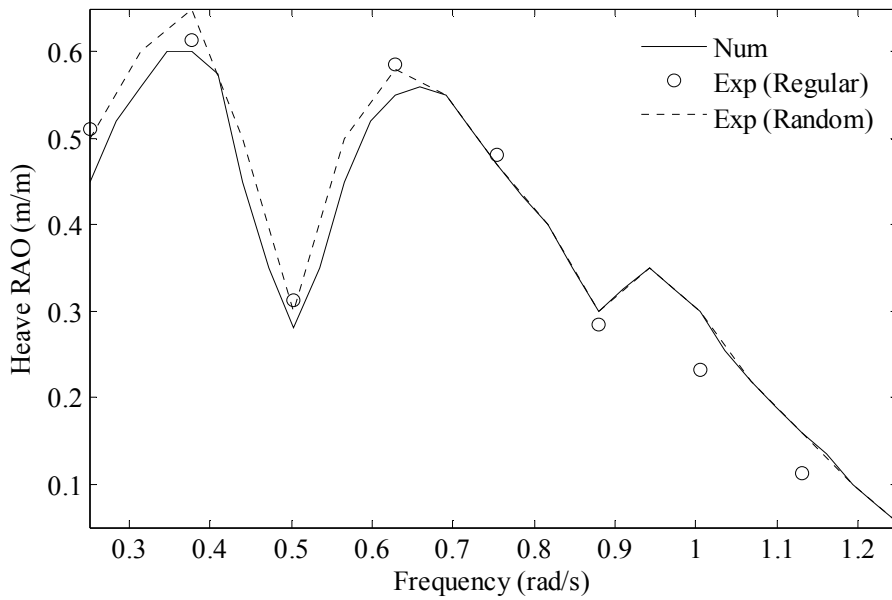


Fig 7.27: Heave RAO to head seas

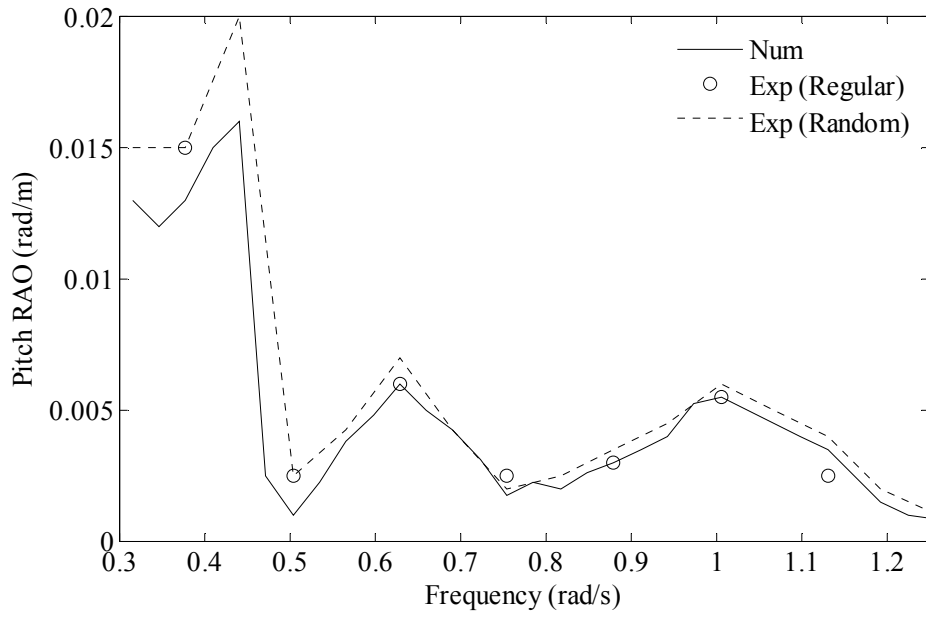


Fig 7.28: Pitch RAO to head seas

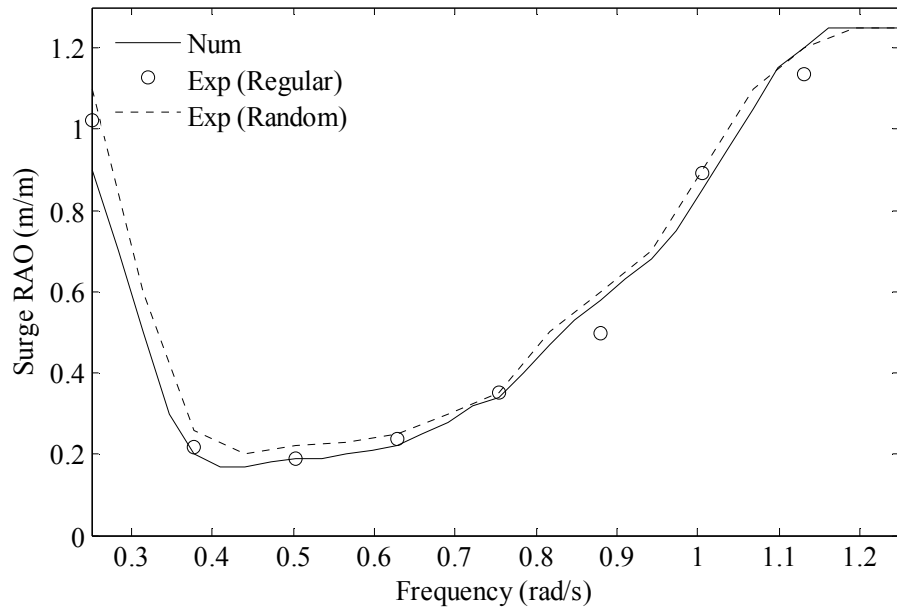


Fig 7.29: Surge RAO to quartering seas

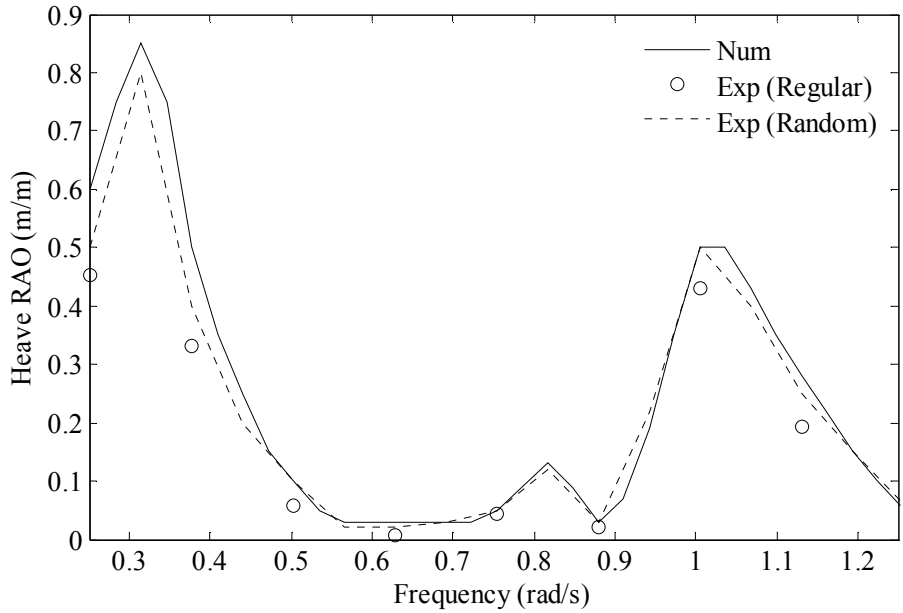


Fig 7.30: Heave RAO to quartering seas

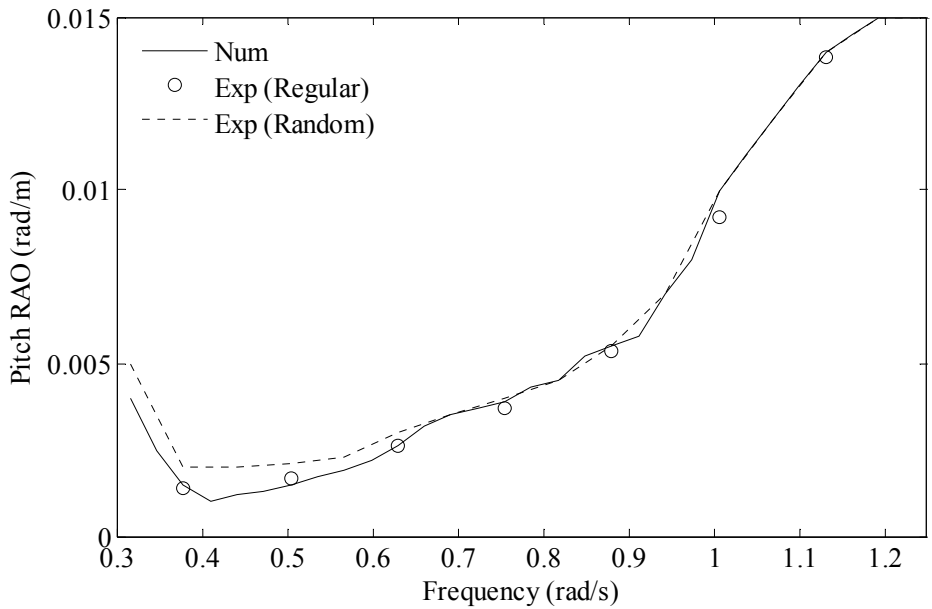


Fig 7.31: Pitch RAO to quartering seas

The typical semi submersible RAOs for sway, heave and roll of the numerical analysis were compared to the experimental processed results for regular and irregular beam waves in Fig 7.32~Fig 7.34. The results of the numerical code agreed well with the experimental results. The maximum differences were 29.2%, 20% and 12% for sway, heave and roll respectively.

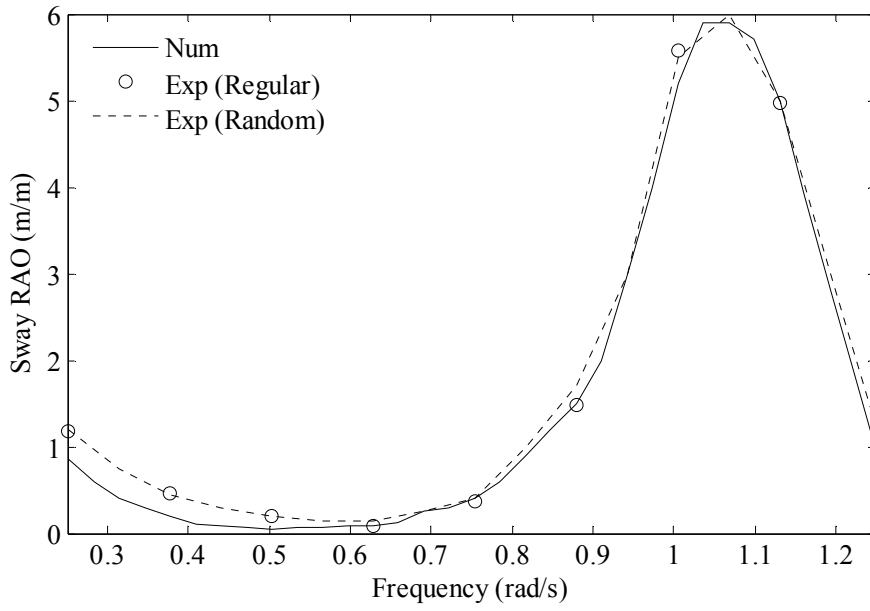


Fig 7.32: Sway RAO to beam seas

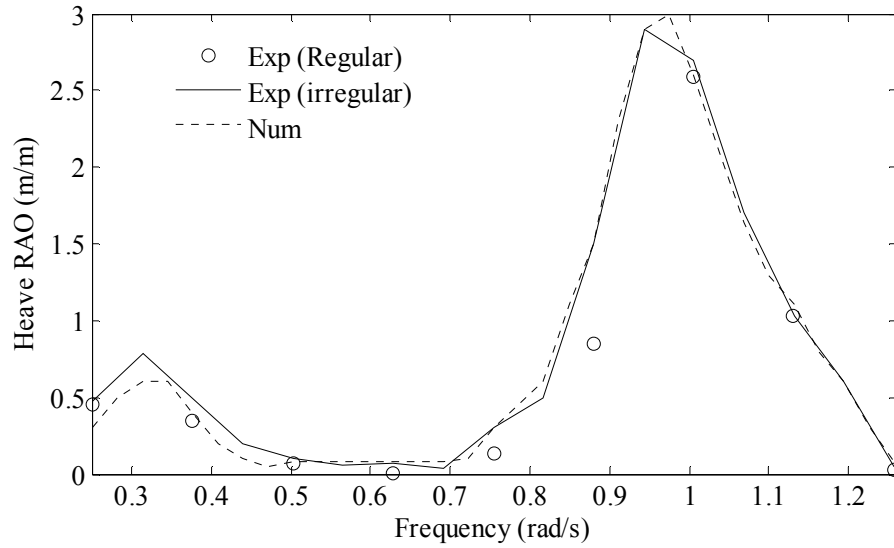


Fig 7.33: Heave RAO to beam seas

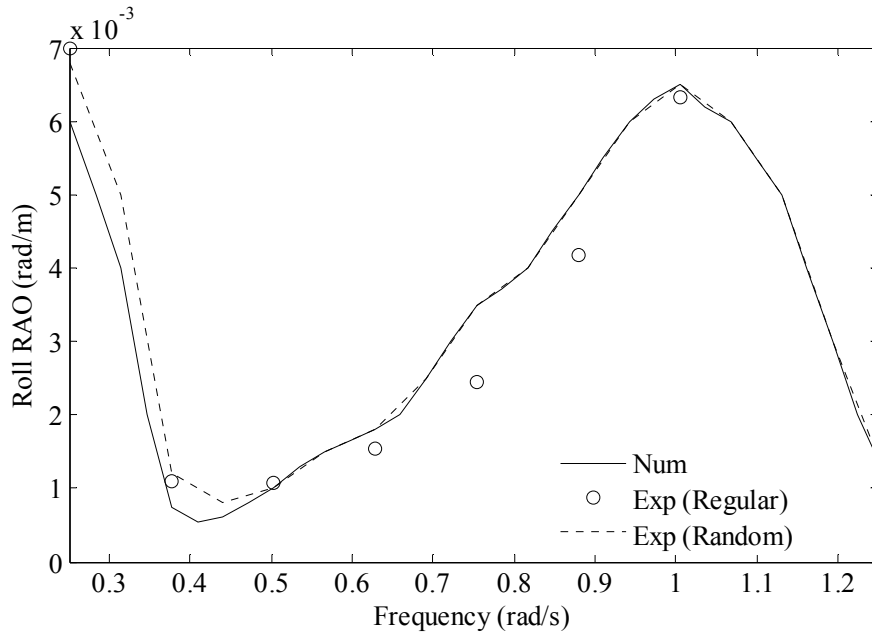


Fig 7.34: Roll RAO to beam seas

From the previous comparisons, it could be observed that all the numerical responses were lower than the physical model responses for low frequency waves. The heave response to quartering waves was the only exception because of neglecting the potential damping. This was because the effects of second order cross modulation low frequency interactions were not taken into account in the mathematical formulation. Also, non-consideration of potential damping resulted in overestimation of heave response to quartering waves. For surge and roll responses bracing members seemed to have considerable contribution to hydrodynamic behavior of the semi submersibles. For this particular model, the bracing members caused about 3% of the total model displacement.

7.4.1 Low frequency responses (experimental vs. numerical)

7.4.1.1 Static-offset test (experimental results)

From the results of the semi submersible-B, it was found that the system spring constant was found about 200 kN/m. The linear and nonlinear regressions were plotted against the collected data as shown in Fig 7.35.

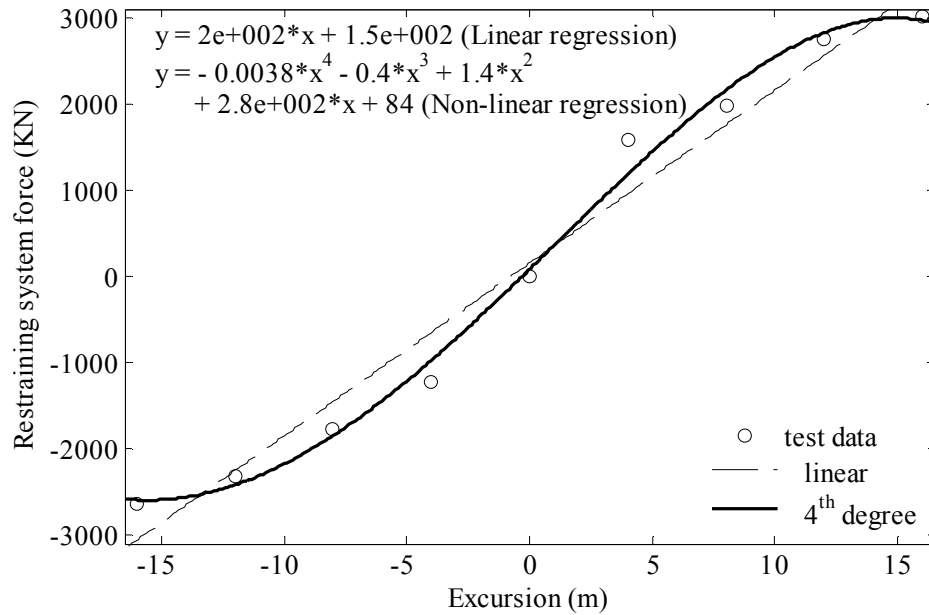


Fig 7.35: Static offset test results with linear and nonlinear data fitting

7.4.1.2 The free-decay test (numerical vs. experimental results)

For the semi submersible-B, response free-decay physical measurements and simulations for surge and sway DOFs are shown in Fig 7.36~Fig 7.37 respectively. The numerical simulations gave good results when compared to the test results. The calculated and measured average natural periods in surge and sway were very close (Table 6.5).

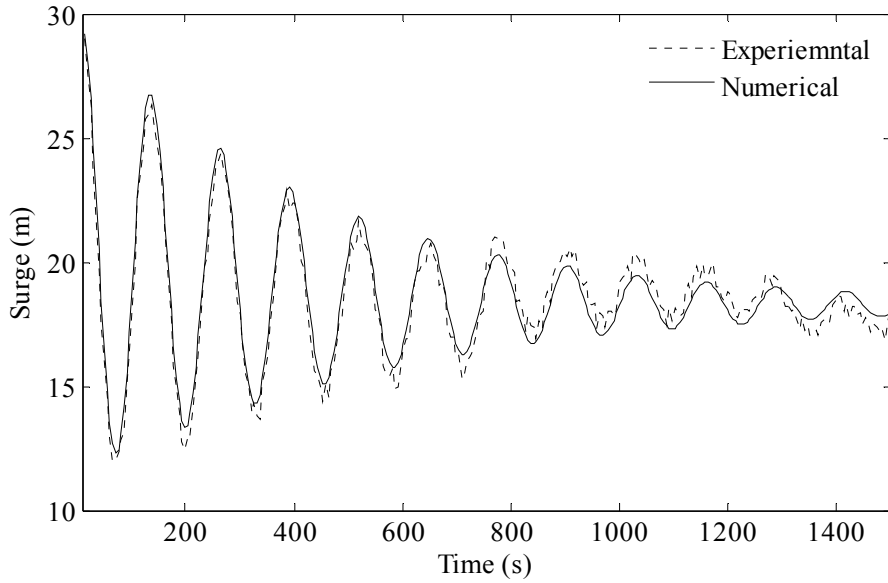


Fig 7.36: Simulation of surge free-decay test

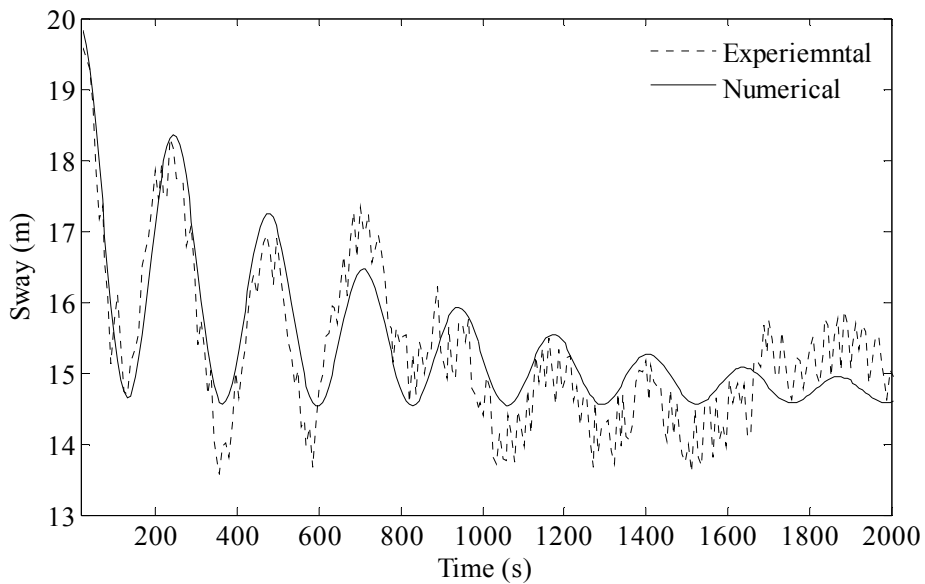


Fig 7.37: Simulation of sway free-decay test

7.4.1.3 Seakeeping tests (numerical vs. experimental results)

The test drive signals for regular, bi-chromatic and random seas for two model orientation (head and beam) are given in Table 6.6~Table 6.10 respectively. The same environment data together with the structure data given in Table 6.5 were used as input data for the numerical analysis algorithms. The measured steady drift forces

in head and beam model orientation were compared with the calculated forces based on [117] formulae as shown in Fig 7.38~Fig 7.39. From Fig 7.38, it is seen that Weggel's formulae follow the same trend of the actual drift force for different frequencies. Weggel's formulae underestimated the drift force for waves having relatively low wave height (waves designated as HRG x.1) with maximum discrepancy of about 40% near the peak frequency. Also, Weggel's formulae overestimated the drift force for waves having relatively high wave height (waves designated as HRG x.2) with maximum discrepancy of about 60% near the peak frequency. On the other hand, for beam model orientation, although Weggel's formulae followed the same trend of the measured drift force, it underestimated the steady drift force to almost 50% of the actual drift force. This was because Weggel's formulae did not take the effect of shallow draft hulls in consideration.

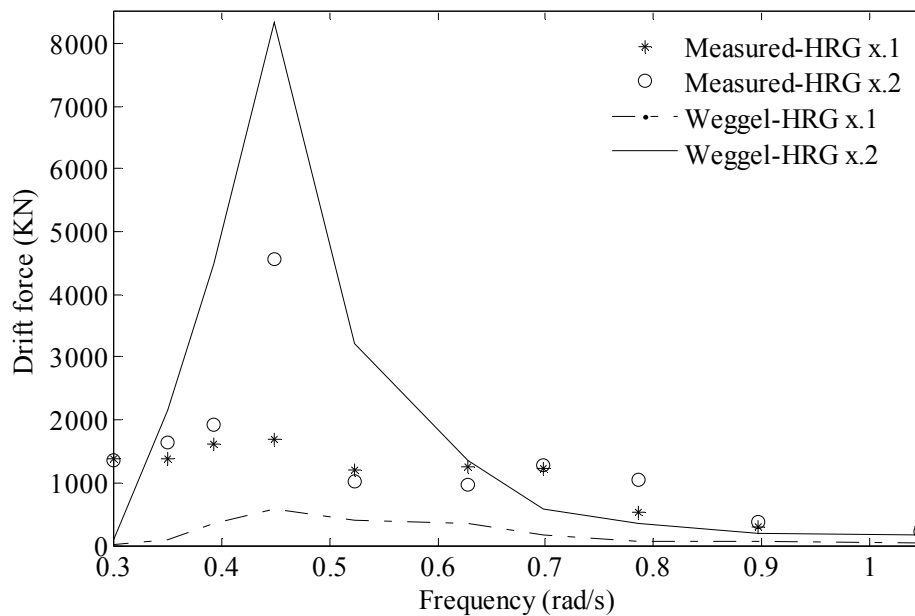


Fig 7.38: Drift force comparisons-head seas

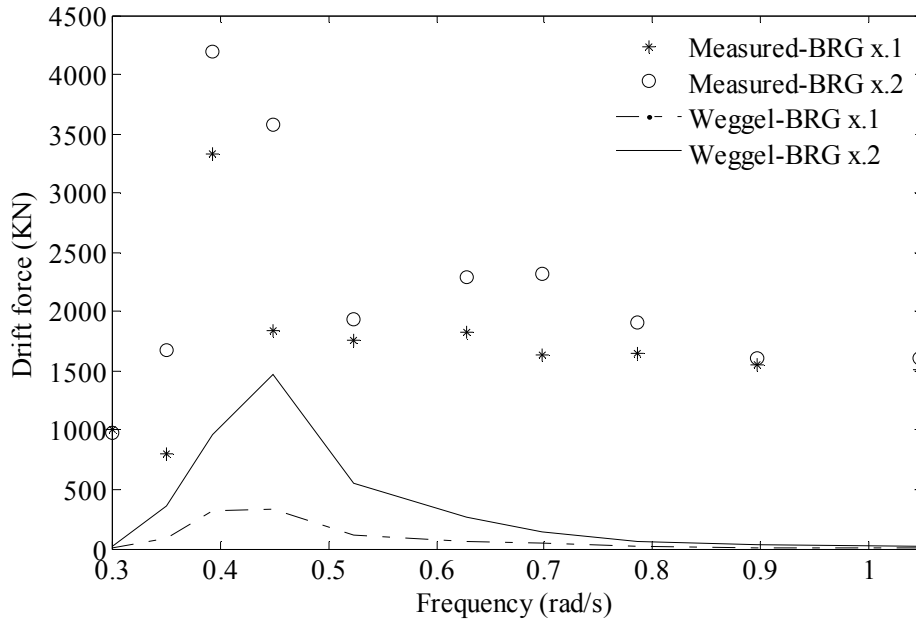


Fig 7.39: Drift force comparisons-beam seas

The calculated drift force coefficient based on the measured drift force for head and beam seas are shown in Fig 7.40~Fig 7.41. It can be seen from these Figures that the drift force coefficient not only depended on the wave frequency but also on the wave height. The existence of the large underwater hulls seemed to have significant effect on the drift force when comparing the drift force coefficient for head and beam seas.

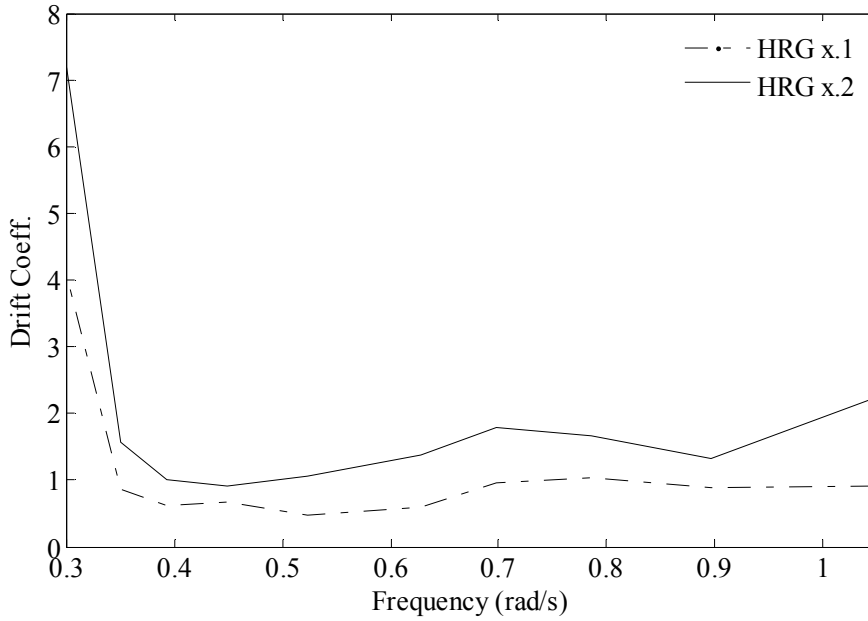


Fig 7.40: Drift coefficient comparisons-head seas

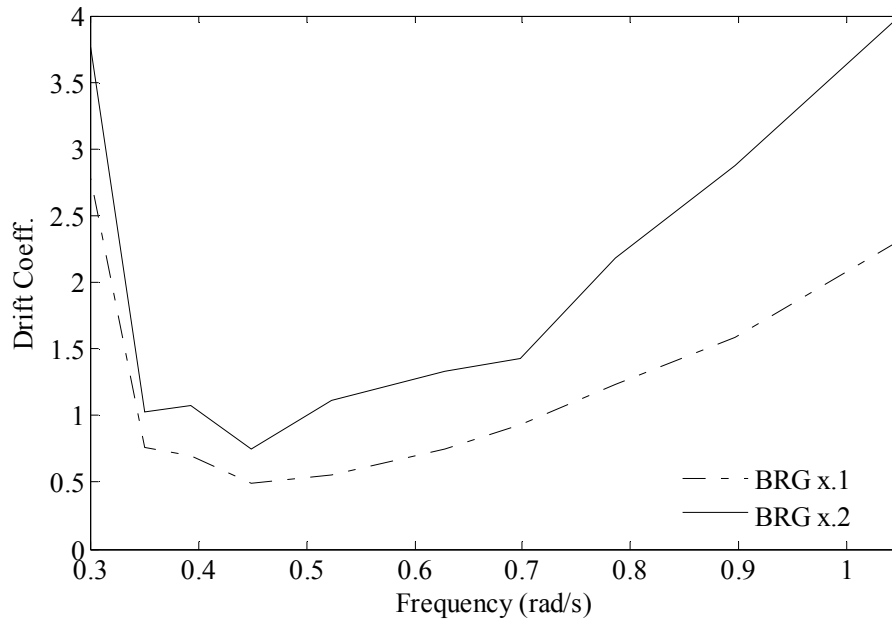


Fig 7.41: Drift coefficient comparisons-beam seas

The simulated and measured model response power density spectra (PSD) for the generated head and beam random seas are presented in Fig 7.42~Fig 7.47. From these figures, it can be seen that the numerical algorithm successfully estimated the low frequency response with slight difference in the peak frequency and maximum energy density.

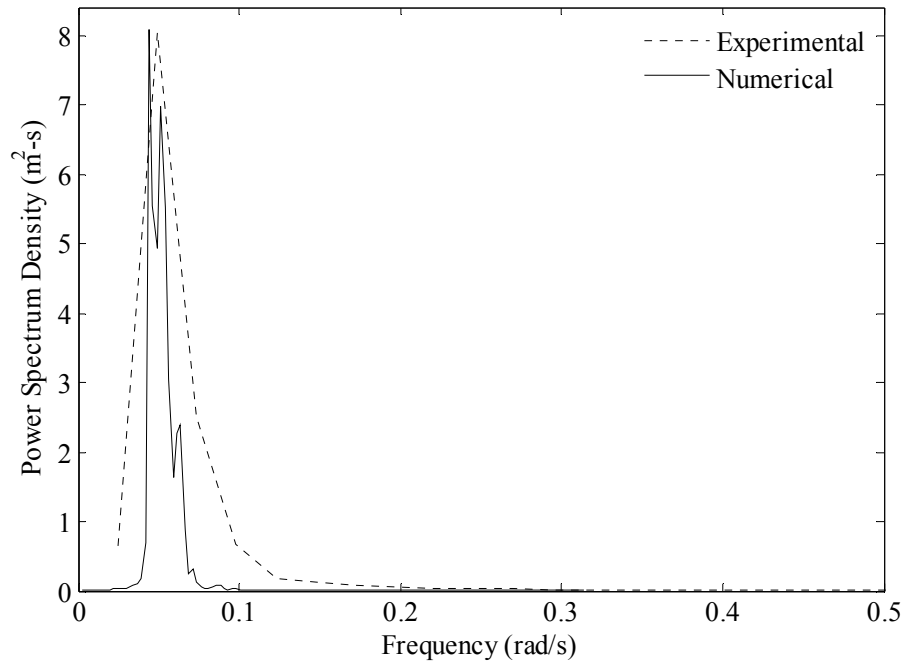


Fig 7.42: Surge response PSD to HRW1

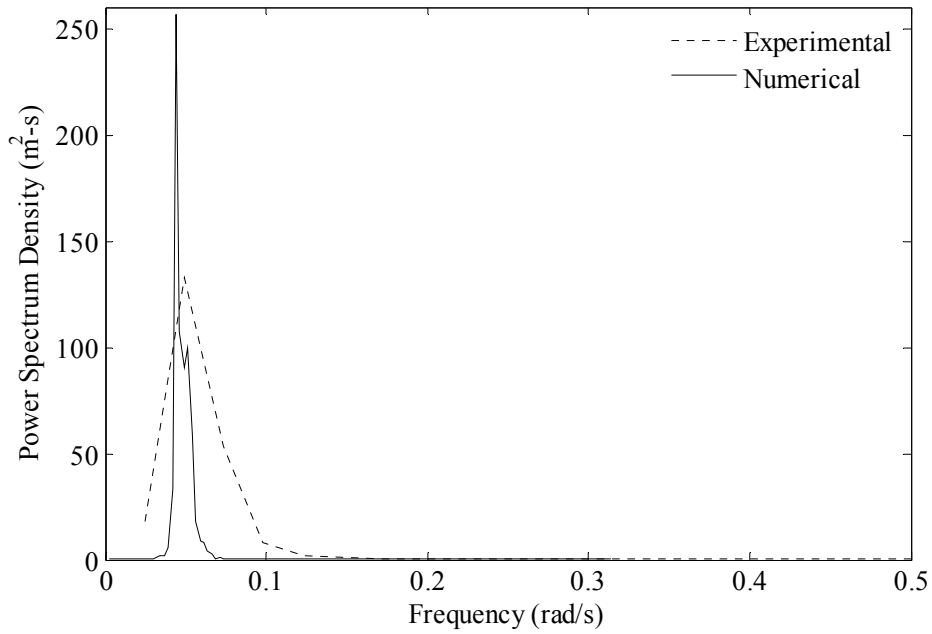


Fig 7.43: Surge response PSD to HRW2

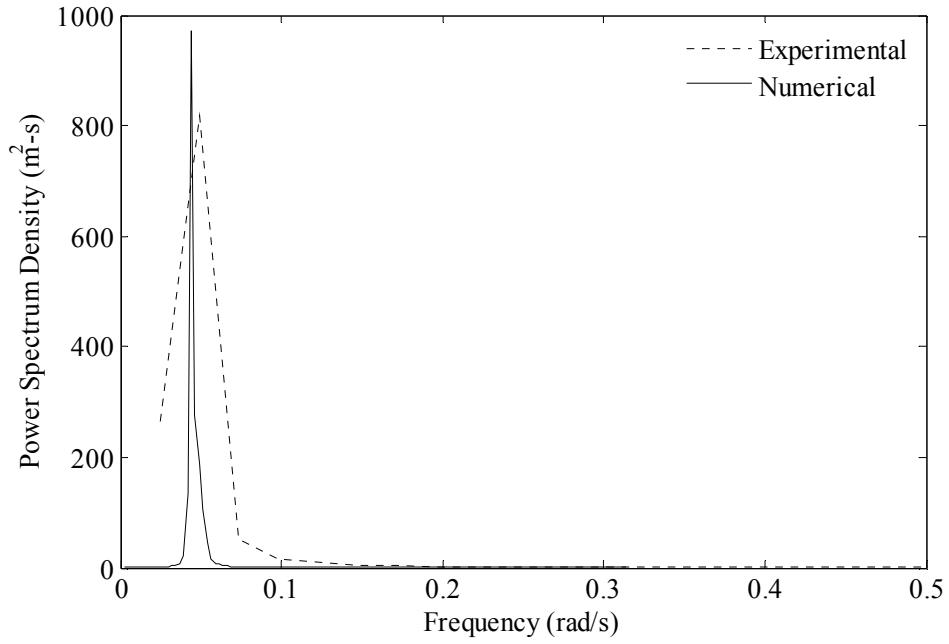


Fig 7.44: Surge response PSD spectrum to HRW3

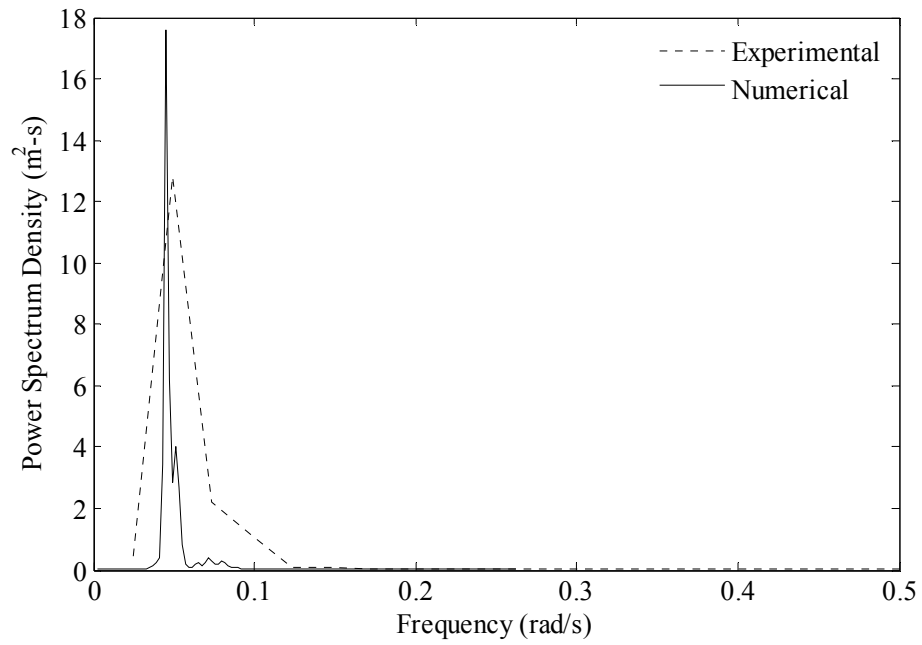


Fig 7.45: Sway response PSD to BRW1

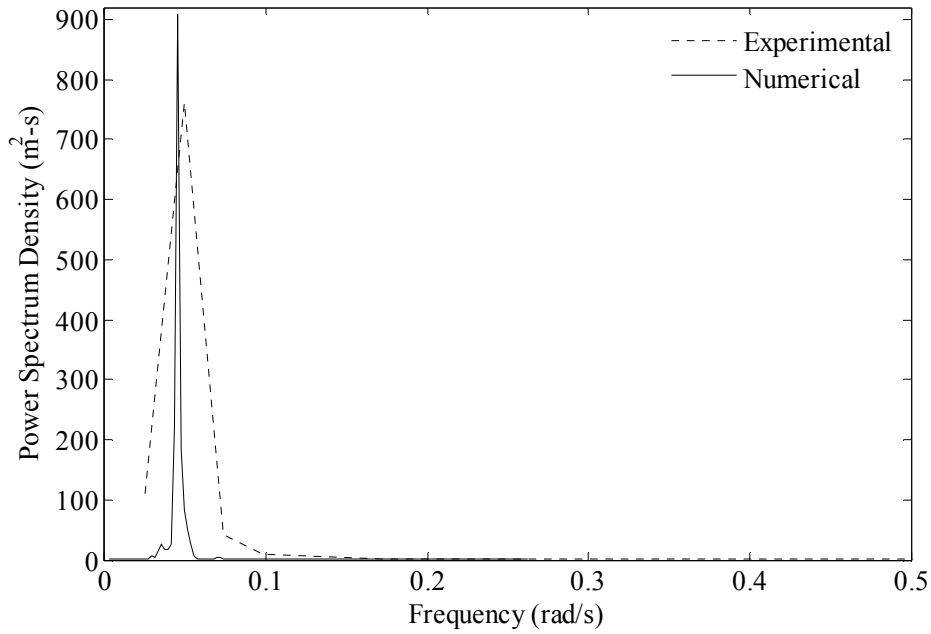


Fig 7.46: Sway response PSD to BRW2

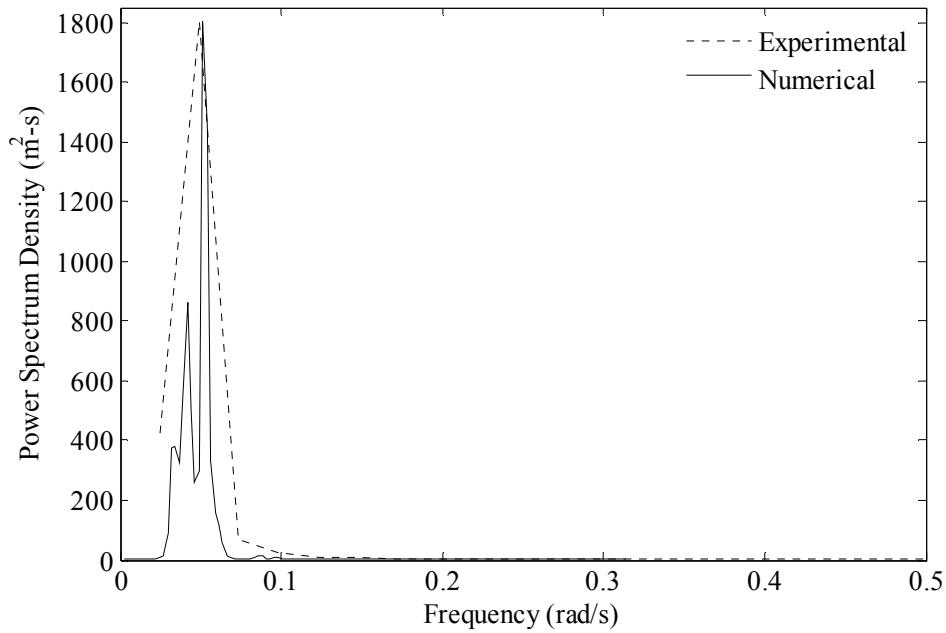


Fig 7.47: Sway response PSD to BRW3

The simulated and measured response amplitudes (RA) to bi-chromatic waves for the head and beam seas are shown in Fig 7.48~Fig 7.49. The simulated surge typically approached the measured surge amplitude with maximum discrepancy of about 8%. The numerical results had more deviations for beam seas with maximum

discrepancy of about 20%. Since these amplitudes were evaluated near the system natural frequency, it is anticipated that the results would improve with better estimate of the nonlinear damping.

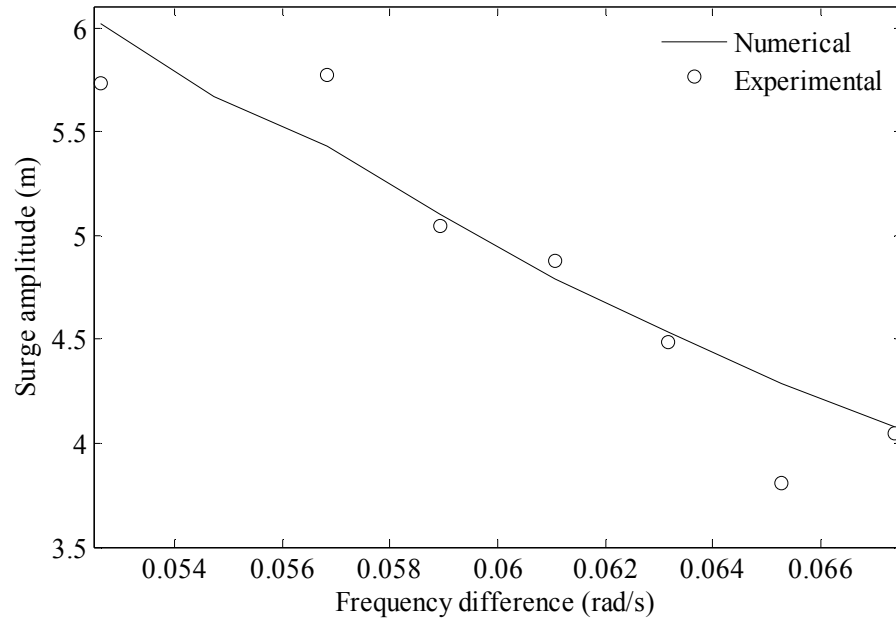


Fig 7.48: Comparisons of surge RA to HBC 1~8

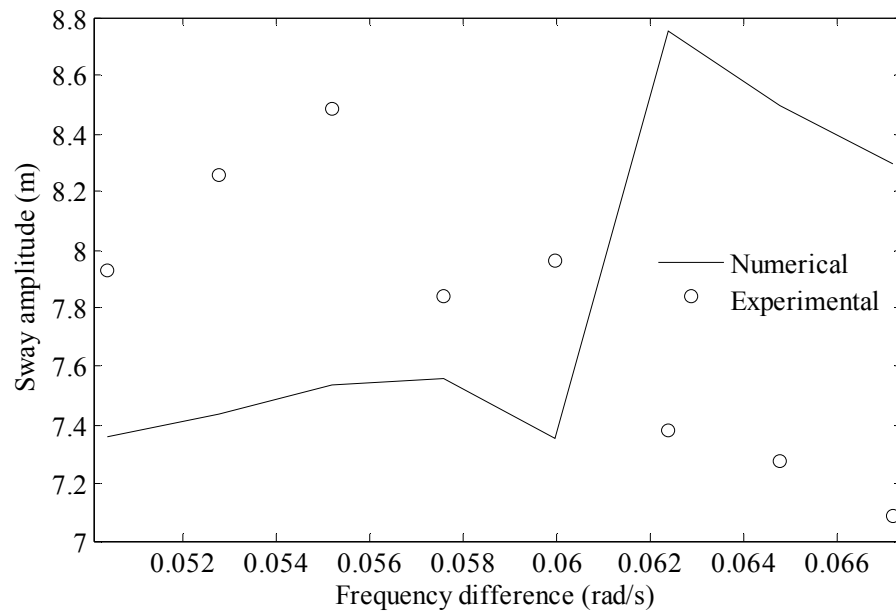


Fig 7.49: Comparisons of sway RA to BBC 1~8

7.4.2 Mooring damage conditions (experimental results)

During the second phase of experimental tests, an attempt was made to investigate the consequences of the line failure on the station-keeping characteristics of semi submersibles. Fig 7.50~Fig 7.51 show the model surge response (full scale) to the random waves MRW1 and MRW2. From these figures, it can be seen that post-failure the platform migrates to another mean position with a remarkable transient response following the line failure directly. Also, it was noted that the migration distance is about 16 m when the wave-ward line (Line M_1) was released while it was about 10 m when the downward line (M_2) was released (Fig 6.14). This indicates that the effect of upstream line failure is greater than the effect of damaging a line lying on downstream. This is because the former line was lying on the positive excursions, while the latter line was lying on the negative excursion zone.

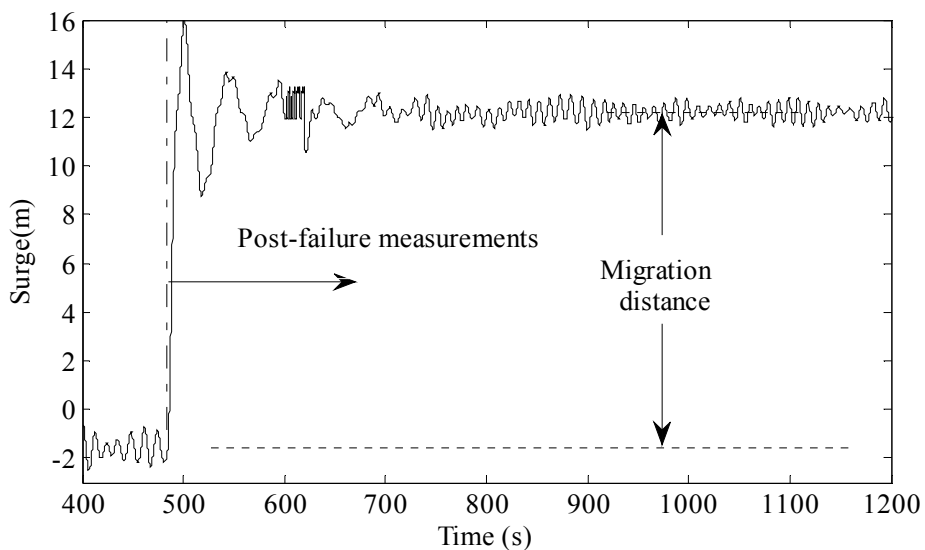


Fig 7.50: Effect of M_1 failure to MRW1 on platform the surge response

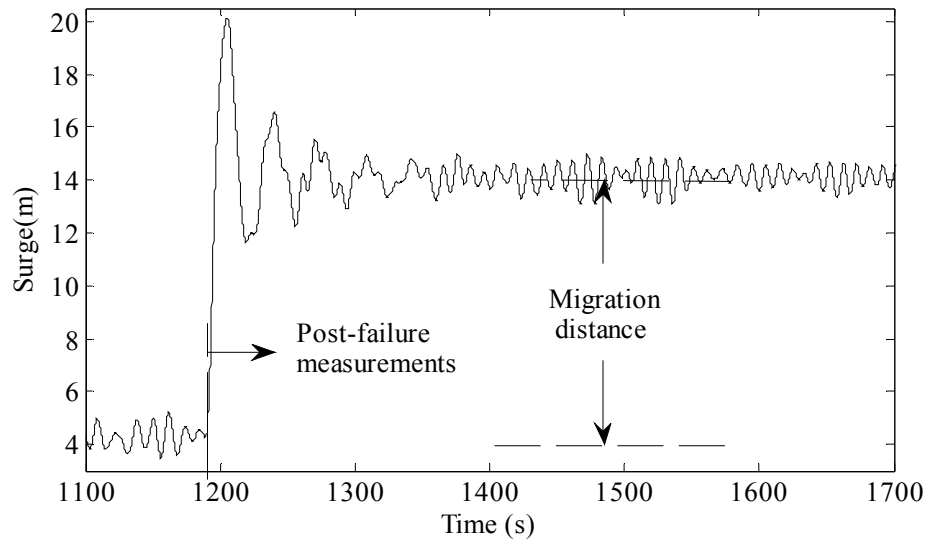


Fig 7.51: Effect of M_2 failure to MRW2 on platform the surge response

The consequences of line failure effects on the intact lines' tension response were measured and are shown in Fig 7.52~Fig 7.55 for the measurements of the two attached load cells LC1 and LC2 (Fig 6.14). For the case of the first line (M_1) failure to wave MRW1, it can be seen from Fig 7.52~Fig 7.53 that all lines' resultant tensions were reduced post-failure with a little increase on the response amplitude for lines on upstream and vice versa for lines on downstream. This true also for the second case (failure of M_2 to MRW2) as can be seen from Fig 7.54~Fig 7.55. This occurred for this particular test setup because all lines lost part of their pretension post-failure.

From these results, a significant migration for the structure was noted due to line failure. This may affect the structure drilling or production operations significantly. Therefore, for crucial assessment of the mooring damaged conditions, typical modeling of the mooring system (stiffness and geometry) and vertical attachments (risers or drilling rigs) is needed.

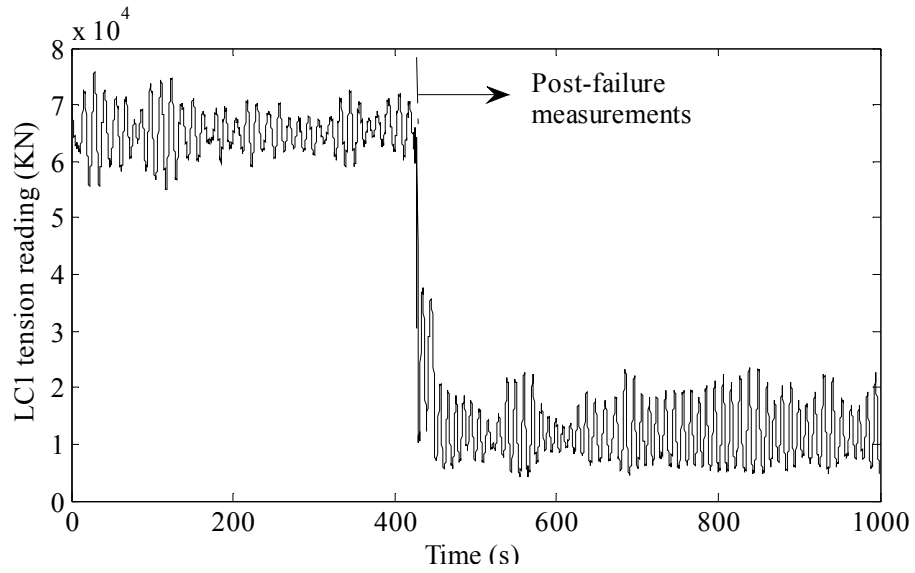


Fig 7.52: LC1 reading for M1 failure to MRW1

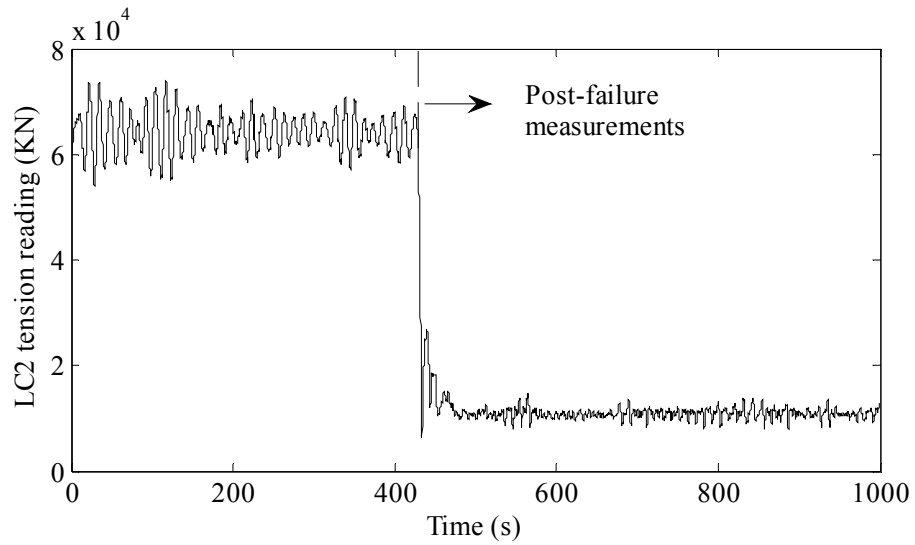


Fig 7.53: LC2 reading for M1 failure to MRW1

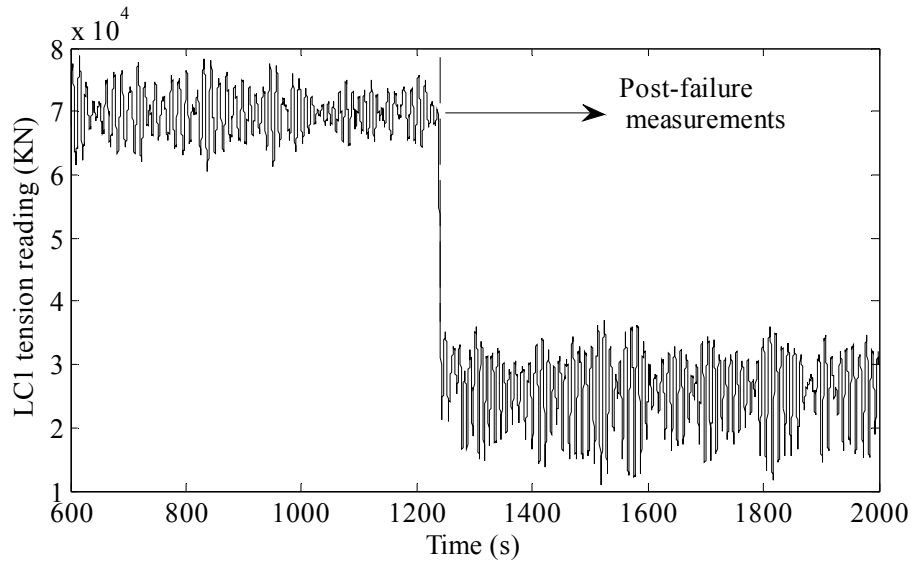


Fig 7.54: LC1 reading for M2 failure to MRW2

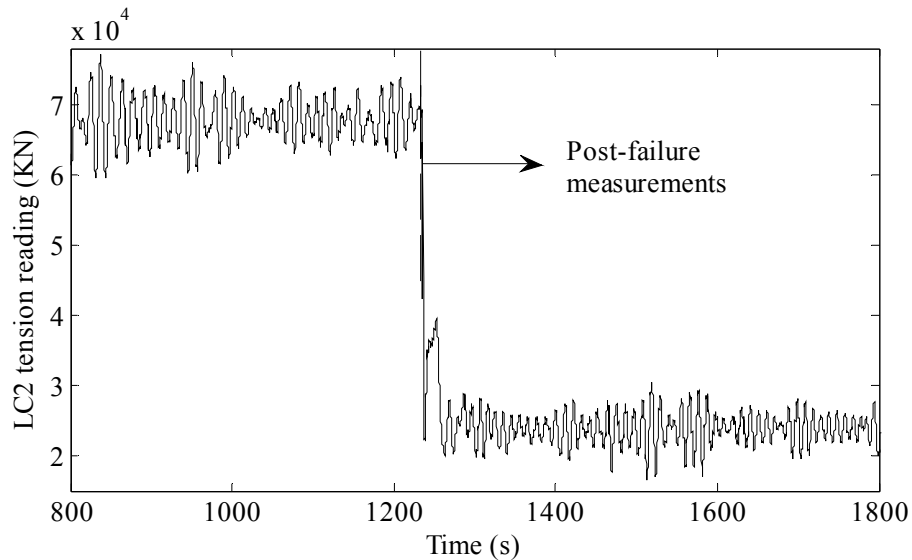


Fig 7.55: LC2 reading for M2 failure to MRW2

7.5 Case studies (Numerical results)

Based on the validated frequency domain numerical model, sixteen case studies were taken for the purpose of investigation of different parameter contributing in the structure response and consequently its design. The general data for these cases are shown in Table 7.8. The notations given in this Table were defined in Fig 7.56~Fig 7.57. The primary aim of this case study is to assess the effect of various parameters on the structure surge and sway motions and mooring line tension responses. It

should be noted that a constant yaw radius of gyration of 24 m was taken for all cases since yaw response was not considered.

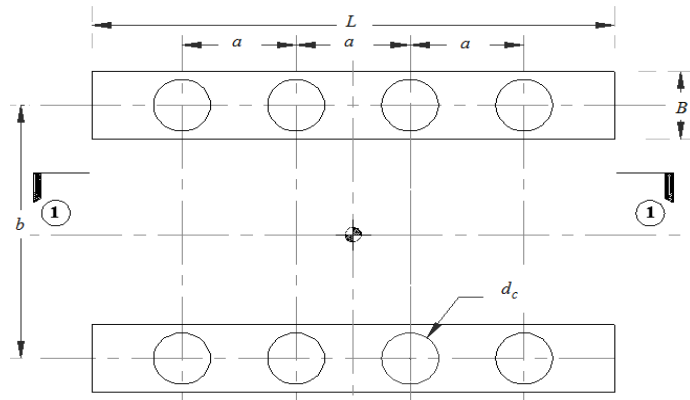


Fig 7.56: Plan of the dimensions related to Table 7.8

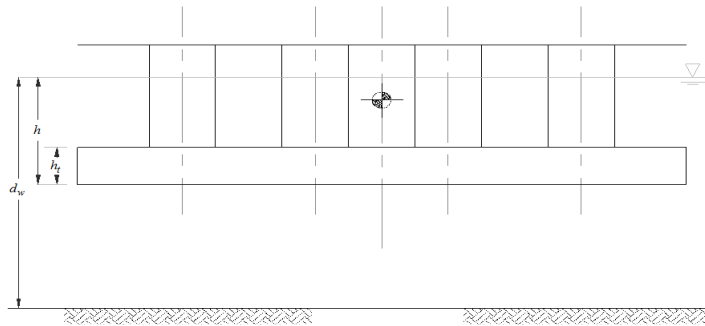


Fig 7.57: Section 1 of the dimensions related to Table 7.8

For this analysis, a partially grounded single-component mooring line was analyzed using Peyrot's method (Appendix-B). For the evaluation of force-excursion relation for the single line and the wholly mooring system for three different cases (All cases except a_1 and a_4 , a_1 and a_4). The cable data are given in Table 7.7.

Table 7.7: Single-component mooring data

Description	Value
Cable cross-sectional area (m^2)	0.05
Cable tangential modulus of elasticity (kN/m^2)	2600E+6
Cable un-stressed length (m)	506.42
Cable unit weight in water (kN/m)	2.0
Cable projection in x-axis	372
Cable projection in z-axis	200 ⁵ , 270 ⁶

⁵ All cases except a_1

⁶ Case a_1

Table 7.8: Case studies general data

Case	m (T)	Dimensions								Spectrum data			N_c	N_m	Wave Spectrum	Mooring condition
		L	B	h_t	a	b	d_w	d_c	h	H_s	T_p					
No	Sym.	(m)	(m)	(m)	(m)	(m)	(m)	(m)	(m)	(m)	(s)					
1	ao	34134.02	100	16	8	24	60	212	10	20	6	11	8	8	JONSWAP	Intact
2	b	36770.82	110	16	8	24	60	212	10	20	6	11	8	8	JONSWAP	Intact
3	c	32486.02	100	15	8	24	60	212	10	20	6	11	8	8	JONSWAP	Intact
4	d	39431.68	100	16	10	24	60	212	10	20	6	11	8	8	JONSWAP	Intact
5	e	34134.02	100	16	8	20	60	212	10	20	6	11	8	8	JONSWAP	Intact
6	f	34134.02	100	16	8	24	50	212	10	20	6	11	8	8	JONSWAP	Intact
7	g	32192.51	100	16	8	30	60	212	10	20	6	11	6	8	JONSWAP	Intact
8	h	31338.25	100	16	8	24	60	212	8	20	6	11	8	8	JONSWAP	Intact
9	i1	35428.35	100	16	8	24	60	212	10	22	6	11	8	8	JONSWAP	Intact
10	i2	37369.86	100	16	8	24	60	212	10	25	6	11	8	8	JONSWAP	Intact
11	a1	34134.02	100	16	8	24	60	282	10	20	6	11	8	8	JONSWAP	Intact
12	a2	34134.02	100	16	8	24	60	212	10	20	8	11	8	8	JONSWAP	Intact
13	a3	34134.02	100	16	8	24	60	212	10	20	6	14	8	8	JONSWAP	Intact
14	a4	34134.02	100	16	8	24	60	212	10	20	6	11	8	12	JONSWAP	Intact
15	a5	34134.02	100	16	8	24	60	212	10	20	6	11	8	8	PM	Intact
16	a6	34134.02	100	16	8	24	60	212	10	20	6	11	8	8	JONSWAP	Damage

Notes:

1. Case a_0 represents the benchmark case -
2. The grey shaded parameter in each case represents the case change from the benchmark case -
3. N_c = number of columns, N_m = number of mooring lines

Force-excursion relationships for single line together and the mooring configuration for static successive excursions (as shown in the internal frame) are shown in Fig 7.58~Fig 7.59. Also, the nonlinear mathematical model evaluated from by data fitting technique are shown in Fig 7.60~Fig 7.61. It should be noted that in these figures, y represents the tension and x denoted the excursion. The comparisons between different cases for the nonlinear force-excursion relationship are shown in Fig 7.62.

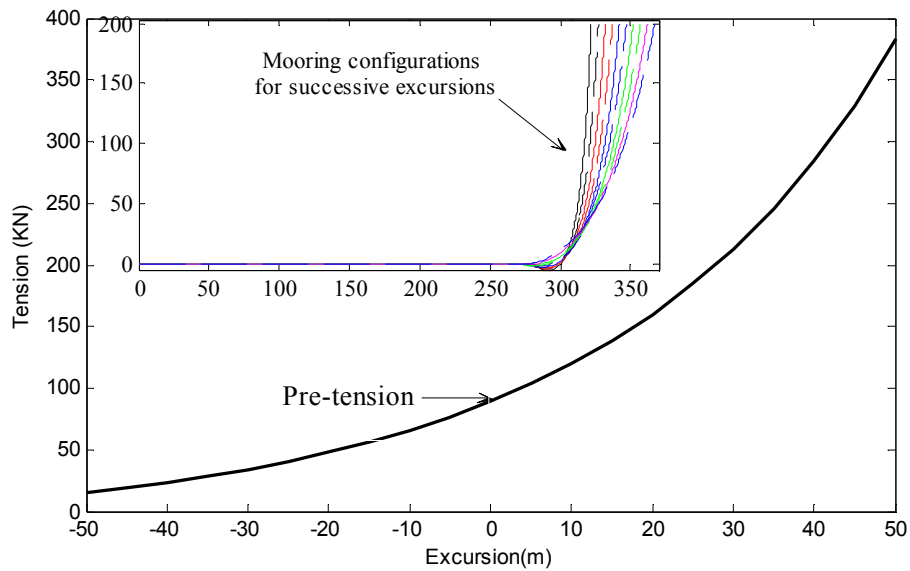


Fig 7.58: Force-excursion relationship for single line (All cases except a₁)

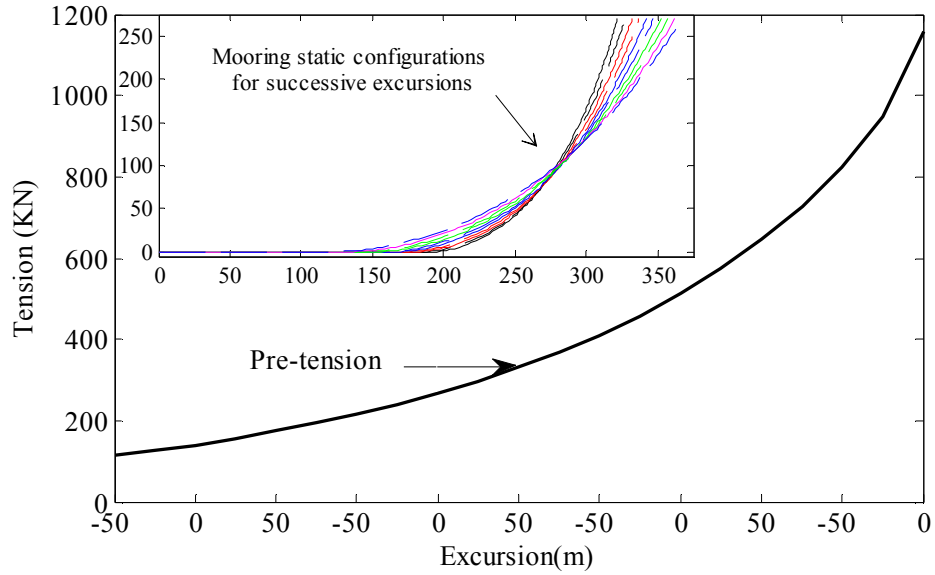


Fig 7.59: Force-excitation relationship for single line (Case a₁)

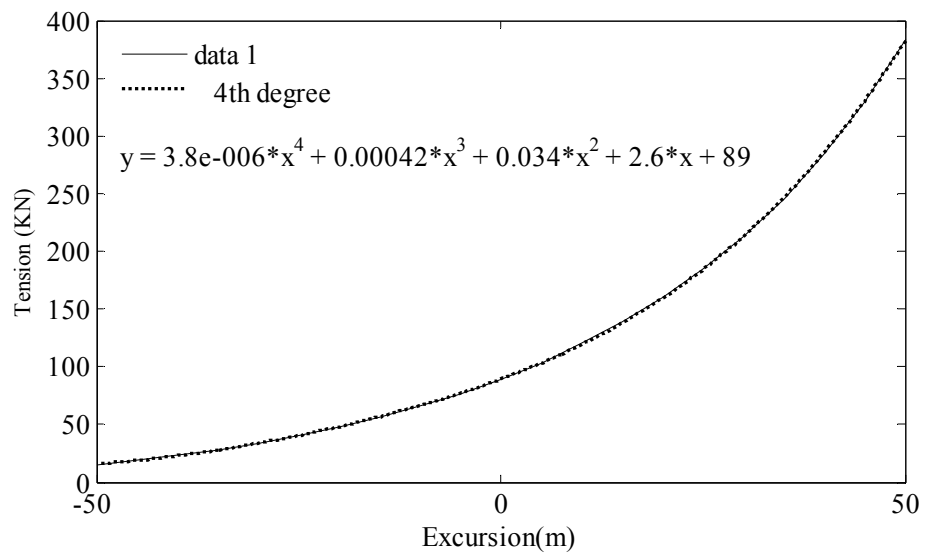


Fig 7.60: Nonlinear mathematical model representing force-excitation relationship for single line (All cases except a₁)

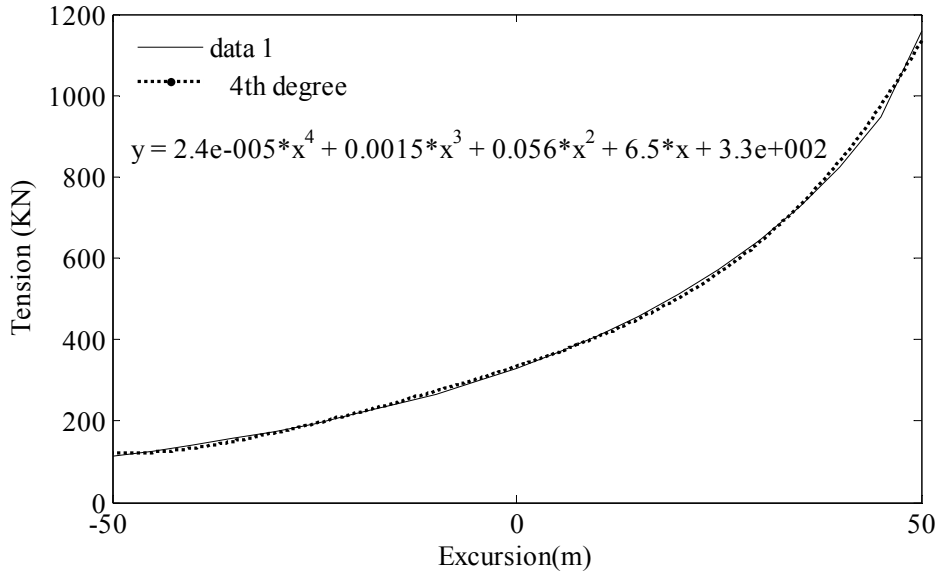


Fig 7.61: Nonlinear mathematical model representing force-excursion relationship for single line (Case a₁)

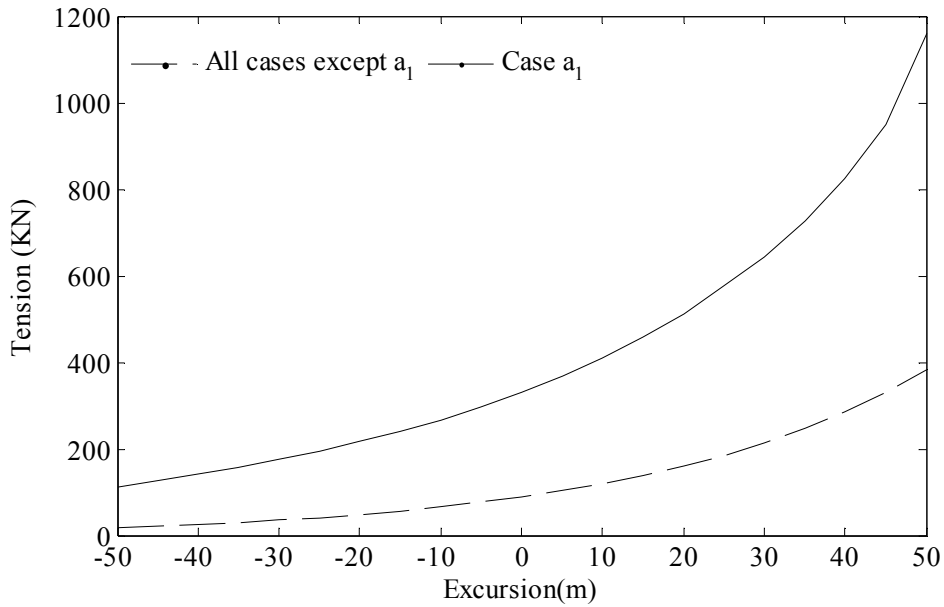


Fig 7.62: Force-excursion relationship for single line (Comparisons)

Mooring system configurations for different cases are given in Fig 7.63~Fig 7.65.

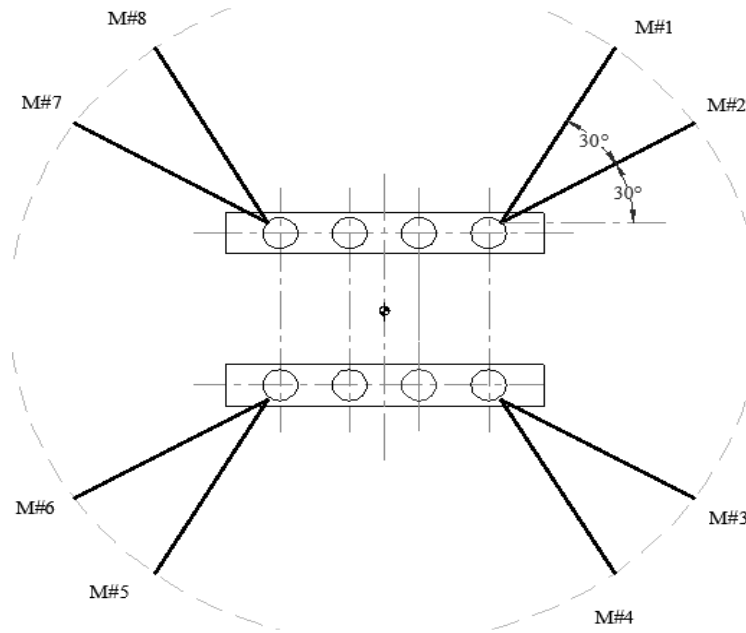


Fig 7.63: Mooring system configuration (All cases except a₄ and a₆)

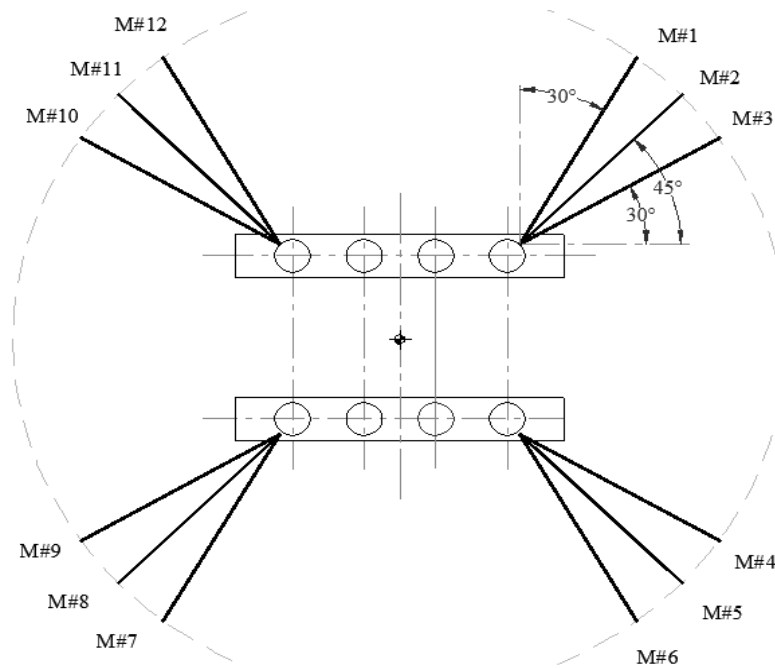


Fig 7.64: Mooring system configuration (Case a₄)

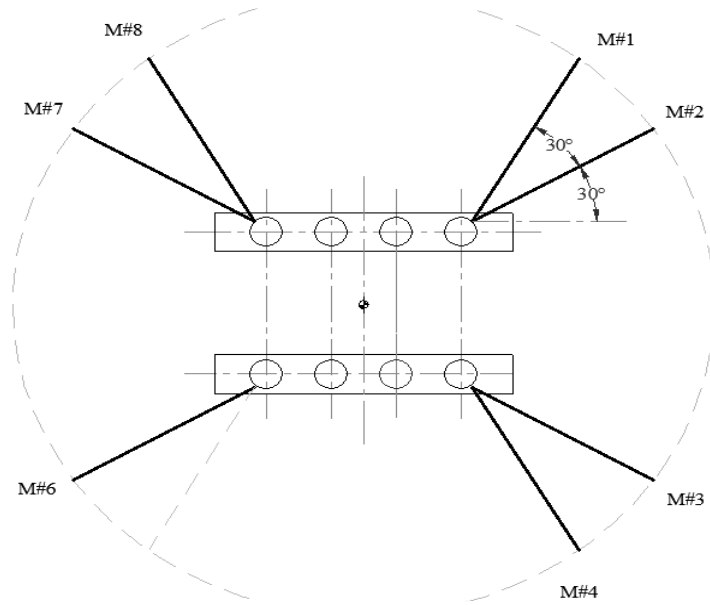


Fig 7.65: Mooring system configuration post-damage (Case a₆)

Comparisons between different mooring systems restoring force for x-excursions and the nonlinear spring mathematical model for x-excursions are given in Fig 7.66~Fig 7.70.

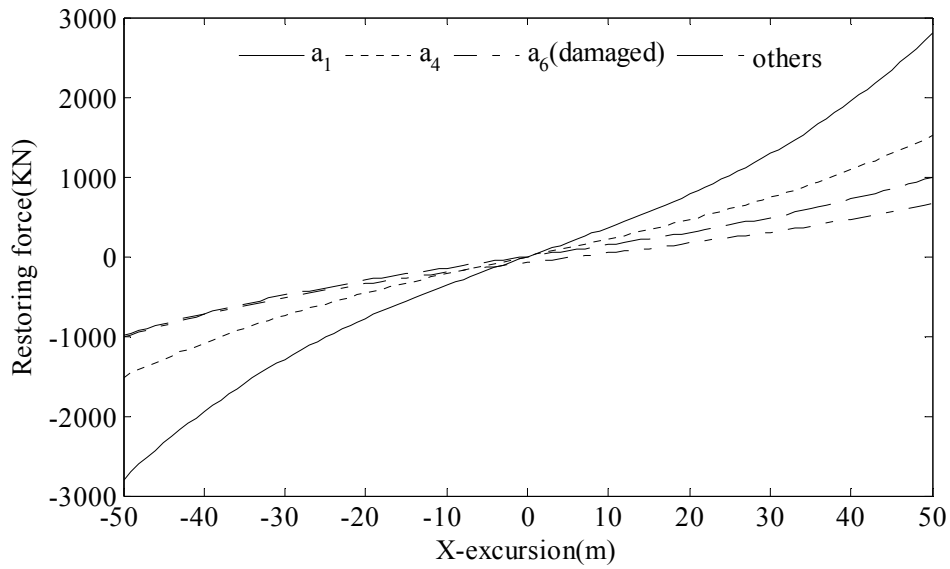


Fig 7.66: Mooring system restoring force-excursion relation (X-axis)

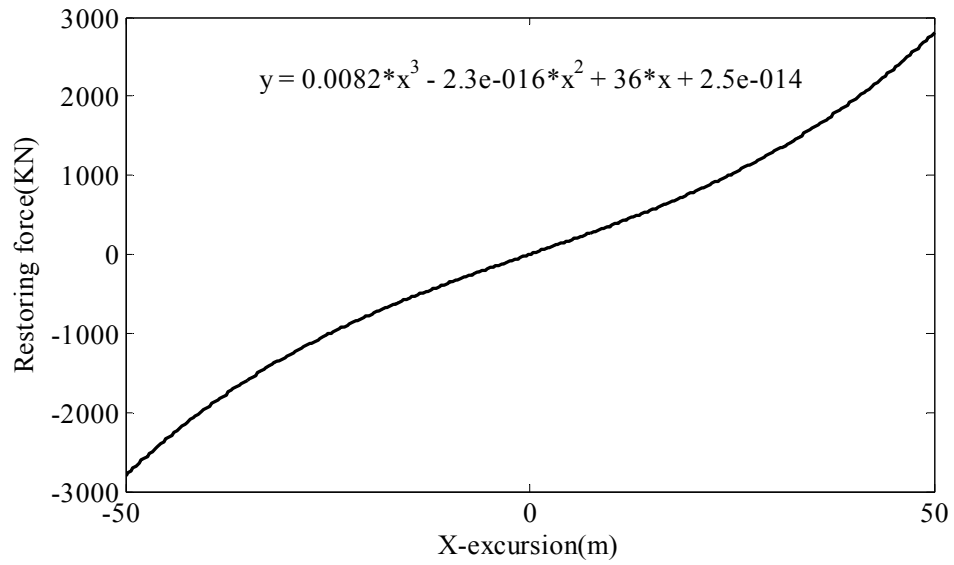


Fig 7.67: Nonlinear X-axis spring mathematical model (case a₁)

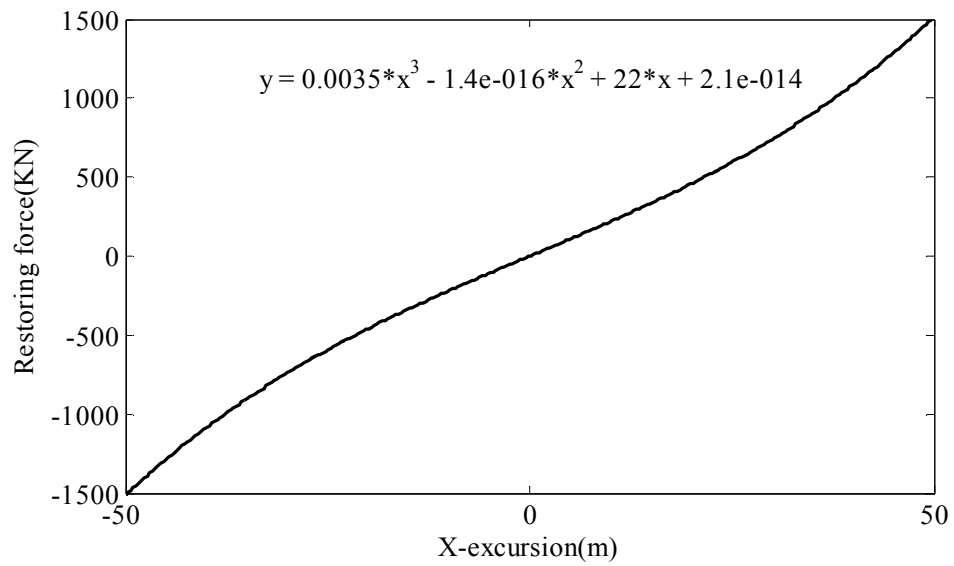


Fig 7.68: Nonlinear X-axis spring mathematical model (case a₄)

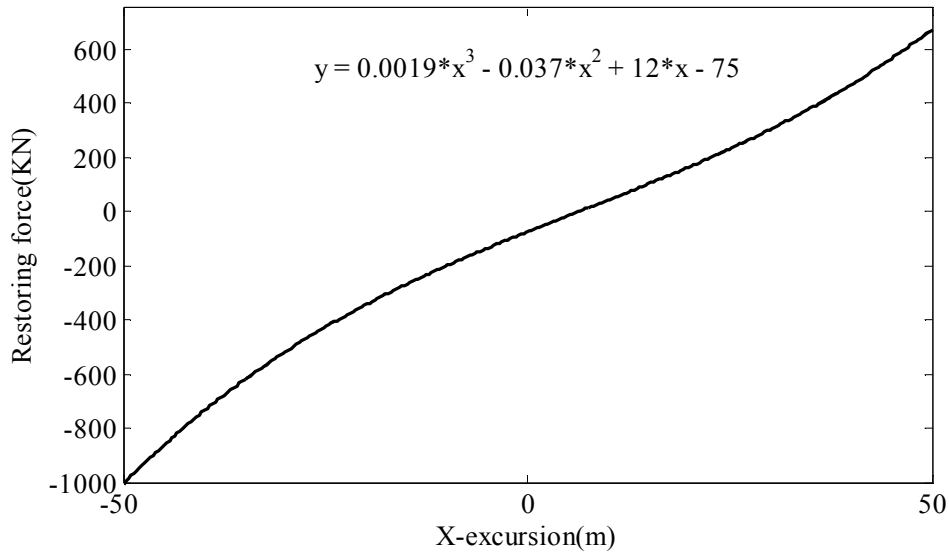


Fig 7.69: Nonlinear X-axis spring mathematical model (case a₆)

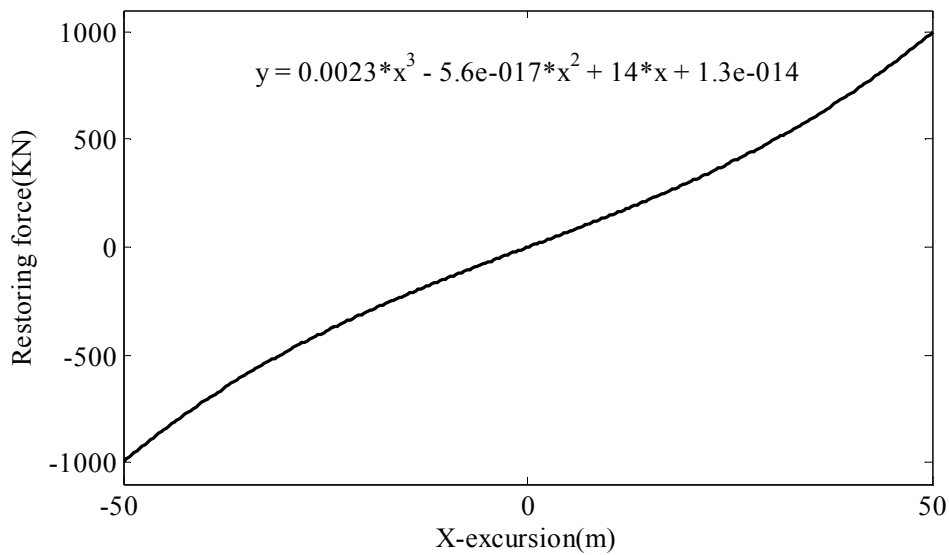


Fig 7.70: Nonlinear X-axis spring mathematical model (All except a₁, a₄ and a₆)

Comparisons between different mooring systems restoring force for y-excursions and the nonlinear spring mathematical model for x-excursions are given in Fig 7.71~Fig 7.75.

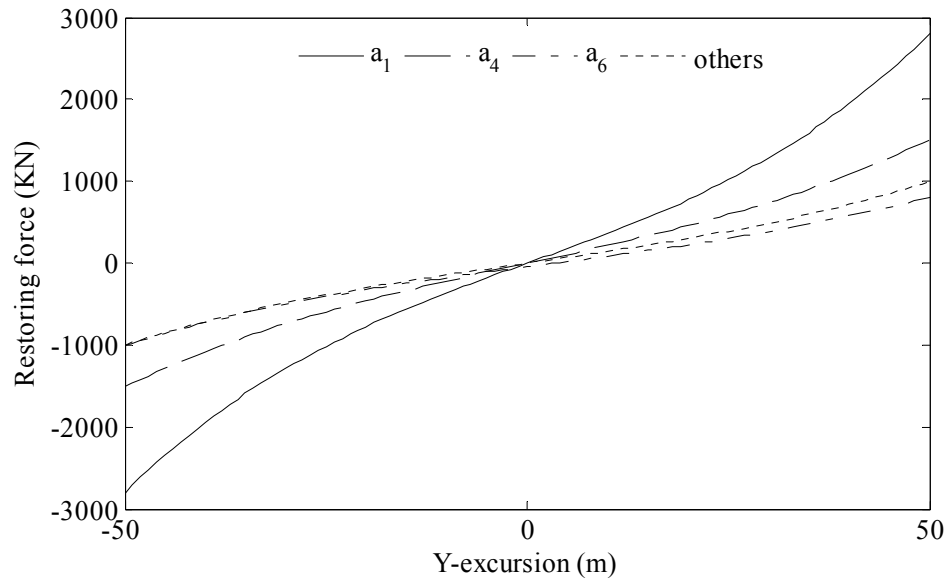


Fig 7.71: Mooring system restoring force-excursion relation (Y-axis)

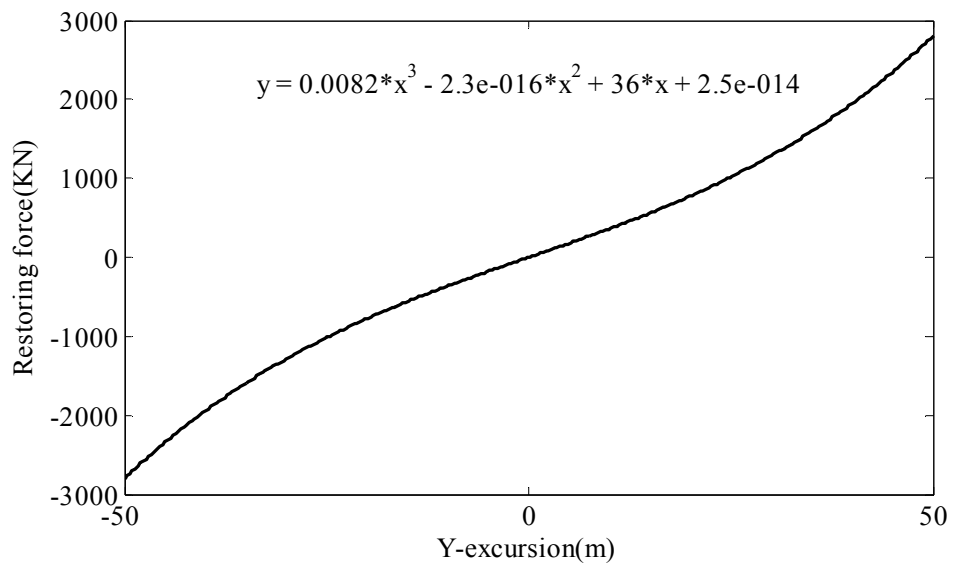


Fig 7.72: Nonlinear Y-axis spring mathematical model (case a₁)

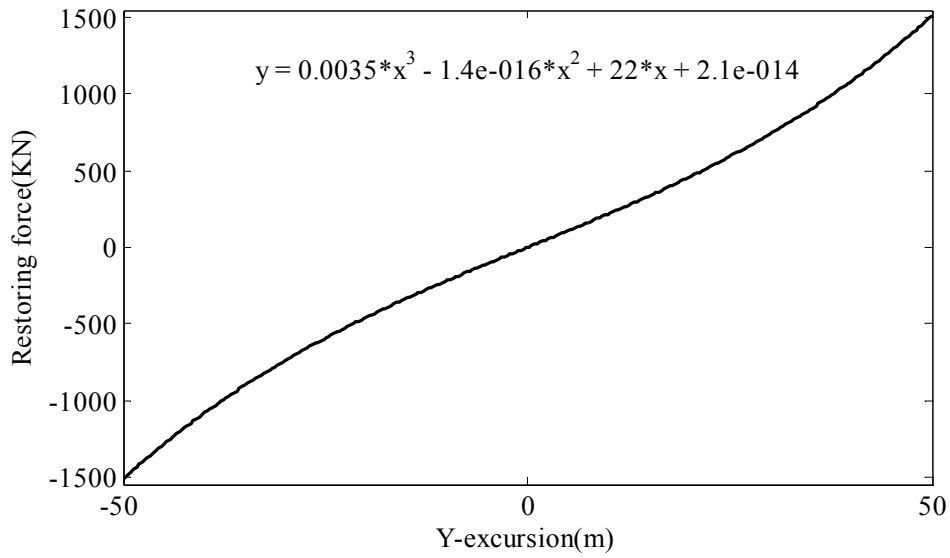


Fig 7.73: Nonlinear Y-axis spring mathematical model (case a₄)

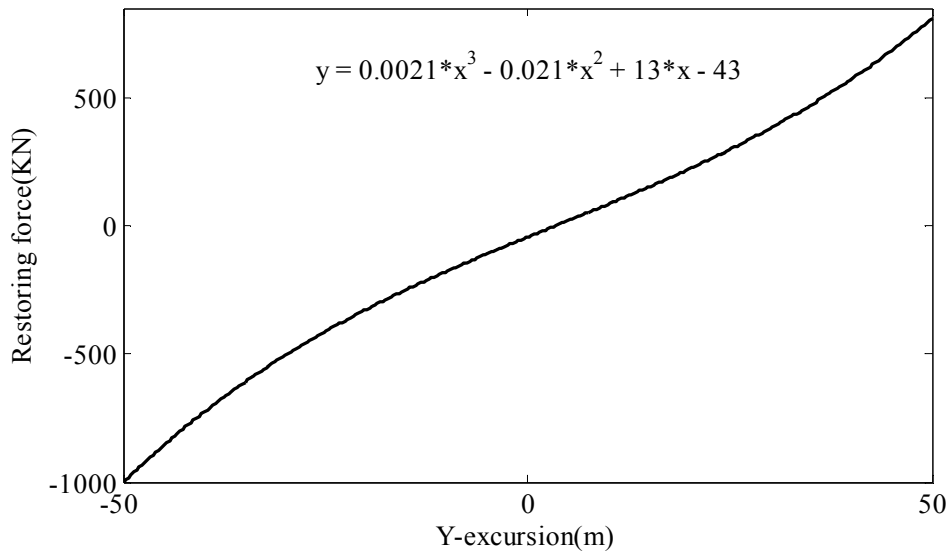


Fig 7.74: Nonlinear Y-axis spring mathematical model (case a₆)

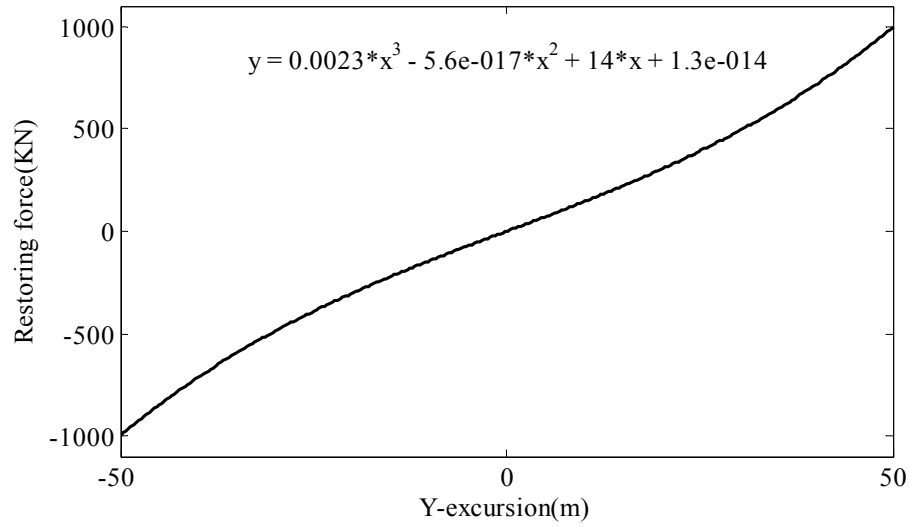


Fig 7.75: Nonlinear Y-axis spring mathematical model (All except a_1 , a_4 and a_6)

For the evaluation of mooring line tension responses, the nonlinear force excursion relationships given in Fig 7.76~Fig 7.79 for negative and positive excursions were used.

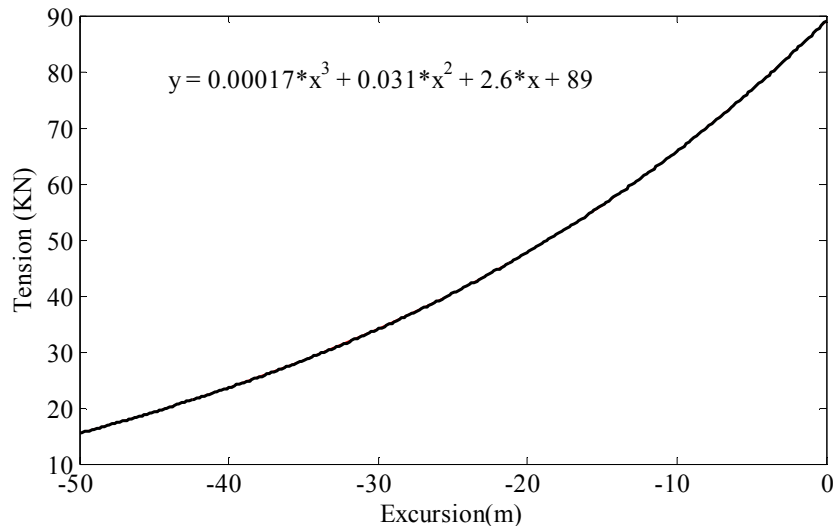


Fig 7.76: Nonlinear mathematical model representing force-negative excursion relationship for single line (All cases except a_1)

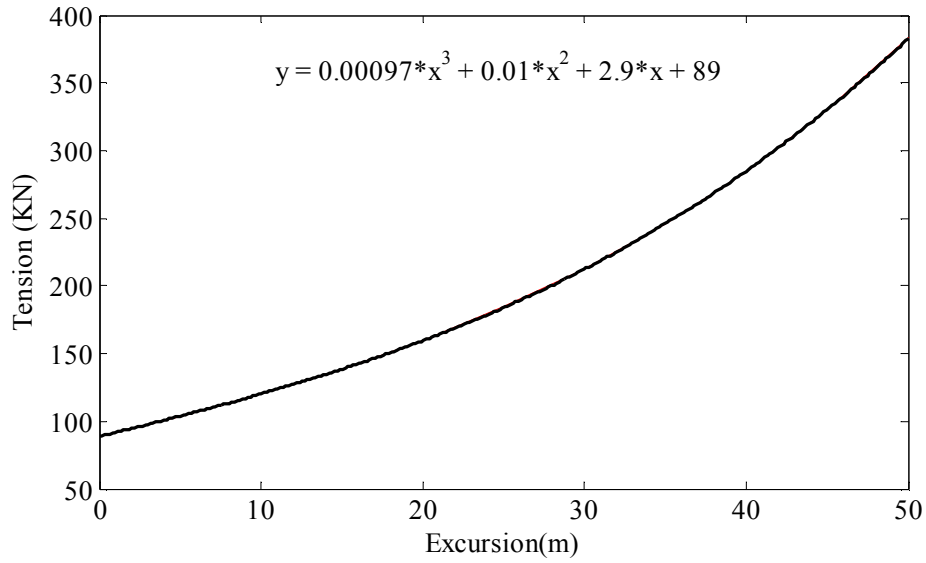


Fig 7.77: Nonlinear mathematical model representing force-positive excursion relationship for single line (All cases except a₁)

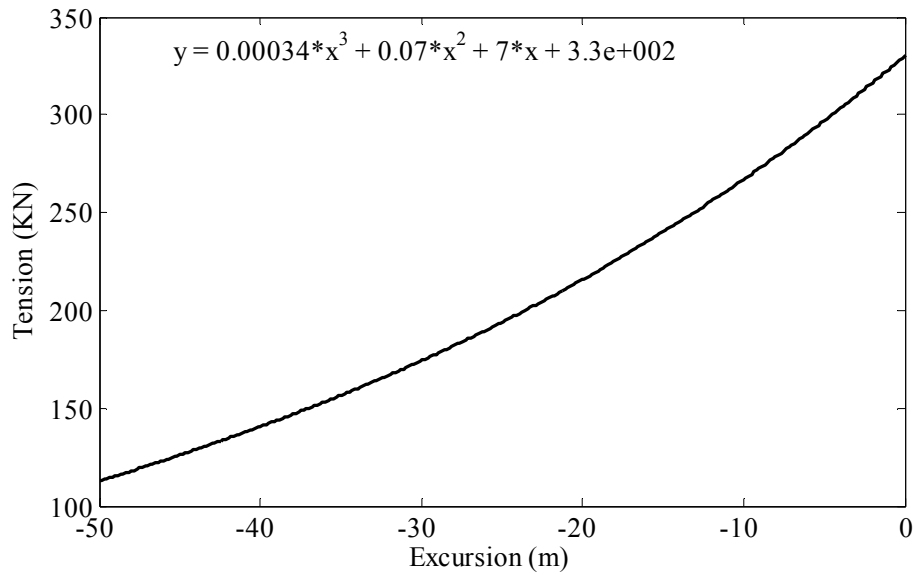


Fig 7.78: Nonlinear mathematical model representing force-negative excursion relationship for single line (Case a₁)

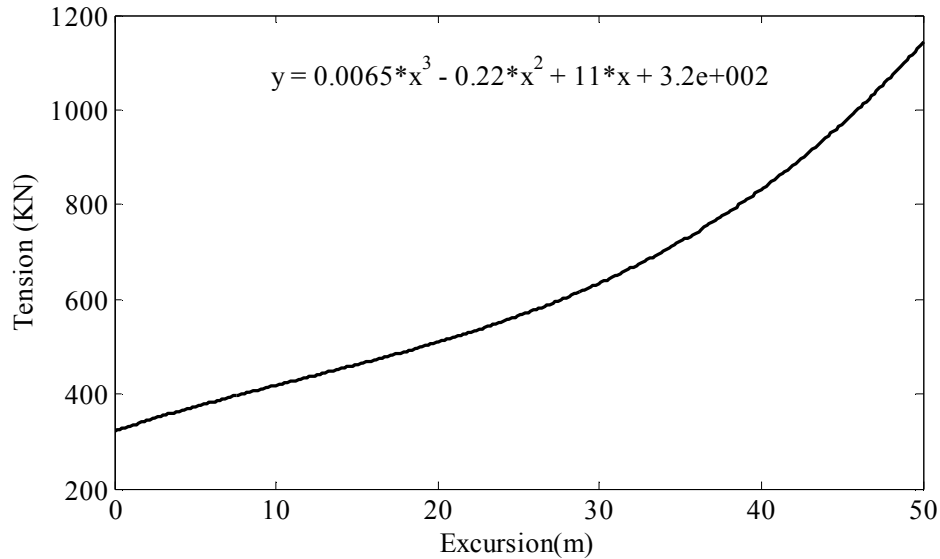


Fig 7.79: Nonlinear mathematical model representing force-positive excursion relationship for single line (Case a₁)

For all the systems, a damping ratio of 5% and seawater specific density of 1.025 T/m³ were taken in the analysis. From free-decay test simulation for the benchmark system, it was found that its natural periods were about 225 s and 300 s for surge and sway degrees of freedom. Thus, it was decided to evaluate the system peak motion and tension responses to bi-chromatic wave having difference frequency approaching the natural frequency of the system. Table 7.9 gives the wave data for the bi-chromatic head.

Table 7.9: Bi-chromatic wave data for case a₀

	Head sea	
	Height (m)	Frequency (rad/s)
Wave 1	1.0	0.572
Wave 2	2.0	0.600

The surge motion and the symmetrical mooring tension response time traces to the head bi-chromatic wave given in Table 7.9 are shown in Fig 7.80~Fig 7.81 respectively. It can be seen from the first figure that the structure is undergoing low frequency response along with an internal first order response. For this particular case, the amplitude of the first order motion is about 0.1 m while the amplitude of the low frequency motion is about 0.6 m. For the line tension response, it can be seen from Fig 7.81 that the most loaded line is mooring #1. Thus, for the assessment of the design parameter for the cases given in Table 7.8 , surge motion and line #1 tension

response to head seas and sway motion and line #2 tension response are the subject of investigations.

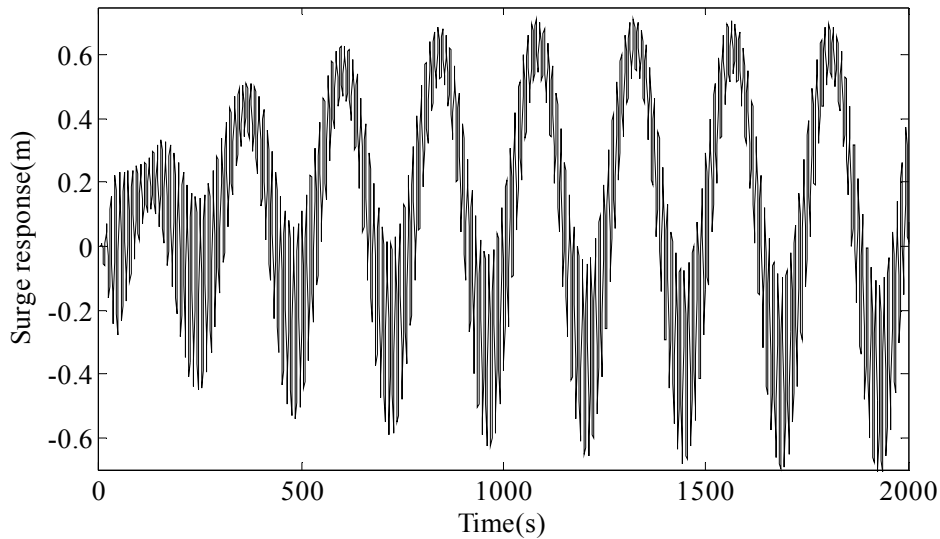


Fig 7.80: Surge response time trace to head bi-chromatic wave given in Table 7.9

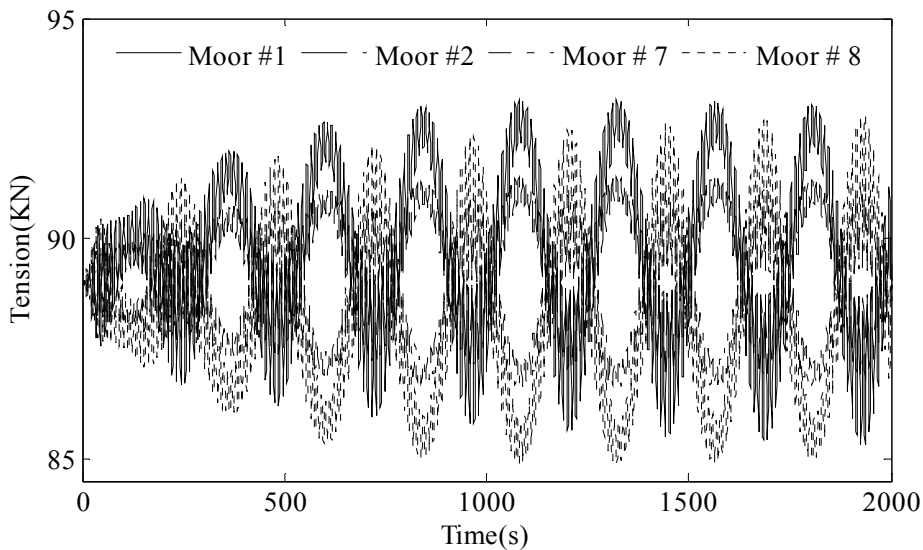


Fig 7.81: mooring tension response time traces to head bi-chromatic wave given in Table 7.9

Fig 7.82~Fig 7.83 shows comparisons between the results for the motion and tension amplitudes in cases a₀ and b respectively. The main difference parameter between the two cases is the underwater hull length and consequently the structure physical mass, since all other parameters were kept constant (Table 7.8). The hull length was increased by 10%. Results indicate that increasing the hull length decrease

the surge and sway amplitudes and the the mooring line tension responses. The percentage decrease in the surge is almost (10.3%) the same as the increase in hull length. This is mainly due to the increase in the structure physical mass, since the added mass and hydrodynamic loads are negligible in this direction. The decrease percentage in sway is about 7.2%. The less ratio in sway direction indicated that the increase in the hydrodynamic load is greater than the increase in the added mass in this sway DOF. The same arguments apply for tension responses with different percentages, since nonlinear mooring line models for force-excursion were adopted.

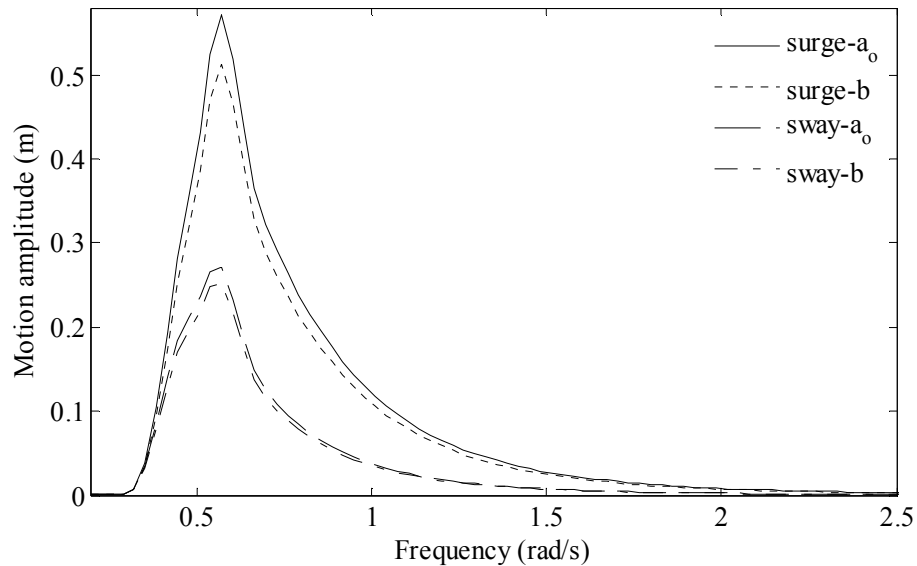


Fig 7.82: Comparison for motion amplitudes between case a₀ and b.

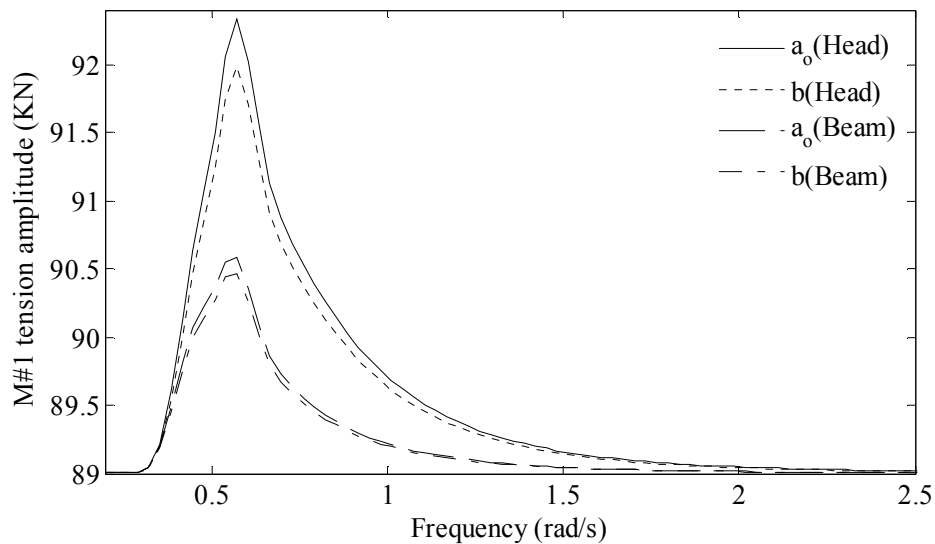


Fig 7.83: Comparison for M#1 tension amplitudes between case a₀ and b.

Comparisons between the motion and tension amplitudes results for case a_0 and c are shown in Fig 7.84~Fig 7.85 respectively. The primary change in case c compared to the benchmark case (a_0) is 6.25% decrease in the hulls x-sectional width (Table 7.8) and consequently decrease in the structure physical mass. This decrease resulted in 7.3% increase in surge and 2.1% decrease in sway. The difference in surge is due to change in the structure mass, while the difference in sway is because the resulted added mass is less than the hydrodynamic load.

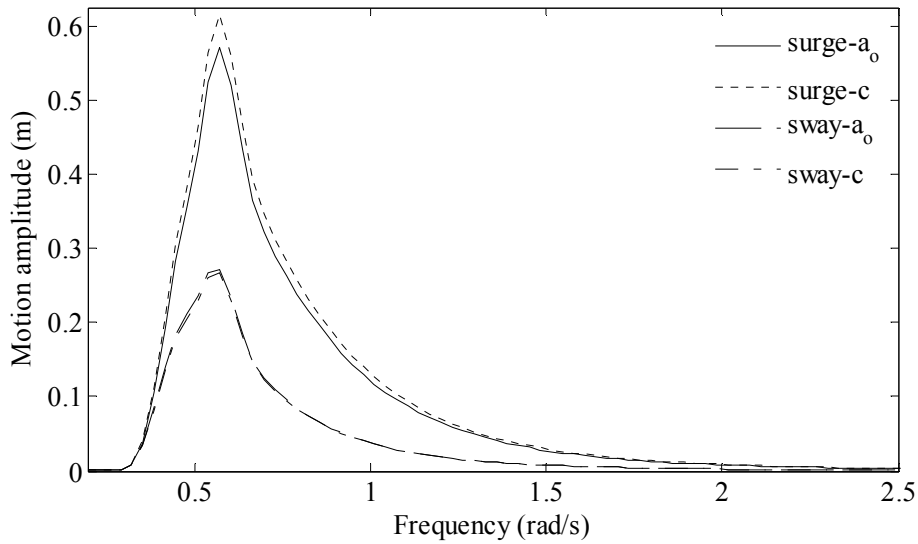


Fig 7.84: Comparison for motion amplitudes between case a_0 and b

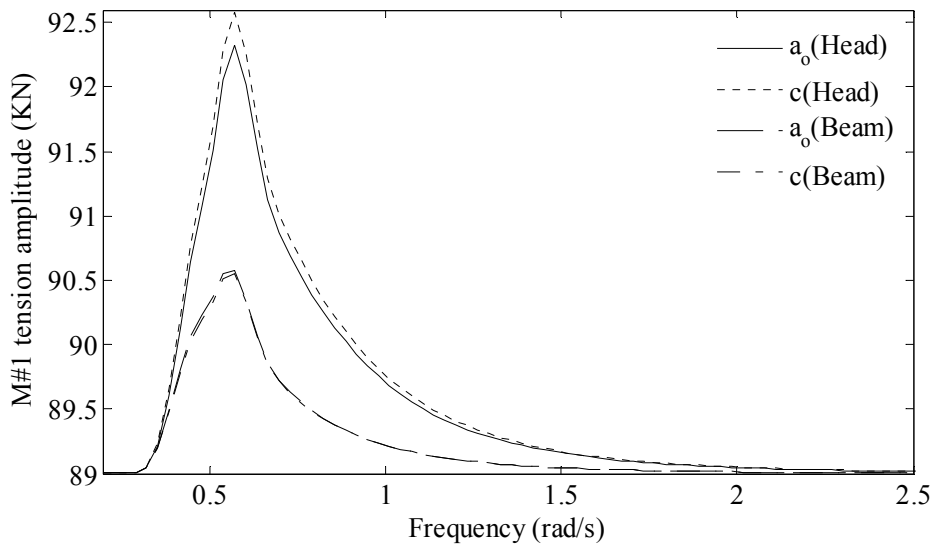


Fig 7.85: Comparison for M#1 tension amplitudes between case a_0 and b

Comparisons between the motion and tension amplitudes results for case a_0 and d are shown in Fig 7.86~Fig 7.87 respectively. In case d , the pontoons x-sectional height was increased by 25% compared to case a_0 . Since all other parameter were kept constant, the structure physical mass increased by 15.5%. These changes decreased the maximum surge and sway amplitudes by 34.5% and 14.1% respectively. The explanation for changes in hull length goes for this case also. For the change in the hull dimensions, it was found that increasing the dimensions lead to better seakeeping performance, especially for the x-sectional depth.

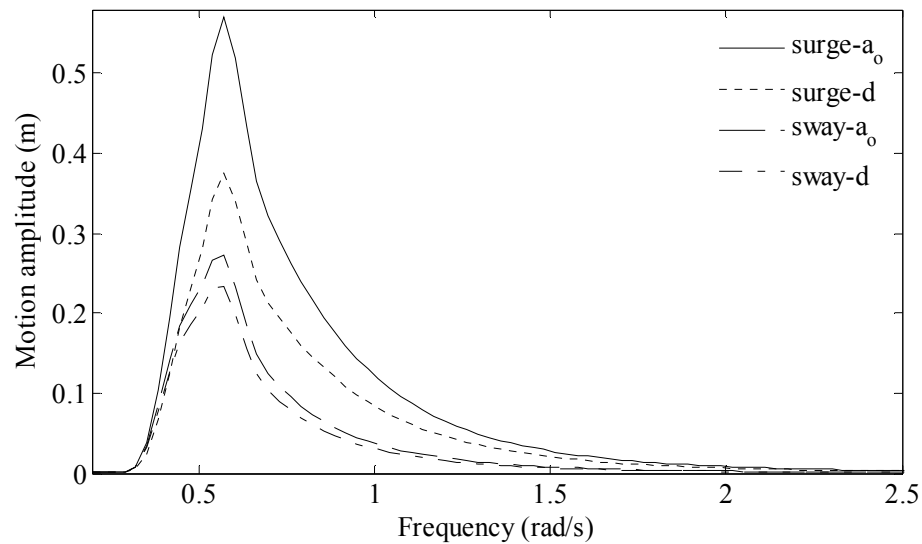


Fig 7.86: Comparison for motion amplitudes between case a_0 and d

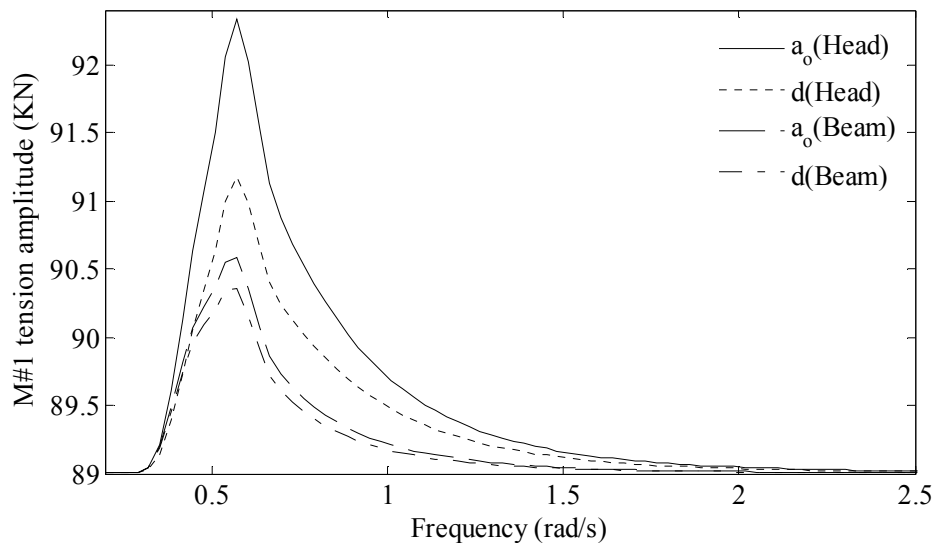


Fig 7.87: Comparison for M#1 tension amplitudes between case a_0 and d

Comparisons between the motion and tension amplitudes results for case a_0 and e are shown in Fig 7.90~Fig 7.91 respectively. The only change in case e compared to the primary case (a_0) is that the columns spacing in x-direction was decreased by 16.7%. This change involves no changes in the structure physical mass or any other parameter. Results of this case when compared to case a_0 , indicated no change in surge response but decrease in sway amplitude by 4.5%. This change occurred due to column proximity in the sway direction.

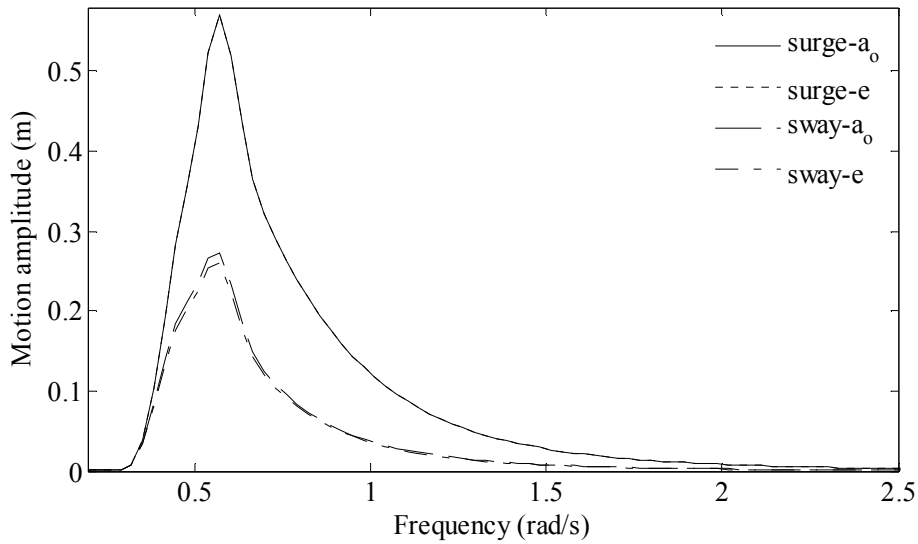


Fig 7.88: Comparison for motion amplitudes between case a_0 and e

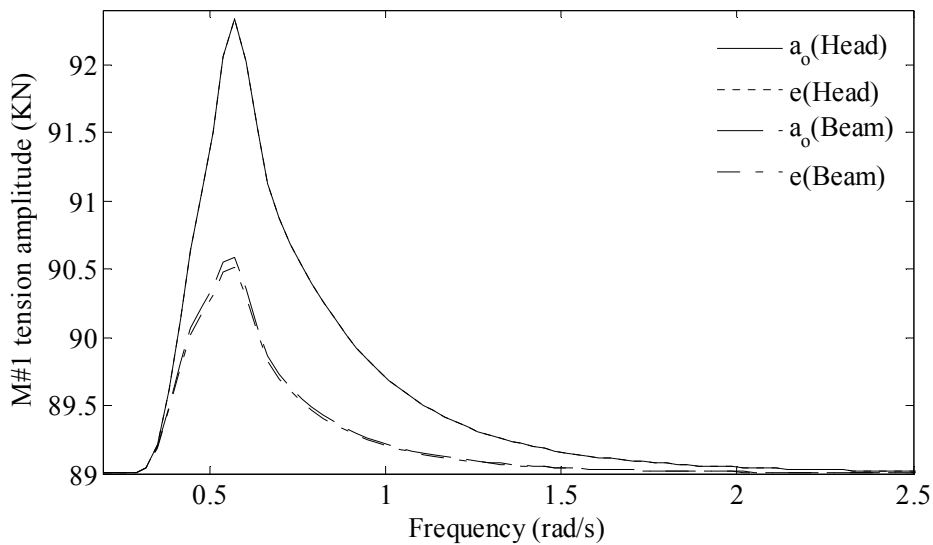


Fig 7.89: Comparison for M#1 tension amplitudes between case a_0 and e

Comparisons between the motion and tension amplitudes results for case a_0 and f are shown in Fig 7.90~Fig 7.91 respectively. In case f , the column spacing in y -direction decreased by 16.7% relative to case a_0 . Typical results as for case e were obtained. The change in sway amplitude may be because of the coupling effects between yaw and sway.

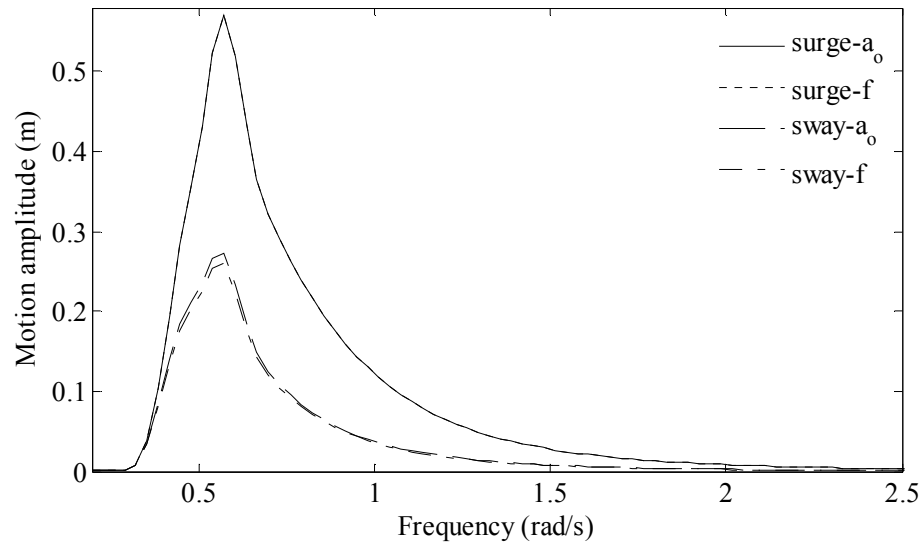


Fig 7.90: Comparison for motion amplitudes between case a_0 and f

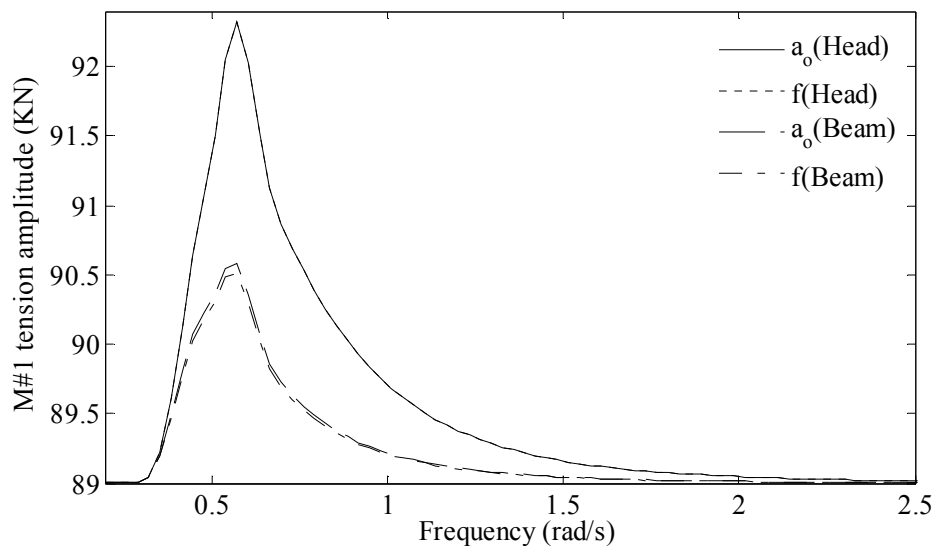


Fig 7.91: Comparison for M#1 tension amplitudes between case a_0 and f

In case g , the number of columns decreased to six (25% less) instead of eight (case a_0). Consequently, the structure physical mass decreased by 5.7% mass and the column spacing in x -direction increased by the same ratio for the number of columns.

Surge and sway amplitudes decreased by 27.7% and 13.5% as shown in Fig 7.92. The comparison of results for tension amplitudes are shown in Fig 7.93.

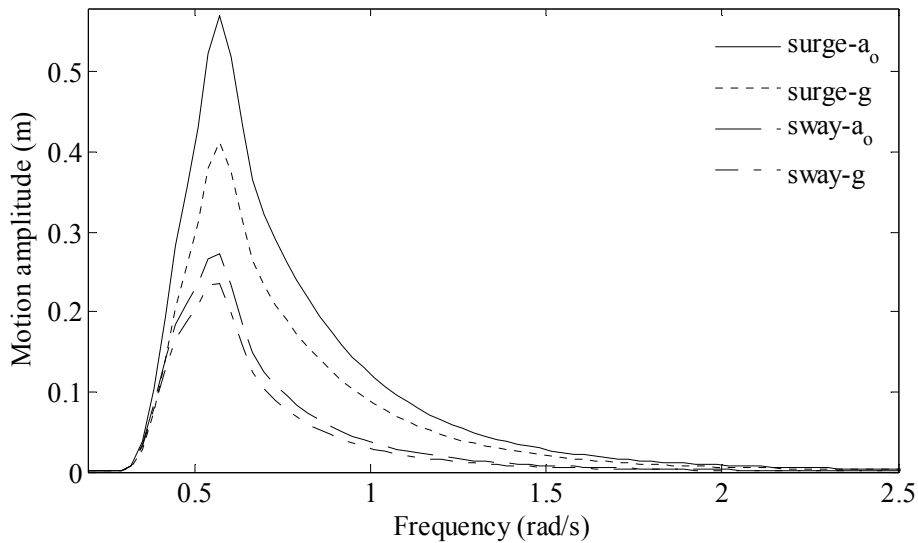


Fig 7.92: Comparison for motion amplitudes between case a₀ and g

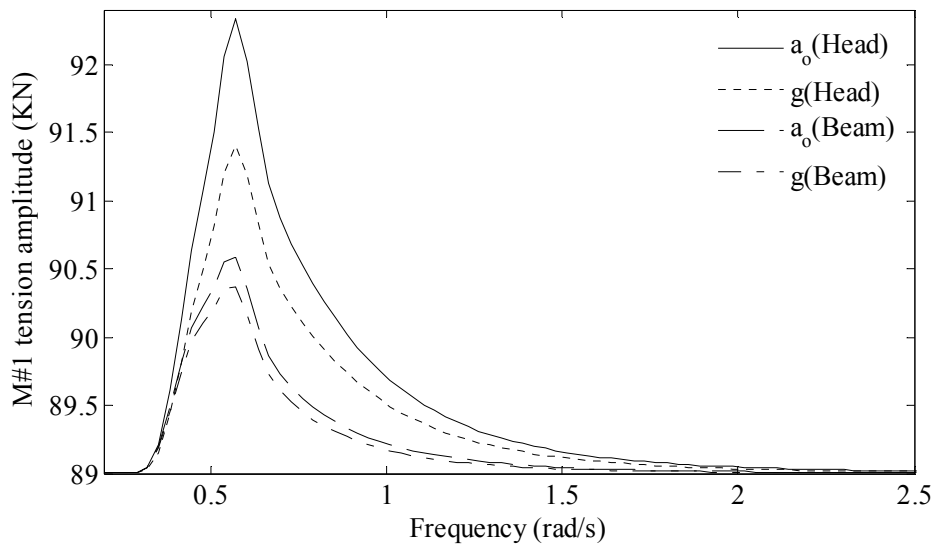


Fig 7.93: Comparison for M#1 tension amplitudes between case a₀ and g

Comparisons between the motion and tension amplitudes results for case a₀ and h are shown in Fig 7.94~Fig 7.95 respectively. In case h, the constant column diameter decreased by 20% relative to case a₀. This change resulted in almost the same percentage for sway amplitude (17.9%) and about 40% less surge amplitude compared to the reference case. It is clear that the effect of column diameter is dominant in surge direction.

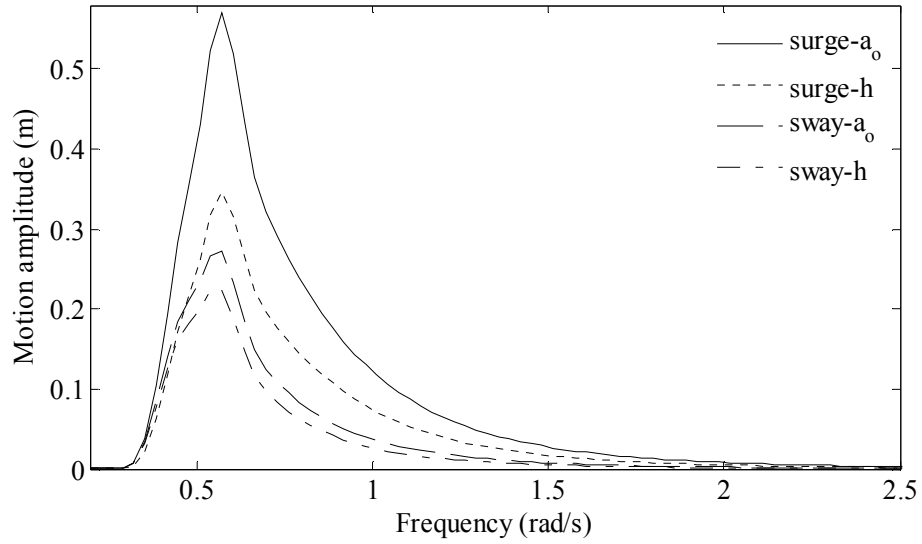


Fig 7.94: Comparison for motion amplitudes between case a₀ and h

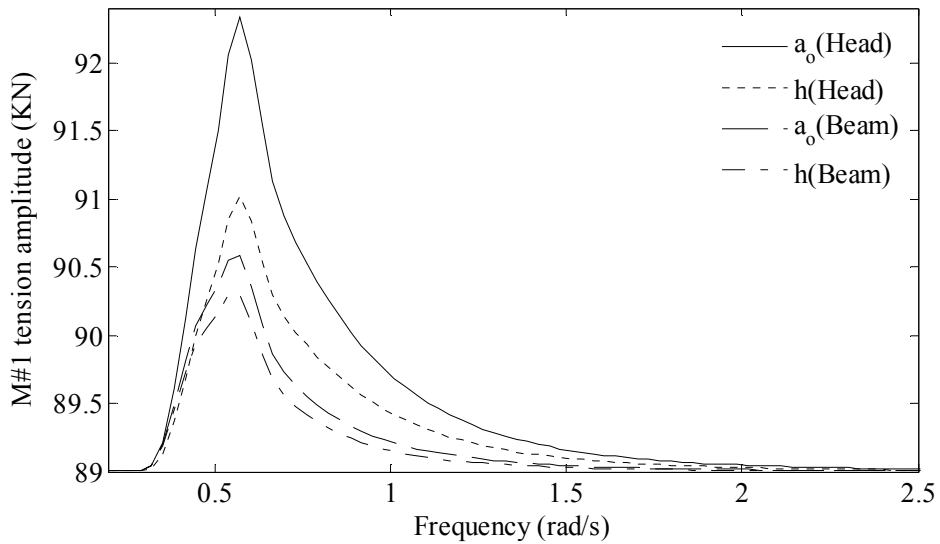


Fig 7.95: Comparison for M#1 tension amplitudes between case a₀ and h

The change in case i_1 and i_2 were corresponding to 10% and 25% increase in structure draft relative to the reference structure. Consequently, the structure physical mass increased by 3.8% and 9.5% for the two cases respectively. Fig 7.96~Fig 7.97 shows comparisons between these cases and the benchmark case (a_0). The surge amplitude in case i_1 increased by 15.9% but decreased by 53.4% in case i_2 . It seems that when increasing the draft by little amount, the increase in the hydrodynamic loads is more than the increase in the added mass and vice versa for significant increase in

the draft. On the other hand, it seems that sway amplitude is independent of the structure draft since very little change was noted as shown in Fig 7.97.

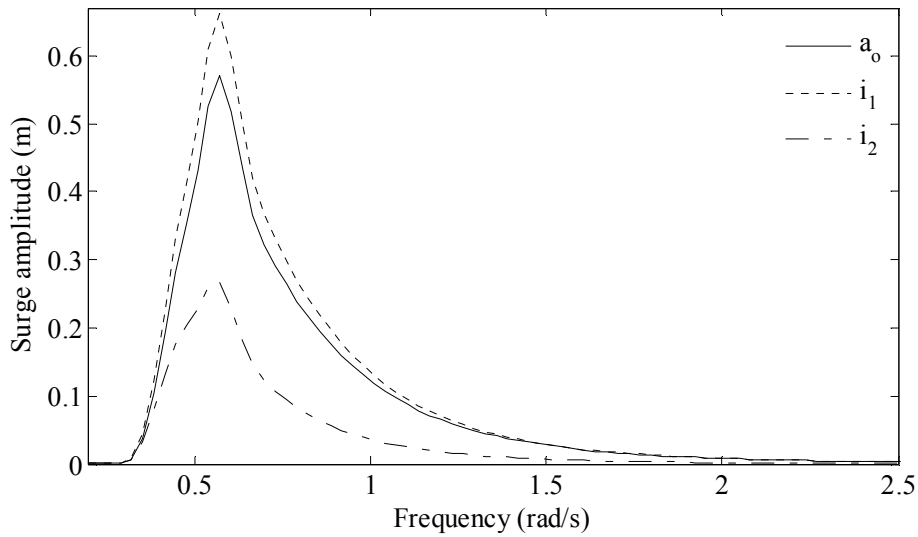


Fig 7.96: Comparison between case a_0 , i_1 and i_2 for surge amplitudes

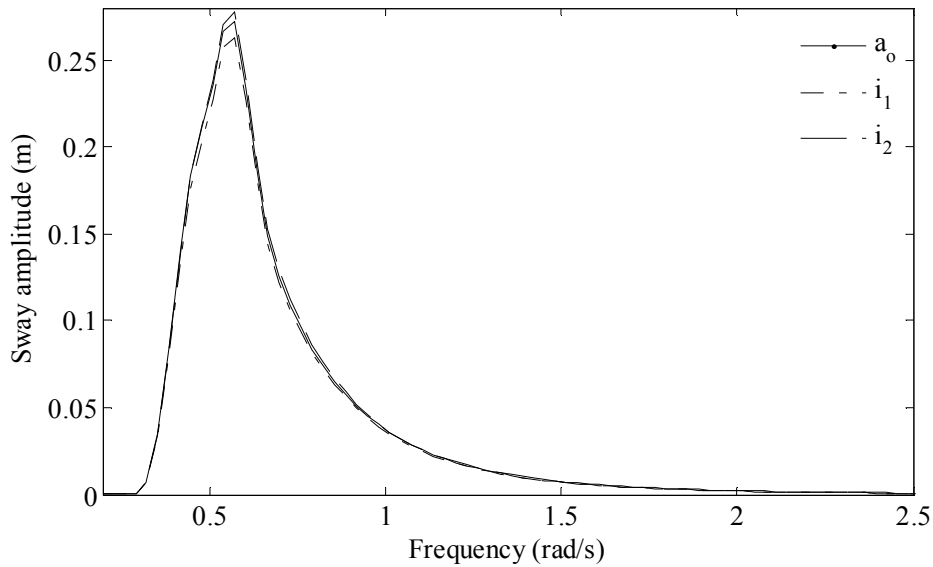


Fig 7.97: Comparison between case a_0 , i_1 and i_2 for sway amplitudes

Fig 7.98~Fig 7.103 shows semi submersible motion amplitudes, which was subjected to different environment and operating conditions (Table 7.8). In Fig 7.98, the reference semi submersible was moved from 212 m to 282 m water depth in case a_1 . Consequently, the mooring system stiffness increased, leading to a little decrease in surge (4.2%). For case a_2 , the wave significant height increased by 33%, which is

the same percentage of increase in surge. The same was observed for sway response as shown in Fig 7.99.

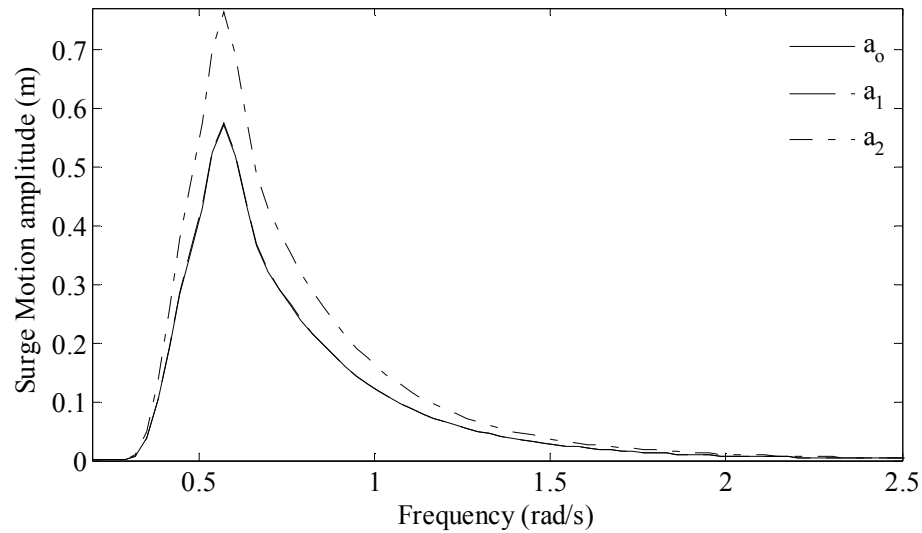


Fig 7.98: Comparison between a_0 , a_1 and a_2 cases for surge amplitudes

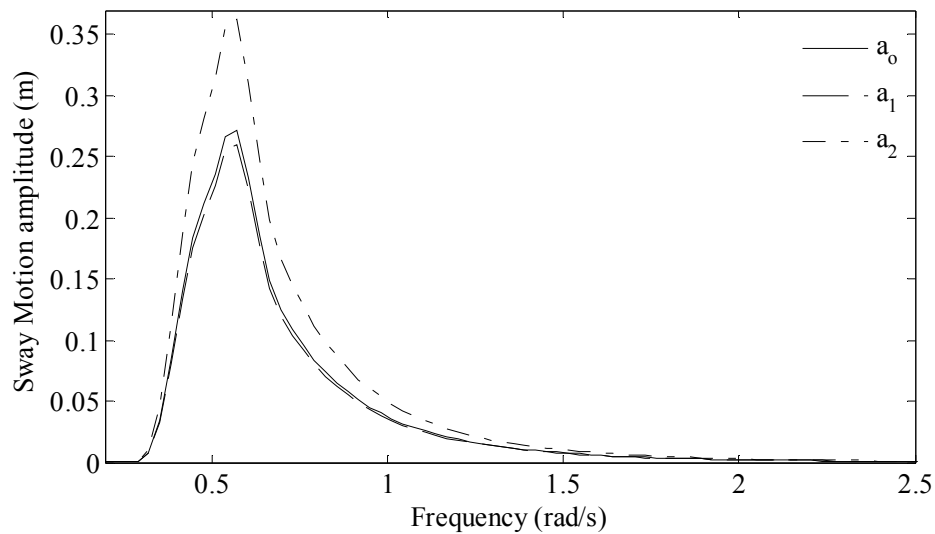


Fig 7.99: Comparison between a_0 , a_1 and a_2 cases for sway amplitudes

Comparisons between case a_0 , a_3 and a_4 for surge amplitudes are shown in Fig 7.100. In case a_3 , the peak period of the wave spectrum increased by 27.3%. This increased the surge by about 21.4% and the peak frequency shifted to low frequency side by the same percentage as the increase in the peak period. The increase in surge is mainly due to the shift in the peak frequency towards the system natural period. In case a_4 , the number of mooring lines was increased to 12. This decreased the surge

response by very little amount (0.4%). For sway amplitudes as shown in Fig 7.101, the response increased by about 66% for using 14 s peak period instead of 11 s and no effect was noted for increasing the number of mooring lines.

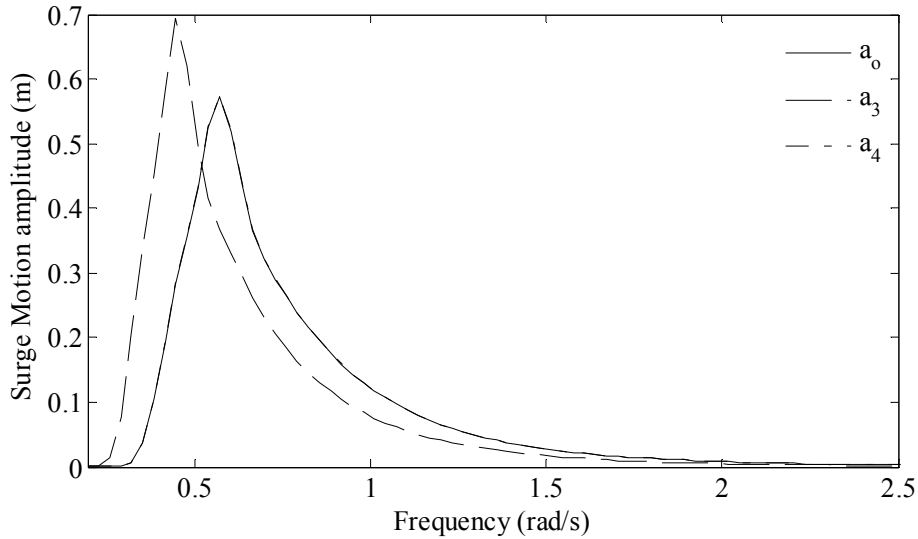


Fig 7.100: Comparison between a_0 , a_3 and a_4 cases for surge amplitudes

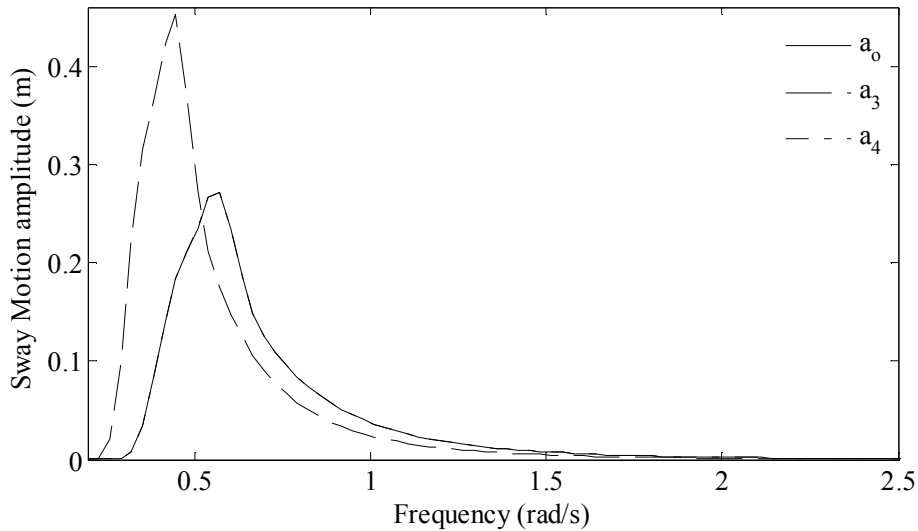


Fig 7.101: Comparison between a_0 , a_3 and a_4 cases for sway amplitudes

Comparisons between case a_0 , a_5 and a_6 for surge amplitudes are shown in Fig 7.102. In case a_5 , the mathematical model representing the sea environment was changed to PM instead of the JONSWAP in case a_0 . As clear in this Figure, the maximum surge amplitude decreased by about 3%. Also, slight shift of the peak frequency was noted. In case a_5 , it was assumed that one of the reference structure

mooring lines was damaged, and consequently the system stiffness decreased little. Results indicated that mooring failure has no effect on the response amplitude. The same argument was noted for sway response as shown in Fig 7.103.

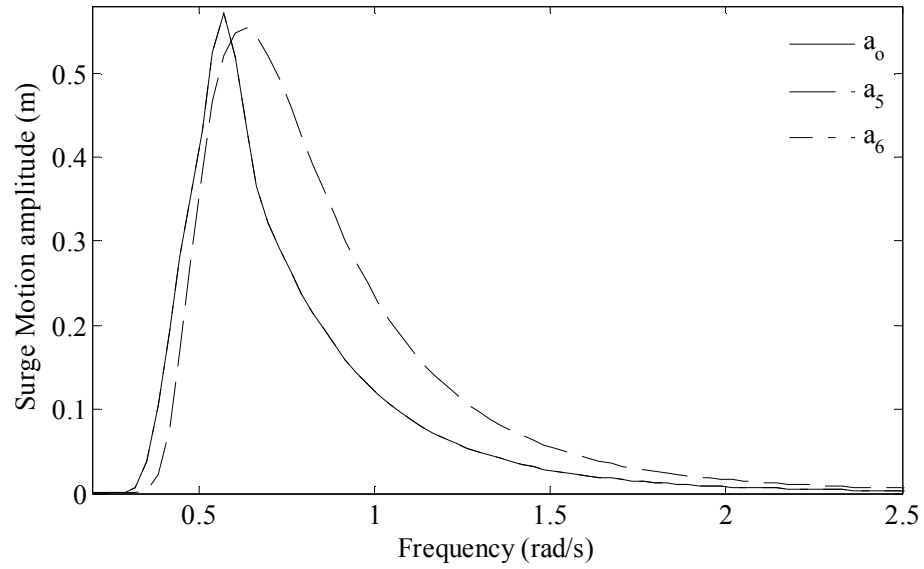


Fig 7.102: Comparison between a_0 , a_5 and a_6 cases for surge amplitudes

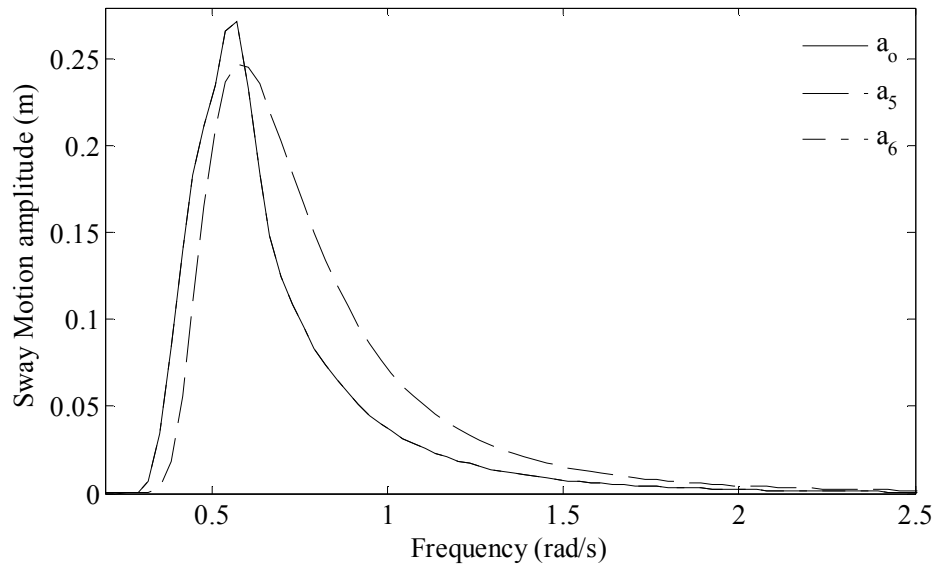


Fig 7.103: Comparison between a_0 , a_5 and a_6 cases for sway amplitudes

7.6 Chapter summary

In this chapter, results and discussion for a parametric study based on nonlinear quasi-static analysis for mooring line were presented. Moreover, results for the hydrodynamic analysis of were compared to available results in the literature and discussed. The effects of different soil seabed on mooring dynamics were investigated. Comparison study between the numerical and experimental studies for semi submersible characteristics was presented. A frequency domain results was presented and discussed for investigating the effects of the structure dimensions and physical mass, the number of columns and mooring lines and the sea/operating conditions on the systems response. In addition, experimental results for mooring system damaged conditions were presented and discussed.

Chapter 8

CONCLUSION

8.1 Conclusions

In this study, an attempt was made to study the nonlinearities associated with moored semi submersibles through numerical, experimental and case studies. These interactions were wave to wave, wave to platform, platform to mooring, fluid to mooring and mooring to seabed nonlinear interactions. In the numerical study, moored semi submersibles were analyzed in the time domain for the wave frequency and the low frequency wave forces. A 6x6 mooring stiffness matrix was derived based on the mooring stiffness and fairlead coordinates relative to the structure CG to simulate the platform to mooring system nonlinear interactions. In addition, for the simulation of the wave-wave and wave-platform interactions, the second order wave forces resulting from the second order temporal acceleration and the structural first order motions were formulated. On the assessment of the mooring system-environment and mooring to seabed nonlinear interactions, a deterministic approach for the dynamic analysis of a multi-component mooring line was formulated. In this approach, seabed-line nonlinear interactions were modeled assuming that the mooring line is rested on an elastic-dissipative foundation.

On the experimental studies, two phases of experimental studies were conducted mainly for verification of the numerical models. In the first phase, the seakeeping performance of eight circular columns semi submersible was studied. The model was built to scale of 1:100 using Froud's law of similitude. The tests were conducted for head, beam and quartering seas. In the second phase, a six circular column semi submersible was modeled using the same scale as for the first semi submersible. Seakeeping tests were conducted for head and beam model orientations. The

measured drift forces were compared to available formulae in the literature to assess the available semi-empirical methods for evaluation these forces.

Based on validated numerical algorithms case studies were conducted for investigating the contributions of various design parameters on the dynamics of moored semi submersibles. The effects of pretension, mooring line configuration, clump weight, cable unit weight, elongation, breaking strength and pretension angle were investigated on the behavior of multi-component mooring line by using an implicit iterative solution of the catenary equations. In addition using a linearized iterative frequency domain analysis, the contributions of platform payload, dimensions, number of columns, number of mooring lines, the wave environment mathematical model, the wave characteristics and the operating (intact or damage) conditions on the wave frequency responses of moored semi submersibles were investigated. Form these studies the following conclusions were drawn:

8.1.1 Wave frequency motion analysis

1. The numerical model developed for assessment of the semi submersible wave frequency responses was able to predict the platform responses due to regular and irregular waves obtaining good agreement with the experimental results.
2. The numerical RAOs obtained for regular and irregular waves agreed very closely for all the cases.
3. The heave response for low frequency sea waves differed by a relatively great value of 13.2% because the heave motions were influenced by water depth at low frequency.
4. The discrepancies for inline responses were due to the wave force evaluation neglecting the influence of bracing members and second order drift forces. Majority of the bracing members had axes in the model transverse direction and hence were not expected to affect the transverse responses. However, the discrepancies could be reduced if the bracing members and potential damping were included in the mathematical formulation.
5. The numerical heave response at low frequency in quartering waves was higher because of neglecting potential damping.

8.1.2 Second order motion analysis model

1. The Weggel's formulae for the evaluation of the steady drift force gave a good estimation for semi submersibles subjected to head seas except for a small range near the wave peak frequency. For beam seas, Weggel's formulae failed to provide reliable results because of the shallow-drafted large underwater hulls.
2. At a given frequency, the drift force coefficient reduces as the wave amplitude increases and this reduction percentage is more for higher amplitudes.
3. The numerical formulation derived for the evaluation of a semi submersible low frequency response successfully estimated the low frequency responses to different head and beam random seas with slight difference in the peak frequency and maximum energy density.
4. The simulated and the measured responses had a maximum discrepancy of about 8% for head bi-chromatic seas. This discrepancy increased to 20% for beam seas.
5. With the proper modifications factors, the Weggel's formulae can be successfully used for the estimation of the steady drift force on semi submersibles.

8.1.3 Consequences following mooring line damage

1. When mooring line is disconnected, structure oscillates around new mean position while the system response amplitude is not affected much.
2. The event of mooring failure is followed by a noticeable transient response.
3. For crucial assessment of the mooring damaged conditions, typical or hybrid modelling of the mooring system (stiffness and geometry) and vertical attachments (risers or drilling rigs) is needed.

8.1.4 The hydrodynamic mooring analysis and the seabed-line interactions

1. The developed numerical model can be used for the analysis and design of the dynamic analysis of multi-component mooring lines with an improved degree

of confidence since a good agreement between numerical simulations and published experimental results was achieved.

2. The mooring line dynamic tension was directly proportional to the upper end motion frequency.
3. For the mooring line attached with spring buoy, the rate of increase of dynamic tension with respect to frequency of mooring upper end motion was generally lower compared to that without spring buoy, and was particularly lower at higher frequency of mooring upper end motion. This strengthens the well-known beneficial effect of the spring buoy.
4. When soil damping and the upper end excursions were constant, the mooring line tension decreased when the soil stiffness increased.
5. Compared to the lifting and grounded seabed model introduced by Nakajima, elastic foundation with dashpot seabed model gave lower mooring tensions, especially at low frequency of upper boundary condition.
6. For very stiff soils, the desired effect of lowering the mooring line tension was achieved at the low frequency of upper end motion, but it produced an adverse effect at the high frequency of upper end motion due to high impact.
7. The soil damping dissipated the impact due to the mooring dynamic responses, which resulted in lower mooring line tensions, especially at a high frequency of the upper end motion. And due to the direction nature of the soil reactive forces, the vertical components of the mooring line tension were more affected by soil damping in comparison to the horizontal components.

8.1.5 Investigations on the moored semi submersible design parameter

1. For multi-component mooring line, the horizontal restoring force is directly proportional to the pretension and to the unit weight parameter and in inversely proportion with pretension angle for positive excursions. The pretension angle and the axial stiffness have little effect on the restoring force for negative excursions. It was noted the mooring restoring force is independent of the clump weight and the mooring length after reaching a certain value of tension.

2. The vertical restoring force is proportional to the pretension and pretension angle before lifting off the whole distributed clump weight and is proportional to the clump unit weight after lifting off the clump weight.
3. The horizontal restoring force for negative excursions is independent of the pretension angle.
4. The force-excursion relationship is linear for low range of excursions before lifting off the clump weight.
5. Among the semi submersible dimensions, the hull x-sectional height parameter seems to have the dominant effect on the platform's sea-keeping performance.
6. A little increase in draft leads to increase in the hydrodynamic loads more than the increase in the added mass. Thus, the system response increases. On the other hand, for a significant increase in draft the increase in added mass predominates the increase in the hydrodynamic load and hence the system response decreases.

8.2 Future studies

The research may be expended to include the following areas:

1. Seakeeping performance of semi submersible platforms for multi-directional waves considering the nonlinear hybrid wave model
2. Assessment of damage conditions with all system attachments like risers
3. Low frequency viscous damping arising from the mooring system
4. Fully coupled integrated dynamic analysis in the time domain for the platform and mooring lines
5. Geometrical modelling of mooring lines in a truncated depth the the experimental testing
6. All the components of the second order wave-wave nonlinear interactions

REFERENCES

- [1] S. Chakrabarti, *Handbook of offshore engineering* vol. 1: Elsevier Science Ltd, 2005.
- [2] M. Patel and J. Witz, *Compliant offshore structures*: Butterworth-Heinemann, 1991.
- [3] J. Herbich, *Developments in offshore engineering: wave phenomena and offshore topics*: Gulf Professional Publishing, 1999.
- [4] API, "2SK, Recommended practice for design and analysis of station-keeping systems for floating structures," *American Petroleum Institute Standards*, 1997.
- [5] T. Utsunomiya, *et al.*, "Experimental validation of hydroelastic analysis of pontoon semi submersible and hybrid type VLFS," in *the 27th International Conference on Offshore Mechanics and Arctic Engineering (OMAE)*, Estoril - Portugal, 2008.
- [6] S. Masanobu, *et al.*, "Estimation of wind loads on VLFS of semi submersible type," *J. of Marine Structures*, vol. 13, pp. 245-260, 2000.
- [7] W. Ye, *et al.*, "Effects of fully coupled and quasi-static semi submersible vessel motions on steel catenary riser's wave loading fatigue," in *the Offshore Technology Conference (OTC)*, Houston, Texas USA, 2003.
- [8] J. Hooft, "Hydrodynamic aspects of semi submersible platforms," PhD thesis, Netherlands Ship Model Basin, 1972.
- [9] M. Takagi and S. Arai, "A Comparison of methods for calculating the motion of a semi submersible," *J. of Ocean Engineering*, vol. 12, pp. 45-97, 1985.

- [10] S. Tan, "Motion prediction of semi submersibles in early design stage," Maritime Research Institute Netherlands 1992.
- [11] D. Sunil and M. Mukhopadhyay, "Free vibration of semi submersibles: A parametric study," *J. of Ocean Engineering*, vol. 22, pp. 489-502, 1995.
- [12] S. Wu, *et al.*, "The motions and internal forces of a moored semi submersible in regular waves," *J. of Ocean Engineering*, vol. 24, pp. 593-603, 1997.
- [13] C. Lewis and M. Griffin, "Evaluating the motions of a semi submersible platform with respect to human response," *J. of Applied Ergonomics*, vol. 28, pp. 193-201, 1997.
- [14] H. Maruo, "The drift of a body floating on waves," *J. of Ship Research*, vol. 4, pp. 1-10, 1960.
- [15] B. Molin, "Computations of wave drift forces," in *the 11th Offshore Technology Conference (OTC)*, Houston, Texas - USA, 1979.
- [16] G. Remery and A. Hermans, "The slow drift oscillations of a moored object in random seas," *Old SPE Journal*, vol. 12, pp. 191-198, 1972.
- [17] J. Pinkser, "Low frequency phenomena associated with vessels moored at sea," *Old SPE Journal*, vol. 15, pp. 487-494, 1975.
- [18] J. Pinkser, "Low frequency second order wave exciting forces on floating structures," PhD thesis, Delft University of Technology, The Netherlands, 1980.
- [19] J. Pinkser, "Mean and low frequency wave forces on semi submersibles," *Old SPE Journal*, vol. 22, pp. 563-572, 1982.
- [20] J. Pinkser, *et al.*, "Hydrodynamic aspects of moored semi submersibles and TLP's," in *the 25th Offshore Technology Conference (OTC)*, Houston, Texas - USA, 1993.
- [21] H. Rye, *et al.*, "On the slow drift oscillations of moored structures," in *the 7th Offshore Technology Conference (OTC)*, Houston, Texas - USA, 1975.

- [22] F. Nielsen, "An approximate method to compute the drift force on an array of vertical cylinders," *J. of Applied Ocean Research*, vol. 10, pp. 35-42, 1988.
- [23] T. Schellin and A. Kirsch, "Low frequency damping of a moored semi submersible obtained from simulated extinction tests and mean wave drift forces," *J. of Applied Ocean Research*, vol. 11, pp. 202-211, 1989.
- [24] H. Prins, "Time domain calculations of drift forces and moments," PhD thesis, Delft University of Technology, The Netherlands, 1995.
- [25] S. Chitrapu, "Nonlinear forces and response of floating platforms in regular and random waves," PhD thesis, University of Hawaii, Manoa - USA, 1992.
- [26] J. Zhang, *et al.*, "Hybrid wave model for unidirectional irregular waves-part I: Theory and numerical scheme," *J. of Applied Ocean Research*, vol. 18, pp. 77-92, 1996.
- [27] C. Spell, *et al.*, "Hybrid wave model for unidirectional irregular waves-part II. Comparison with laboratory measurements," *J. of Applied Ocean Research*, vol. 18, pp. 93-110, 1996.
- [28] P. Cao, "Slow motion responses of compliant offshore structures," MSc thesis, Texas A & M University, 1997.
- [29] I. Anam, "Evaluation of the dynamic response of spar platforms," PhD thesis, Texas A& M University, 2000.
- [30] H. Lie and K. Kaasen, "Viscous drift forces on semi submersibles in irregular seas: A frequency domain approach," in *the International Conf. of Offshore Mechanics and Arctic Engineering (OMAE)*, Estoril - Portugal, 2008.
- [31] B. Stone, "An experimental study of the motion response in regular waves of a semi submersible under damage conditions," Memorial University of Newfoundland, Canada 1986.

- [32] B. Stone, *et al.*, "Model studies of the motion response of a damaged four column semi submersible in regular and irregular waves," *J. of Ocean Engineering*, vol. 17, pp. 235-261, 1990.
- [33] O. Yilmaz and A. Incecik, "Extreme motion response analysis of moored semi submersibles," *J. of Ocean Engineering*, vol. 23, pp. 497-517, 1996.
- [34] G. Clauss, *et al.*, "Freak wave impact on semi submersibles time domain analysis of motions and forces," in *the 21st International Conference on Offshore Mechanics and Arctic Engineering (OMAE)*, Oslo - Norway, 2002.
- [35] G. Clauss, *et al.*, "Freak wave impact on semi submersibles: Timedomain analysis of motions and forces," Technical University of Berlin, Germany 2003.
- [36] M. Rudman, *et al.*, "Rogue wave impact on a semi submersible offshore platform," in *the 27th International Conference on Offshore Mechanics and Arctic Engineering (ASME)* Estoril - Portugal, 2008.
- [37] A. Cruz and E. Krausmann, "Damage to offshore oil and gas facilities following hurricanes Katrina and Rita: An overview," *J. of Loss Prevention in the Process Industries*, vol. 21, pp. 620-626, 2008.
- [38] G. Tahchiev and J. Zhang, "Numerical prediction of MODUs drift during Hurricane Katrina," *J. of Ocean Engineering*, vol. 35, pp. 995-1005, 2008.
- [39] M. Patel and J. Harrison, "The mechanics of compliant motion suppression system for semi submersibles," *J. of Sound and Vibration*, vol. 106, pp. 491-507, 1986.
- [40] J. Halkyard, *et al.*, "A deep draft semi submersible with a retractable heave plate," in *the Offshore Technology Conference (OTC)*, Houston, Texas - USA, 2002.
- [41] A. Gupta, *et al.*, "Riser analysis for a dry tree semi submersible," in *the 27th International Conference on Offshore Mechanics and Arctic Engineering (OMAE)*, Estoril-Portugal, 2008.

- [42] J. Murray, *et al.*, "Hydrodynamics of dry tree semi submersibles," in *the Offshore Technology Conference (OTC)*, Houston, Texas - USA, 2007, pp. 2275-2281.
- [43] A. Aubault, *et al.*, "Parametric optimization of a semi submersible platform with heave plates," in *the 26th International Conference on Offshore Mechanics and Arctic Engineering (OMAE)*, San Diego, California - USA, 2007, pp. 11-16.
- [44] C. Chen, *et al.*, "Improving the motions of a semi submersible by the addition of heave plates," in *the 27th International Conference on Offshore Mechanics and Arctic Engineering (OMAE)*, Estoril - Portugal, 2008.
- [45] J. Murray, *et al.*, "Two dry tree semi submersible designs for ultra-deep water post Katrina GOM," in *the 27th International Conference on Offshore Mechanics and Arctic Engineering (OMAE)*, Estoril - Portugal, 2008.
- [46] M. Patel and S. Walker, "A compliant semi submersible for offshore production," University College London 1988.
- [47] C. Hu, *et al.*, "The design of a variable draft semi submersible floating production vessel," SLP Engineering London - UK 1991.
- [48] O. Often, *et al.*, "Dry tree semi submersible for Brazil and GOM," in *the Offshore Technology Conference (OTC)*, Houston, Texas - USA, 2001.
- [49] R. Souza, *et al.*, "The next generation production drilling semi submersible based deepwater field development system," in *the Offshore Technology Conference (OTC)*, Houston, Texas - USA, 2002.
- [50] S. Chakrabarti, *et al.*, "Design analysis of a truss pontoon semi submersible concept in deep water," *J. of Ocean Engineering*, vol. 34, pp. 621-629, 2007.
- [51] T. Kendon, *et al.*, "Ultra-deepwater model testing of a semi submersible and hybrid verification," in *the 27th International Conference on Offshore Mechanics and Arctic Engineering (OMAE)* Estoril - Portugal, 2008.

- [52] Y. Watanabe and K. Yoshida, "Wave response of a semi submersible structure model with mechanical connectors," in *the 27th International Conference on Offshore Mechanics and Arctic Engineering (OMAE)*, Estoril - Portugal, 2008.
- [53] O. Rijken and S. Leverette, "Experimental study into vortex induced motion response of semi submersible with square columns," in *the International Conference on Offshore Mechanics and Arctic Engineering (OMAE)*, Estoril - Portugal, 2008.
- [54] J. Kim, *et al.*, "Global performance and sloshing analysis of a new deep draft semi submersible LNG FPSO," in *the International Conference on Offshore Mechanics and Arctic Engineering Conf. (OMAE)*, Estoril - Portugal 2008.
- [55] A. Peyrot and A. Goulois, "Analysis of cable structures," *J. of Computers & Structures*, vol. 10, pp. 805-813, 1979.
- [56] A. Peyrot, "Marine cable structures," *J. of the Structural Division*, vol. 106, pp. 2391-2404, 1980.
- [57] A. Agarwal and A. Jain, "Dynamic behavior of offshore spar platforms under regular sea waves," *J. of Ocean Engineering*, vol. 30, pp. 487-516, 2003.
- [58] A. Agarwal and A. Jain, "Nonlinear coupled dynamic response of offshore Spar platforms under regular sea waves," *J. of Ocean Engineering*, vol. 30, pp. 517-551, 2003.
- [59] F. Ramzan and R. Robinson, "An engineering assessment of the validity of the quasi-static approach to semi submersible mooring design," in *the 18th Offshore Technology Conference (OTC)*, Houston, Texas - USA, 1986.
- [60] M. Patel and D. Brown, "Analysis and design of catenary mooring systems," *J. of Advances in Underwater Technology, Ocean Science and Offshore Engineering*, vol. 13, pp. 139-157, 1987.
- [61] T. Walton and H. Polachek, "Calculation of transient motion of submerged cables," *J. of Mathematics of computation*, vol. 14, pp. 27-46, 1960.

- [62] T. Nakajima, *et al.*, "On the dynamic analysis of multi-component mooring lines," in *the 14th Offshore Technology Conference*, Houston, Texas - USA, 1982.
- [63] H. Boom, "Dynamic behaviour of mooring lines," in *the 4th International Conference on the Behaviour of Offshore Structures*, The Netherlands, 1985.
- [64] G. Hearn and D. Thomas, "The Influence of practical time integration schemes on dynamic mooring line analysis," in *the 23rd Offshore Technology Conference (OTC)*, Houston - Texas, 1991.
- [65] D. Thomas and G. Hearn, "Deepwater mooring line dynamics with emphasis on seabed interference effects," in *the 26th Offshore Technology Conference* Houston - Texas, 1994.
- [66] K. Cho and W. Yi, "Development of a dynamic analysis scheme of cable for ROV Operation," in *the 12th International Society of Offshore and Polar Engineers Conference*, Kitakyushu - Japan, 2002, pp. 249-254.
- [67] S. Mavrakos, *et al.*, "Deep water mooring dynamics," *J. of Marine Structures*, vol. 9, pp. 181-209, 1996.
- [68] R. Webster, "Nonlinear static and dynamic response of underwater' cable structures using the Finite Element Method," in *the Offshore Technology Conference (OTC)*, Dallas, Texas - USA, 1975.
- [69] O. Aomo and T. Fossen, "Finite element modeling of mooring lines," *J. of Mathematics & Computers in Simulation*, vol. 53, pp. 415-422, 2000.
- [70] E. Kreuzer and U. Wilke, "Dynamics of mooring systems in ocean engineering," *J. of Archive of Applied Mechanics*, vol. 73, pp. 270-281, 2003.
- [71] T. Hyakudome, *et al.*, "Experimental study on dynamic positioning control for semi submersible platform," in *the International Society of Offshore and Polar Engineers conf. (ISOPE)*, Brest - France, 1999.

- [72] Y. Xiao and Y. Wang, "Analysis of deepwater mooring system for a semisubmerged drilling platform," Dalian University of Technology Dalian-China 2004.
- [73] F. Papoulias, "Dynamic analysis of mooring systems," PhD thesis, Department of Naval Architecture and Marine Engineering, University of Michigan, Ann Arbor, MI, 1987.
- [74] B. Kim, *Stability analysis and design of spread mooring systems*. Michigan - USA: University of Michigan, 1999.
- [75] S. Sivaji, "Nonlinear analysis of mooring lines," MSc thesis, Ocean Engineering Centre, Indian Institute of Technology (IIT), Madras-India, 1991.
- [76] H. Yin, "Nonlinear analysis of mooring lines and marine risers," Memorial University of Newfoundland, Canada 2007.
- [77] E. Loukogeorgaki and D. Angelides, "Stiffness of mooring lines and performance of floating breakwater in three dimensions," *J. of Applied Ocean Research*, vol. 27, pp. 187-208, 2005.
- [78] S. Wu, "Adaptive dynamic relaxation technique for static analysis of catenary mooring," *J. of Marine Structures*, vol. 8, pp. 585-599, 1995.
- [79] Y. Liu and L. Bergdahl, "Frequency domain dynamic analysis of cables," *J. of Engineering Structures*, vol. 19, pp. 499-506, 1997.
- [80] R. Smith and C. MacFarlane, "Statics of a three component mooring line," *J. of Ocean Engineering*, vol. 28, pp. 899-914, 2001.
- [81] L. Yu, "Numerical investigation of seabed interaction in time domain analysis of mooring cables," *J. of Hydrodynamics*, vol. 18, pp. 424-430, 2006.
- [82] S. Sannasiraj, *et al.*, "Mooring forces and motion responses of pontoon-type floating breakwaters," *J. of Ocean Engineering*, vol. 25, pp. 27- 48, 1998.
- [83] X. Chen, *et al.*, "Dynamic analysis of mooring lines with inserted springs," *J. of Applied Ocean Research*, vol. 23, pp. 277-284, 2001.

- [84] C. Wung, *et al.*, "Effect of soil on mooring system dynamics," in *the 27th Offshore Technology Conference (OTC)* Houston, Texas - USA, 1995.
- [85] Y. Liu and L. Bergdahl, "Influence of current and seabed friction on mooring cable response: Comparison between time-domain and frequency-domain analysis," *J. of Engineering Structures*, vol. 19, pp. 945-953, 1997.
- [86] J. Gobat and M. Grosenbaugh, "Dynamics in the touchdown region of catenary moorings," *International Journal of Offshore and Polar Engineering (IJOPE)*, vol. 11, pp. 273-281, 2001.
- [87] P. Ong and S. Pellegrino, "Modelling of seabed interaction in frequency domain analysis of mooring cables," *J. of Structural Engineer*, vol. 81, pp. 13-14, 2003.
- [88] C. Gatti-Bono and N. Perkins, "Numerical simulations of cable-seabed interaction," *International Journal of Offshore and Polar Engineering (IJOPE)*, vol. 14, pp. 118-124, 2004.
- [89] C. Martin, "Exact bearing capacity calculations using the method of characteristics," University of Oxford, London - UK 2005.
- [90] A. Palmer, "Touchdown indentation of the seabed," *J. of Applied Ocean Research*, vol. 30, pp. 235-238, 2008.
- [91] E. Clukey, *et al.*, "Soil response and stiffness laboratory measurements of SCR pipe-soil interaction," in *the Offshore Technology conference (OTC)*, Houston, Texas - USA, 2008.
- [92] M. Hodder and B. Byrne, "3D experiments investigating the interaction of a model SCR with the seabed," *J. of Applied Ocean Research*, vol. 35, 2009.
- [93] O. Yilmaz, *et al.*, "Wave enhancement due to blockage in semi submersible and TLP structures," *J. of Ocean Engineering*, vol. 28, pp. 471-490, 2001.
- [94] M. Atlar, "Towards the understanding of the steady tilt phenomenon in semi submersibles," PhD thesis, University of Glasgow Scotland- UK, 1986.

- [95] R. Rainey, "A new theory and its application for stability criteria covering wave-induced tilt phenomena on semi submersibles," *J. of Advances in Underwater Technology, Ocean Science and Offshore Engineering*, vol. 9, pp. 41-59, 1986.
- [96] T. Wu, "Effect of second order forces on steady tilt behaviours and some applications in dynamic positioning aspects of twin hulled marine vehicles," PhD thesis, University of Glasgow, Scotland - UK, 1993.
- [97] M. Soeylemez, "Motion tests of a twin-hulled semi submersible," *J. of Ocean Engineering*, vol. 22, pp. 643-660, 1995.
- [98] T. Nakajima, "A new 3D quasi-static solution for the multi-component mooring systems," in *the 5th International Conference on Ocean, Offshore and Arctic Engineering (OMAE)*, 1986, pp. 487-493.
- [99] C. Teng and H. Wang, "Mooring of surface wave following buoys in shallow water," in *the 14th international Conference on Ocean, Offshore and Arctic Engineering (OMAE)*, Copenhagen - Denmark, 1995, pp. 223-232.
- [100] Y. Inoue and S. Surendran, "Dynamics of the interaction of mooring lines with the seabed," in *the 4th International Society of Offshore and Polar Engineers Conf. (ISOPE)*, Osaka - Japan, 1994.
- [101] J. Leonard, *et al.*, "Deterministic fluid Forces on Structures: A Review," *J. of the Structural Division*, vol. 107, pp. 1041-1057, 1981.
- [102] S. K. Chakrabarti, Ed., *Hydro-dynamics of Offshore Structures*. Illinois CBI Industries, Inc. Plainfield, USA, 1987, p. ^pp. Pages.
- [103] S. Chakrabarti, *Hydrodynamics of Offshore Structures* WIT Press, 1987.
- [104] Z. Ran, "Coupled dynamic analysis of floating structures in waves and currents," PhD thesis, Texas A & M University, 2000.

- [105] M. Longuet-Higgins and R. Stewart, "Changes in the form of short gravity waves on long waves and tidal currents," *J. of Fluid Mechanics*, vol. 8, pp. 565-583, 1960.
- [106] J. Wilson, *Dynamics of offshore structures*. Newjersey - USA: John Wiley & Sons, 2003.
- [107] J. Morison, *The force exerted by surface waves on piles*: University of California, Dept. of Engineering, Fluid Mechanics Laboratory, 1949.
- [108] R. C. T. Rainey, "A new theory and its application for stability criteria covering wave induced tilt phenomena on semi submersibles," *Advances in Underwater Technology, Ocean Science and Offshore Engineering*, vol. 9, pp. pp. 41-59, 1986.
- [109] Y. Li and A. Kareem, "Computation of wave-induced drift forces introduced by displaced position of compliant offshore platforms," *J. of Offshore Mechanics and Arctic Engineering*, vol. 114, pp. 175-184, 1992.
- [110] J. F. Wilson, *Dynamics of Offshore Structures*, second ed. Newjersey-USA: John Wiley & Sons, 2003.
- [111] S. Alexandar, "Bearing capacity of shallow foundation " PhD thesis, Civil Eng. Dept., Duke University, North Carolina - USA, 1987.
- [112] R. Clough and J. Penzien, *Dynamics of structures*, 3rd ed. Perkeley - USA: Computer and Strucures Inc, 2003.
- [113] HR, "Multi-element wave generation system with AC derives and dynamic wave absorption for Universiti Teknologi PETRONAS: user manual ", Wallingford - UK CQR 4187, 2008.
- [114] S. Chakrabarti, *Offshore structure modeling*: World Scientific, 1994.
- [115] E. Dudgeon, "Hydrodynamic model studies of the ocean Ranger marine disaster," in *the Stationing and Stability of Semi submersibles Conference*, Glasgow - UK, 1986.

- [116] G. Clauss and T. Schellin, "Slow drift forces and motions on a barge-type structure comparing model tests with calculated results," in *the Offshore Technology Conference*, Houston, Texas - USA, 1982.
- [117] D. Weggel, "Nonlinear Dynamic Response of Large-diameter Offshore Structures," PhD thesis, A & M University of Texas Austin - USA, 1997.

APPENDIX A EVALUATION OF FIRST ORDER WAVE FORCES

Introduction

The following is a detailed wave force evaluation on the semi submersible platform based on the modified version of Morison equation (Eq 3.23~3.24). It was assumed the total wave force on the structure is equal to the sum of the forces on each individual member (Hooft [8] hypothesis). The hulls of the semi submersible platform, which have rectangular cross sections, were treated as cylinders with equivalent hydrodynamic characteristics. The latter assumption was applied because Morison equation is applicable only for cylindrical members. The evaluated forces were the horizontal inertia and drag forces and moments on columns, the horizontal surge force and pitch moments on hull faces due to undisturbed dynamic pressure, the horizontal inertia and drag sway force and roll moments on hulls and vertical inertia and drag force and moments on hulls.

Horizontal inertia force and moments on columns

The instantaneous position of the CG of the structure taken in the direction of the wave propagation as defined in Fig A.1 is given by Eq A.1.

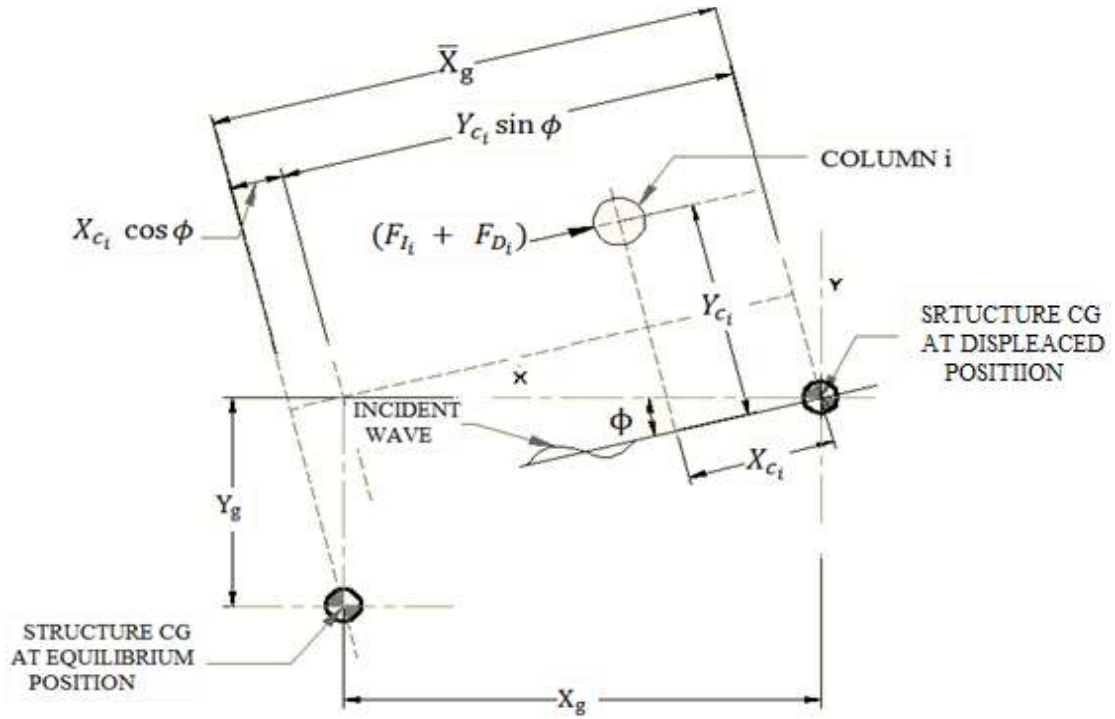


Fig A.1: Structure CG at the instantaneous position definition

$$\bar{X}_g = X_g \cos \phi + Y_g \sin \phi \quad (\text{A.1})$$

Assuming the semi submersible behaved as rigid platform, the instantaneous x-coordinate for column i (Fig A.1) \bar{X}_{c_i} taken in the direction of the wave is given by Eq A.2.

$$\bar{X}_{c_i} = X_{c_i} + \bar{X}_g \quad (\text{A.2})$$

were X_{c_i} are the elements of column vector $\{X_c\}$, which represents the x-coordinate of elements 3 to 10 (Fig 3.5) in the direction of wave propagation, given by Eq A.3.

$$\{X_c\} = \begin{cases} -1.5a_{st} \cos \phi + b_{st} \sin \phi \\ 1.5a_{st} \cos \phi + b_{st} \sin \phi \\ 1.5a_{st} \cos \phi - b_{st} \sin \phi \\ -1.5a_{st} \cos \phi - b_{st} \sin \phi \\ -0.5a_{st} \cos \phi + b_{st} \sin \phi \\ 0.5a_{st} \cos \phi + b_{st} \sin \phi \\ 0.5a_{st} \cos \phi - b_{st} \sin \phi \\ -0.5a_{st} \cos \phi - b_{st} \sin \phi \end{cases} \quad (\text{A.3})$$

It should be noted that Eq A.3 notations are defined in Fig A.2.

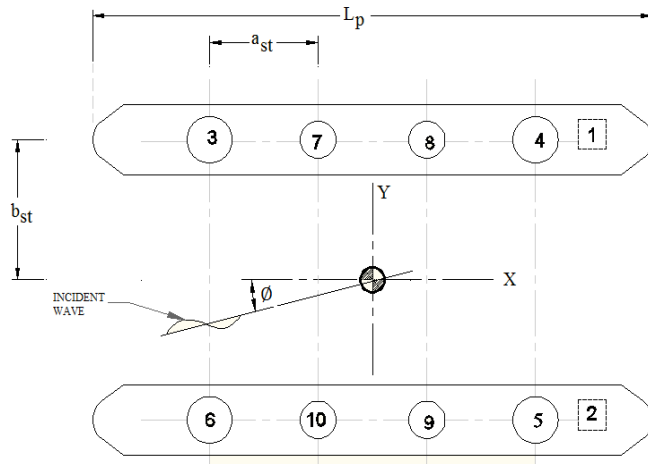


Fig A.2: Definition of the structure plan dimensions

The wetted length of column i was estimated based on the free surface level at the column instantaneous location by Eq A.4. The notations of this equation are defined in Fig A.3.

$$h_{c_i} = -h - b - Z_g + \frac{H}{2} \cos(kX_{c_i} - \omega t) \quad (\text{A.4})$$

Column i was divided number of elements in order to achieve an appropriate estimation for the wave force numerical integration evaluation. The number of elements N is based on the instantaneous wetted length h_{c_i} and the elements length dz as shown in Eq A.5.

$$N = \text{Rounddown} \left(\frac{h_{c_i}}{dz}, 0 \right) \quad (\text{A.5})$$

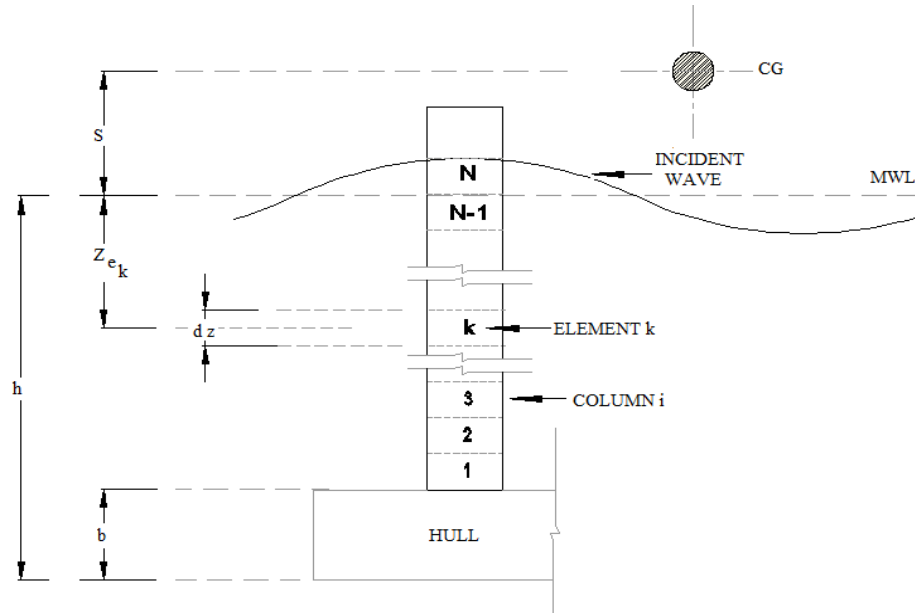


Fig A.3: Column element characteristics

For each element, the wave forces are evaluated and summed up to evaluate the total wave force on the column i applying the following steps:

Inertia force $F_{I_{c_i}}$ and moment $M_{I_{c_i}}$ on column i :

1. The element z -coordinate measured from MSL is given by Eq A.6 (Fig A.3.)

$$Z_k = -(h - b - Z_g) + (k - 1/2)dz \quad (A.6)$$

2. The wave velocity u_k and acceleration \dot{u}_k at each column element were evaluated using Airy linear wave theory by Eq 3.15 and Eq 3.17 respectively.

3. The acceleration at element k , \ddot{x}_k , in the wave direction was evaluated by Eq A.7. where \ddot{x}_g is given by Eq A.8, \ddot{x}_x, \ddot{x}_y are the structure CG linear accelerations in the x, y directions respectively and $\ddot{\alpha}_g$ is the structure CG angular acceleration evaluated in the wave direction by Eq A.9. In which, $\ddot{\theta}_x, \ddot{\theta}_y$ are the structure CG angular accelerations in the x, y directions respectively.

$$\ddot{x}_k = \ddot{x}_g - \ddot{\alpha}_g (Z_{e_k} - s) + 0.5 \bar{X}_{c_i} \ddot{\alpha}_g^2 \quad (A.7)$$

$$\ddot{x}_g = \ddot{x}_x \cos\phi + \ddot{x}_y \sin\phi \quad (\text{A.8})$$

$$\ddot{\alpha}_g = \ddot{\theta}_x \cos\phi + \ddot{\theta}_y \sin\phi \quad (\text{A.9})$$

For element k in column i , the inertia force and moment are given by Eq

A.10~A.11 respectively, where C_{m_c} is the inertia coefficient for columns.

$$\delta F_{I_k} = \rho \left(\pi D_i^2 / 4 \right) \left[C_{m_c} \dot{u}_k - (C_{m_c} - 1) \ddot{x}_k \right] dz \quad (\text{A.10})$$

$$\delta M_{I_k} = (z_{e_k} - s) \delta F_{I_k} \quad (\text{A.11})$$

4. For the evaluation of the column i total inertia force and moment at each time step at the structure displaced position and on the wave propagation direction, the elemental inertia force is summed up for the total number, N of the elements as give in Eq A.12~A.13.

$$F_{I_{c_i}} = \sum_{k=1}^N \delta F_{I_k} \quad (\text{A.12})$$

$$M_{I_{c_i}} = \sum_{k=1}^N \delta M_{I_k} \quad (\text{A.13})$$

Drag force $F_{I_{c_i}}$ and moment $M_{I_{c_i}}$ on column i :

The following steps were applied for each element to estimate the column i drag force:

1. The fluid-column structure element relative velocity, u_{krel} was evaluated by Eq A.14, where u_k is the element k velocity in the wave direction, given by Eq A.15. In which, \dot{x}_g is the structure CG velocity evaluated in the direction of wave propagation, given by Eq A.16, where \dot{x}_x, \dot{x}_y are the structure CG linear velocities in the x, y directions respectively and $\dot{\alpha}_g$ is The structure CG angular velocity evaluated in the wave direction, given by Eq A.17. In the latter equation, $\dot{\theta}_x, \dot{\theta}_y$ are the structure CG angular velocities in the x, y directions respectively.

$$u_{krel} = u_k - \dot{x}_k \quad (\text{A.14})$$

$$\dot{x}_k = \dot{x}_g - \dot{\alpha}_g (Z_{e_k} - s) + (1/2) X_{c_i} \dot{\alpha}_g^2 \quad (\text{A.15})$$

$$\dot{x}_g = \dot{x}_x \cos\phi + \dot{x}_y \sin\phi \quad (\text{A.16})$$

$$\dot{\alpha}_g = \dot{\theta}_x \cos\phi + \dot{\theta}_y \sin\phi \quad (\text{A.17})$$

2. For the element k in column i , the drag force and moment were evaluated by using Eq A.18~A.19 respectively.

$$\delta F_{D_k} = \rho C_d (D_i/2) u_{krel} |u_{krel}| dz \quad (\text{A.18})$$

$$\delta M_{D_k} = \delta F_{D_k} (Z_{ek} - s) \quad (\text{A.19})$$

3. To evaluate the column i total drag force and moment at each time step at the structure displaced position and on the wave propagation direction, the elemental inertia force is summed up for the total number, N , of the elements as give in Eq A.20~A.21 respectively.

$$F_{d_{ci}} = \sum_{k=1}^N \delta F_{d_k} \quad (\text{A.20})$$

$$M_{d_{ci}} = \sum_{k=1}^N \delta M_{d_k} \quad (\text{A.21})$$

Surge load and pitch moments due to dynamic pressure on hull faces:

The following steps were applied for the evaluation of this force component:

1. Evaluation of the first order un-disturbed dynamic pressure, p_j as given by Airy linear theory on each face j (Fig 3.5) is given by Eq A.22. In which, \bar{X}_{h_j} is the instantaneous hulls face j location, given by Eq A.23 and $Z_{h_{1,2}}$ is the instantaneous z-coordinate of hulls given by Eq A.24. In Eq A.23, X_{h_j} are the elements of column vector $\{X_h\}$, which represents the x-coordinate of hull faces 1 to 4 in the direction of wave propagation (Fig 3.5), given by Eq A.25.

$$p_j = \rho g \frac{H \cosh k(d + Z_{h_{1,2}})}{2 \cosh kd} \cos(k\bar{X}_{h_j} - \omega t) \quad (\text{A.22})$$

$$\bar{X}_{h_j} = X_{h_j} + \bar{X}_g \quad (\text{A.23})$$

$$Z_{h_{1,2}} = -[h - (b/2) - Z_g] \quad (\text{A.24})$$

$$\{X_h\} = \begin{cases} -0.5L_p \cos \phi + b_{st} \sin \phi \\ 0.5L_p \cos \phi + b_{st} \sin \phi \\ -0.5L_p \cos \phi - b_{st} \sin \phi \\ 0.5L_p \cos \phi - b_{st} \sin \phi \end{cases} \quad (\text{A.25})$$

2. The force in x-axis and moment about y-axis on face j of the hulls are given by Eq A.26~A.27 respectively, where a, b denotes the hull cross sectional dimensions.

$$F_{p,x_j} = p_j abc \cos \phi \quad (\text{A.26})$$

$$M_{p,y_j} = -F_{p,x_j} (h - b/2 + s) \quad (\text{A.27})$$

3. The total x-direction force and y-direction moment due to the first order undisturbed dynamic pressure in the four hull faces are given by Eq A.28~A.29 respectively.

$$F_{p,x_{hull1,2}} = \sum_{j=1}^4 F_{p,x_j} \quad (\text{A.28})$$

$$M_{yp} = \sum_{j=1}^4 M_{p,y_j} \quad (\text{A.29})$$

Sway forces, roll and yaw moments on hull due to inertia and drag forces:

The rectangular x-sectional hulls are transformed to equivalent circular hulls with the same x-sectional area; where $D_{h_{1,2}}$ the equivalent diameter of the circular hull is given by Eq A.30.

$$D_{h_{1,2}} = (4ab/\pi)^{1/2} \quad (\text{A.30})$$

The hull is divided into M elements with 1.0 meter width as presented in Fig A.4, a procedure for evaluation of the inertia and drag force on the hull is stated in the following steps:

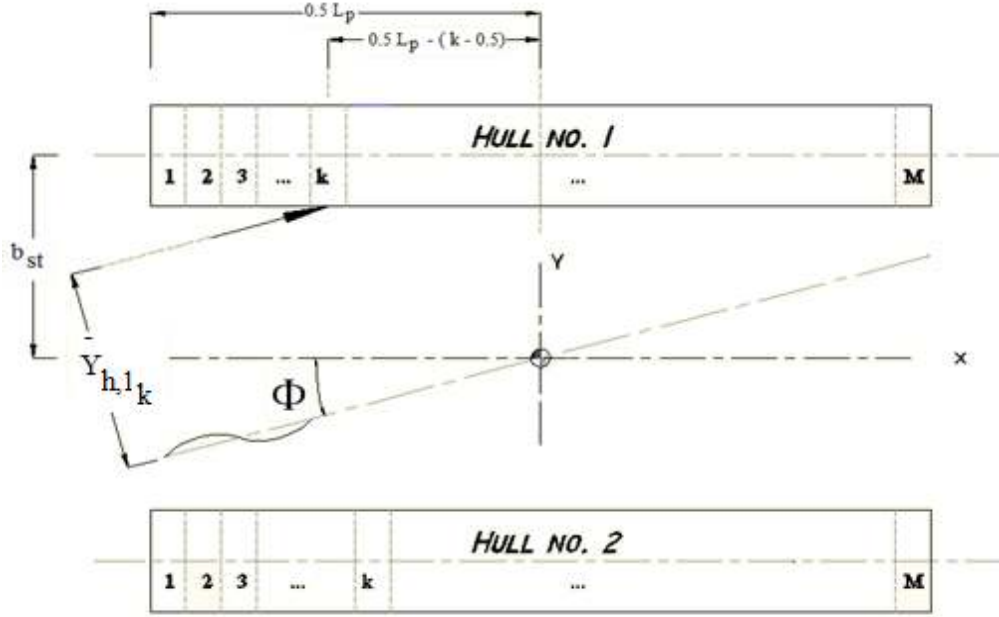


Fig A.4: Hull discretisation

Hull No.1:

The inertia and drag wave forces and moments applied on the hull are evaluated on each element of the hull and summed up for the total number of elements, M , applying the following steps:

1. For each element, the instantaneous x-coordinate in the wave direction is given by Eq A.31, where $X_{h,1k}$ is the hull no. 1 k element x-coordinate, relative to the structure CG, in the wave direction given by Eq A.32.

$$\bar{X}_{h,1k} = X_{h,1k} + \bar{X}_g \quad (\text{A.31})$$

$$X_{h,1k} = \left[\left(-L_p/2 \right) + k - (1/2) \right] \cos\phi + b_{st} \sin\phi \quad (\text{A.32})$$

2. The horizontal (in the wave direction) and vertical directions wave kinematics on each element were evaluated using Eq A.33~A.36.

$$u_{h,1k} = \frac{\pi H}{T} \frac{\cosh k(d + Z_{h,2})}{\cosh kd} \cos(k\bar{X}_{h,1k} - \omega t) \quad (\text{A.33})$$

$$v_{h,1k} = \frac{\pi H \sinh k(d + Z_{h,2})}{T \cosh kd} \sin(k\bar{X}_{h,1k} - \omega t) \quad (\text{A.34})$$

$$\dot{u}_{h,1k} = \frac{2\pi^2 H \cosh k(d + Z_{h,2})}{T^2 \cosh kd} \sin(k\bar{X}_{h,1k} - \omega t) \quad (\text{A.35})$$

$$\dot{v}_{h,1k} = -\frac{2\pi^2 H \sinh k(d + Z_{h,2})}{T^2 \cosh kd} \cos(k\bar{X}_{h,1k} - \omega t) \quad (\text{A.36})$$

3. The acceleration of element k in the wave direction is given by Eq A.37.

$$\ddot{x}_{h,1k} = \ddot{x}_g - (Z_{h,2} - s)\ddot{\alpha}_g + (1/2)X_{h,1k} \ddot{\alpha}_g^2 \quad (\text{A.37})$$

4. The wave-hull element relative velocity is given by Eq A.38, where is the hull no. 1 element k velocity, given by Eq A.39.

$$(u_{h,1k})_{rel} = u_{h,1k} - \dot{x}_{k,1k} \quad (\text{A.38})$$

$$\dot{x}_{k,1k} = \dot{x}_g - (Z_{h,2} - s)\dot{\alpha}_g + (1/2)X_{h,1k} \dot{\alpha}_g^2 \quad (\text{A.39})$$

5. The sway drag wave force and yaw drag moments are given by Eq A.40~A.41 respectively.

$$\delta F_{D_y, h, 1k} = \rho C_{dh} (D_{h,2} / 2) (u_{h,1k})_{rel} |(u_{h,1k})_{rel}| \sin \phi \quad (\text{A.40})$$

$$\delta M_{D_y, h, 1k} = -\delta F_{D_y, h, 1k} X_{h,1k} \quad (\text{A.41})$$

6. The sway inertia wave force and yaw inertia moments are given by Eq A.42~A.43 respectively.

$$\delta F_{I_y, h, 1k} = \rho (\pi D_{h,2}^2 / 4) [C_{mh} \dot{u}_{h,1k} - (C_{mh} - 1) \ddot{x}_{h,1k}] \sin \phi \quad (\text{A.42})$$

$$\delta M_{I_y, h, 1k} = \delta F_{D_y, h, 1k} (0.5Lp - k + 0.5) \quad (\text{A.43})$$

7. The heave drag wave force and pitch drag moments are given by Eq A.44~A.45 respectively.

$$\delta F_{d_z, h, 1k} = \rho C_{dh} (D_{h,2i} / 2) (v_{h,1k})_{rel} |(v_{h,1k})_{rel}| \sin \phi \quad (\text{A.44})$$

$$\delta M_{d_y, h, 1k} = -\delta F_{d_z, h, 1k} [(Lp/2) - k + (1/2)] \quad (\text{A.45})$$

8. The heave inertia wave force and pitch inertia moments are given by Eq A.46~A.47 respectively.

$$\delta F_{I_{z,h,1k}} = \rho \left(\pi D_{h1,2}^2 / 4 \right) \left[C_{m_h} \dot{v}_{h,1k} - (C_{m_h} - 1) Z_g \right] \quad (\text{A.46})$$

$$\delta M_{I_{y,h,1k}} = \delta F_{I_{z,h,1k}} (0.5Lp - k + 0.5) \quad (\text{A.47})$$

9. The total wave sway and heave forces and yaw and pitch moments applied on hull no. 1 are given by Eq A.48~A.51 respectively.

$$F_{y_{hull1}} = \sum_{k=1}^M \left(\delta F_{I_{y,h,1k}} + \delta F_{d_{y,h,1k}} \right) \quad (\text{A.48})$$

$$F_{z_{hull1}} = \sum_{k=1}^M \left(\delta F_{I_{z,h,1k}} + \delta F_{d_{z,h,1k}} \right) \quad (\text{A.49})$$

$$M_{z_{hull1}} = \sum_{k=1}^M \left(\delta M_{I_{z,h,1k}} + \delta M_{d_{z,h,1k}} \right) \quad (\text{A.50})$$

$$M_{y_{hull1}} = \sum_{k=1}^M \left(\delta M_{I_{y,h,1k}} + \delta M_{d_{y,h,1k}} \right) \quad (\text{A.51})$$

Hull No.2:

The same steps (step 1 to 9) as for hull no. 1 were followed to evaluate the wave excitation forces on hull no.2 except the element x-coordinate in the wave direction is given by Eq A.52.

$$X_{h,2k} = \left[(L_p/2) - k + (1/2) \right] \cos\phi - b_{st} \sin\phi \quad (\text{A.52})$$

The total forces and moments are given by Eq A.53~A.57.

$$F_{y_{hull2}} = F_{y_{hull1}} + F_{y_{hull2}} \quad (\text{A.53})$$

$$F_{z_{hull2}} = F_{z_{hull1}} + F_{z_{hull2}} \quad (\text{A.54})$$

$$M_{x_{hull2}} = 2b_{st} \left(F_{z_{hull1}} - F_{z_{hull2}} \right) \quad (\text{A.55})$$

$$M_{y_{hull2}} = M_{y_{hull1}} + M_{y_{hull2}} \quad (\text{A.56})$$

$$M_{z_{hull2}} = M_{z_{hull1}} + M_{z_{hull2}} \quad (\text{A.57})$$

Yaw moments due to inertia and drag forces on columns

Yaw moments due to inertia and drag forces on columns are function of y-coordinate (perpendicular to wave direction) of each column as stated in Eq A.42, which are given by Eq A.58.

$$\{Y_c\} = \begin{Bmatrix} 1.5a_{st} \sin \phi + b_{st} \cos \phi \\ -1.5a_{st} \sin \phi + b_{st} \cos \phi \\ -1.5a_{st} \sin \phi - b_{st} \cos \phi \\ 1.5a_{st} \sin \phi - b_{st} \cos \phi \\ 0.5a_{st} \sin \phi + b_{st} \cos \phi \\ -0.5a_{st} \sin \phi + b_{st} \cos \phi \\ -0.5a_{st} \sin \phi - b_{st} \cos \phi \\ 0.5a_{st} \sin \phi - b_{st} \cos \phi \end{Bmatrix} \quad (\text{A.58})$$

APPENDIX B
BEYROT METHOD FOR MOORING LINES QUASI-STATIC ANALYSIS

A numerical procedure was developed by Peyrot and Goulouis [55] and Peyrot [56] for the analysis of complex 3D cable structures. The procedure was based on the nonlinear catenary equations and applicable to guyed towers, transmission lines, roof cables and mooring lines. For mooring cables, the mathematical model provided applicable procedures for the analysis of cables rapidly changing from a slack to taut configuration, cables having variable contact with the sea floor and cables with multi-component network. Fig B.1 shows a mooring multi-component network cable element stretched in its plane.

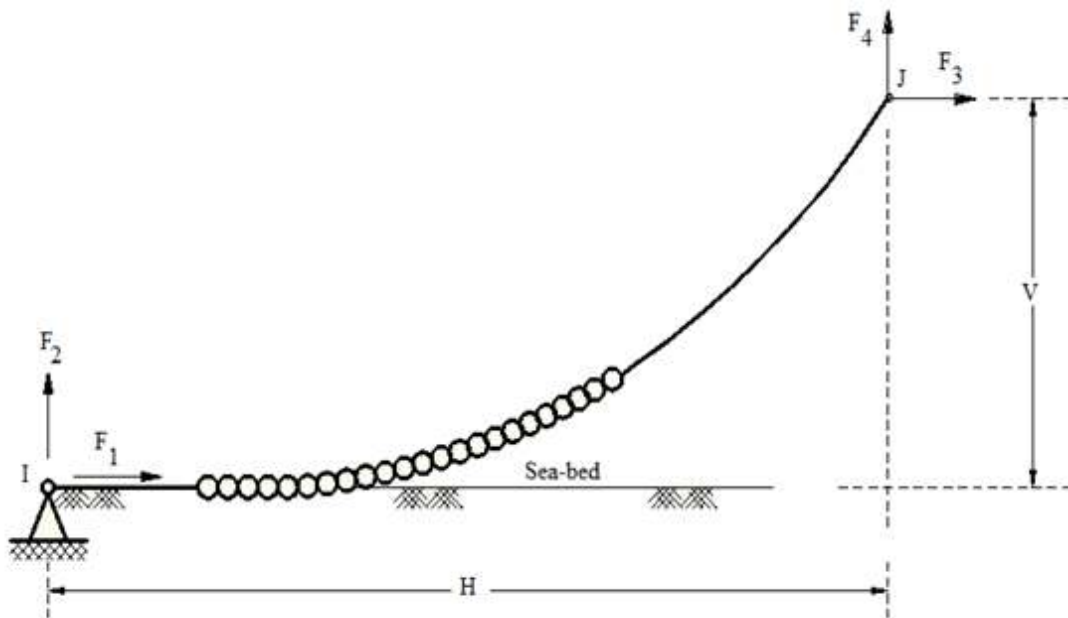


Fig B.1: Multi-component mooring line partially lies on the seabed

The well-known catenary equations are given by Eq B.1~B.3.

$$L^2 = V^2 + \frac{H^2 \sinh^2 \lambda}{\lambda^2} \tag{B.1}$$

$$F_2 = \frac{w}{2}(L - V \coth \lambda) \quad (\text{B.2})$$

$$\lambda = \frac{w|H|}{2F_H} \quad (\text{B.3})$$

where L is the stressed cable length between I and J and F_H is the horizontal component of the cable tension ($F_H = |F_1| = |F_3|$). Three additional geometrical relationships were derived by integrating the projections and the lengths of elemental segments along the length of the cable as given by Eq B.4~B.6.

$$H = -F_1 \left[\frac{L_u}{EA} + \frac{1}{w} \log \left(\frac{F_4 + T_J}{T_I - F_2} \right) \right] \quad (\text{B.4})$$

$$V = \frac{1}{2EAw} (T_J^2 - T_I^2) + \frac{T_J - T_I}{w} \quad (\text{B.5})$$

$$L = L_u + \frac{1}{2EAw} \left[F_4 T_I + F_2 T_I + F_1^2 \log \left(\frac{F_4 + T_J}{T_I - F_2} \right) \right] \quad (\text{B.6})$$

where T_I, T_J are the cable tensions at joints I and J respectively and L_u is the unstressed length between I and J (original). Because the relations given by Eq B.10~B.13 are exists, Eq B.4~B.6 are written in-terms F_1 and F_2 only, as the forms given in Eq B.7~B.9.

$$H = f_H(F_1, F_2) \quad (\text{B.7})$$

$$V = f_V(F_1, F_2) \quad (\text{B.8})$$

$$L = f_L(F_1, F_2) \quad (\text{B.9})$$

$$F_4 = -F_2 + w \cdot L_u \quad (\text{B.10})$$

$$F_3 = -F_1 \quad (\text{B.11})$$

$$T_I = (F_1^2 + F_2^2)^{1/2} \quad (\text{B.12})$$

$$T_J = (F_3^2 + F_4^2)^{1/2} \quad (\text{B.13})$$

where H is the constant component of cable tension. Considering the cable shown in Fig B.2, the following iterative procedure was used for the evaluation of the cable force-excurion nonlinera relationship.

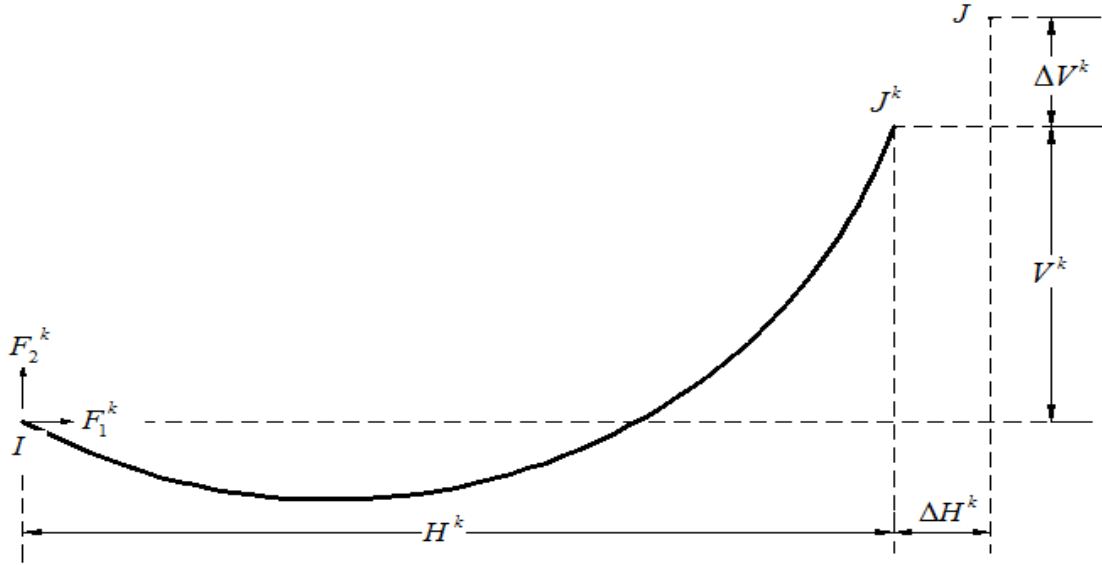


Fig B.2: Cable configuration at iteration step k

Fully suspended single component mooring lines

In this case, the following steps were used for evaluation of the force-excursion relationship:

1. Assuming F_1^k and F_2^k are joint I forces at the k^{th} iteration step, the corresponding cable projections H^k and V^k can be evaluated by Eq B.7 directly.
2. ΔH^k and ΔV^k are evaluated based on the known J^k location, the total step error, ζ^k is given by Eq B.14.

$$\zeta^k = \left[(\Delta H^k)^2 + (\Delta V^k)^2 \right]^{1/2} \quad (\text{B.14})$$

3. If ζ^k exceeds certain tolerance value, linear corrections are added to F_1^k and F_2^k to get new step origin forces according to Eq B.15, where F_1^k, F_2^k are the Forces of joint I at the k^{th} iteration step.

$$\begin{Bmatrix} F_1^{k+1} \\ F_2^{k+1} \end{Bmatrix} = \begin{Bmatrix} F_1^k \\ F_2^k \end{Bmatrix} + \begin{bmatrix} \alpha & \beta \\ \gamma & \delta \end{bmatrix} \begin{Bmatrix} \Delta H^k \\ \Delta V^k \end{Bmatrix} \quad (\text{B.15})$$

4. If the portion of Eq B.15 is inverted, it becomes as given by Eq B.16.

$$\begin{Bmatrix} \Delta H^k \\ \Delta V^k \end{Bmatrix} = \begin{bmatrix} \varepsilon & \xi \\ \eta & \theta \end{bmatrix} \begin{Bmatrix} \Delta F_1^k \\ \Delta F_2^k \end{Bmatrix} \quad (\text{B.16})$$

where

$$\begin{bmatrix} \alpha & \beta \\ \gamma & \delta \end{bmatrix} = \frac{1}{(\varepsilon\theta - \eta\xi)} \begin{bmatrix} \theta & -\xi \\ -\eta & \varepsilon \end{bmatrix} \quad (\text{B.17})$$

The constants ε , θ , η and ξ were approximated by Eq B.18~B.21.

$$\varepsilon = \frac{\partial f_{H^k}}{\partial F_1^k} = \frac{H^k}{F_1^k} + \frac{1}{w} \left(\frac{F_4^k}{T_J^k} + \frac{F_2^k}{T_I^k} \right) \quad (\text{B.18})$$

$$\xi = \frac{\partial f_{H^k}}{\partial F_2^k} = \frac{F_1^k}{w} \left(\frac{1}{T_J^k} - \frac{1}{T_I^k} \right) \quad (\text{B.19})$$

$$\eta = \frac{\partial f_{V^k}}{\partial F_1^k} = \frac{F_1^k}{w} \left(\frac{1}{T_J^k} - \frac{1}{T_I^k} \right) \quad (\text{B.20})$$

$$\theta = \frac{\partial f_{V^k}}{\partial F_2^k} = \frac{-L}{EA} - \frac{1}{w} \left(\frac{F_4^k}{T_J^k} + \frac{F_2^k}{T_I^k} \right) \quad (\text{B.21})$$

5. The iterative procedure requires starting values of F_1^k and F_2^k at the first iteration step ($k = 1$), this was achieved by replacing the stretching length in Eq B.1 by the un-stretched length and retaining only the first term of a series expansion of $\sinh^2(\lambda)/\lambda^2$, noting that the sign of F_1^1 always opposite that of H as given by Eq B.22.

$$F_1^1 = -\frac{wH}{2\lambda^1} \quad (\text{B.22})$$

where

$$\lambda^1 = \sqrt{3} \left(\frac{L_u^2 - V^2}{H^2} - 1 \right)^{1/2} \quad (\text{B.23})$$

Special cases were considered for Eq B.23 by conservative assumptions according to

Table B.1.

Table B.1: Special assumptions for Eq B.23

Case	Condition	Assumption
1	When Eq. B. 17 gives imaginary result ($L_u < V$)	$\lambda^1 = 0.2$
2	When Eq 17 gives infinity result ($H=0$)	$\lambda^1 = 10^6$

Eq B.2 was used to obtain the starting value of F_2 as given by Eq B.24.

$$F_2^1 = \frac{w}{2} [L_u - V \coth(\lambda)] \quad (\text{B.24})$$

The above-mentioned iterative procedure converges quickly on F_1 and F_2 . Then, the corresponding values of F_3 , F_4 , T_I and T_J were obtained from Eq B.8. The coordinates of any number of points along the cable were determined from Eq B.4~B.6 by replacing L_u by any fraction of L_u and the geometry of the cable was stored in matrix named “COORD”.

Single component mooring lines lying partially on the seabed

For mooring lines lying partially on the seabed, the above analysis was modified. Using an iterative procedure so that additional increments of line are progressively laid on the bed until the suspended line is in equilibrium as shown in Fig B.3, the following steps were followed:

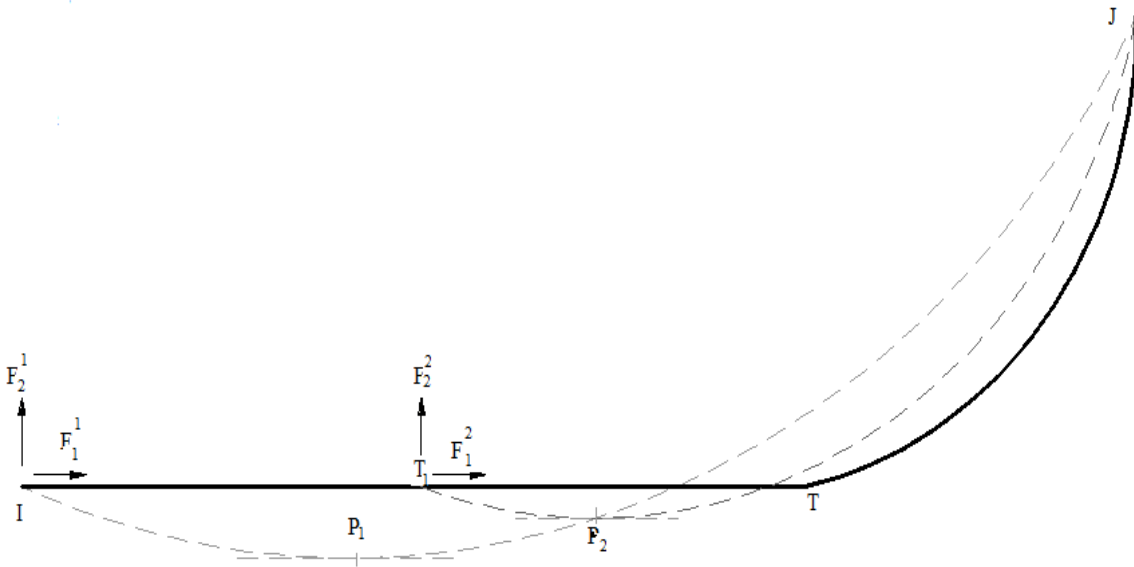


Fig B.3: Mooring line partially lies on seabed

1. Ignoring the sea-floor, the configuration IP_1J was found (point P_1 on the fictitious cable, where the tangent is parallel to the flat sea floor).
2. Point P_1 was located directly by its distance to I , which depends on the values of F_1^1 and F_1^2 . This step was completed when the length IP_1 is stretched along the sea-floor [IP_1 (curved) = IT_1 (straight)]. The remaining part is suspended [T_1 (1) P (2) J].
3. Step 2 was repeated till $T(k-1)P(k)$ gets smaller than specified value.

It should be noted that in the above procedure, it was assumed that the final tension in the grounded part, IT , is equal tension in the suspended segment, TJ .

PUBLICATIONS LIST

- [1] **M. A. Yassir** and V. J. Kurian, "Dynamic analysis for Mobile Offshore Drilling Unit," in *the National Post-graduate Conference on Engineering Science and Technology (NPC)*, Tronoh - Malaysia, 2009.
- [2] **M. A. Yassir** and V. J. Kurian, "Time domain hydrodynamic analysis of semi-submersible platforms," in *the 2nd International Conference on Engineering Technology (ICET)*, Kuala Lumpur - Malaysia, 2009.
- [3] **M. A. Yassir**, V. J. Kurian, I. S. Harahap, and N. Abu Bakar, "Numerical study on the dynamic response of a semi submersible platform with experimental validation," in *Conference on Scientific and Social Science Research (CSSR 2010)*, Kuala Lumpur - Malaysia, 2010.
- [4] **M. A. Yassir**, V. J. Kurian, and N. Abu Bakar, "Motion responses of a semi submersible: experimental study," in *the International Conference on Sustainable Building & Infrastructure (ICSBI)*, Kuala Lumpur - Malaysia, 2010.
- [5] V. J. Kurian, **M. A. Yassir**, and I. S. Harahap, "Nonlinear coupled dynamic response of a semi submersible platform " in *the 20th International Offshore (Ocean) and Polar Engineering Conference (ISOPE)*, Beijing - China, 2010.
- [6] C. Ng, V. J. Kurian, and **M. A. Yassir**, "Regression analysis for the dynamic responses of semi submersible platform," in *the 7th International Conference on Steel & Aluminum Structures (ICSAS)*, Kuching, Sarawak - Malaysia, 2011. *(Approved)*
- [7] **M. A. Yassir**, V. J. Kurian, I. S. Harahap, and N. Abu Bakar, "Parametric study on multi-component catenary mooring lines for offshore floating structures," in *the Asia-Pacific Offshore Conference (APOC)*, Kuala Lumpur - Malaysia, 2010.

- [8] **M. A. Yassir**, V. J. Kurian, and I. S. Harahap, "Second order motion responses of semi submersibles: numerical and experimental study," in the 21th International Offshore (Ocean) and Polar Engineering Conference (ISOPE), Maui, Hawaii - USA, 2011. (Approved)
- [9] **M. A. Yassir**, V. J. Kurian, and I. S. Harahap, "Nonlinear dynamic analysis of multi-component mooring lines incorporating mooring to seabed interaction," International Journal of Offshore and Polar Engineering (IJOPE), 2011. (Approved for publication)

Under preparation

- [1] **M. A. Yassir**, V. J. Kurian, and I. S. Harahap, "The consequences following mooring line loss on the dynamic responses of moored semi submersibles: experimental study," in the 22th International Offshore (Ocean) and Polar Engineering Conference (ISOPE), Rhodes - Greece, 2012.
- [2] **M. A. Yassir**, V. J. Kurian, and I. S. Harahap, "The wave frequency response of semi submersibles with different configurations: parametric study," International Journal of Offshore and Polar Engineering (IJOPE), 2011.